FIU Electronic Theses and Dissertations   University Graduate School

3-8-2006

Origin of the Grande Ronde Formation flows, Columbia River Flood Basalt Group

Sedelia Rodriguez Durand
Florida International University

FLORIDA INTERNATIONAL UNIVERSITY

Miami, Florida

ORIGIN OF THE GRANDE RONDE FORMATION FLOWS, COLUMBIA RIVER

FLOOD BASALT GROUP

A dissertation submitted in partial fulfillment of the

requirements for the degree of

DOCTOR OF PHILOSOPHY

in

GEOSCIENCES

by

Sedelia Rodriguez Durand

2006

To: Interim Dean Mark Szchuman
     College of Arts and Sciences

This dissertation, written by Sedelia Rodriguez Durand, entitled Origin of the Grande Ronde Formation Flows, Columbia River Flood Basalt Group, having been approved in respect to style and intellectual content, is referred to you for judgment.

We have read this dissertation and recommend that it be approved.

Grenville Draper

Stephen Haggerty

Rosemary Hickey-Vargas

Andrew Macfarlane

Stephen P. Reidel

Gautam Sen, Major Professor

Date of Defense: March 8, 2006

The dissertation of Sedelia Rodriguez Durand is approved.

Interim Dean Mark Szchuman
College of Arts and Sciences

Interim Dean Stephan L. Mintz
University Graduate School

Florida International University, 2006

DEDICATION

I would like to dedicate this dissertation to my son Xavier, who gave me the strength to move forward no matter what obstacles stood in my way and who made me realize that anything was possible.

ACKNOWLEDGMENTS

ABSTRACT OF THE DISSERTATION

ORIGIN OF THE GRANDE RONDE FORMATION FLOWS, COLUMBIA RIVER

FLOOD BASALT GROUP

by

Sedelia Rodriguez Durand

Florida International University, 2006

Miami, Florida

Professor Gautam Sen, Major Professor

Lavas belonging to the Grande Ronde Formation (GRB) constitute about 63% of the Columbia River Basalt Group (CRBG), a flood basalt province in the NW United States. A puzzling feature is the lack of phenocrysts (< 5%) in these chemically evolved lavas. Based mainly on this observation it has been hypothesized that GRB lavas were nearly primary melts generated by large-scale melting of eclogite. Another recent hypothesis holds that GRB magmas were extremely hydrous and rose rapidly from the mantle such that the dissolved water kept the magmas close to their liquidi. I present new textural and chemical evidence to show that GRB lavas were neither primary nor hydrous melts but were derived from other melts via efficient fractional crystallization and mixing in shallow intrusive systems. Texture and chemical features further suggest that the melt mixing process may have been exothermic, which forced variable melting of some of the existing phenocrysts.

Finally, reported here are the results of efforts to simulate the higher pressure histories of GRB using COMAGMAT and MELTS softwares. The intent was to evaluate (1) whether such melts could be derived from primary melts formed by partial melting of a peridotite source as an alternative to the eclogite model, or if bulk melting of eclogite is required; and (2) at what pressure such primary melts could have been in equilibrium with the mantle. I carried out both

forward and inverse modeling. The best fit forward model indicates that most primitive parent melts related to GRB could have been multiply saturated at ~1.5–2.0 GPa. I interpret this result to indicate that the parental melts last equilibrated with a peridotitic mantle at 1.5-2.0 GPa and such partial melts rose to ~0.2 GPa where they underwent efficient mixing and fractionation before erupting. These models suggest that the source rock was not eclogitic but a fertile spinel lherzolite, and that the melts had ~0.5% water.

TABLE OF CONTENTS

LIST OF TABLES

LIST OF FIGURES

xi

CHAPTER 1

INTRODUCTION

Large Igneous Provinces

Continental flood basalts (CFB) or large igneous provinces (LIP) are formed by the eruption of large volumes of lava onto the continental and oceanic crust. Lava volumes can range from 200,000 km^3 (Columbia River Basalt Group) up to 1.5 million cubic kilometers (Siberian Traps); (Hooper et al., 2002; Reichow et al., 2002; Renne, 2002; Camp et al., 2003; Camp and Ross, 2004). The maximum flux of these eruptions is generated in relatively short time scales, usually less than a million years. These eruptions have occurred throughout Earth's history in different locations around the world. The eruptions can release large amounts of greenhouse gases such as carbon dioxide, sulfur dioxide and hydrogen sulfide. When these gases are released into the upper troposphere and lower stratosphere they can create global warming effects and affect Earth's climate for many years (Thordarson and Self, 1996; Self et al., 1997). Consequently, these types of eruptions have been linked to mass extinction events throughout Earth's history. For example, the largest recorded extinction event, when approximately 90% of the species on Earth became extinct (Permian Extinction), occurred around the same time as the Siberian Traps (largest LIP eruption), approximately 250 million years ago (Renne, 2002).

Most CFB's are assumed to have been formed by hot spot or mantle plume activity. It has been proposed that a mantle plume is necessary to account for the unique characteristics of LIPs (Brandon and Goles, 1988; Richards et al., 1989; Campbell and Griffiths, 1990; Hooper, 1990). Studying flood basalt eruptions, therefore, may yield

important information on melt generation processes in LIPs and other products of plume related activity such as ocean island basalts (OIB) like those of the Hawaiian Islands.

In addition, the study of LIPs can lead to information on magma generation and transport and the role of global tectonics. For example, at approximately 30 Ma the North American plate collided with the East Pacific Rise changing the tectonic setting of the Pacific Northwest. This change caused the strike slip motion that created the San Andreas Fault system (Atwater, 1970), and an extensional regime further east which created the Basin and Range province (Christiansen and Lipman, 1972). Dickinson (1997) proposed that torsional deformation of the North American continental block that occurred in response to shear movement imposed by the Pacific plate, created a mantle perturbation. This mantle perturbation in turn could have caused a type of decompressional melting in the CRBG plateau that perhaps aided in the formation of the voluminous Columbia River Basalt Group (CRBG) flows (Dickinson, 1997).

Columbia River Basalt Group

The CRBG of the Pacific Northwest is the smallest, youngest and most well-preserved continental flood basalt province (Waters, 1961; Watkins and Baksi, 1974; McKee et al., 1977; 1981; Swanson et al., 1979; Hooper, 1982, 1984, 2000, Hooper et al., 2002; Reidel, 1983, Reidel et al., 1989, Reidel and Tolan, 1992; Swanson, et al., 1989). The CRBG has been extensively studied for insights into the processes that create rapid voluminous basalt eruptions on continents as well as on the ocean floor (Waters, 1961; Watkins and Baksi, 1974; McKee et al., 1977; 1981; Baksi, 1989). Although small when compared to other flood basalts, the CRBG contains over 234,000 km^3 of lava (Camp and Ross, 2004). Some individual lava flows extend from western Idaho all the way to the

Pacific Ocean approximately 600 km away (Shaw and Swanson, 1970; Reidel et al., 1989), making them the longest known lava flows on Earth. Major and trace-element compositions do not change over the entire lengths of some of these flows (Shaw and Swanson, 1970). Typical flow volumes are 10 to 20 km^3 (Basaltic Volcanism on Terrestrial Planets, BVTP, 1981). Lava flow thickness range from a few meters up to 45 m, with an average thickness of 30 m (BVTP, 1981). The basalts cover an area of approximately 200,000 km^2 occupying parts of Washington, Oregon and Idaho (Waters, 1961); (Figure 1).

The lavas of the CRBG erupted between 17 and 6 million years ago (Watkins and Baksi, 1974; McKee et al., 1977, 1981; Swanson et al., 1979), through fissures that became the Chief Joseph dike swarm near the mutual borders of Idaho, Washington, and Oregon. Recently, Hooper et al. (2002) and Camp (1995), Camp et al. (2003) and Camp and Ross (2004) have proposed the inclusion of lava formations south of the CRBG plateau, mainly the Steens Mountain Basalt, and younger eruptions of high alumina basalts, termed the Oregon Plateau Basalts (OPB in Figure 1). Furthermore, Coe et al. (2005) propose that the Lovejoy Basalts of northeastern and central California could possibly be related to the same magma generation event. The addition of these formations would increase both the areal extent and volume of the CRBG. It is doubtful however, that this increase would change the current status of the CRBG, considering that other flood basalt provinces such as the Siberian Traps and Ontong Java Plateau are orders of magnitude larger than the CRBG (Reichow et al., 2002) and have erupted over a million km^3 of basalt (Reichow et al., 2002; and others).
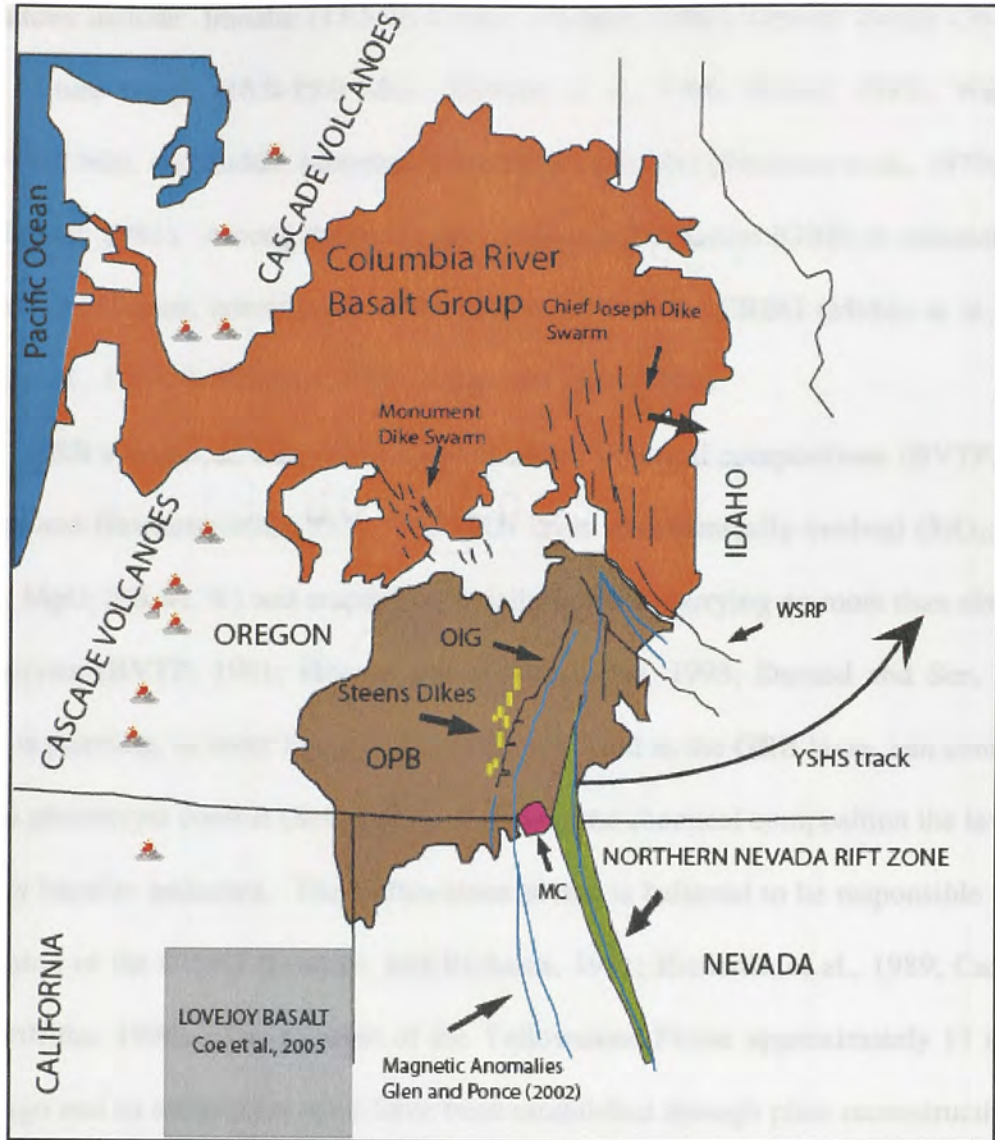
Figure 1-Map of Columbia River Basalt Group adapted from Camp and Ross, 2004; Coe et al., 2005. Map shows proposed additions to the flood basalt province, namely the Oregon Plateau Basalt and the Lovejoy Basalt. OIG-Oregon Idaho Graben; OPB-Oregon Plateau Basalt; MC-McDermitt Caldera; YSHS-Yellowstone Hotspot; WSRP-Western Snake River Plain.

4

The CRBG has been formally divided into five formations based on age and first order geochemical differences (Waters, 1961; Swanson et al., 1979) (Figure 2). These formations include: Imnaha (17.5-16.5 Ma); (Hooper, 1984), Grande Ronde (16.5-15.6 Ma); Picture Gorge (16.0-15.0 Ma), (Mangan et al., 1986; Reidel, 1983), Wanapum (15.6-14.5 Ma), and Saddle Mountain Basalt (14.5-6.0 Ma) (Swanson et al., 1979; Camp and Hooper, 1981). Among them, the Grande Ronde Formation (GRB) is volumetrically the most significant, constituting about 63% to 87% of the CRBG (Mckee et al., 1977; Reidel et al., 1989; Tolan et al., 1989; Camp and Ross, 2004).

GRB consists of 4 km of flows with varied chemical compositions (BVTP, 1981; Hooper and Hawkesworth, 1993). The GRB lavas are chemically evolved (SiO_2: 52-57 wt. %, MgO: 3-6 wt. %) and erupted essentially as melts carrying no more than about 5% phenocrysts (BVTP, 1981; Hooper and Hawkesworth, 1993; Durand and Sen, 2004), which is puzzling, as other lavas as chemically evolved as the GRB lavas, can contain up to 15% phenocryst content (Sen, 1983). Based on the chemical composition the lavas are actually basaltic andesites. The Yellowstone plume is believed to be responsible for the generation of the CRBG (Duncan, and Richards, 1991; Richards, et al., 1989; Campbell and Griffiths, 1990). The location of the Yellowstone Plume approximately 17 million years ago and its subsequent track have been established through plate reconstructions by Engebretson et al. (1984) and Pierce and Morgan (1992); they place the plume near the CRBG eruptive center in southeastern Oregon during the time of the eruptions of the Grande Ronde Formation.

Group	Formation	Member	Samples	Age	Magnetic Polarity
		Saddle Mountain	See Reidel and others (1989)		6.0	
	Wanapum	See Reidel and others (1989)		14.5	
	Grande Ronde Basalts	SentinelBluffs Unit	GR-SBM2269, GR-SBM2570, GR-SBM2978	15.6	N2
		Slack Canyon Unit			
		Field Spring Unit			
		Winter Water Unit			
		Umtanum Unit	GR-U3406		
		Ortley Unit	GR-O4014, GR-O4352		
		Armstrong Canyon Unit			
		Meyer Ridge Unit			R2
		Wapshilla Ridge Unit			
		Grouse Creek Unit			
		Mt. Horrible Unit			
		China Creek Unit	CHI-40		N1
		Downey Gulch Unit	CHI-38, 39, 41 44, 45		
Picture Gorge		Center Creek Unit	GR-17, 18, CHI-30-32, CHI-34, 36		
		Rogersburg Unit	GR-13, 16 CHI-29		
	Grande Ronde Basalts	Teepee Butte Unit	GR-3, 8-10, CHI-28		R1
		Buckhorn Springs Unit	GR-1, 2, CHI-17-22, 24	16.5	
	Imnaha	See Hooper and others (1984)		17.5	

Figure 2- Stratigraphic column of the Columbia River Basalts Group. Samples from the Grande Ronde Basalt Formation analyzed during this study are shown adjacent to the specific GRB units they were collected from.

The plume or hot spot track can be traced from the site of the initial eruptions which produced a rhyolitic field approximately 16.5 Ma through the silicic Eastern Snake River Plain (ESRP) and ending in Wyoming at the Yellowstone caldera, where the plume is thought to be at the present time.

Several questions remain unanswered regarding the genesis of the CRBG. For example, if the Yellowstone Plume was indeed responsible for the CRBG eruptions, then why was it located 500 km south of the eruptive vents that fed the CRBG at 16.5 Ma? There is also no evidence of a plume prior to this event (Geist and Richards, 1993). Furthermore, the lavas are different from other plume or hot spot related lavas in the lack of hot temperature magmas such as picrites. Picrites can be generated by the elevated temperatures associated with mantle plumes (Hooper, 1990 and others). In addition, the lavas erupted directly above the plume location are silicic, rather than the usual tholeiitic lavas associated with mantle plumes (Hooper, 1990 and others). Some investigators have attributed the silicic compositions to crustal anextesis of the continental and accreted oceanic crust in the area (Carlson et al., 1981; Carlson, 1984; Carlson & Hart, 1988).

There are several other inconsistencies with a typical plume model. For example, it is coincidental that the purported plume track along ESRP eruptions also follows an ancient tectonic boundary (www.mantleplumes.org/CRB.html). In addition, volcanism directly above the projected plume path 16.5 million years ago appears to extend to the north (CRBG), east (ESRP), and west (Newberry Trend). This "mirror" volcanism is difficult to explain with a simple eastern-tracking plume migration hypothesis. Volcanism appears to move northward to create the mostly tholeiitic CRBG, while at the same time producing a rhyolite field directly above, the silicic Brothers Fault volcanics

7

(Newberry trend) to the northwest, and the ESRP to the east (Camp et al., 2003; and others).

Because the eruptive vents for the CRBG are located approximately 500 km north of the projected plume location at the time of major eruptions (~16.5 Ma), it has been proposed that the lava traveled long distances in a similar manner to what has been seen on other planets (e.g., Mars), where giant radiating dike swarms have been seen around plume-like structures (Ernst et al., 1995). Camp and Ross (2004) suggest that the CRBG dikes are similar in scale and pattern to radiating swarms indicating a radial geometry. Ernst and Buchan (2003) reconstructed the orientation of the Chief Joseph dike swarm, the Monument dike swarm, and the Northern Nevada Rift Zone and found that these triangulate to a focal point east of Steens Mountain. Camp and Ross (2004) suggest that this point may have been the central location of a mantle plume at 17 Ma. This point also marks the site of the earliest eruptions of Steens Mountain (Hooper et al., 2002), which has been described as a shield volcano (Mankenin et al., 1987). A circular magnetic anomaly near the crest of the mountain delineates the volcano's central vent (Camp and Ross, 2004). The lavas are tholeiitic (becoming mildly alkalic up section) and are thinner and more complex, typical of shield volcano development (Clague and Moore, 1991). Camp and Ross (2004) postulate that giant radiating dike swarms fed the CRBG as well as the Steens Mountain basalts. In spite of difficulties with plume models, both plume and non-plume models continue to be invoked for the origin of CRBG lavas. An alternative non-plume proposal is that the CRBG magmas formed due to back arc spreading behind the Cascade arc and at the northern end of the Basin and Range province (Hart and Carlson, 1987; Carlson and Hart, 1988; Swanson et al., 1989; Smith,

8

1992). White and Mackenzie (1989) proposed that the lithospheric thinning was caused by plume-related extension. Whether the extension was the cause or a consequence of the eruptions remains a topic of some debate (Hooper, et al., 2002; White and Mackenzie, 1989; Richards et al., 1989; Hooper, 1990).

The absence of the proposed mantle plume directly beneath the CRBG plateau prior the eruption of the CRBG is intriguing. Geist and Richards (1993) propose that the mantle plume was blocked by the subducting Farallon plate and thus the surface did not exhibit any prior mantle plume activity. At approximately 17.5 Ma, They suggest that the plume head penetrated the subducting plate and broke through the slab. This event caused the plume head to be deflected north, placing the plume head beneath the eruptive center for the CRBG (Figure 3). Once the plume head was sheared off as the North American plate moved over the plume, the plume tail recovered to a near vertical conduit and continued on its original northeast path forming the Snake River plain and Yellowstone plateau. The Geist and Richards model explains both the absence of plume activity prior to the CRBG and why the eruptive vents for the CRBG were located so far north (approximately 500 km) of the projected plume path. Pierce and Morgan (1992) proposed a similar model in which a mantle plume intercepted the base of the lithosphere approximately 16.5 Ma. The plume head spread outward to generate the CRBG and other volcanic outpourings near the Oregon-Idaho-Nevada border (Pierce and Morgan, 1992).

A petrologic model has been proposed by Takahashi et al. (1998); that calls for a subducted component (eclogite) entrained in a mantle plume (Figure 4).
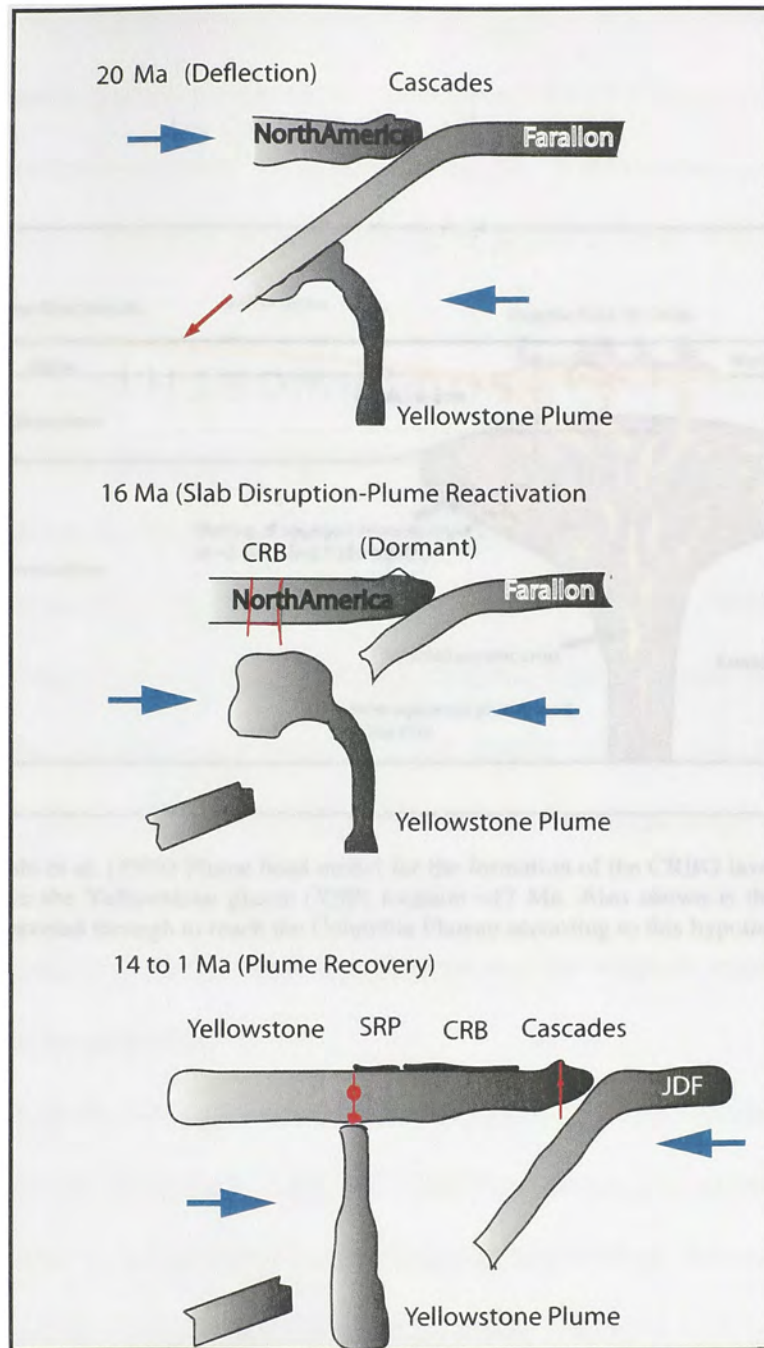
Figure 3-Geist and Richards model depicting the Yellowstone plume being deflected by the Farallon plate. This caused the plume head to move under the Columbia plateau approximately 17.5 Ma. The plume tail recovered and continue to its present location beneath the Yellowstone caldera in Wyoming. CRB-Columbia River Basalts; SRP-Snake River Plain; JDF-Juan de Fuca Plate.
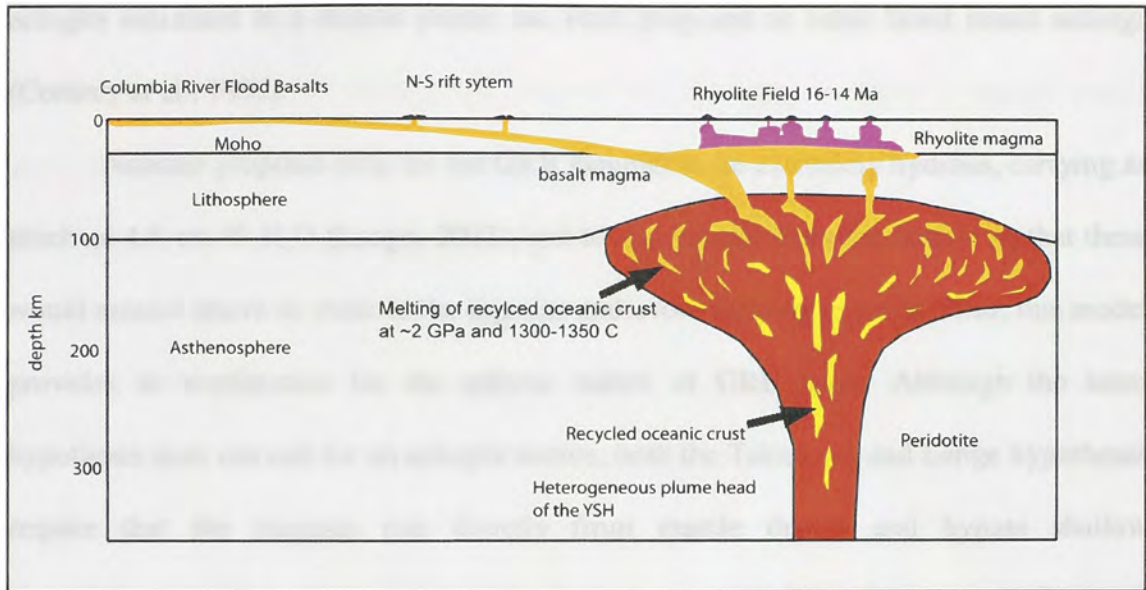
Figure 4- Takahashi et al. (1998) Plume head model for the formation of the CRBG lavas and the rhyolitic field directly above the Yellowstone plume (YSP) location ~17 Ma. Also shown is the North South rift system the lavas traveled through to reach the Columbia Plateau according to this hypothesis.

The authors proposed that many of the GRB magmas were produced by 30-50% melting of the eclogite. The Takahashi et al. (1998) model suggests that the GRB are primary or near-primary melts that originated near the crust-mantle boundary and bypassed any shallow-level fractionation prior to eruption (Figure 4). A subducted component such as eclogite entrained in a mantle plume has been proposed in other flood basalt settings (Cordrey et al., 1997).

Another proposal calls for the GRB magmas to be extremely hydrous, carrying as much as 4.4 wt. % H_2O (Lange, 2002), and to rise rapidly from the mantle so that these would remain above or close to the liquidus and avoid forming crystals. Thus, this model provides an explanation for the aphyric nature of GRB lavas. Although the latter hypothesis does not call for an eclogite source, both the Takahashi and Lange hypotheses require that the magmas rise directly from mantle depths and bypass shallow crystallization. This scenario is required because shallow-level crystallization-differentiation processes would result in degassing of the magmas and would also sufficiently modify the original melt signature so that the original mantle-equilibration history could not be unraveled.

Analysis of the GRB phenocrysts (Durand and Sen, 2004; Caprarelli and Reidel, 2004, 2005); provide evidence for shallow level fractionation. For example, GRB lavas plot near the 1-atm pseudo cotectic on the cpx-ol-qz and pl-ol-qz diagrams (Durand and Sen, 2004, see figure 28 in Chapter 3). The presence of a shallow level magma chamber, where such fractionation could occur, has been disputed by Hooper et al. (1982) and others. They point to the lack of large collapse structures, such as calderas, on the surface. Others (Reidel et al., 1984) suggest that the Pasco Basin subsided both before,

during and after the main lava eruptions, perhaps as a result of the collapse of a large magma chamber at shallow depths. If crystal fractionation of a partial melt of an upper mantle peridotite (thought to be the source rock of most plumes) was the source for the CRBG lavas, then the source magma must have fractionated in a crustal magma chamber(s) before erupting; and extremely efficient crystal separation had to occur in order for these magmas to erupt with virtually no phenocrysts. Such a process would leave behind gabbro cumulates at shallow depths beneath the feeder dikes. Seismic velocity and density measurements beneath the Columbia River plateau suggest that a high density layer is not present (Catching and Mooney, 1988; Saltus, 1993) however, geophysical data in the area is difficult to obtain and therefore the findings thus far are not conclusive and more analyses are needed to verify this assumption (Reidel, S.P., pers. comm.).

As is apparent from the numerous petrogenic models presented above, there is no consensus on what caused the eruption of large volumes of lava in the Columbia Plateau, or whether the resultant basaltic andesites are low-pressure fractionates or primary melts. This study focuses primarily on the Grande Ronde Basalts given that they constitute over 63% of the entire volume of the CRBG (Camp and Ross, 2004 and others).

The remainder of this dissertation will be subdivided into four parts. Chapter two will include field and petrographic studies. Chapter 3 will discuss the mineral chemistry of the Grande Ronde lavas, emphasizing the phenocrysts, since these constitute one of the most puzzling aspects of this formation. Although phenocrysts comprise less than 5% phenocryst in these rocks, a substantial study of major and minor element variations was conducted. Groundmass analyses of major and minor elements were also performed.

Both a petrographic study using a transmitted light microscope and an electron microprobe study were conducted. Chapter 4 focuses on computer simulations of the potential Grande Ronde parental magmas in order to explain the origin of the lavas, i.e., pressure, temperature, H_2O content and phase appearance. The computer simulation programs COMAGMAT (Ariskin, 1993) and MELTS (Sack and Ghiorso, 1994) were used in the simulations. Chapter 5 presents the summary and conclusions followed by a discussion of two tectonic models for the generation of the CRBG, and finally a proposal for future work.

CHAPTER 2.

FIELD STUDY AND PETROGRAPHY

Lava flows

The CRBG lavas were generated as large fissure eruptions that poured from large dike swarms concentrated in the eastern edge of the plateau near the Idaho-Washington border. Flows up to >600 km in length have been reported (Ho and Cashman, 1997; Tolan et al., 1989). The Pomona flow traveled from the site of eruption in western Idaho to the Pacific Ocean 600 km away, making it one of the longest known lava flows on Earth (Tolan et al., 1989). If not impeded by the ocean, this flow could have possibly been longer (Keszthelyi and Self, 1998). Additionally, the Gingko flow of the Wanapum Formation, traveled approximately 500 km covering more than 37,000 km^2 (Ho and Cashman, 1997). Interestingly these flows have been reported to be extremely homogenous in bulk composition and texture. The GRB in particular seems to be remarkably homogenous considering its large volume (149,000 km^3) (Swanson et al., 1979). During peak activity of the CRBG, the average interval between major eruptions was approximately 13,500 years and the average volume per major flow was about 1350 km^3 (Tolan et al., 1989).

Columnar Jointing

In general, columnar basalts have internal jointing classified as colonnades and entablatures (Figure 5). The term colonnade refers to small columns of fine-grained basalt that are generally restricted to the top and bottom of the lava flow.

Figure 5- Lava flows of the Columbia River Basalt Group in Washington State. The CRBG flows form extensive plateaus composed of numerous layers of lava. Picture displays the columnar basalt features seen throughout the CRBG plateau, with upper and lower colonnade and entablature structures (see text below for discussion).

Colonnades show quench textures which indicate they cooled more rapidly than the coarser and therefore slower cooling entablature structure that lies in between the upper and lower colonnades (Long and Wood, 1987). According to Reidel (1983), a typical basalt flow in the CRBG plateau is composed of three parts, a well-developed colonnade, a thin entablature and a thin scoriaceous flow top. Most flows have stubby, irregular columns and lack well-defined entablature (Reidel, 1983; Figure 6).

Vent Systems

Dikes and vents that fed the CRBG are concentrated in the southeast corner of the plateau (Swanson et al., 1979). These dikes are generally a few meters wide but can be wider than 20 meters in some locations (Swanson, 1970; Figure 7). NNW-oriented fissures 10 to over 100 km in length and up to several meters wide fed the extensive lava flows of the CRBG (Swanson et al., 1979). Average lava flows are 30 to 50 m thick but can be as much as 100 m thick (Reidel, 1983, 2005). Most of the dikes are restricted to the thinner, and more mafic, accreted terrains of the Blue Mountain province in northeastern Oregon (Hooper, 2003). Evidence for multiple magmatic intrusions within a single dike can be seen in thin sections analyzed in this study. Mingling of at least two different magmas is evident from the textures illustrated in figure 8. One of the magmas is fine grained and glassy while the other is more coarse grained. This observation suggests that magma conduits were long-lived and were replenished more than once.

The two major feeder dike swarms are the Chief Joseph dike swarm, and the Monument dike swarm (Waters, 1961; Swanson et al., 1979; see figure 1 in INTRODUCTION).

Figure 6- Basaltic columns of the Roza flow (Wanapum Basalt Formation) of the Columbia River Basalt Group, located in Washington State.

Figure 7- Exposed Roza dike that fed the Roza flow of the CRBG Wanapum Formation located in Washington State.

The majority of the CRBG lavas were erupted from the Chief Joseph dike swarm, including the Imnaha, GRB, Wanapum, and Saddle Mountain basalt formations. The Monument dike swarm produced the Picture Gorge Basalt, which has similar chemical compositions to the Imnaha Formation but, are more primitive and are similar to some of the Basin and Range lavas (Hooper, 1984; Hooper and Hawkesworth, 1993).

Here, I report the textural features and mineral chemistry of the phenocrysts in Grande Ronde Formation lavas from two well-known field sections—the Grande Ronde Formation section (type section), the China Creek section (cf. Reidel, 1983), the Sentinel Bluffs Member, and informal members; Umtanum and Ortley (See Figure 2 in INTRODUCTION). GR and China Creek samples were previously analyzed for major, trace, and isotope chemistry by others (Hooper, 1982; Reidel et al., 1989; Swanson et al., 1979; Hooper and Hawkesworth, 1993; Mangan et al., 1986; Hooper et al., 2002, and references therein).

SAMPLE SELECTION

Samples examined in the present study encompass the lower to middle sections of the Grande Ronde Formation, from the Buckhorn Springs unit to the China Creek unit, representing two magnetostratigraphic units, R1 and N1 (See Figure 2 in INTRODUCTION). Samples were also analyzed from the middle to upper sections of the GRB formation (Umtanum and Ortley) and from the youngest member of the GRB, the Sentinel Bluffs Member. These represent the N2 magnetostratigraphic unit (See Figure 2 in INTRODUCTION). The bulk of the samples analyzed here were collected by S.P. Reidel and P.R. Hooper and were previously analyzed for elemental and isotopic compositions by Reidel (1983) and Hooper and Hawkesworth (1993).

Figure 8-Cross-polarized image of a dike thin section showing products of at least two different magmas, indicating that the same dike was used by at least two or more batches of magma that mingled in the dike. (Width of field of view represents 5.2 mm).

Additionally, I collected samples across the width of a GRB dike, from chilled margin, through the interior, to chilled margin of each dike. Imnaha dike samples were collected by H. Petcovic.

METHOD OF STUDY

Thirty-one rock thin sections were initially inspected using an optical microscope and were then analyzed at the Florida Center for Analytical Electron Microscopy (FCAEM), Florida International University (FIU), on a fully automated electron microprobe (JEOL Superprobe, JSM-8900R) equipped with five wavelength dispersive spectrometers (WDS) and an energy dispersive spectrometer (EDS). All analyses reported here were analyzed with WDS. The operating conditions included an accelerating voltage of 15 kV and 20 nA current at the Faraday cup. The probe diameter was 1-2 µm and all analyses were performed in a fixed spot mode. Standards used for Mg, and Fe were olivine (ol), ol and plagioclase (An$_{65}$) for Si, plagioclase (An$_{65}$) and pyrope-garnet for Al, plagioclase (An$_{65}$) and diopside-2 for Ca, Cr$_2$O$_3$ for Cr, rutile for Ti, albite-2 for Na, orthoclase and sanidine for K, and rhodonite (2) for Mn. The on-peak time was 10 seconds for both standard and unknown and five seconds for the high and low background on each element mentioned above. The electron beam was extremely stable and counting statistics were excellent, so that standard analysis was reproducible to within +/- 2% of the absolute values for all major elements. The φρZ (CITZAF) correction program (Goldstein et al., 1992) was utilized to correct for the effects of matrix, density, and atomic number. Several spot analyses were performed on the samples in order to minimize analytical uncertainties of sodium loss on all the phenocryst

phases. Methods similar to Keshav and Sen (2001) were adopted for analyzing for sodium.

In addition, backscatter electron images were collected on the various textural features found in GRB lavas. These include: zoning patterns and resorption features of major minerals, generally plagioclase and clinopyroxene.

PETROGRAPHY

Basaltic andesites from the GRB flows are generally aphyric to sparsely phyric (<5%). The modal percent of phenocrysts in individual flows stays relatively constant with stratigraphic height. The phenocrysts mainly consist of plagioclase and augite (60% Plagioclase, 40% pyroxene). Textures vary from slightly porphyritic to intergranular and intersertal.

Plagioclase (average size 1.5 mm) and augite (0.3-1.0 mm) are the most common phenocryst phases, with plagioclase being dominant. Some small relatively Fe-rich, olivine (Fo_{30-50}) crystals do occur in the groundmass of some samples, but whether they are a part of the groundmass or are microphenocrysts is not clear. Larger phenocrysts of olivine (altered to iddingsite) are present (<1%) in some flows. Pigeonite and orthopyroxene phenocrysts are generally rare (see also Reidel, 1983). Iron-titanium oxide phenocrysts were not found in any of the flows studied.

The groundmass is generally microcrystalline to glassy composed of plagioclase, augite, olivine (rare), pigeonite, Fe-Ti oxides and black and light brown glass. Iron oxides are generally restricted to the groundmass and these are Ti-magnetites and ilmenites with euhedral to subhedral morphologies.

Pockets of rhyolitic glass are found in the groundmass of several of the thin sections analyzed (CHI-45). Rhyolitic glass is also found as inclusions in several plagioclase grains (CHI-45). The glass found in these thin sections is similar to those found by Lambert et al (1989) in all CRBG formations. They find two phases, described as a chlorophaeite-rich glass and a granite-glass. Several quartz (xenocrysts?) were found in some of the sections (GRB-2, GRB-17, and CHI-45). Secondary interstitial shallow level carbonate phases are sparsely located throughout the flows sections sampled.

Plagioclase

Plagioclase is the most abundant phase and has the largest sized phenocrysts in the GRB basaltic flows. Generally the phenocryst size averages approximately 1.5 mm in length and 0.002 mm in width. The rare larger phenocrysts can be up to 5.0 mm in length and 0.012 mm in width. The smaller phenocrysts or microphenocrysts are as small as 0.002 mm. Crystals are labeled microphenocrysts if the grain is significantly larger than groundmass grains, but smaller than typical phenocryst grains (>0.3 mm). Although the plagioclase phenocrysts are the most abundant, these are still small in modal abundance (<5%) compared to the total Grande Ronde flow volumes and as such the flows are considered aphyric to sparsely phyric. Phyric flows are found intermittingly in some of the GRB flows (i.e., GRB-10, GRB-16), however the overall majority of the formation is aphyric. Plagioclase phenocrysts and microphenocrysts are found as single crystals and as crystal aggregates or as glomeroporphyritic clusters. These clusters in some cases contain only plagioclase grains (Figure 9). However, plagioclase clusters are found with clusters of pyroxene grains (Figure 10). Most plagioclase phenocrysts are tabular with euhedral to subhedral morphologies.

Figure 9- Glomeroporphyritic cluster of plagioclase grains in a GRB flow (Sample GR-16). (Crossed polars: Width of field of view represents 2.5 mm).

Figure 10- Glomeroporphyritic cluster of plagioclase, augite (blue) and opx (brown) grains in a GRB flow (Sample O-4352). (Crossed polars: Width of field of view represents 2.5 mm).

In general however, the largest phenocrysts are euhedral. Some of these phenocrysts show resorption along rims. Melt (glass and mineral) inclusions are often trapped in a ring-like manner around the resorbed areas (Figure 11). These ring-like inclusions are mostly found in the lower units. Mesh resorption, or spongy resorption in the core of some phenocrysts, is also observed (Figure 11). The existing anhedral crystals show extensive evidence of resorption (sieve texture). Of interest are several phenocrysts which are extremely resorbed (Figures 12 and 26). Some of these resorbed phenocrysts have An contents of up to 96 (Figure 26). Overall the plagioclase phenocrysts are better preserved than the pyroxene phenocrysts.

Zoning is present in plagioclase phenocrysts throughout the GRB formation. The zoning patterns persist throughout the formation from the lower flows to the upper flows in the samples analyzed. The lower members however appear to have more zoned phenocrysts than the middle to upper members. Many plagioclase phenocrysts exhibit reverse zoning (Figure 13). In some cases both normal and reverse zoned plagioclase can be found in individual samples. Oscillatory zoning is also found within the same samples that exhibit normal and reverse zoning patterns (Figure 14). Some crystals have patchy zoning trends where patches of varied compositions occur throughout the grain. Plagioclase morphology in the groundmass ranges from euhedral to subhedral. Zoning in groundmass plagioclase is not as evident as it is in the phenocryst population however zoning is seen in some of the plagioclase crystals analyzed. The type of zoning is generally oscillatory. Zoning is even less evident in the younger GRB flows. Resorption features are also not seen as often in the groundmass.
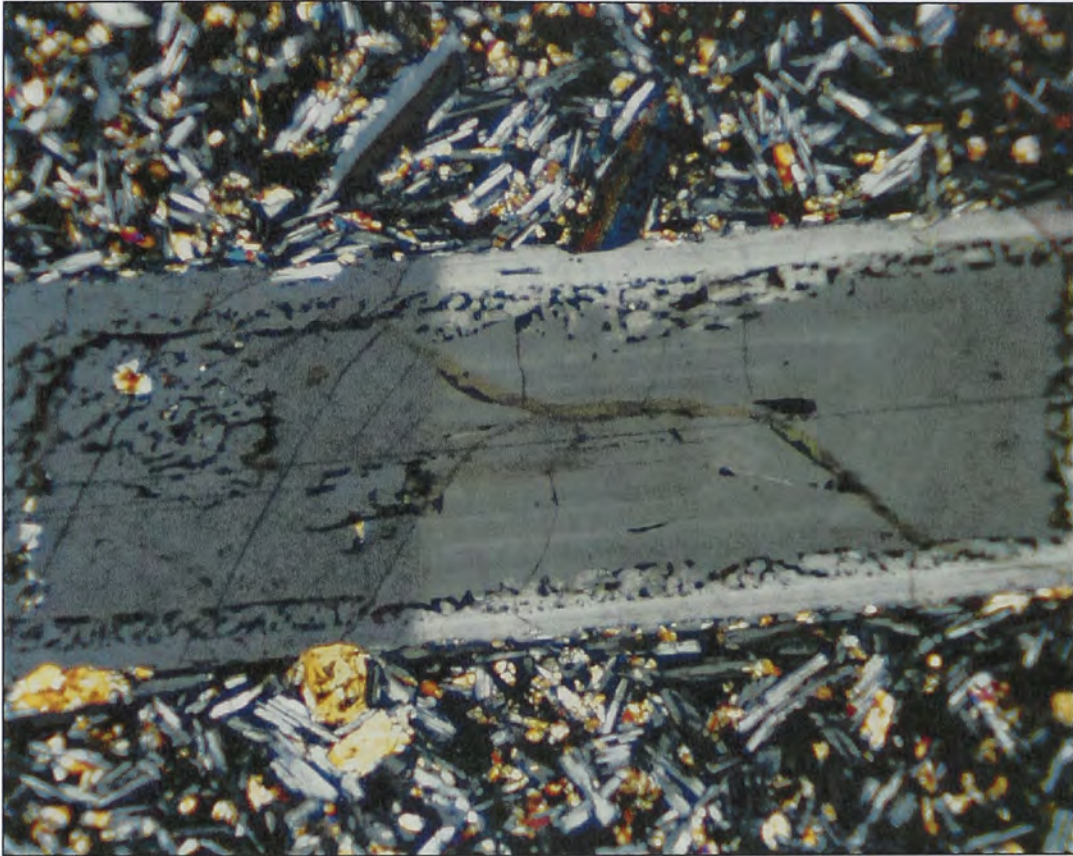
Figure 11- Large zoned and partially resorbed plagioclase phenocryst with melt (glass) inclusions. Outer rim is more anorthitic (An_{60}) than core (An_{47}) (Sample GR-3). (Crossed polars: Width of field of view represents 3 mm).
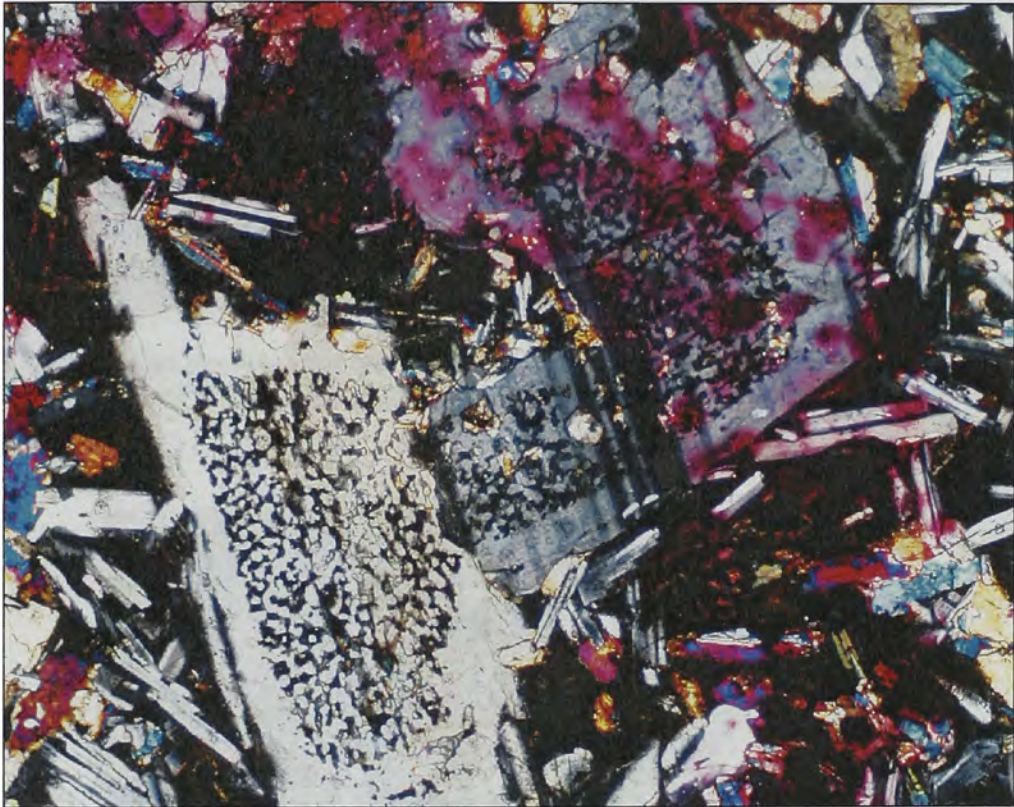
Figure 12- Several plagioclase phenocrysts showing extensive resorption of the core surrounded by euhedral rims (GR-2269). This is a typical sieve texture. (Crossed polars: Width of field of view represents 2.5 mm).
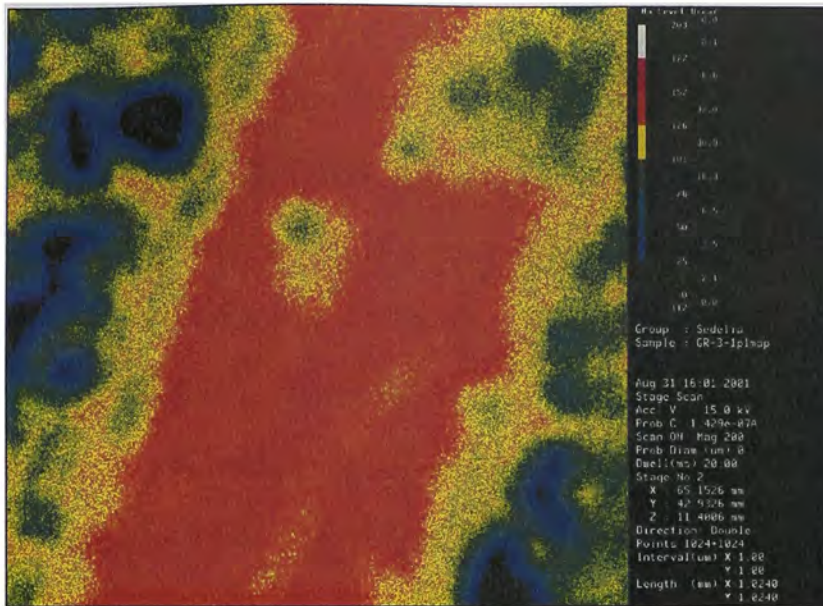
Figure 13- X-ray map depicting oxide concentrations, Red area indicates higher Na, the yellow area indicates lower Na, higher Ca. This is an example of a GRB reversely zoned plagioclase phenocryst (Sample GR-3).
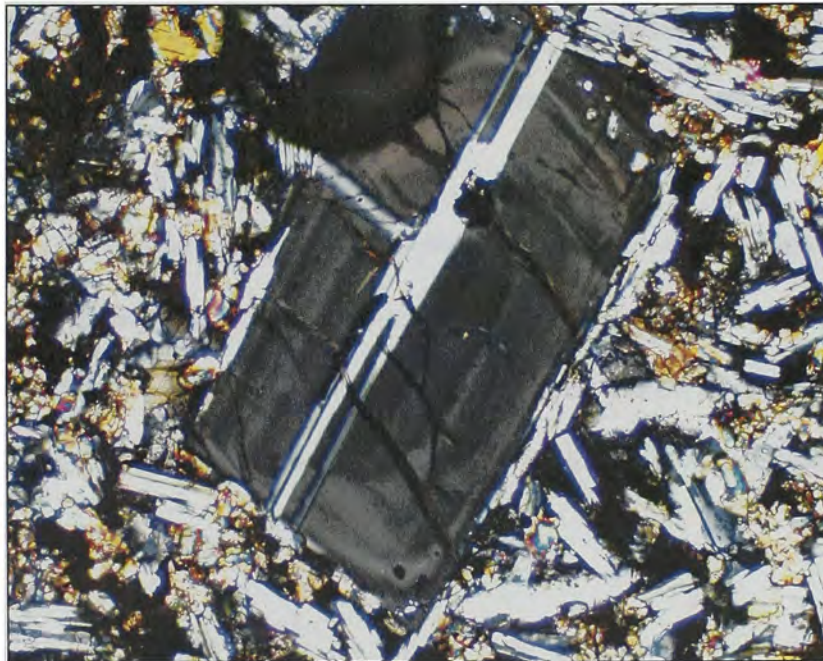
Figure 14- Plagioclase phenocrysts with oscillatory zoning (Sample CHI-20). (Crossed polars: Width of field of view represents 1.1 mm).

Pyroxene

Euhedral crystals of augite occur as isolated phenocrysts or in clusters, sometimes showing a thin but distinct outer zone. Where present, pigeonite phenocrysts show disequilibrium characteristics: for example, Figure 15 shows a pigeonite phenocryst with a rounded (resorbed) outline and surrounded by a thin rim of augite. A euhedral augite phenocryst is juxtaposed to it. Furthermore, low-Al orthopyroxene phenocrysts or microphenocrysts are also rimmed by augite (Figure 16, and Reidel, 1978). Euhedral pyroxene phenocrysts are found in all sections, but more commonly pyroxene grains are subhedral to anhedral in these lavas. An extremely resorbed pyroxene (CHI-20) has an augitic composition throughout most of the crystal however some parts of the crystal have lower-Ca compositions and glassy spots (Figure 17). This could indicate that this augite was in the process of being resorbed by a new magma and that pigeonite was beginning to form, then the magma was erupted interrupting this process and quenching some partial melt areas into glass.

Low-Ca pyroxenes are represented primarily by pigeonite, which is ubiquitous throughout the GRB. It occurs both in the groundmass and as microphenocrysts. Pigeonite crystals are commonly anhedral; rarely are any euhedral grains found. Some pigeonite phenocrysts are rimmed by augite and some others are highly resorbed but lack the augite rims (Figure 17).
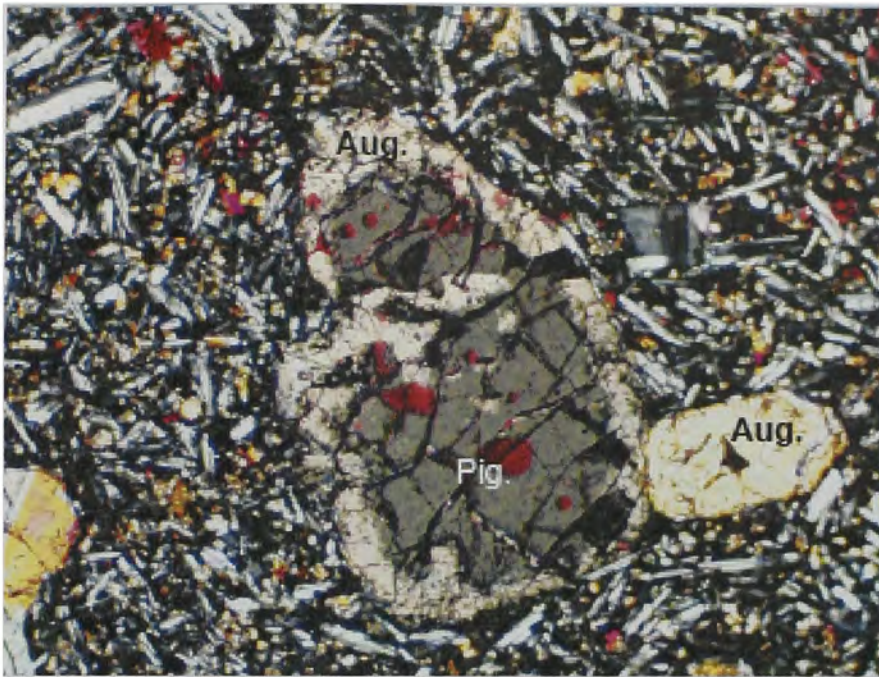
Figure 15- Augite-rimmed resorbed pigeonite (darker grain in the center of image) juxtaposed against a euhedral augite phenocryst (Sample CHI-24). (Crossed polars: Width of field of view represents 1.1 mm).
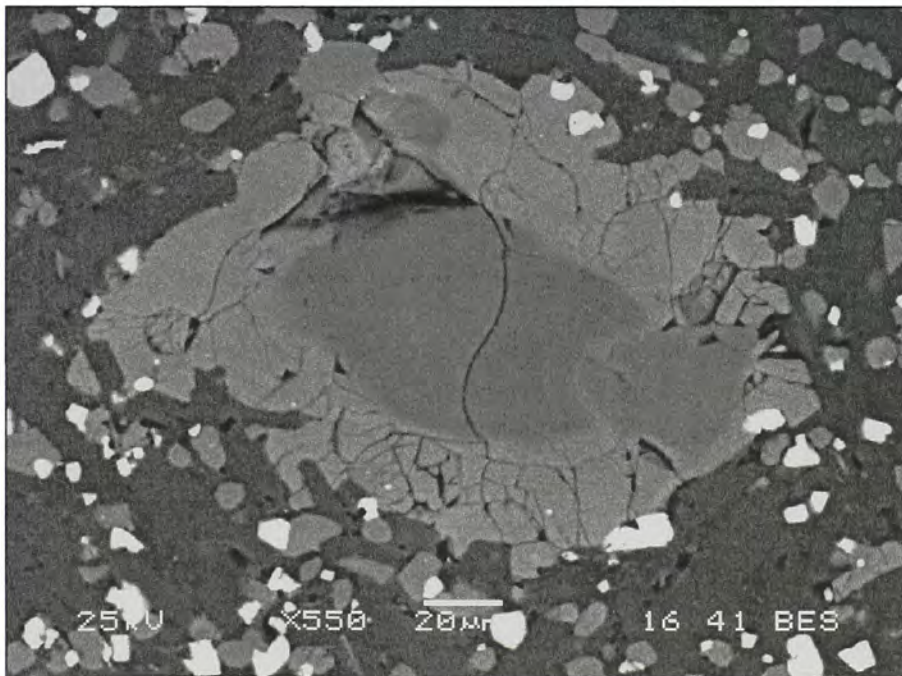
Figure 16-Back-scatter image of an orthopyroxene grain rimmed by augite, Dog 39, (sample provided by S.P. Reidel). Darker grains are plagioclase crystals and bright grains are Fe-Ti oxides.
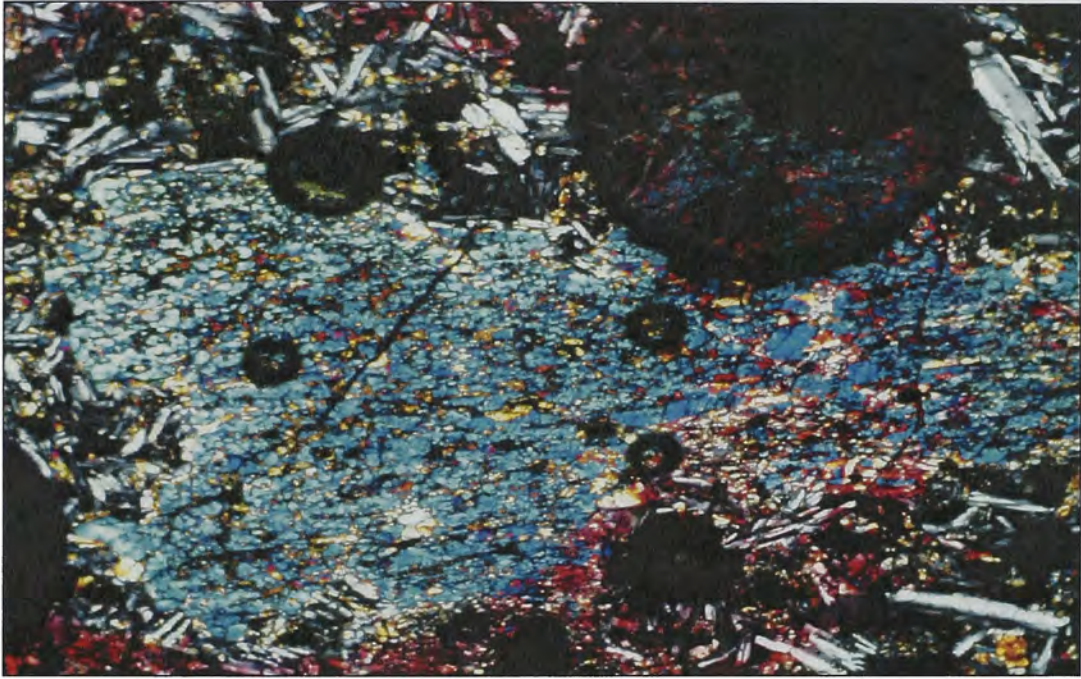
Figure 17- Crossed polar photomicrograph of a highly resorbed clinopyroxene phenocryst (CHI-20). (Width of field of view represents 2.5 mm).

Orthopyroxene is rare as a phenocryst phase as well as in the groundmass. Grande Ronde sample GRB-O4352 is the only sample that contains an opx phenocryst (0.45 mm) in the samples studied (Figure 10). This opx phenocryst appears to have been in the initial process of resorption, and has a thin glassy rim. A smaller resorbed subophitic augite phenocryst and a larger subhedral plagioclase phenocryst are adjacent to this grain. Reidel (1983) has also found opx in his samples. For example, an opx rimmed by pigeonite is found in sample number Dog 39 of Reidel (Figure 16). Sub-ophitic and ophitic textures are seen in the phenocryst clusters throughout the sections. Many pyroxenes, both pigeonite and augite, are not only resorbed along the rims but also within the cores. Many of the phenocrysts and microphenocrysts are found as glomeroporphyritic clusters with plagioclase phenocrysts.

In summary, some spectacular reaction textures are shown by the pyroxenes- opx rimmed by pigeonite, pigeonite rimmed by augite, and augite rimmed by pigeonite. In the middle and upper flows analyzed, patchy zoning is found within individual groundmass and microphenocrysts grains.

Olivine

Unaltered olivine phenocrysts are not present in any of the flows studied. The olivines are altered to iddingsite and can only be recognized by the euhedral olivine shape (Figure 18). These altered olivine crystals can be as large as 3 mm. Modal abundance of altered olivine (iddingsite) averages 1.03% with no more than 3.0% in any flow (Camp, 1976). Reidel (1978) found one partially altered olivine phenocryst in only one China Creek flow (CHI-27). This olivine has a Fo_{67} core and Fo_{47} rim (Reidel, 1978).
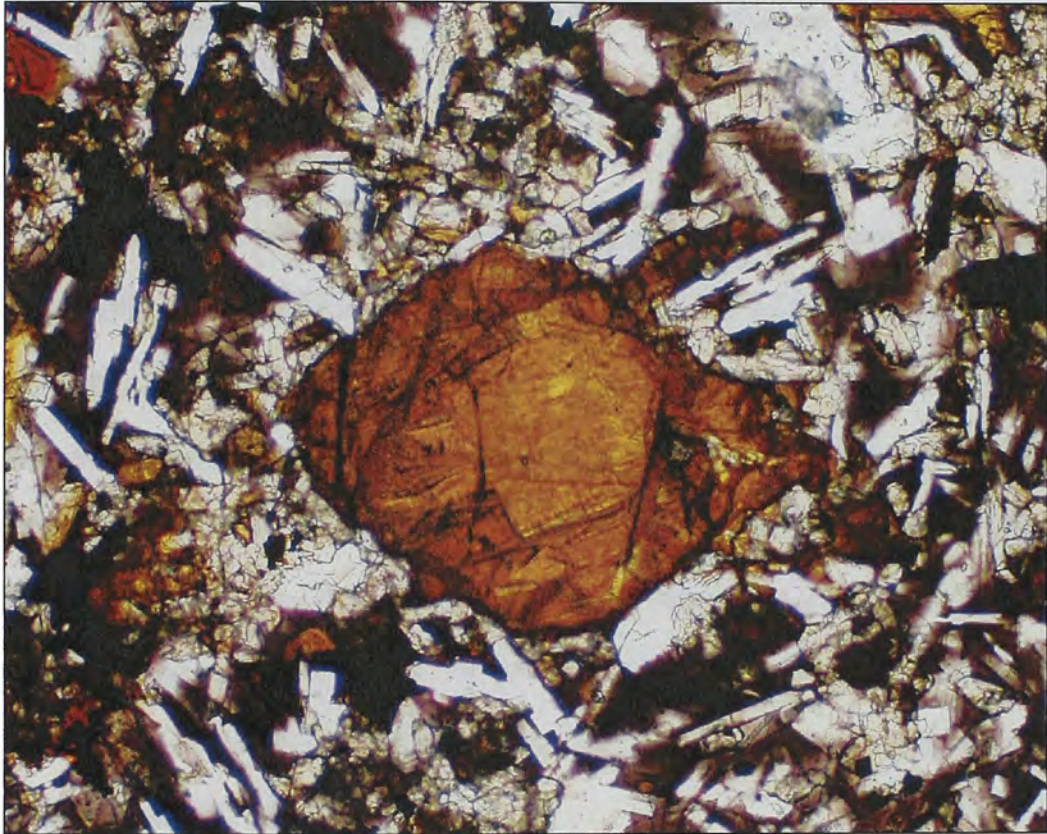
Figure 18-Crossed polar photomicrograph of Iddingsite, believed to be the alteration product of altered olivine phenocryst. Notice the distinct euhedral olivine shape of the crystal (Sample CHI-32). (Plane polarized light: Width of field of view represents 1.15 mm).

Olivine crystals are present as groundmass crystals of some samples, but whether these are really part of the groundmass or are extensively resorbed phenocrysts is not clear. Most groundmass crystals are anhedral to subhedral and are homogenous with no evidence of zoning. Mg numbers $[100*Mg/(Mg+Fe^{2+})]$ in groundmass crystals range from Fo_{21} to Fo_{60}. In addition, olivine (Fo_{60}) is observed as an inclusion in several groundmass pyroxene grains.

DIKE PETROGRAPHY

Samples were collected across the width of two dikes, one that fed the Imnaha Formation (Big Lookout Mountain dike) and another that fed the GRB Formation (Joseph Creek dike). The GRB dike shows features that suggest that at least two different magmas mingled and flowed through the same dike (Figure 19). There appear to be two or three magmas of different degree of darkness due to variation in glass content. Magma mingling can only be seen in the interior of the GRB dike and not along the rims of the dike, which suggests that the interior of the dike was open to distinct magma intrusion episodes. The Imnaha dike does not display these features and is significantly coarser grained than the GRB dike.

Joseph Creek dike (GRB Formation)

Samples collected across the width of the Joseph Creek dike captured only one of the chill margins (sample # W-1). The chilled margin is fine-grained to glassy with black and yellow-brown glass. The chill margin has both plagioclase (<5%) and clinopyroxene (<1%) microphenocrysts (<0.3 mm), but no phenocrysts (>0.3 mm). Several clusters of plagioclase and clinopyroxene microphenocrysts occur.

Morphologies range from euhedral to subhedral for plagioclase, and subhedral to anhedral for clinopyroxene grains. Anhedral unaltered olivine crystals (<1%) are seen only in the groundmass. Slight zoning is seen in a few plagioclase microphenocrysts.

Samples W-2 and W-3, which were collected farther in from the chilled margin, are both glass-rich. Petrographically, there appears to be two distinct magmas mingled in these samples: one of these has a darker glassy texture; the other has a lighter more coarse-grained texture (Figure 19). Both W-2 and W-3 have 5-10% modal plagioclase (up to 0.4 mm) and 1-5% modal clinopyroxene (up to 0.3 mm) phenocrysts and microphenocrysts. Plagioclase and cpx crystals are more resorbed in W-2 and W-3. Plagioclase and cpx phenocrysts and microphenocrysts range from euhedral to anhedral in these two samples.

Samples W-4, W-6 and W-7 are all glass-rich to fine-grained; sample W-7 has the highest glass content. The glass is black, and yellow-orange where altered. Textures and modal percent of phenocrysts and microphenocrysts in these samples are similar to W-2 and W-3. Sample W-5 is medium to coarse-grained comes from the center of the dike. The texture ranges from intergranular to intersertal. There are less than 1% plagioclase phenocrysts and 5-10% euhedral to subhedral microphenocrysts. Pyroxene is only present as microphenocrysts (<1%) and in the groundmass. The largest plagioclase phenocrysts are 0.5 mm in width. Largest cpx phenocrysts are 0.4 mm in width. Ti-magnetite and ilmenite are only present as groundmass crystals.

Big Lookout Mountain Dike (Imnaha Formation)

Unlike the majority of GRB dike and flow samples, the Imnaha Formation is coarse grained, with large plagioclase, olivine and clinopyroxene grains occurring in

most of the samples studied. Typically these phenocrysts have unzoned cores, but some larger plagioclase grains display oscillatory zoning. The matrix is typically intergranular, with some subophitic textures. Ti-magnetite and ilmenite are only present in the groundmass. Brown to yellow glass is seen in the mesostasis. Needles of apatite, alkali feldspar and microgranophyric textures are also found in minor amounts in the groundmass.

The Imnaha Formation has unaltered olivine grains, unlike the GRB Formation (Figure 20). These crystals are euhedral to subhedral. In some cases skeletal olivine is also found in the groundmass. These skeletal olivines generally have higher Mg number [Mg/(Mg+Fe*)] of ~71. Generally the olivine (1-2 mm) and plagioclase grains are larger than the pyroxene grains (~1 mm). Many of these olivine grains include melt and mineral (Fe-oxide) inclusions.

Subhedral to euhedral plagioclase grains in the Imnaha Formation dikes are often of considerable size (>3 cm in length). They are also modally more abundant than both olivine and pyroxene crystals. The plagioclase grains mark a clear distinction from the younger GRB formation. Zoning is not a common feature of these crystals although some oscillatory zoning is present in some of the smaller plagioclase grains. Reverse zoning is not detected in any of the grains analyzed. In some cases, plagioclase grains completely enclose olivine grains. Plagioclase grains also contain melt inclusions. The pyroxenes in all flows are augites. These augites are usually smaller with subhedral to anhedral grains. Some of the augite crystals contain small melt inclusions.
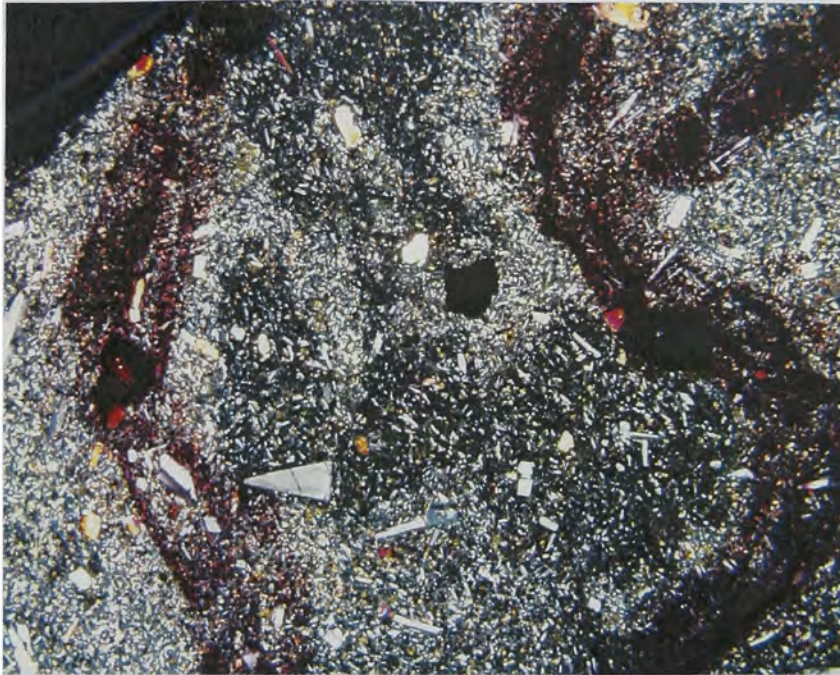
Figure 19-Crossed polars image of the GRB dike showing two magmas, lighter coarser grained and darker more glassy (W-2). (Width of field of view represents 5.2 mm).
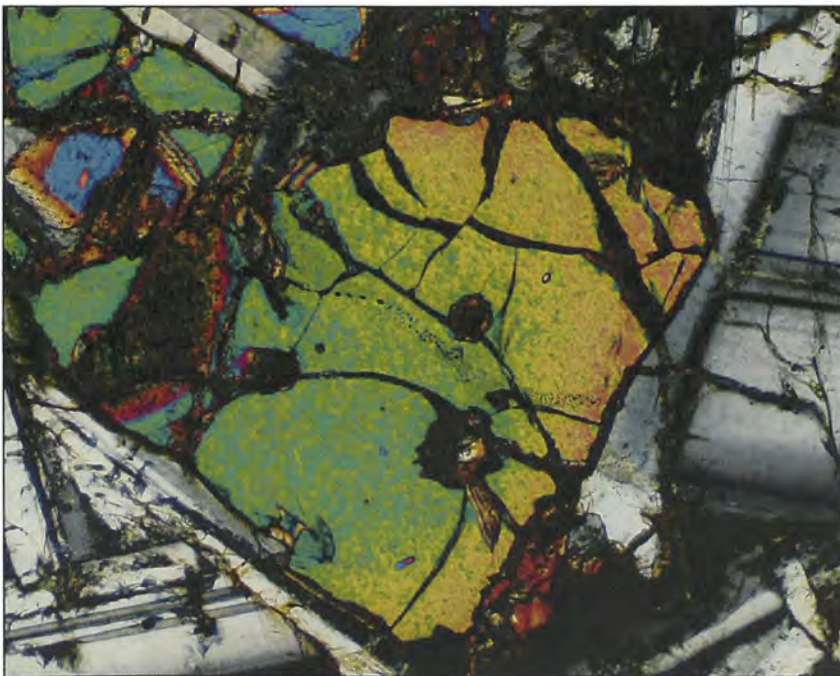
Figure 20- Photomicrograph of an olivine crystal in the Imnaha dike (BLM). Olivine has several small melt inclusions and is surrounded by plagioclase (gray) and pyroxene (blue). Crossed polarized light: Width of field of view represents 1.15 mm).

CHAPTER 3

GEOCHEMISTRY AND MINERAL CHEMISTRY

GRANDE RONDE FORMATION

Major Elements

Some general aspects of geochemistry that have been discussed by previous researchers are presented first as background material. Then, I present my mineral chemical data. Imnaha basalts are relatively rich in MgO (4.5-7.1 wt %) with intermediate SiO_2 values and low K_2O content relative to MgO (Hooper, 1984; Hooper and Hawkesworth, 1993). The Grande Ronde Formation on the other hand comprises basaltic andesites based on the higher SiO_2 concentrations in these rocks (Hooper and Hawkesworth, 1993). The GRB basaltic andesites generally have low MgO contents (3.0-5.5 wt %) with the highest SiO_2 (52-58 wt %) relative to MgO in the CRBG. The Wanapum Basalt has high TiO_2 and FeO contents and low SiO_2 when compared with GRB. Saddle Mountain Formation shows the greatest chemical dispersion among CRBG lavas with the lowest MgO (2.7 wt %) and highest MgO (8.2 wt %) values. The SMB lavas also have some of the highest total FeO (17.5 wt %) (Hooper and Hawkesworth, 1993). Whole rock Mg numbers $[(100*Mg/(Mg+Fe^{2+})]$ of GRB lavas range from 30 to 64, and SiO_2 values range from 52-58. TiO_2 values range from 0.7 to 3.6 wt. % (Erlank et al., 1988).

Trace Elements

All CRBG lavas are enriched in light-REE and are similar to ocean island basalts (Hooper and Hawkesworth, 1993; figure 21). Many flows have relatively high large ion lithophile elements (LILE)/high field strength elements (HFSE) ratios (Ba/Nb = 10-80).
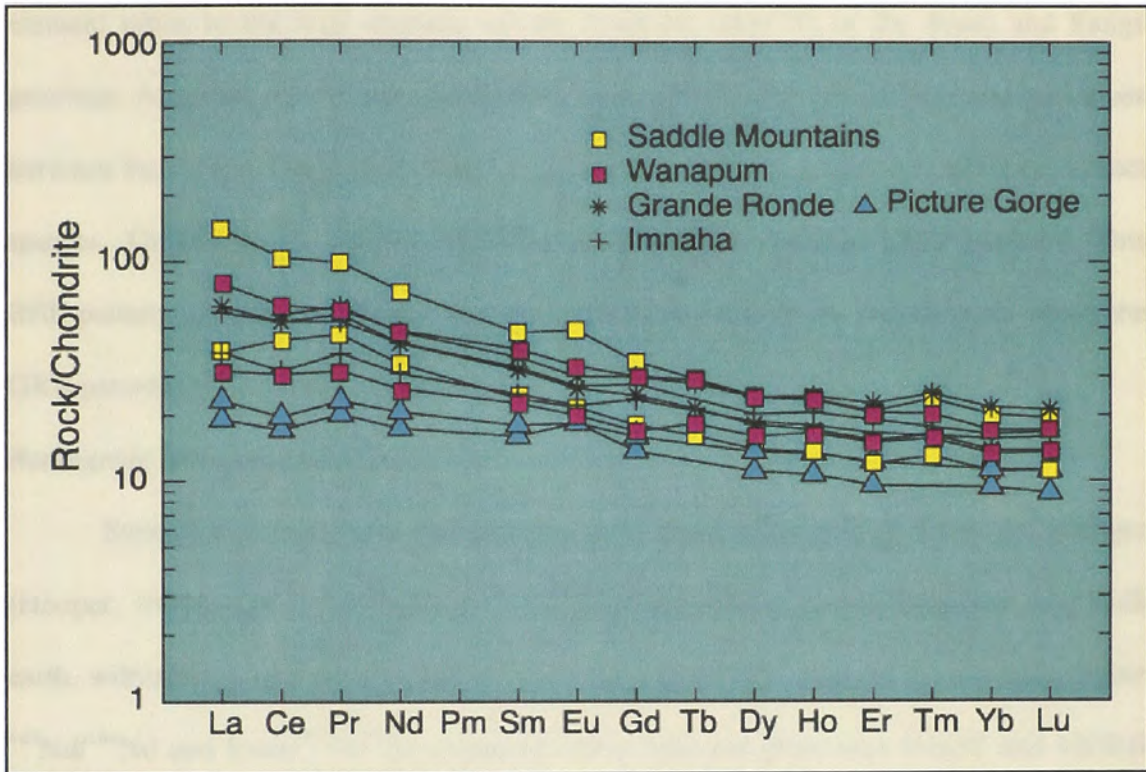
Figure 21-Chondrite-normalized rare earth element patterns of some typical CRBG samples. Winter (2001). An Introduction to Igneous and Metamorphic Petrology. Prentice Hall. Data from Hooper and Hawkesworth (1993) *J. Petrol.*, 34, 1203-1246.

High LILE/HFSE ratios are commonly attributed to the preferential mobilization of LILE in hydrous fluids derived from the subducted slab (Pearce, 1983; Hawkesworth et al., 1991). The Picture Gorge Basalt, which is coeval with the Grande Ronde Basalt, erupted from a different set of fissures, namely the Monument dike swarm, and has similar trace element ratios to the high alumina olivine tholeiites (HAOT) of the Basin and Range province. According to Hooper and Hawkesworth (1993), the lack of intermediate values between the Picture Gorge and CRBG suggests that these were derived from two distinct sources. Grande Ronde lavas exhibit a flat MREE-HREE enriched LREE patterns. This REE pattern suggests that garnet was not a residual phase in the mantle with which the GRB parental magmas last equilibrated

Radiogenic Isotope Compositions

Strontium isotope ratios become generally more radiogenic as flows get younger (Hooper, 1984). On ^{143}Nd/^{144}Nd vs. ^{87}Sr/^{86}Sr plots, Grande Ronde lavas plot near bulk earth, within the ocean island basalt (OIB) field (Figure 22). Imnaha basalts have higher ^{143}Nd/^{144}Nd and lower ^{87}Sr/^{86}Sr values (0.703-0.704) and plots near HAOT and MORB fields, but still within the OIB field (McDougall, 1976; Hooper and Hawkesworth, 1993). Wanapum basalts also plot near bulk earth, but with lower ^{143}Nd/^{144}Nd values than Grande Ronde basalts. Average Grande Ronde and Wanapum ^{87}Sr/^{86}Sr values are approximately 0.705 (McDougall, 1976). Saddle Mountain basalts, the youngest formation, are very different from the rest of the group: these lavas are highly enriched and ^{87}Sr/^{86}Sr ratios have a large range from approximately 0.708 to 0.715 (De Paolo and Wasserburg, 1979; Nelson, 1980; BVTP, 1981; Carlson, et al., 1981; Hooper and Hawkesworth, 1993) (See figure 22).
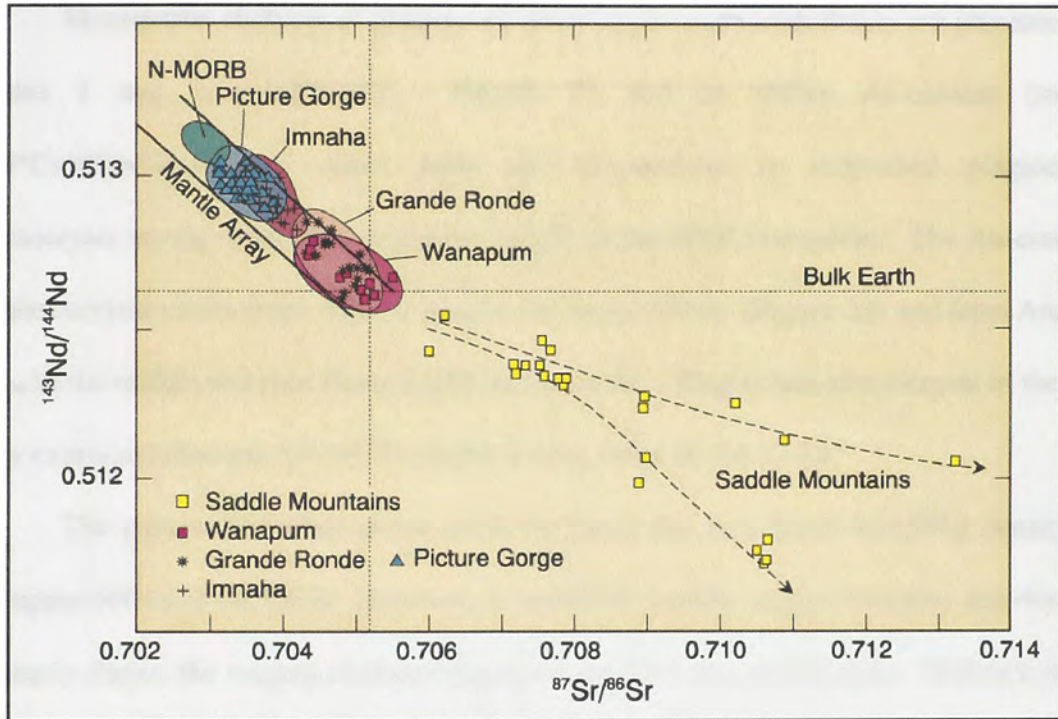
Figure 22- 87Sr/86Sr vs. 143Nd/144Nd for the CRBG. Winter (2001). An Introduction to Igneous and Metamorphic Petrology. Prentice Hall.

Helium and neon isotope analysis of Imnaha basalt fluid inclusions have yielded $^3He/^4He$ ratios of 11.4 times atmosphere, and $^{20}Ne/^{22}Ne$, and $^{21}Ne/^{22}Ne$ characteristic of a plume component (Dodson et al., 1997).

PHASE CHEMISTRY

Plagioclase

Microprobe analyses of plagioclase phenocrysts and Groundmass are presented in Tables 1 and 3, respectively. Figures 23 and 24 shows An-content (molar $100*Ca/(Ca+Na+K)$) of cores, rims and groundmass in individual plagioclase phenocrysts versus relative stratigraphic height of the GRB Formation. The An-content of phenocrysts varies from An_{59} to An_{96} in the lower 250 m (Figure 23) and from An_{65} to An_{79} in the middle to upper flows (>250 m; figure 24). Plagioclase phenocrysts in the top flow examined (Sample SB-2978) exhibit a wide range of An 37-74.

The pattern described above could be partly due to a lesser sampling density in the upper 600 m of the GRB. However, it could also signify magma chamber activity. In the early stages, the magma chamber may not have been in a steady state. Different input melts carrying phenocrysts incompletely mixed in the chamber and then erupted as lavas with highly variable phenocrysts. With time, as the chamber reached a steady state, phenocrysts formed in well mixed magmas. The top flow shows a larger An range, which includes the lowest An compositions in the phenocrysts. A straightforward interpretation is that this lava was formed as the last liquid that was squeezed out of GRB magma chamber, carrying with it crystals that not only formed from the most differentiated melts, but also from more primitive crystals that probably formed from earlier magma batches.
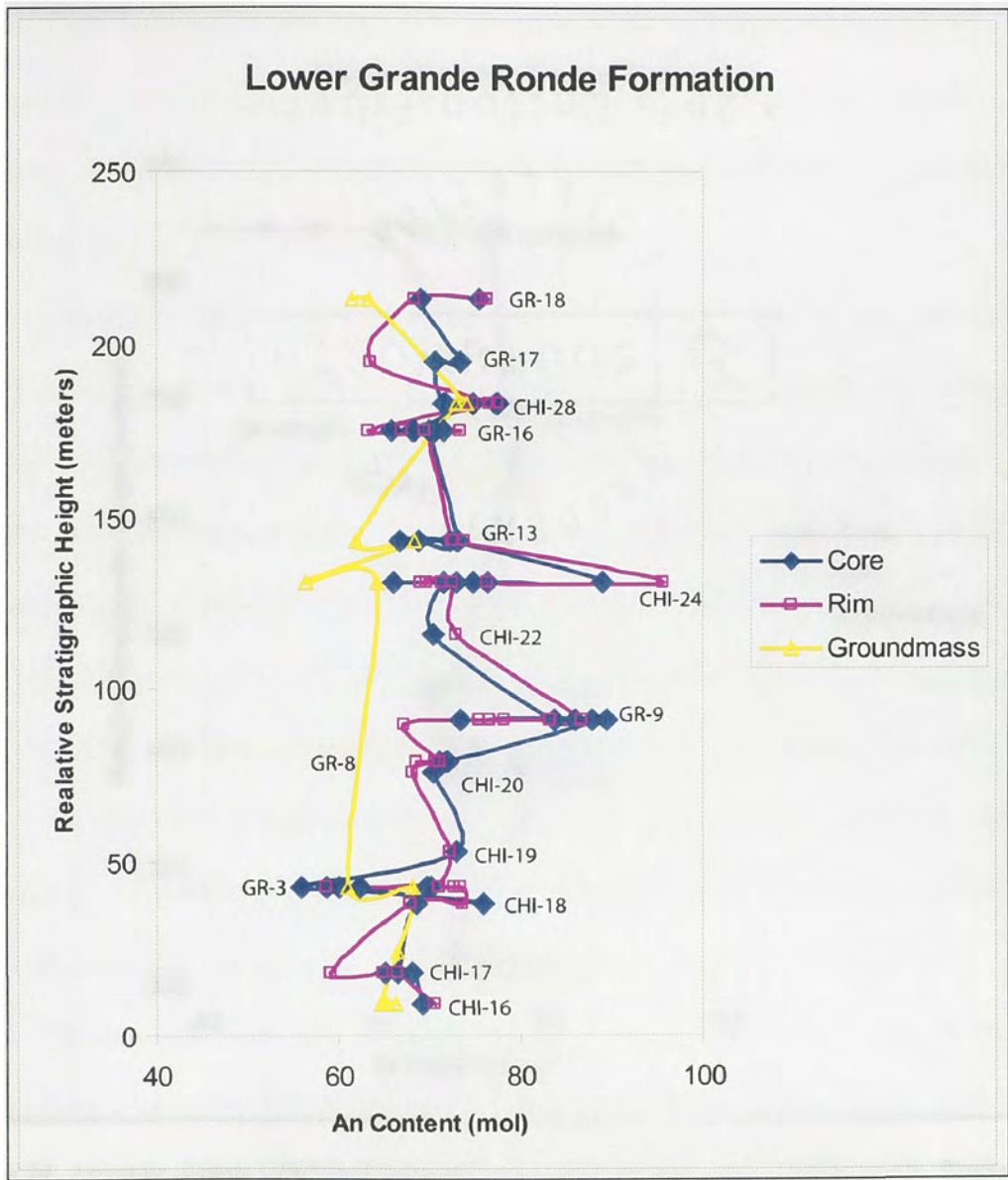
Figure 23- Anorthite content (100*Ca/(Ca+Na+K)) of older sections of the Grande Ronde. Plagioclase phenocrysts are plotted against relative stratigraphic height depicting core, rim, and groundmass compositions for the samples analyzed by electron microscopy in this study.

45
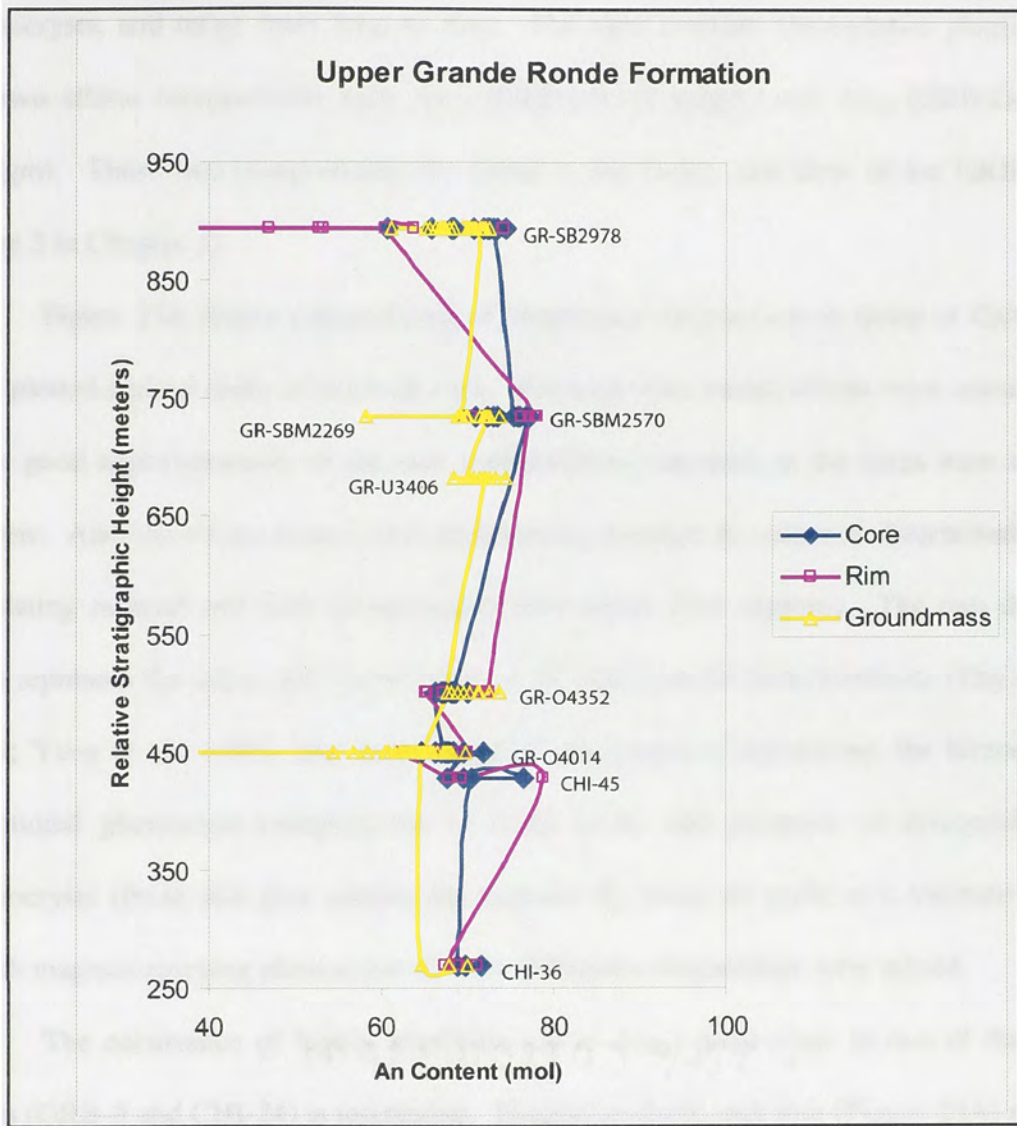
Figure 24- Anorthite content (100*Ca/(Ca+Na+K)) of younger sections of the Grande Ronde. Plagioclase phenocrysts are plotted against relative stratigraphic height depicting core, rim, and groundmass compositions for the samples analyzed by electron microscopy in this study.

Groundmass plagioclase compositions are also plotted in figure 23, which shows that the groundmass crystals generally have lower An contents than the phenocrysts. Groundmass plagioclases do not have the large compositional range shown by the phenocrysts, and range from An_{56} to An_{74}. The most extreme Groundmass plagioclase are two albitic compositions with An_{17} (GRB-O4352-1plgm) and An_{24} (GRB-O4352-12plgm). These two compositions are found in the Ortley unit flow of the GRB (See figure 2 in Chapter 1).

Figure 25A shows compositions of plagioclase phenocrysts in terms of Ca/(Ca + Na), plotted against those of the bulk rock. The bulk-rock compositions were considered to be good approximations of the melt compositions inasmuch as the lavas were nearly aphyric. Also shown are dashed lines representing constant K_d values as determined from coexisting mineral and melt compositions (See figure 25A caption). The two dashed lines represent the upper and lower limits of all experimental determinations (Thy et al., 1999; Yang et al., 1996). The large range of phenocryst compositions, the bimodal to polymodal phenocryst compositions in some lavas, and presence of disequilibrium phenocrysts (those that plot outside the constant K_d lines) all point to a mechanism in which magmas carrying phenocrysts of very different compositions were mixed.

The occurrence of highly anorthitic (up to An_{96}) plagioclase in two of the lava flows (GRB-9 and CHI-24) is interesting. Plagioclase/bulk rock plot (Figure 25A) shows that phenocrysts were clearly out of equilibrium with their host lava. This is also supported by the highly resorbed texture (Figure 26).

A.
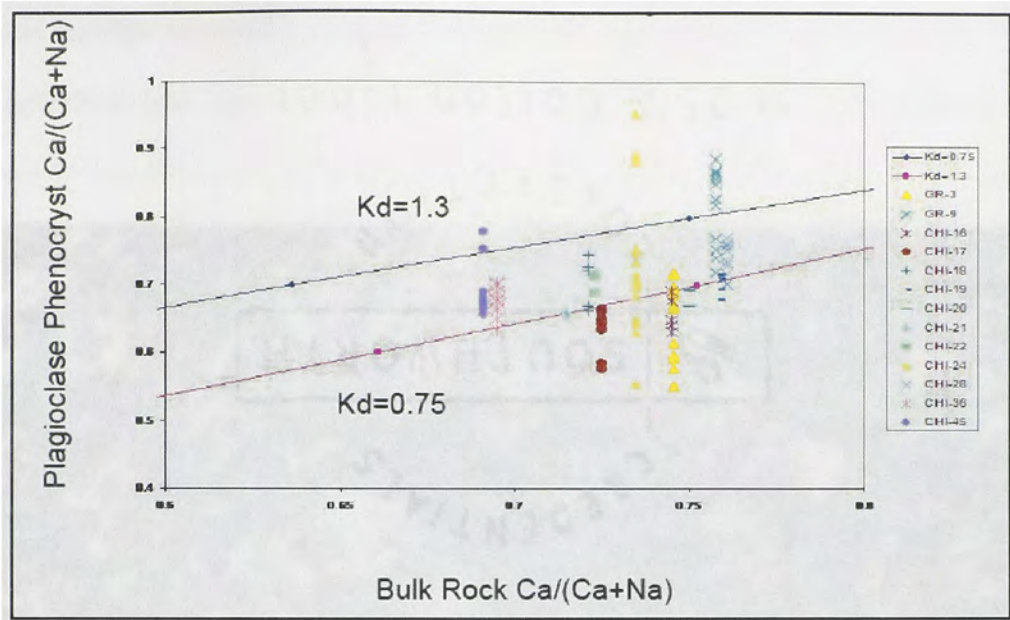
B.
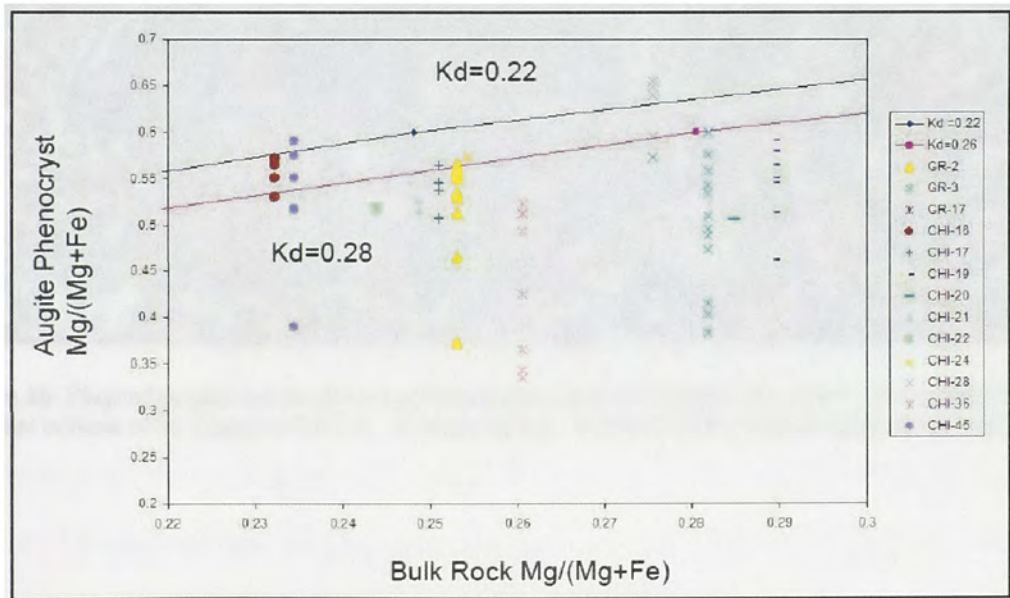
Figure 25- A and B: Anorthite (An) content [= molar Ca/(Ca + Na)] of plagioclase plotted against that of whole rock (= melt). Dashed lines—two constant values of K_d (= $[X_{Ca}^{pl}][X_{Na}^{melt}])/([X_{Ca}^{melt}][X_{Na}^{pl}])$ representing extremes of experimentally constrained values (Thy et al., 1999).

Figure 26- Plagioclase phenocryst showing extreme resorption throughout the crystal. This crystal has an anorthite content of 96 (Sample CHI-24). (Crossed polars: Width of field of view represents 2.5 mm).

Phase-equilibrium experiments on hydrous mafic to intermediate-composition basaltic systems and the common occurrence of highly anorthitic plagioclase in high-Al basalts and andesites from convergent plate boundaries indicate that such high-An plagioclase commonly crystallizes from H_2O-rich basaltic magma (see discussion and references in Sen, 2001).

This finding lends some support to Lange's (2002) contention that GRB magmas were extremely hydrous. The rarity of the highly anorthitic plagioclase phenocrysts may indicate that only a few formed from hydrous parent melts prior to any degassing, whereas most plagioclase phenocrysts formed at shallow crustal depths after their parent magmas had mostly degassed. Alternatively, only a few input melts may have been hydrous, while the bulk, were relatively anhydrous.

Pyroxene

Mg numbers [$100*Mg/(Mg+Fe^{2+})$] for pyroxene phenocrysts range from 36 to 79, with the mean at 65. The lower sections (GR and China Creek type sections) have Mg #'s ranging from 48 to 79, middle sections (Umtanum, Ortley) have Mg#'s ranging from 36 to 71, and upper sections (Sentinel Bluffs) range from 48 to 76. Mg numbers for Groundmass pyroxene range from 34 to 76, with an average value of 62. Groundmass pyroxene in the lower sections (GR and China Creek type sections) have Mg #'s ranging from 41-73 while middle sections (Umtanum, Ortley) have Mg#'s ranging from 34 to 73 and upper sections (Sentinel Bluffs) range from 45 to 76. There does not appear to be a consistent trend in the Mg#'s in either the Groundmass or in the phenocrysts.

Figure 25B shows compositions of augite phenocrysts in terms of $Mg/(Mg + Fe*)$ plotted against those of the bulk rock. Also shown are constant K_d (dashed) lines defined

by experimentally determined coexisting mineral and melt compositions (See figure 25 caption). The two dashed lines represent the upper and lower limits of all experimental determinations (Thy et al., 1999; Yang et al., 1996). This figure, like figure 25A, shows a large range of phenocryst compositions, many of which are clearly out of equilibrium.

This provides further evidence for a mechanism in which magmas carrying phenocrysts of very different compositions were well mixed. Resorption features and the presence of normally and reversely zoned phenocrysts in individual samples point to preeruption magma mixing as an important mechanism that controlled the erupted lava compositions (cf. Kuo and Kirkpatrick, 1982; Sen, 1983; Durand and Sen, 2004).

Figure 27 shows augite and pigeonite phenocryst compositions in a pyroxene quadrilateral, which also includes some experimentally determined isotherms for pyroxenes that crystallize from tholeiitic basalt magmas at 1 atm pressure (Lindsley, 1983). This diagram indicates that the pyroxene phenocrysts formed between 1200° and 1000 °C. Schiffman and Lofgren (1982) performed 1-atm melting experiments on pillow basalts from the GRB. They were able to duplicate the pillow basalt textures in most cases indicating that indeed the basalts evolved in a low pressure environment. Pillow outer rim textures were duplicated in runs cooled from 1125 °C at very fast cooling rates (>2100 °C/hr), inner rim textures were duplicated in runs cooled at rates between 450° and 84°C/hr and the pillow interiors were duplicated in experiments at cooling rates between 42° and 10°/hr (Schiffman and Lofgren, 1982). Cooling rates less than 10°C/hr were not found in any of the runs for the pillow basalts. The colonnade basalt that overlies the pillow basalts, however, exhibits a texture analogous to those produced in an experiment cooled at 1°C/hr (Schiffman and Lofgren, 1982).
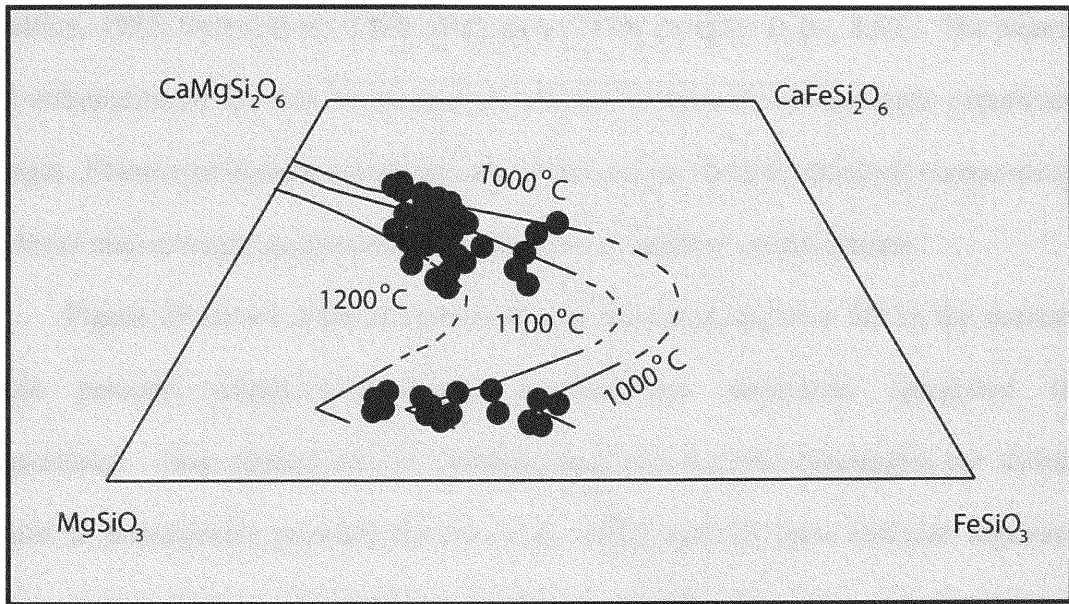
Figure 27- Pyroxene quadrilateral showing 1 atm isotherms (Lindsley, 1983) and compositions of augite and pigeonite phenocrysts in Grande Ronde lavas. The temperature of crystallization was between 1200 – 1000°C.

DISCUSSION

Evidence for Low-Pressure Equilibration

Plagioclase, pigeonite, augite, olivine (altered), and a few orthopyroxene phenocrysts are typical crystallization assemblages in experimental crystallization studies of tholeiitic basalts at 1 atm pressure (cf. Basaltic Volcanism Study Project, 1981; Lindsley, 1983; Grove et al., 1989; Thy et al., 1999; Latypov et al., 2001). The pigeonite and orthopyroxene are low in Al, and are similar to those in low-pressure experimental charges. Phase-equilibrium considerations of the major element chemical composition of the lavas also strongly suggest their equilibration at shallow crustal depths.

Figure 28 shows plots of Grande Ronde lava analyses ($n = 50$) in the normative (mole percent) augite-olivine-quartz pseudoternary projection (projected from plagioclase). Also plotted are (1) multiply saturated liquidus boundaries for tholeiitic basalts at atmospheric pressure (Grove et al., 1982) and (2) glass analyses reported in high-pressure melting experiments on Grande Ronde Formation starting materials (Takahashi et al., 1998). Grande Ronde lavas form a tight cluster close to the atmospheric-pressure liquidus boundary, suggesting that the erupted lavas last equilibrated at or near atmospheric conditions. The linear cluster of Grande Ronde lavas can be explained by magma mixing (mixing line from A to B is shown in Figure 28) between a less differentiated liquid, such as B (with olivine, augite, and plagioclase phenocrysts), and a more evolved melt saturated with pigeonite (± orthopyroxene, plagioclase and augite). Note that such magma mixing would force pigeonite crystals to become unstable and, therefore, react with the mixed melt, which is consistent with the
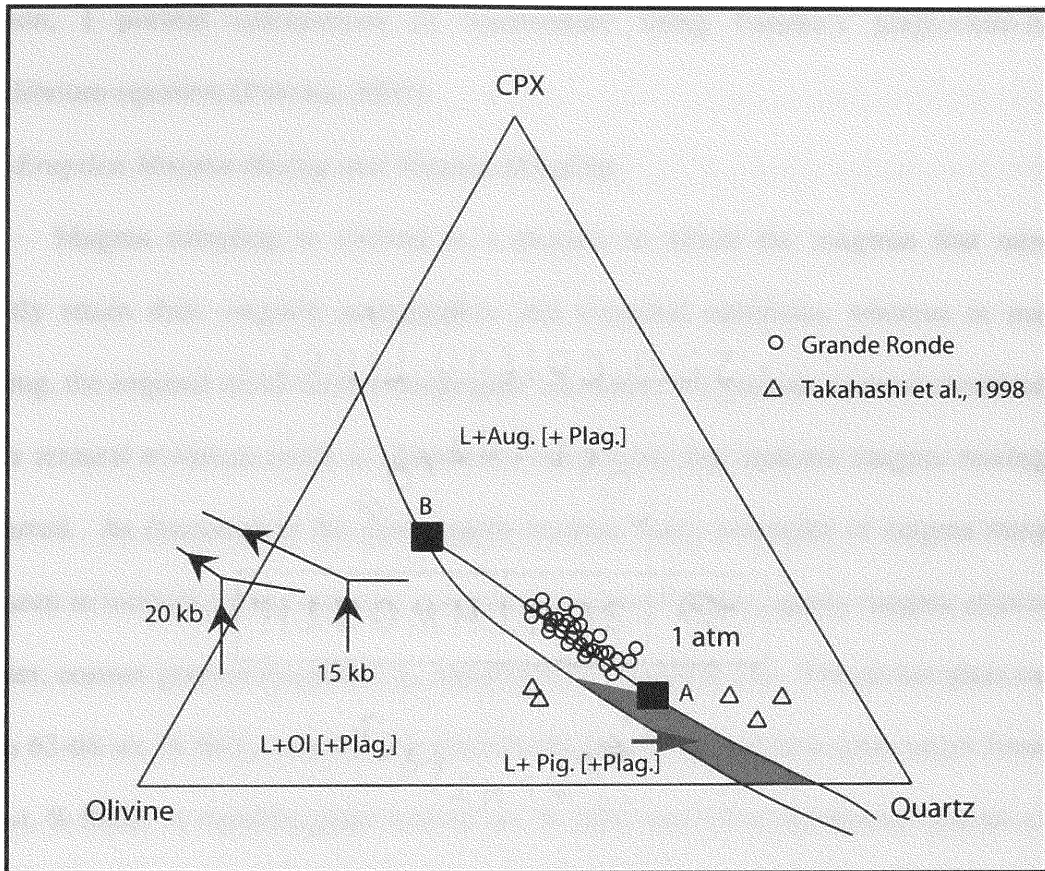
Figure 28- Liquidus (L) phase diagram (mol%, projected from plagioclase) for tholeiitic basalts at atmospheric pressure (Grove et al., 1982). Circles-Grande Ronde lavas. Triangles-experimentally produced partial melts from eclogite at high-pressure (Takahashi et al., 1998). Thick line-a hypothetical mixing line between two end-member melts, B and A. I contend that the linear cluster of Grande Ronde Formation lavas is due to low-pressure mixing between a less evolved melt (such as B) and a highly evolved, pigeonite-saturated melt (A).

petrography of these rocks (resorbed pigeonite: discussed earlier). Augite would be stable in the mixed melt and would therefore nucleate on the resorbed pigeonite phenocrysts (and orthopyroxene, if present), forming a rim around them. In a later section, I present calculations of temperature using Putirka's plagioclase-liquid equilibrium equation (Putirka, 2005).

Pre-Eruption Magma Mixing and Magma Mingling

Magma mingling is viewed as a process in which the magmas that mingled mostly retain their original petrographic and chemical identities, whereas in magma mixing, the original melts loose petrographic identities, but provide mineral chemical and other textural evidence (such as phenocryst resorption) that indicate magma mixing has occurred. As discussed in the petrography section, many examples of magma mingling are seen in individual thin sections, comprising veins of darker, glassy magma adjacent to lighter, coarser grained magma (e.g., samples CHI-38, GRB-16). The darker glass ranges from 63-68 wt. % SiO_2, whereas the glass in the lighter, crystal rich area ranges from 58-63 wt. % SiO_2. A rhyolitic glass with 82 wt. % SiO_2 was found juxtaposed against a dark glass with 63 wt. % SiO_2. Anorthite content of plagioclase in the lighter areas is 68-70, while in the darker areas, it is 65-66. In, GRB dike and GRB flows, the lighter colored area is coarser grained than the darker, glassier and fine grained area it interacts with (see Figures 8 and 19). The plagioclase compositions associated with lighter glass is An68-70, whereas it is An65-66 in the dark glass.

Reverse zoned and resorbed plagioclase phenocrysts, resorbed pigeonite phenocrysts, and euhedral augite rims on resorbed pigeonite and low-Al opx cores in some lavas all point to an extensive melt mixing process that forced such disequilibrium

textures. The augite rims on the resorbed pigeonite would point to a reaction relationship such as L+Pig → Aug; however, such a reaction does not occur in experimental phase equilibrium studies of tholeiitic basalts (BVTP, 1981). On the other hand, such a texture is easily explained by magma mixing between a less differentiated magma (melt B in Figures 28 and 29) carrying pigeonite phenocrysts and another magma (melt A) carrying augite (+olivine and plagioclase) phenocrysts. Such mixing would lead to a new magma whose composition would fall inside the augite liquidus field, forcing the pigeonite crystals to be out of equilibrium with the new magma. In such a scenario, pigeonite crystals would start to dissolve while augite would nucleate. In sample CHI-24 from GRB (Figure 15), the growth of the augite rim on the dissolving pigeonite reached a point where the pigeonite crystal became isolated from the melt (rimmed by augite) and could no longer dissolve. In contrast, the spongy pyroxene in sample CHI-20 (Figure 17) kept dissolving because the mixed melt may have been superheated so that it did not reach augite saturation. Reverse zoning and resorption of plagioclase (see figures 11-13 and 26) also point to a rise in temperature during the mixing process. This could have dissolved some of the phenocrysts making the lavas aphyric to near-aphyric.
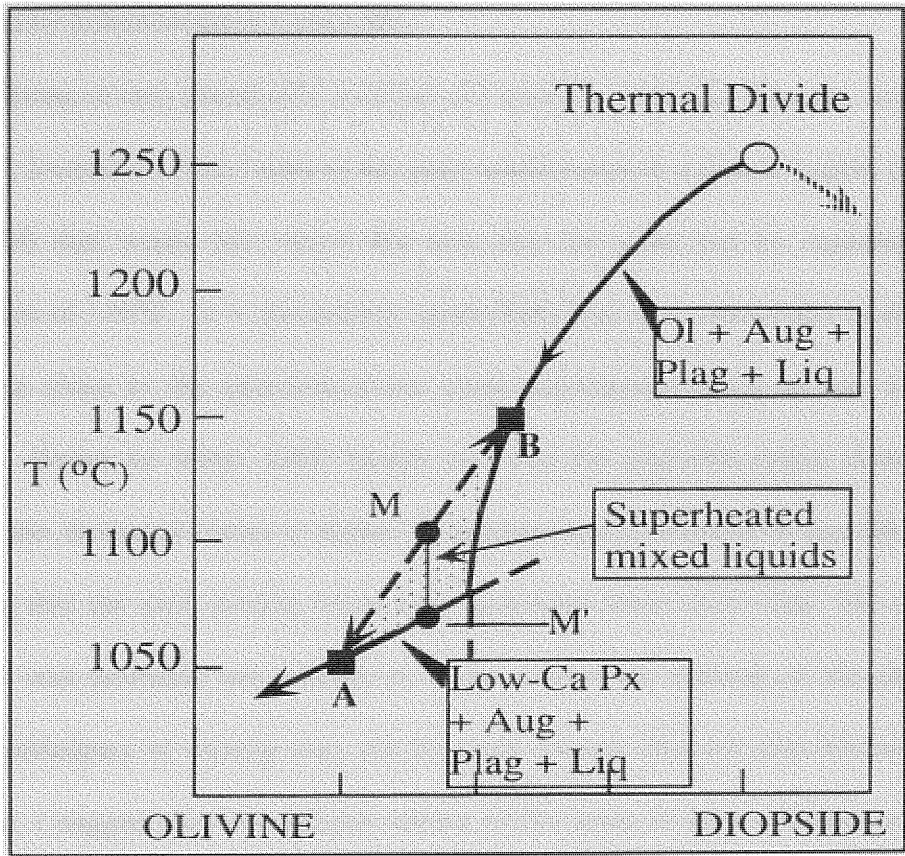
Figure 29- This diagram is projected from plagioclase onto the join formed by olivine-diopside boundary (from Walker et al., 1979). Gray curves represent liquidus surfaces. When melts A and B are mixed to produce a new melt, M, it is going to lie above its corresponding liquidus temperature (i.e., it will be superheated), which is at M. This diagram implies that mixed melts are going to be slightly superheated. Ol—olivine; aug—augite; plag—plagioclase; liq—liquid; px—pyroxene.

Walker et al. (1979) experimentally examined how melt mixing within similar compositional range can generate extra heat. Of particular relevance is the low temperature 'cusp' that occurs on the liquidus where the curves *Ca-poor px+pl+aug+liq* and *ol+aug+plag+liq* meet in the system *pl-ol-aug-silica* (Figs. 28 and 29). Such a cusp is required by Schreinemaker's principle.

Mixing of two chemically evolved and multiply saturated magmas, say A and B in Fig. 29, located on either sides of the cusp would result in a mixed magma (magma M in Fig. 29) that would plot above the area near the cusp and be superheated by a temperature of ~50°C. It is particularly noteworthy that M is chemically quite evolved, as it plots close to the pseudoinvariant point aug+pig+pl+ol+liq at one atmosphere pressure. Based on where GRB basalts plot and the pigeonite-augite disequilibrium textures, the mixing scenario in figure 29 appears highly relevant to the GRB basalts, indicating that the melt mixing could have generated some extra heat. The amount of superheat was probably not enough to cause wholescale melting of the phenocrysts because enthalpies of mixing may not be large enough [Russell and Nicholls, 1990]. Therefore, I suggest the near-aphyric nature of the lavas to very efficient near-surface fractional crystallization process that removed the bulk of the crystals from the magma by a mechanism such as solidus front crystallization in shallow magma chambers (Marsh, 1989, 1996; discussed in Durand and Sen, 2004).

Phenocryst Residence Times in GRB Magma Chambers

I used a simple approach to calculate the residence time of a GRB phenocryst in a magma chamber. Crystal growth time-[(t) =L (length of the phenocryst)/G (growth rate)]. The largest phenocryst found in my samples is 1.2 mm (length). Using growth

rate of 10^{-10} cm/s (Marsh, 1996), I obtain 3.8 years for residence time. This result is very similar to that of Ramos et al. (2005) who used diffusion relations of $^{87}Sr/^{86}Sr$ across plagioclase zone boundaries to determine phenocryst residence times. This result indicates that GRB phenocrysts had extremely short residence times. This implies that the GRB magma chamber was partially flushed out every 4 to 5 years.

More on Shallow Fractionation and Mixing

The volatile contents of magmas are controlled by the laws of phase equilibria, which do not permit a high percentage of dissolved water in basaltic melts within the shallow crust (Lange, 2002). If all parent magmas of the Grande Ronde Formation contained high amounts of H_2O and were therefore essentially crystal free at depth (as proposed by Lange, 2002), these would have lost dissolved volatiles by degassing during extensive shallow-level magma mixing and fractionation. Shallow degassing would in turn result in rapid crystallization along the walls of the shallow conduits (perhaps a network of dikes and sills: Marsh, 1989, 1996). The efficient removal of phenocrysts could have been accomplished by *punctuated differentiation* (Marsh, 1989, 1996). In punctuated differentiation, magma which formed at higher pressures is emplaced in a shallow chamber already phenocrysts. Inward-propagating solidification fronts within the shallow chamber captures many phenocrysts along the margins, and a largely molten zone forms in the center of the chamber. Successive batches of melt equilibrated at higher pressure, and then emplaced in this chamber would mix with the resident melt, while breaking off phenocrysts from the partly solidified zones. The magma replenishment would create volume instability within the chamber and would force some of the nearly

crystal-free mixed melts to be erupted via dike-like conduits (Marsh, 1989, 1996). It is suggested that this flushing out of melt happened on a frequency of 4-5 year time scales.

Lava Flow Cooling Rates and Speed

Cooling rates of CRBG lavas have been the subject of much discussion. In order to explain the presence of long lava flows in the CRBG, Shaw and Swanson (1970) have proposed that flows were erupted at high eruption rates (>1 km^3/day/km). Model calculations performed by Shaw and Swanson (1970) indicate that flows traveled 5-15 km per hour, or faster, and advanced as sheet floods. Furthermore, calculations of viscosity based on the chemical composition showed that the viscosity of the flows was not unusually low and that the viscosity of the CRBG lava flows (500 poise) was only slightly greater than that of modern Kilauea lava. According to Shaw and Swanson (1970), the high rate of eruption combined with the huge volume of available magma enabled the flows to travel so far. Also, Shaw and Swanson (1970) suggest that the textural and compositionally homogeneous nature of the lavas can be explained by turbulent flow conditions which would mix and homogenize the flows constantly as these traveled. Evidence for rapid rates of eruption include the presence of sideromelane in water quenched rims of pillows in areas that are far away from the vents that these were erupted from (Swanson et al., 1979). In addition, glass in these flows contains less than 5% crystals, and many crystals have branching, skeletal shapes typical of rapid quenching events (Lofgren, 1982). Ho and Cashman (1997) also find that in the 500 km long Ginkgo flow (Wanapum Formation) temperatures do not change significantly over the extent of the flow. The temperature change is only about 15-20 °C over the entire length. Shaw and Swanson propose that for a 1000 km^3 flow, emplacement took place in days to

weeks. They contend that the CRBG eruption rates are very similar to historical Kilauea which has average eruption rates of 10^{-3} to 10^{-4} km^3/day/km (Shaw and Swanson, 1970; Swanson et al., 1975).

On the other hand, Self et al. (1997) suggest that emplacement took place over months to years. They propose that for the lava to flow long distances, tube-like emplacement and emplacement by lava inflation is necessary. Lava tubes form when the surface of a lava flow cools and solidifies, while the still-molten interior flows through and drains away, forming a tunnel. This mechanism insulates lava from the surface, as a result the hotter lava can travel longer distances without significant cooling. Similarly, in lava inflation, the solid upper crust is uplifted above a still molten lava interior. As more lava is injected into the interior of the flow, the rigid outer crust inflates. Multiple lava injections cause the lava flow to increase in thickness. Initial thicknesses can range from 20-30 cm and can increase up to 5 m or more (Hon et al., 1994). Tube-like emplacement (lava tubes) and lava inflation mechanisms are typically observed in the pahoehoe lava flows of Hawaii. Lava tubes have not been observed in CRBG flows; however, Reidel (2005), reports that the Cohassett Flow (Sentinel Bluffs Member) of the GRB shows evidence of inflated lava flows.

The average magma supply rate for the CRBG was 0.1 cubic kilometer per year (Swanson, 1972), which is identical to those calculated for present day Mauna Loa and Kilauea volcanoes (Jackson et al., 1972). Jackson et al. (1972) assert that this is the approximate modern rate of magma production in a melting spot that is approximately 7 x 10^4 km^2 in area. Utilizing similar parameters, Jackson et al. (1972) calculated that the melting regime beneath the CRBG plateau would be approximately 2 x 10^5 km^2.

Some workers however believe that the maximum rate of supply, in late Grande Ronde time, was 2-3 times that at Kilauea based on revisions of the geomagnetic time scale (Baksi, 1989).

A large number of lava flows appear to have traveled up to 500 km without ample crystallization or a significant decrease in temperature (Shaw and Swanson, 1970; Ho and Cashman, 1997). Ho and Cashman (1997) found that flows quenched to glass when they entered water even after traveling for hundreds of kilometers and that the crystal content of the glass was not much higher than that found in the chilled margins of the feeder dikes (11% at the vent to ~16% at the end of the flow). These findings provide evidence for very little cooling of the long lava flow of the CRBG. Several scenarios have been proposed to explain this finding; for example, the lava flows could have been superheated and therefore the flows did not cool enough to form a significant number of crystals (Ho and Cashman, 1997; Durand and Sen, 2004), or the lava flows were insulated by a crust thick enough to prevent the internal lava from cooling (inflated flows) and allowing it to flow a long distance, as has been observed in Hawaiian lava flows (Shaw and Swanson, 1970).

Measured crystallinities and phase compositions of natural and experimental samples from one of the long CRBG flows (the Gingko flow) tightly constrain the minimum temperature of this particular flow to 1085 °C ± 5 °C (Ho and Cashman, 1997). Ho and Cashman concluded that the maximum temperature change throughout the 500 km length of the flow was only 20 °C, which implies cooling rates between 0.02 to 0.04 °C/km. These cooling rates are much smaller than for Hawaiian aa flows (1.0-4.4 °C/km) and for active Kilauea lava tubes (0.6-1.0 °C/km) (Helz, et al., 1992; Cashman et al.,

1994). Low cooling rates mean rapid emplacement or that transport was extremely thermally efficient (Ho and Cashman, 1997).

I obtained cooling rates for Grande Ronde lavas using a very different method based on Al_2O_3 and TiO_2 contents of groundmass pyroxenes. This method makes use of an earlier experimental determination of Grove and Bence, (1977) that the partitioning of TiO_2 and Al_2O_3 in pyroxenes is strongly cooling rate dependent (Figure 30). Both augite and low-calcium pyroxenes show the same rate dependency.

Grande Ronde groundmass pyroxene Al and Ti, normalized to 6 oxygen, contents were plotted on a graph with the 1:1, 1:2, 1:4 trends of Grove and Bence (1977). The majority of GRB lavas plot inside the 4°C per hour cooling rate trend, although it appears that the magma (s) had a range of cooling rates from less than 1°C per hour to greater than 10°C per hour (Figure 30). A flow rate for an average GRB long lava flow (100 km) was obtained by taking the cooling rate obtained from the Ti-Al plot (4°C/hr) (Figure 31) and the change in temperature of the melt (ΔT). This change in temperature indicates the difference between the eruption temperature (liquidus) and the temperature of crystallization (solidus) for the GRB melts. Temperatures were obtained from MELTS thermodynamics software calculations (Sack and Ghiorso, 1994)

Time=ΔT/ Cooling Rate (4°C/hr)

- ΔT=(difference between the temperature of eruption (liquidus) minus temperature at which the melt solidifies)
- 1159 °C -799°C (Obtained from MELTS)
- Time = 90 hours
- Flow velocity=distance/time;

Therefore, flow velocity for a 100 km long lava flow would be 100 km/90 hr or 1.1 km/hr, and of a 600 km lava flow it would be 6.7 km/hr.
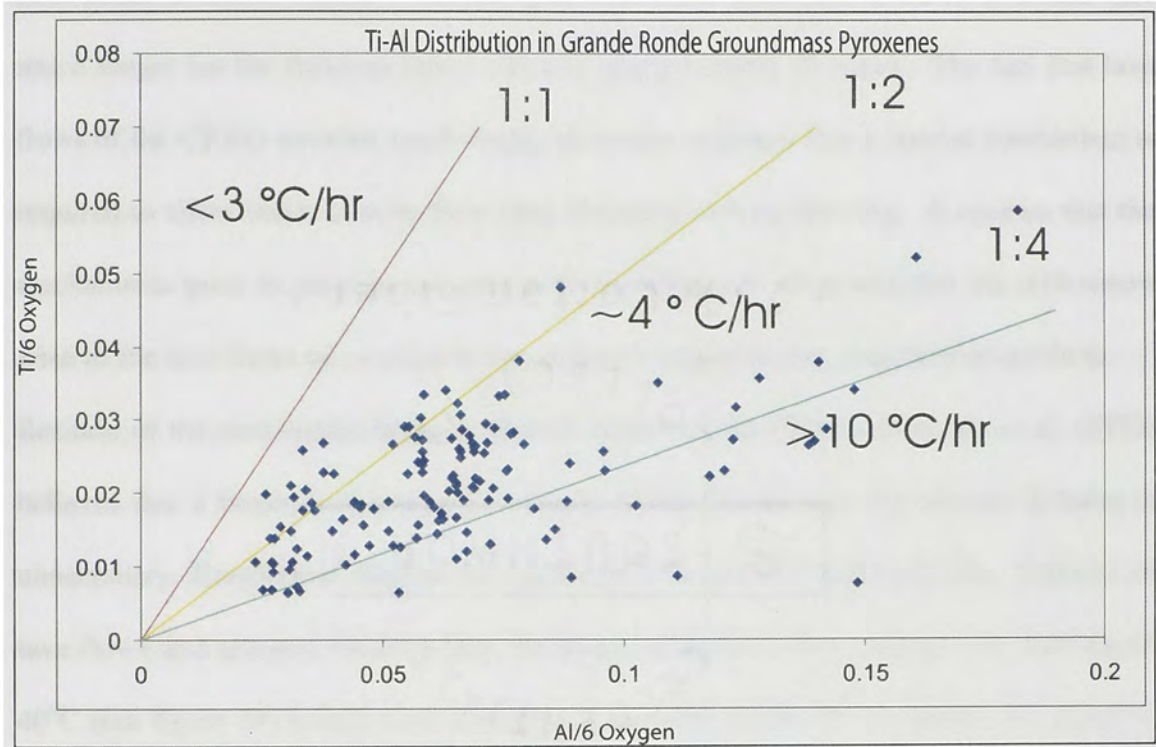
Figure 30- Graph showing Ti vs. Al Groundmass data indicating Grande Ronde lava cooling rates for Groundmass pyroxene.

For the sake of comparison, an aa flow from Hawaii's Mauna Loa volcano had a measured velocity of approximately 1.98 km/hour (Decker et al., 1987). Considering that aa is more viscous and has a lower temperature than pahoehoe flows, this rate is at the lower end of the spectrum of lava flow rates. At this rate, it would take this Hawaii flow 50.5 hours to travel 100 km. At the calculated flow rates for the GRB, it would take much longer for the flows to travel 100 km, approximately 91 hours. The fact that lava flows of the CRBG traveled much longer distances indicates that a special mechanism is required to allow these lavas to flow long distances without freezing. It appears that the mechanisms prior to eruption are similar to the Hawaiian lavas and that the differences arise as the lava flows on or close to the surface in upper crustal chambers or conduits.

Because of the similarities between Hawaii lavas and the CRBG, Swanson et al. (1975) believes that a larger heat source for Grande Ronde Basalt than for modern Kilauea is unnecessary. Exothermal magma mixing could have lowered the kinematic viscosity of lava flows and allowed these to flow for longer distances. For example, an increase of $40^{\circ}C$ (see figure 29) would have lowered the viscosity of the mixed magma by about 50 poise, which is a significant number. The center of a 30 m thick near-liquidus lava flow with a Newtonian viscosity of 300 poise would travel at 15 km/hour over a slope of 1 degree based on the following equations (http://www.geo.ua.edu/volcanology/lecture notes.html).

$$\acute{\eta} = g\rho sinAd2/3V$$

[where $\acute{\eta}$ is the viscosity, g is acceleration of gravity, ρ is density of magma (2.8 g/cm^3),

A is slope angle, V is velocity, and d is depth of flow.]

The same lava flow superheated by 40° will travel at 25 km/hour. These numbers represent appropriate average velocities for GRB lava flows [Shaw and Swanson, 1970].

Eruption Conditions: Thermometry and Barometry

I calculated eruption conditions using the plagioclase phenocryst data obtained during this study and whole rock data from Hooper and Hawkesworth (1993). Pressure and temperature conditions were calculated for plagioclase crystals that were in equilibrium with appropriate liquid compositions (whole rock data was assumed to be the same as the liquid in this case since most of the GRB is aphyric).

Plagioclase-liquid thermo barometers of Putirka (2005) were used to estimate the pressure and temperature of crystallization and the water contents of the GRB lavas. Although the Sugawara (2001) and Ghiorso (1994) thermometers provide more accurate temperature estimates than earlier calibrations, these do not provide a means for calculating pressure from plagioclase-liquid equilibrium (Putirka, 2005). To remedy this shortcoming Putirka developed a plagioclase-liquid thermometer and barometer. Putirka's (2005) thermometers (below) yield an error that is 30-40% lower than Sugawara (2001) and Ghiorso (1994) models:

Putirka's Plagioclase-liquid thermometer based on his Model [A] as:

$$104/T(K) = 68.8 - 0.86\ln(An^P/(Ca^{liq}(Al^{liq})2(Si^{liq})^2) + 179(Al^{liq}) - 113(Al/(Al+Si))^{liq} -$$

$$7.92(AbAn^P) - 6.13 \times 10 - 2(P(kb)) - 91.6(CaAl^{liq}) - 155(Si^{liq}) + 110.3(Si^{liq})^2 - 149(Al^{liq})^2$$

(Where P and liq denote plagioclase and liquid phases, respectively and Ca^{liq}, Al^{liq}, and Si^{liq} represent the abundances of these elements in the liquid).

Temperatures calculated using Putirka's Model [A] range from 1089 °C to 1127 °C, which are slightly lower than those calculated by Caprarelli and Reidel (2005) using Putirka's clinopyroxene-liquid geothermometer (1120-1222 °C). Caprarelli and Reidel (2005) interpret these results as consistent with crustal-level magma chamber evolution. Note that their calculations were not limited to the GRB Formation, however, but included the entire CRBG stratigraphy. Interestingly, one of the younger members of the CRBG, the Pomona Member (12 Ma), had the highest temperature calculated. Higher potential temperatures are expected to translate into larger volumes of erupted magmas (Caprarelli and Reidel, 2005); however in this case, the Pomona Member is part of the Late Saddle Mountain Formation comprising 1% by volume of the CRBG (Hooper, 1988). Caprarelli and Reidel (2005) suggest that the temperature differences reflect magma chamber heterogeneities.

I also calculated pressure using Putirka's (2005) Model [C]:

$$P(kb) = -42.2 + 4.94 \times 10\text{-}2(T(K)) + 1.16 \times 10\text{-}2T(K)\ln(Ab^{Pl}Al^{liq}Ca^{liq}/(An^{Pl}Na^{liq}Si^{liq})) - 382.3(Si^{liq})^2 + 514.2(Si^{liq})^3 - 19.6\ln(Ab^{Pl}) - 139.8(Ca^{liq}) + 287.2(Na^{liq}) + 163.9(K^{liq})$$

(Where Pl and liq denote plagioclase and liquid phases, respectively and Ca^{liq}, Al^{liq}, and Si^{liq} represent the abundances of these elements in the liquid).

Although my calculated temperatures for the GRB obtained from the plagioclase-liquid geothermometer of Putirka are lower than those calculated from the clinopyroxene-liquid thermometer, my pressure results are very close to that of Caprarelli and Reidel (2005). Clinopyroxene-liquid barometry gave pressures ranging from 0 to 0.66 GPa, while I obtain pressures of 0.35 GPa to 0.61 GPa from the plagioclase-liquid barometer.

The results of the two sets of pressure estimates by using very different barometry are very similar (Figure 31).

H_2O contents of the magmas were derived by using Putirka's Model [H] and the temperatures calculated above.

$$H_2O \text{ (wt. \%)} = 24.757 - 2.26 \times 10^{-3} T(K) \ln(An^{Pl}/(Ca^{liq}(Al^{liq})^2 Si^{liq})^2) -$$

$$3.847(Ab^{Pl}) + 1.927(An^{Pl}/(Ca^{liq}/(Ca^{liq} + Na^{liq})))$$

(Where Pl and liq denote plagioclase and liquid phases, respectively and Ca^{liq}, Al^{liq}, and Si^{liq} represent the abundances of these elements in the liquid).

The results of the H_2O calculations show that water contents are very low reaching the limits of the model, and some results are negative. I obtain dissolved H_2O contents ranging from 0 to 0.29 wt. % H_2O, which indicate either that the GRB magmas were very dry to begin with, or that, even if the original magmas were wet, they degassed significantly during ascent.
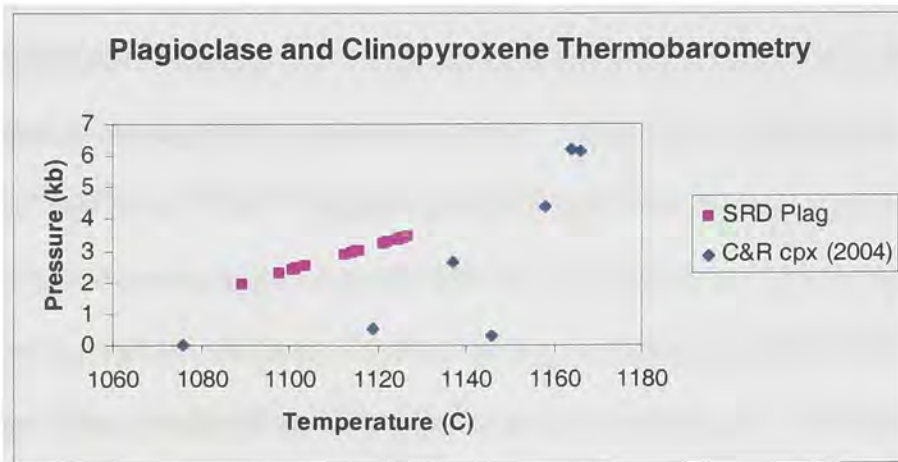
Figure 31- A comparison between plagioclase thermobarometric calculations conducted in this study and data from pyroxene calculations of Caprarelli and Reidel (2004). Plagioclase seems to fall in between the pyroxene values, both show low pressure and temperature values.

SUMMARY

The results of petrographic and mineral chemistry analyses of the Grande Ronde basalts provide considerable insight into the generation of the formation. The following is a summary of the findings and observations outlined earlier. The largest and most abundant phenocryst phase in the GRB is plagioclase followed by augite and pigeonite. Olivine phenocrysts are rarely observed because most olivine phenocrysts have been completely altered to iddingsite. Unaltered olivine grains are generally only found in the groundmass. The Imnaha formation being fairly phyric with phenocryst of plagioclase, augite, and olivine, differs dramatically from the GRB. Many phenocrysts in the GRB show extensive resorption and evidence of magma mixing. For example, reverse and normal zoning patterns are seen throughout the flows, some of this zoning within single thin sections. Several of these crystals are also resorbed. In addition, magma mingling is seen in the flows and dikes of the GRB.

The GRB is generally chemically evolved with low Mg numbers [$(100*Mg/(Mg+Fe^{2+})$ ranging from 30 to 64] and high SiO_2 (52-58 wt %). These lavas are enriched in incompatible elements and show a relatively flat HREE pattern. When plotted on $^{87}Sr/^{86}Sr$ vs. $^{143}Nd/^{144}Nd$ graph, the GRB (and Wanapum) plot near bulk earth.

Several features suggest that the GRB last fractionated at shallow depths before erupting on the surface. Evidence for this shallow processing includes the GRB's phase assemblage (Plag.+Augite+Pigeonite) which typical of magma that fractionated in the middle to upper crust. GRB lavas also plot near the 1-atm cotectic on an augite-olivine-quartz pseudoternary projection, indicating once more that the lavas last equilibrated in shallow conduits. Because of the extensive resorption and zoning seen in the

phenocrysts, it is suggested that superheated mixing of the magma is responsible for the lack of some of the phenocrysts in the GRB.

Other findings in the GRB include the presence of a few high-An plagioclase phenocrysts. These are interpreted to be due to the presence of a H_2O-rich source in the mantle. Many of these plagioclase phenocrysts (and pyroxenes) are out of equilibrium with the groundmass. Residence time in magma chamber(s) calculations indicate that if indeed these magmas last resided in shallow level conduits, they were processed rather rapidly as residence time calculation indicate very short durations (<5 years). Lava flow rates obtained from calculated GRB cooling rates indicate that GRB lava flow rates are not significantly different than modern Hawaiian flow lava flow rates. This finding indicates that a special mechanism is required to generate the larger volumes observed at the CRBG plateau.

As a final point, calculations to determine the temperature, pressure and H_2O content of the GRB were performed. The temperature results range from 1089 °C to 1127 °C while pressures from 0.35 GPa to 0.61 GPa were obtained. The erupted lavas had a maximum of 0.3 wt. % H_2O, indicating that magmas were largely degassed at shallow depths or were dry to begin with.

Table 1A - Microprobe Analyses of Plagioclase Phenocrysts

	GRB-3-01c	GRB-3-1c	GRB-3-02r	GRB-3-03c	GRB-3-rim	GRB-3-D-c	GRB3-1PLInf
SiO2	59.70	55.82	55.25	55.56	53.80	58.90	58.73
TiO2	0.01	0.08	0.09	0.05	0.01	0.01	0.00
Al2O3	25.63	28.47	27.87	27.83	28.78	26.26	25.30
Cr2O3	0.03	0.03	0.00	0.01	0.00	0.01	0.00
MgO	0.04	0.07	0.07	0.07	0.08	0.03	0.00
CaO	7.69	11.03	10.82	10.44	11.50	8.44	8.34
FeO	0.39	0.58	0.53	0.59	0.57	0.41	0.34
MnO	0.06	0.04	0.01	0.01	0.03	0.01	0.00
Na2O	6.24	5.05	4.67	4.65	4.58	6.20	6.13
K2O	0.70	0.38	0.33	0.40	0.33	0.56	0.60
Total	**100.49**	**101.56**	**99.65**	**99.60**	**99.69**	**100.83**	**99.45**
Structural Formulae							
Cations per 8 Oxygen							
Si	2.66	2.49	2.50	2.51	2.44	2.62	2.64
Ti	0.00	0.00	0.00	0.00	0.00	0.00	0.00
Al (IV)	1.34	1.50	1.49	1.48	1.54	1.38	1.34
Al (VI)							
Cr	0.00	0.00	0.00	0.00	0.00	0.00	0.00
Mg	0.00	0.00	0.00	0.00	0.01	0.00	0.00
Ca	0.37	0.53	0.52	0.51	0.56	0.40	0.40
Fe	0.01	0.02	0.02	0.02	0.02	0.02	0.01
Mn	0.00	0.00	0.00	0.00	0.00	0.00	0.00
Na	0.54	0.44	0.41	0.41	0.40	0.53	0.53
K	0.04	0.02	0.02	0.02	0.02	0.03	0.03
Cation Sum	**4.96**	**4.99**	**4.97**	**4.96**	**5.00**	**4.98**	**4.97**
An	0.56	0.70	0.71	0.70	0.73	0.59	0.59
Ab	0.41	0.29	0.28	0.28	0.26	0.39	0.39
Or	0.03	0.01	0.01	0.02	0.01	0.02	0.03

Table 1B - Microprobe Analyses of Plagioclase Phenocrysts

	GRB3-1PLlnf	GRB3-1PLlnf	GRB3-1PLlnf	GRB-8-1plag	GRB-8-1plc2	GRB-8-1plrm2	GRB-8-2plagcr
SiO2	57.86	58.69	54.34	54.37	53.81	54.67	54.39
TiO2	0.06	0.04	0.07	0.07	0.08	0.08	0.08
Al2O3	25.78	25.37	27.85	28.64	28.34	28.10	27.38
Cr2O3	0.01	0.00	0.00	0.00	0.02	0.01	0.00
MgO	0.00	0.01	0.07	0.15	0.12	0.12	0.14
CaO	8.87	8.43	11.56	11.24	11.17	11.09	10.91
FeO	0.47	0.43	0.53	0.52	0.50	0.70	0.53
MnO	0.00	0.00	0.00	0.00	0.00	0.00	0.00
Na2O	5.56	5.82	4.49	4.63	4.67	4.79	4.70
K2O	0.55	0.61	0.27	0.31	0.32	0.34	0.31
Totals	**99.15**	**99.40**	**99.18**	**99.93**	**99.04**	**99.89**	**98.44**
Structural Formulae							
Cations per 8 Oxygen							
Si	2.62	2.64	2.48	2.46	2.46	2.48	2.50
Ti	0.00	0.00	0.00	0.00	0.00	0.00	0.00
Al (IV)	1.37	1.35	1.50	1.53	1.53	1.50	1.48
Al (VI)							
Cr	0.00	0.00	0.00	0.00	0.00	0.00	0.00
Mg	0.00	0.00	0.00	0.01	0.01	0.01	0.01
Ca	0.43	0.41	0.56	0.55	0.55	0.54	0.54
Fe	0.02	0.02	0.02	0.02	0.02	0.03	0.02
Mn	0.00	0.00	0.00	0.00	0.00	0.00	0.00
Na	0.49	0.51	0.40	0.41	0.41	0.42	0.42
K	0.03	0.03	0.02	0.02	0.02	0.02	0.02
Cation sum	**4.96**	**4.96**	**4.98**	**4.99**	**4.99**	**4.99**	**4.98**
An	0.62	0.60	0.73	0.72	0.72	0.71	0.71
Ab	0.35	0.37	0.26	0.27	0.27	0.28	0.28
Or	0.02	0.03	0.01	0.01	0.01	0.01	0.01

72

Table 1C- Microprobe Analyses of Plagioclase Phenocrysts

	GRB-8-2plaGRBm	GRB-8-3plcr	GRB-8-3plrm2	GRB-8-3plrm3	GRB-9-1plc	GRB-9-1ln1	GRB-9-1ln2
SiO_2	54.00	54.59	54.86	54.37	50.52	49.53	47.47
TiO_2	0.10	0.06	0.12	0.08	0.22	0.00	0.00
Al_2O_3	28.36	28.49	27.16	27.93	31.36	31.73	32.69
Cr_2O_3	0.01	0.02	0.00	0.01	0.00	0.00	0.00
MgO	0.13	0.13	0.15	0.14	0.31	0.16	0.15
CaO	10.98	11.34	10.53	10.93	14.63	15.38	16.29
FeO	0.53	0.48	0.55	0.48	0.78	0.50	0.62
MnO	0.03	0.01	0.01	0.00	0.18	0.01	0.00
Na_2O	4.76	4.72	5.09	4.85	3.05	2.56	2.08
K_2O	0.31	0.32	0.36	0.32	0.15	0.08	0.04
Totals	**99.20**	**100.16**	**98.84**	**99.11**	**101.20**	**99.95**	**99.33**

Structural Formulae

Cations per 8 Oxygen

Si	2.46	2.47	2.51	2.48	2.29	2.27	2.20
Ti	0.00	0.00	0.00	0.00	0.00	0.00	0.00
Al (IV)	1.53	1.52	1.46	1.50	1.68	1.71	1.78
Al (VI)							
Cr	0.00	0.00	0.00	0.00	0.00	0.00	0.00
Mg	0.01	0.01	0.01	0.01	0.02	0.01	0.01
Ca	0.54	0.55	0.52	0.53	0.71	0.75	0.81
Fe	0.02	0.02	0.02	0.02	0.03	0.02	0.02
Mn	0.00	0.00	0.00	0.00	0.00	0.00	0.00
Na	0.42	0.41	0.45	0.43	0.27	0.23	0.19
K	0.02	0.02	0.02	0.02	0.01	0.00	0.00
Cation sum	**4.99**	**4.99**	**4.99**	**4.99**	**5.01**	**4.99**	**5.01**
An	0.71	0.72	0.69	0.70	0.84	0.87	0.90
Ab	0.28	0.27	0.30	0.28	0.16	0.13	0.10
Or	0.01	0.01	0.01	0.01	0.01	0.00	0.00

73

Table 1D- Microprobe Analyses of Plagioclase Phenocrysts

	GRB-9-1ln3	GRB-9-1ln4	GRB-9-2plcr	GRB-9-2plrm	GRB-9-3plcr1	GRB-9-3rm2	GRB-9-3rm3
SiO_2	49.36	50.78	54.36	51.97	48.39	52.57	52.68
TiO_2	0.00	0.00	0.00	0.00	0.00	0.06	0.00
Al_2O_3	31.50	30.69	27.93	29.48	32.08	28.83	29.04
Cr_2O_3	0.00	0.00	0.00	0.00	0.00	0.00	0.00
MgO	0.16	0.17	0.25	0.14	0.17	0.15	0.16
CaO	15.11	14.30	11.48	12.62	15.55	11.96	12.55
FeO	0.66	0.51	0.77	0.69	0.47	0.67	0.65
MnO	0.00	0.02	0.02	0.00	0.00	0.02	0.00
Na_2O	2.67	3.15	4.47	3.78	2.38	4.19	4.11
K_2O	0.05	0.08	0.21	0.20	0.03	0.22	0.18
Totals	**99.51**	**99.69**	**99.50**	**98.88**	**99.07**	**98.67**	**99.37**
Structural Formulae							
Cations per 8 Oxygen							
Si	2.27	2.32	2.47	2.39	2.24	2.42	2.41
Ti	0.00	0.00	0.00	0.00	0.00	0.00	0.00
Al (IV)	1.71	1.65	1.50	1.60	1.75	1.56	1.56
Al (VI)							
Cr	0.00	0.00	0.00	0.00	0.00	0.00	0.00
Mg	0.01	0.01	0.02	0.01	0.01	0.01	0.01
Ca	0.74	0.70	0.56	0.62	0.77	0.59	0.61
Fe	0.03	0.02	0.03	0.03	0.02	0.03	0.02
Mn	0.00	0.00	0.00	0.00	0.00	0.00	0.00
Na	0.24	0.28	0.39	0.34	0.21	0.37	0.36
K	0.00	0.00	0.01	0.01	0.00	0.01	0.01
Cation sum	**5.00**	**4.99**	**4.98**	**4.99**	**5.00**	**4.99**	**5.00**
An	0.86	0.83	0.73	0.78	0.88	0.75	0.77
Ab	0.14	0.17	0.26	0.21	0.12	0.24	0.23
Or	0.00	0.00	0.01	0.01	0.00	0.01	0.01

74

Table 1E- Microprobe Analyses of Plagioclase Phenocrysts

	GRB-13-1plc	GRB-13-1plr	GRB-13-2plc	GRB-13-3PL1c	GRB-13-3PL2c	GRB-13-5PL1	GRB-13-5PL2
SiO2	55.07	55.51	56.36	55.66	53.48	53.83	57.52
TiO2	0.07	0.07	0.10	0.05	0.08	0.03	0.07
Al2O3	27.96	27.82	27.01	27.57	27.90	28.25	26.69
Cr2O3	0.00	0.00	0.00	0.00	0.00	0.01	0.00
MgO	0.13	0.11	0.08	0.10	0.16	0.11	0.12
CaO	11.66	11.71	10.64	11.70	11.71	11.97	10.16
FeO	0.66	0.74	0.78	0.56	0.66	0.64	0.57
MnO	0.00	0.00	0.02	0.00	0.02	0.01	0.00
Na2O	4.60	4.72	5.12	4.79	4.59	4.54	5.37
K2O	0.26	0.29	0.34	0.26	0.26	0.26	0.39
Totals	**100.42**	**100.97**	**100.45**	**100.68**	**98.86**	**99.65**	**100.90**

Structural Formulae

Cations per 8 Oxygen

Si	2.48	2.49	2.54	2.50	2.46	2.45	2.57
Ti	0.00	0.00	0.00	0.00	0.00	0.00	0.00
Al (IV)	1.49	1.47	1.43	1.46	1.51	1.52	1.40
Al (VI)							
Cr	0.00	0.00	0.00	0.00	0.00	0.00	0.00
Mg	0.01	0.01	0.01	0.01	0.01	0.01	0.01
Ca	0.56	0.56	0.51	0.56	0.58	0.58	0.49
Fe	0.02	0.03	0.03	0.02	0.03	0.02	0.02
Mn	0.00	0.00	0.00	0.00	0.00	0.00	0.00
Na	0.40	0.41	0.45	0.42	0.41	0.40	0.46
K	0.02	0.02	0.02	0.01	0.02	0.02	0.02
Cation sum	**4.98**	**4.99**	**4.98**	**4.98**	**5.00**	**5.00**	**4.97**
An	0.73	0.72	0.69	0.72	0.73	0.74	0.67
Ab	0.26	0.26	0.30	0.27	0.26	0.25	0.32
Or	0.01	0.01	0.01	0.01	0.01	0.01	0.02

75

Table 1F- Microprobe Analyses of Plagioclase Phenocrysts

	GRB-13-3PL1	GRB-13-6pl1	GRB1-16-1plc	GRB1-16-1plr	GRB-16-1plln2	GRB-16-1plln3	GRB-16-1plln4
SiO2	55.66	55.85	56.93	58.19	55.33	56.58	57.91
TiO2	0.05	0.06	0.12	0.06	0.09	0.09	0.09
Al2O3	27.57	27.85	27.22	26.26	28.24	27.52	27.05
Cr2O3	0.00	0.00	0.00	0.00	0.01	0.01	0.01
MgO	0.10	0.14	0.14	0.11	0.11	0.11	0.11
CaO	11.70	11.41	10.71	9.68	12.02	11.07	10.17
FeO	0.56	0.64	0.67	0.50	0.64	0.54	0.60
MnO	0.00	0.00	0.01	0.00	0.04	0.00	0.02
Na2O	4.79	4.57	5.30	5.88	4.64	4.89	5.59
K2O	0.26	0.26	0.39	0.51	0.32	0.35	0.44
Totals	**100.68**	**100.78**	**101.49**	**101.19**	**101.44**	**101.16**	**101.99**
Structural Formulae							
Cations per 8 Oxygen							
Si	2.50	2.50	2.54	2.59	2.47	2.52	2.56
Ti	0.00	0.00	0.00	0.00	0.00	0.00	0.00
Al (IV)	1.46	1.47	1.43	1.38	1.49	1.45	1.41
Al (VI)							
Cr	0.00	0.00	0.00	0.00	0.00	0.00	0.00
Mg	0.01	0.01	0.01	0.01	0.01	0.01	0.01
Ca	0.56	0.55	0.51	0.46	0.58	0.53	0.48
Fe	0.02	0.02	0.02	0.02	0.02	0.02	0.02
Mn	0.00	0.00	0.00	0.00	0.00	0.00	0.00
Na	0.42	0.40	0.46	0.51	0.40	0.42	0.48
K	0.01	0.02	0.02	0.03	0.02	0.02	0.02
Cation sum	**4.98**	**4.97**	**4.99**	**4.99**	**4.99**	**4.97**	**4.99**
An	0.72	0.73	0.68	0.63	0.73	0.71	0.66
Ab	0.27	0.26	0.30	0.35	0.26	0.28	0.33
Or	0.01	0.01	0.01	0.02	0.01	0.01	0.02

76

Table 1G- Microprobe Analyses of Plagioclase Phenocrysts

	GRB-16-1plln5	GRB-16-2plc	GRB1-16-3pl	GRB1-16-6pl	GRB-16-8c	GRB-16-83	GRB-17-2pl
SiO_2	56.59	57.81	54.11	55.70	56.16	56.65	54.76
TiO_2	0.08	0.09	0.09	0.05	0.09	0.07	0.01
Al_2O_3	27.15	26.87	27.44	28.01	26.91	27.06	27.11
Cr_2O_3	0.03	0.00	0.01	0.02	0.00	0.03	0.01
MgO	0.09	0.13	0.15	0.14	0.09	0.11	0.13
CaO	10.55	10.34	11.06	11.44	10.71	10.58	11.47
FeO	0.72	0.53	0.65	0.57	0.51	0.51	0.69
MnO	0.01	0.00	0.02	0.01	0.00	0.05	0.00
Na_2O	5.49	5.08	4.64	4.64	4.89	4.87	4.44
K_2O	0.42	0.38	0.32	0.30	0.36	0.39	0.24
Totals	**101.13**	**101.22**	**98.48**	**100.88**	**99.72**	**100.32**	**98.87**

Structural Formulae

Cations per 8 Oxygen

	GRB-16-1plln5	GRB-16-2plc	GRB1-16-3pl	GRB1-16-6pl	GRB-16-8c	GRB-16-83	GRB-17-2pl
Si	2.53	2.57	2.487	2.495	2.540	2.545	2.503
Ti	0.00	0.00	0.000	0.000	0.000	0.000	0.000
Al (IV)	1.43	1.41	1.487	1.479	1.435	1.433	1.461
Al (VI)							
Cr	0.00	0.00	0.000	0.000	0.000	0.000	0.000
Mg	0.01	0.01	0.010	0.009	0.006	0.007	0.009
Ca	0.51	0.49	0.545	0.549	0.519	0.509	0.562
Fe	0.03	0.02	0.025	0.021	0.019	0.019	0.026
Mn	0.00	0.00	0.000	0.000	0.000	0.000	0.000
Na	0.48	0.44	0.414	0.403	0.429	0.424	0.394
K	0.02	0.02	0.019	0.017	0.021	0.022	0.014
Cation sum	**5.00**	**4.96**	**4.986**	**4.975**	**4.968**	**4.961**	**4.970**
An	0.67	0.68	0.72	0.72	0.70	0.70	0.73
Ab	0.31	0.30	0.27	0.27	0.29	0.29	0.26
Or	0.02	0.01	0.01	0.01	0.01	0.02	0.01

77

Table H- Microprobe Analyses of Plagioclase Phenocrysts

	GRB-17-3plc	GRB-17-plr	GRB-18-3plr	GRB-18-3plln1c	GRB-18-3plln	GRB-18-5plln3	GRB-18-5plln4
SiO2	56.13	57.52	54.24	54.96	54.00	56.73	56.97
TiO2	0.03	0.04	0.03	0.00	0.00	0.01	0.01
Al2O3	27.44	26.27	28.52	27.65	28.18	26.83	26.84
Cr2O3	0.00	0.00	0.00	0.00	0.00	0.01	0.00
MgO	0.12	0.07	0.14	0.17	0.15	0.11	0.10
CaO	10.97	9.40	12.57	12.17	12.02	10.77	10.75
FeO	0.66	0.77	0.58	0.64	0.69	0.87	0.77
MnO	0.00	0.00	0.00	0.00	0.02	0.00	0.01
Na2O	4.85	5.72	4.18	4.26	4.14	5.19	5.32
K2O	0.34	0.44	0.22	0.19	0.19	0.29	0.29
Totals	100.55	100.24	100.46	100.04	99.40	100.81	101.06

Structural Formulae

Cations per 8 Oxygen

	GRB-17-3plc	GRB-17-plr	GRB-18-3plr	GRB-18-3plln1c	GRB-18-3plln	GRB-18-5plln3	GRB-18-5plln4
Si	2.520	2.583	2.45	2.49	2.46	2.54	2.55
Ti	0.000	0.000	0.00	0.00	0.00	0.00	0.00
Al (IV)	1.452	1.391	1.52	1.47	1.51	1.42	1.41
Al (VI)							
Cr	0.000	0.000	0.00	0.00	0.00	0.00	0.00
Mg	0.008	0.005	0.01	0.01	0.01	0.01	0.01
Ca	0.528	0.452	0.61	0.59	0.59	0.52	0.51
Fe	0.025	0.029	0.02	0.02	0.03	0.03	0.03
Mn	0.000	0.000	0.00	0.00	0.00	0.00	0.00
Na	0.422	0.498	0.37	0.37	0.37	0.45	0.46
K	0.019	0.025	0.01	0.01	0.01	0.02	0.02
Cation sum	**4.97**	**4.98**	**4.98**	**4.97**	**4.97**	**4.98**	**4.99**
An	0.71	0.63	0.76	0.75	0.76	0.69	0.68
Ab	0.28	0.35	0.23	0.24	0.24	0.30	0.31
Or	0.01	0.02	0.01	0.01	0.01	0.01	0.01

78

Table I- Microprobe Analyses of Plagioclase Phenocrysts

	CHI-16-1pl	CHI-16-2pl	CHI-17-1plln2	CHI-17-1plln3	CHI-17-2pllnc1	CHI-17-2plln3	CHI-17-3pl2c
SiO_2	57.01	54.70	58.23	56.65	56.73	56.51	56.07
TiO_2	0.08	0.08	0.08	0.07	0.07	0.03	0.08
Al_2O_3	26.72	28.04	25.05	26.40	26.06	26.09	26.56
Cr_2O_3	0.00	0.01	0.00	0.02	0.02	0.00	0.00
MgO	0.11	0.11	0.09	0.10	0.08	0.09	0.12
CaO	10.72	11.03	8.41	10.12	9.78	9.85	10.43
FeO	0.84	0.82	0.73	1.01	0.80	0.93	0.74
MnO	0.00	0.03	0.00	0.00	0.03	0.01	0.00
Na_2O	5.09	4.93	6.17	5.49	5.64	5.66	5.24
K_2O	0.26	0.24	0.39	0.29	0.36	0.32	0.26
Totals	**100.83**	**99.99**	**99.16**	**100.14**	**99.56**	**99.50**	**99.50**

Structural Formulae

Cations per 8 Oxygen

	CHI-16-1pl	CHI-16-2pl	CHI-17-1plln2	CHI-17-1plln3	CHI-17-2pllnc1	CHI-17-2plln3	CHI-17-3pl2c
Si	2.55	2.48	2.64	2.56	2.57	2.56	2.57
Ti	0.00	0.00	0.00	0.00	0.00	0.00	0.00
Al (IV)	1.41	1.50	1.34	1.40	1.39	1.40	1.39
Al (VI)							
Cr	0.00	0.00	0.00	0.00	0.00	0.00	0.00
Mg	0.01	0.01	0.01	0.01	0.01	0.01	0.01
Ca	0.51	0.54	0.41	0.49	0.47	0.48	0.49
Fe	0.03	0.03	0.03	0.04	0.03	0.04	0.04
Mn	0.00	0.00	0.00	0.00	0.00	0.00	0.00
Na	0.44	0.43	0.54	0.48	0.50	0.50	0.47
K	0.01	0.01	0.02	0.02	0.02	0.02	0.02
Cation sum	**4.97**	**5.00**	**4.98**	**4.99**	**4.99**	**5.00**	**4.98**
An	0.69	0.71	0.59	0.66	0.65	0.65	0.68
Ab	0.30	0.29	0.39	0.33	0.34	0.34	0.31
Or	0.01	0.01	0.02	0.01	0.01	0.01	0.01

79

Table J - Microprobe Analyses of Plagioclase Phenocrysts

	CHI-17-3plr	CHI-18-1plcra	CHI-18-1rm2a	CHI-18-1plcb	CHI-18-1pl3a	CHI-19-2plln2	CHI-19-2plln3
SiO_2	56.53	52.36	53.45	55.25	56.20	55.39	55.07
TiO_2	0.01	0.05	0.04	0.09	0.04	0.03	0.06
Al_2O_3	25.90	28.52	28.06	26.95	26.94	27.88	28.03
Cr_2O_3	0.00	0.00	0.00	0.00	0.00	0.00	0.00
MgO	0.11	0.13	0.12	0.12	0.12	0.12	0.12
CaO	10.00	12.23	11.62	10.62	10.19	11.35	11.86
FeO	0.98	0.85	0.80	0.86	0.87	0.67	0.67
MnO	0.01	0.00	0.03	0.04	0.01	0.02	0.00
Na_2O	5.36	4.18	4.47	5.22	5.17	4.61	4.69
K_2O	0.31	0.16	0.20	0.28	0.23	0.33	0.32
Totals	**99.21**	**98.48**	**98.79**	**99.43**	**99.77**	**100.41**	**100.83**
Structural Formulae							
Cations per 8 Oxygen							
Si	2.57	2.42	2.45	2.52	2.54	2.49	2.48
Ti	0.00	0.00	0.00	0.00	0.00	0.00	0.00
Al (IV)	1.39	1.55	1.52	1.45	1.44	1.48	1.49
Al (VI)							
Cr	0.00	0.00	0.00	0.00	0.00	0.00	0.00
Mg	0.01	0.01	0.01	0.01	0.01	0.01	0.01
Ca	0.49	0.60	0.57	0.52	0.49	0.55	0.57
Fe	0.04	0.03	0.03	0.03	0.03	0.03	0.03
Mn	0.00	0.00	0.00	0.00	0.00	0.00	0.00
Na	0.47	0.37	0.40	0.46	0.45	0.40	0.41
K	0.02	0.01	0.01	0.02	0.01	0.02	0.02
Cation sum	**5.00**	**5.00**	**4.99**	**5.00**	**4.98**	**4.98**	**4.99**
An	0.67	0.76	0.74	0.68	0.68	0.72	0.73
Ab	0.32	0.23	0.26	0.30	0.31	0.27	0.26
Or	0.01	0.01	0.01	0.01	0.01	0.01	0.01

80

Table K- Microprobe Analyses of Plagioclase Phenocrysts

	CHI-20-1plcr	CHI-20-1plrm	CHI-21-3plrm	CHI-22-3cr	CHI-22-3plc	CHI-24-pl3c	CHI-24-pl4c
SiO2	55.55	56.35	55.60	53.58	55.89	48.50	53.37
TiO2	0.00	0.06	0.28	0.09	0.11	0.01	0.02
Al2O3	27.55	26.97	27.68	28.34	26.96	32.23	28.64
Cr2O3	0.00	0.00	0.00	0.00	0.02	0.02	0.00
MgO	0.14	0.09	0.27	0.13	0.13	0.10	0.03
CaO	10.92	10.59	10.22	11.35	10.98	15.03	12.15
FeO	0.51	0.64	0.88	0.89	0.73	1.18	0.36
MnO	0.02	0.04	0.17	0.03	0.01	0.00	0.03
Na2O	4.85	5.23	5.27	4.50	4.95	1.98	4.02
K2O	0.33	0.38	0.42	0.26	0.29	0.10	0.24
Totals	**99.87**	**100.35**	**100.79**	**99.16**	**100.08**	**99.14**	**98.85**
Structural Formulae							
Cations per 8 Oxygen							
Si	2.51	2.54	2.50	2.45	2.53	2.24	2.44
Ti	0.00	0.00	0.00	0.00	0.00	0.00	0.00
Al (IV)	1.47	1.43	1.47	1.53	1.44	1.75	1.55
Al (VI)							
Cr	0.00	0.00	0.00	0.00	0.00	0.00	0.00
Mg	0.01	0.01	0.02	0.01	0.01	0.01	0.00
Ca	0.53	0.51	0.49	0.56	0.53	0.74	0.60
Fe	0.02	0.02	0.03	0.03	0.03	0.05	0.01
Mn	0.00	0.00	0.00	0.00	0.00	0.00	0.00
Na	0.42	0.46	0.46	0.40	0.43	0.18	0.36
K	0.02	0.02	0.02	0.01	0.02	0.01	0.01
Cation sum	**4.98**	**4.99**	**5.00**	**4.99**	**4.98**	**4.97**	**4.97**
An	0.70	0.68	0.67	0.73	0.70	0.89	0.76
Ab	0.28	0.30	0.31	0.26	0.29	0.11	0.23
Or	0.01	0.01	0.02	0.01	0.01	0.00	0.01

81

Table 1L- Microprobe Analyses of Plagioclase Phenocrysts

	CHI-24-1pl	CHI-24-pl5c	CHI-24-pl6c	CHI-24-3plr	CHI-24-3lnc1	CHI-24-3ln2	CHI-24-3ln4
SiO_2	46.18	56.99	54.85	55.21	53.94	54.25	56.10
TiO_2	0.01	0.07	0.08	0.06	0.06	0.06	0.07
Al_2O_3	34.05	26.32	26.56	27.00	28.43	28.41	26.95
Cr_2O_3	0.00	0.00	0.00	0.00	0.00	0.00	0.00
MgO	0.03	0.07	0.29	0.15	0.15	0.16	0.12
CaO	17.99	9.89	10.95	10.94	12.46	11.93	11.00
FeO	0.41	0.75	1.66	0.70	0.58	0.70	0.57
MnO	0.02	0.04	0.03	0.01	0.00	0.00	0.00
Na_2O	0.90	5.31	4.59	4.72	4.17	4.34	5.06
K_2O	0.03	0.50	0.32	0.26	0.20	0.22	0.34
Total	**99.63**	**99.93**	**99.33**	**99.06**	**99.99**	**100.07**	**100.21**
Structural Formulae							
Cations per 8 Oxygen							
Si	2.13	2.57	2.51	2.52	2.45	2.46	2.53
Ti	0.00	0.00	0.00	0.00	0.00	0.00	0.00
Al (IV)	1.85	1.40	1.43	1.45	1.52	1.52	1.43
Al (VI)							
Cr	0.00	0.00	0.00	0.00	0.00	0.00	0.00
Mg	0.00	0.00	0.02	0.01	0.01	0.01	0.01
Ca	0.89	0.48	0.54	0.53	0.61	0.58	0.53
Fe	0.02	0.03	0.06	0.03	0.02	0.03	0.02
Mn	0.00	0.00	0.00	0.00	0.00	0.00	0.00
Na	0.08	0.46	0.41	0.42	0.37	0.38	0.44
K	0.00	0.03	0.02	0.02	0.01	0.01	0.02
Cation Sum	**4.98**	**4.98**	**4.99**	**4.97**	**4.98**	**4.98**	**4.99**
An	0.96	0.66	0.72	0.71	0.76	0.75	0.70
Ab	0.04	0.32	0.27	0.28	0.23	0.25	0.29
Or	0.00	0.02	0.01	0.01	0.01	0.01	0.01

Table 1M- Microprobe Analyses of Plagioclase Phenocrysts

	CHI-24-5PLC	CHI-24-5PLR	CHI-24-6PL	CHI-24-7PLr	CHI-28-1pli	CHI-28-2plc	CHI-28-4plc
SiO_2	54.79	56.15	55.52	55.08	55.46	54.00	54.33
TiO_2	0.05	0.04	0.09	0.06	0.04	0.05	0.09
Al_2O_3	27.67	26.96	27.46	27.80	27.47	29.18	28.97
Cr_2O_3	0.00	0.00	0.00	0.02	0.00	0.00	0.00
MgO	0.12	0.12	0.14	0.13	0.18	0.15	0.16
CaO	11.32	10.76	11.28	11.37	11.45	12.55	12.78
FeO	0.62	0.64	0.73	0.83	0.74	0.45	0.44
MnO	0.01	0.00	0.00	0.00	0.05	0.00	0.01
Na_2O	4.46	5.13	4.79	4.66	4.83	3.95	4.07
K_2O	0.27	0.34	0.28	0.24	0.28	0.17	0.16
Totals	**99.31**	**100.14**	**100.28**	**100.18**	**100.50**	**100.50**	**101.01**
Structural Formulae							
Cations per 8 Oxygen							
Si	2.49	2.53	2.50	2.49	2.50	2.43	2.44
Ti	0.00	0.00	0.00	0.00	0.00	0.00	0.00
Al (IV)	1.48	1.43	1.46	1.48	1.46	1.55	1.53
Al (VI)							
Cr	0.00	0.00	0.00	0.00	0.00	0.00	0.00
Mg	0.01	0.01	0.01	0.01	0.01	0.01	0.01
Ca	0.55	0.52	0.55	0.55	0.55	0.61	0.61
Fe	0.02	0.02	0.03	0.03	0.03	0.02	0.02
Mn	0.00	0.00	0.00	0.00	0.00	0.00	0.00
Na	0.39	0.45	0.42	0.41	0.42	0.35	0.35
K	0.02	0.02	0.02	0.01	0.02	0.01	0.01
Cation sum	**4.97**	**4.99**	**4.98**	**4.98**	**4.99**	**4.97**	**4.98**
An	0.73	0.69	0.71	0.72	0.72	0.77	0.77
Ab	0.26	0.30	0.27	0.27	0.27	0.22	0.22
Or	0.01	0.01	0.01	0.01	0.01	0.01	0.01

Table 1N- Microprobe Analyses of Plagioclase Phenocrysts

	CHI-28-4pllnc1	CHI-28-4plln2	CHI-28-4plln3	CHI-28-5plc	CHI-28-5plr	CHI-36-2plln1en	CHI-36-2plln3
SiO_2	53.86	55.96	54.80	54.55	54.08	55.79	55.14
TiO_2	0.03	0.05	0.05	0.08	0.05	0.28	0.30
Al_2O_3	28.98	27.42	28.24	28.24	28.62	25.71	26.16
Cr_2O_3	0.02	0.00	0.02	0.01	0.00	0.14	0.16
MgO	0.16	0.18	0.18	0.16	0.18	0.26	0.21
CaO	12.89	11.11	11.74	12.09	12.65	10.42	10.56
FeO	0.57	0.53	0.53	0.42	0.55	0.79	0.91
MnO	0.00	0.04	0.01	0.00	0.00	0.00	0.00
Na_2O	4.00	4.72	4.21	4.39	4.14	5.27	5.03
K_2O	0.22	0.24	0.25	0.19	0.20	0.40	0.41
Total	**100.72**	**100.25**	**100.02**	**100.13**	**100.47**	**99.07**	**98.88**
Structural Formulae							
Cations per 8 Oxygen							
Si	2.43	2.52	2.48	2.47	2.44	2.56	2.59
Ti	0.00	0.00	0.00	0.00	0.00	0.00	0.00
Al (IV)	1.54	1.45	1.50	1.51	1.52	1.39	1.35
Al (VI)							
Cr	0.00	0.00	0.00	0.00	0.00	0.00	0.00
Mg	0.01	0.01	0.01	0.01	0.01	0.02	0.02
Ca	0.62	0.54	0.57	0.59	0.61	0.51	0.49
Fe	0.02	0.02	0.02	0.02	0.02	0.03	0.04
Mn	0.00	0.00	0.00	0.00	0.00	0.00	0.00
Na	0.35	0.41	0.37	0.38	0.36	0.47	0.47
K	0.01	0.01	0.01	0.01	0.01	0.02	0.03
Cation Sum	**4.98**	**4.97**	**4.96**	**4.98**	**4.98**	**5.00**	**4.99**
An	0.77	0.72	0.75	0.75	0.77	0.68	0.69
Ab	0.22	0.28	0.24	0.25	0.23	0.31	0.30
Or	0.01	0.01	0.01	0.01	0.01	0.02	0.02

84

Table 1O- Microprobe Analyses of Plagioclase Phenocrysts

	CHI-36-2plc	CHI-36-2plr	CHI-36-3pllnlen	CHI-36-3plln3	CHI-36-3plln4	CHI-45-1plc	CHI-45-1pl3
SiO_2	55.49	55.28	54.76	54.20	54.03	56.05	55.45
TiO_2	0.30	0.33	0.26	0.28	0.26	0.29	0.28
Al_2O_3	26.16	26.22	26.35	27.10	26.70	26.61	25.90
Cr_2O_3	0.17	0.15	0.14	0.14	0.16	0.13	0.16
MgO	0.25	0.24	0.22	0.25	0.28	0.27	0.30
CaO	10.97	10.71	10.67	11.46	11.10	10.47	10.50
FeO	1.04	1.04	0.83	1.02	1.16	0.96	0.88
MnO	0.00	0.00	0.00	0.00	0.00	0.17	0.17
Na_2O	5.01	5.04	5.10	4.81	4.73	5.25	5.22
K_2O	0.37	0.39	0.40	0.35	0.39	0.39	0.40
Total	**99.75**	**99.40**	**98.74**	**99.60**	**98.82**	**100.59**	**99.25**
Structural Formulae							
Cations per 8 Oxygen							
Si	2.53	2.53	2.52	2.48	2.49	2.53	2.54
Ti	0.00	0.00	0.00	0.00	0.00	0.00	0.00
Al (IV)	1.41	1.42	1.43	1.46	1.45	1.42	1.40
Al (VI)							
Cr	0.00	0.00	0.00	0.00	0.00	0.00	0.00
Mg	0.02	0.02	0.02	0.02	0.02	0.02	0.02
Ca	0.54	0.53	0.53	0.56	0.55	0.51	0.52
Fe	0.04	0.04	0.03	0.04	0.04	0.04	0.03
Mn	0.00	0.00	0.00	0.00	0.00	0.00	0.00
Na	0.44	0.45	0.46	0.43	0.42	0.46	0.46
K	0.02	0.02	0.02	0.02	0.02	0.02	0.02
Cation sum	**5.00**	**5.00**	**5.00**	**5.01**	**5.00**	**5.00**	**5.00**
An	0.70	0.69	0.69	0.72	0.71	0.68	0.68
Ab	0.29	0.29	0.30	0.27	0.27	0.31	0.31
Or	0.01	0.01	0.02	0.01	0.01	0.01	0.02

Table 1P- Microprobe Analyses of Plagioclase Phenocrysts

	CHI-45-2plc	CHI-45-2pl2c	CHI-45-2pl3r	CHI-45-2pl5r	CHI-45-2pl6c	GRB-O4014-3pl	GRB-O4014-4plmp
SiO_2	54.21	52.41	54.86	51.80	53.95	54.78	55.19
TiO_2	0.28	0.28	0.27	0.27	0.26	0.37	0.08
Al_2O_3	26.53	27.95	26.30	28.35	27.35	26.86	26.90
Cr_2O_3	0.15	0.15	0.15	0.12	0.16	0.13	0.00
MgO	0.28	0.24	0.25	0.26	0.26	0.29	0.13
CaO	10.66	12.27	10.69	12.98	10.81	10.85	10.40
FeO	0.54	0.48	0.54	0.47	0.52	0.97	0.69
MnO	0.18	0.15	0.14	0.15	0.15	0.09	0.00
Na_2O	4.97	4.02	5.01	3.69	4.84	5.73	6.02
K_2O	0.28	0.24	0.32	0.24	0.27	0.39	0.33
Total	**98.08**	**98.19**	**98.52**	**98.32**	**98.57**	**100.46**	**99.73**
Structural Formulae							
Cations per 8 Oxygen							
Si	2.51	2.43	2.53	2.41	2.49	2.49	2.51
Ti	0.00	0.00	0.00	0.00	0.00	0.00	0.00
Al (IV)	1.45	1.53	1.43	1.55	1.49	1.44	1.44
Al (VI)							
Cr	0.00	0.00	0.00	0.00	0.00	0.00	0.00
Mg	0.02	0.02	0.02	0.02	0.02	0.02	0.01
Ca	0.53	0.61	0.53	0.65	0.53	0.53	0.51
Fe	0.02	0.02	0.02	0.02	0.02	0.04	0.03
Mn	0.00	0.00	0.00	0.00	0.00	0.00	0.00
Na	0.45	0.36	0.45	0.33	0.43	0.51	0.53
K	0.02	0.01	0.02	0.01	0.02	0.02	0.02
Cation sum	**4.99**	**4.99**	**4.99**	**4.99**	**4.99**	**5.05**	**5.04**
An	0.70	0.76	0.69	0.79	0.70	0.67	0.65
Ab	0.29	0.23	0.29	0.20	0.29	0.32	0.34
Or	0.01	0.01	0.01	0.01	0.01	0.01	0.01

Table 1Q- Microprobe Analyses of Plagioclase Phenocrysts

	GRB-O4014-4plmp	GRB-O4014-4plmp	GRB-O4014-4plmp	GRB-O4014-5pl	GRB-O4014-6pl	GRB-O4014-6pl	GRB-O4352-7pl
SiO_2	54.18	53.45	55.15	53.89	54.61	54.89	53.12
TiO_2	0.06	0.09	0.07	0.10	0.36	0.38	0.36
Al_2O_3	27.38	28.05	26.90	27.50	27.12	26.89	28.34
Cr_2O_3	0.00	0.01	0.00	0.01	0.18	0.11	0.16
MgO	0.10	0.11	0.07	0.08	0.29	0.30	0.28
CaO	11.01	11.98	10.49	10.79	10.92	10.90	11.96
FeO	0.80	0.86	0.84	1.19	0.83	1.01	0.97
MnO	0.00	0.00	0.02	0.01	0.11	0.16	0.10
Na_2O	5.70	5.20	4.94	5.73	5.68	5.74	5.20
K_2O	0.35	0.28	1.02	0.38	0.40	0.41	0.35
Total	**99.58**	**100.02**	**99.49**	**99.68**	**100.50**	**100.78**	**100.83**
Structural Formulae							
Cations per 8 Oxygen							
Si	2.47	2.44	2.52	2.47	2.49	2.49	2.42
Ti	0.00	0.00	0.00	0.00	0.00	0.00	0.00
Al (IV)	1.47	1.51	1.45	1.48	1.46	1.44	1.52
Al (VI)							
Cr	0.00	0.00	0.00	0.00	0.00	0.00	0.00
Mg	0.01	0.01	0.00	0.01	0.02	0.02	0.02
Ca	0.54	0.59	0.51	0.53	0.53	0.53	0.58
Fe	0.03	0.03	0.03	0.05	0.03	0.04	0.04
Mn	0.00	0.00	0.00	0.00	0.00	0.00	0.00
Na	0.50	0.46	0.44	0.51	0.50	0.51	0.46
K	0.02	0.02	0.06	0.02	0.02	0.02	0.02
Cation Sum	**5.05**	**5.05**	**5.01**	**5.06**	**5.05**	**5.05**	**5.06**
An	0.67	0.71	0.67	0.67	0.67	0.67	0.71
Ab	0.31	0.28	0.29	0.32	0.32	0.32	0.28
Or	0.01	0.01	0.04	0.01	0.01	0.02	0.01

87

Table 1R- Microprobe Analyses of Plagioclase Phenocrysts

	GRB-O4352-7pl	GRB-O4352-7pl	GRB-O4014-9pl	GRB-O4014-10pl	GRB-O4014-10pl	GRB-O4014-10pl	GRB-O4352-3pl
SiO_2	52.63	53.10	53.42	56.20	54.07	55.17	54.15
TiO_2	0.40	0.37	0.03	0.04	0.00	0.07	0.36
Al_2O_3	28.13	27.93	27.60	27.21	28.00	27.09	27.11
Cr_2O_3	0.15	0.19	0.02	0.00	0.05	0.06	0.15
MgO	0.32	0.29	0.11	0.08	0.12	0.11	0.30
CaO	12.23	12.08	11.30	9.92	11.27	9.93	11.28
FeO	1.03	0.97	0.72	0.91	0.91	0.69	0.95
MnO	0.12	0.08	0.00	0.03	0.00	0.00	0.09
Na_2O	5.08	5.15	5.62	5.86	5.39	5.60	5.50
K_2O	0.32	0.31	0.35	0.65	0.35	0.65	0.52
Total	**100.41**	**100.48**	**99.18**	**100.89**	**100.16**	**99.37**	**100.41**
Structural Formulae							
Cations per 8 Oxygen							
Si	2.41	2.43	2.45	2.52	2.46	2.52	2.47
Ti	0.00	0.00	0.00	0.00	0.00	0.00	0.00
Al (IV)	1.52	1.51	1.49	1.44	1.50	1.46	1.46
Al (VI)							
Cr	0.00	0.00	0.00	0.00	0.00	0.00	0.00
Mg	0.02	0.02	0.01	0.01	0.01	0.01	0.02
Ca	0.60	0.59	0.56	0.48	0.55	0.49	0.55
Fe	0.04	0.04	0.03	0.03	0.03	0.03	0.04
Mn	0.00	0.00	0.00	0.00	0.00	0.00	0.00
Na	0.45	0.46	0.50	0.51	0.47	0.49	0.49
K	0.02	0.02	0.02	0.04	0.02	0.04	0.03
Cation sum	**5.06**	**5.06**	**5.06**	**5.03**	**5.04**	**5.02**	**5.06**
An	0.72	0.71	0.68	0.64	0.69	0.65	0.68
Ab	0.27	0.28	0.31	0.34	0.30	0.33	0.30
Or	0.01	0.01	0.01	0.02	0.01	0.03	0.02

Table 1S- Microprobe Analyses of Plagioclase Phenocrysts

	GRB-O4352-3pl	GRB-O4352-5pl	GRB-O4352-5pl	GRB-O4352-6pl	GRB-O4352-7pl	GRB-O4352-7pl	GRB-O4352-10pl
SiO_2	54.55	53.13	53.35	55.41	53.12	52.63	53.91
TiO_2	0.35	0.36	0.36	0.37	0.36	0.40	0.38
Al_2O_3	27.13	27.91	27.72	26.61	28.34	28.13	26.66
Cr_2O_3	0.17	0.12	0.14	0.14	0.16	0.15	0.16
MgO	0.28	0.31	0.32	0.26	0.28	0.32	0.37
CaO	10.90	12.06	11.79	10.02	11.96	12.23	11.03
FeO	1.04	1.02	1.06	0.98	0.97	1.03	1.96
MnO	0.11	0.09	0.10	0.07	0.10	0.12	0.10
Na_2O	5.95	5.02	5.38	6.33	5.20	5.08	5.27
K_2O	0.48	0.30	0.31	0.49	0.35	0.32	0.45
Total	**100.96**	**100.31**	**100.54**	**100.68**	**100.83**	**100.41**	**100.31**
Structural Formulae							
Cations per 8 Oxygen							
Si	2.48	2.43	2.44	2.51	2.42	2.41	2.47
Ti	0.00	0.00	0.00	0.00	0.00	0.00	0.00
Al (IV)	1.45	1.51	1.49	1.42	1.52	1.52	1.44
Al (VI)							
Cr	0.00	0.00	0.00	0.00	0.00	0.00	0.00
Mg	0.02	0.02	0.02	0.02	0.02	0.02	0.03
Ca	0.53	0.59	0.58	0.49	0.58	0.60	0.54
Fe	0.04	0.04	0.04	0.04	0.04	0.04	0.08
Mn	0.00	0.00	0.00	0.00	0.00	0.00	0.00
Na	0.52	0.45	0.48	0.56	0.46	0.45	0.47
K	0.03	0.02	0.02	0.03	0.02	0.02	0.03
Cation Sum	**5.07**	**5.05**	**5.06**	**5.07**	**5.06**	**5.06**	**5.05**
An	0.66	0.72	0.70	0.62	0.71	0.72	0.69
Ab	0.33	0.27	0.29	0.36	0.28	0.27	0.30
Or	0.02	0.01	0.01	0.02	0.01	0.01	0.02

89

Table 1T- Microprobe Analyses of Plagioclase Phenocrysts

	GRB-O4352-13pl	GRB-SB2978-1pl	GRB-SB2978-1pl	GRB-SB2978-5pl	GRB-SB2978-5pl	GRB-SB2978-6pl	GRB-SBM2269-1pl
SiO_2	54.76	53.27	53.64	52.65	60.41	53.00	54.47
TiO_2	0.07	0.05	0.08	0.07	0.05	0.01	0.10
Al_2O_3	27.21	28.84	28.40	28.86	24.48	28.36	28.16
Cr_2O_3	0.00	0.00	0.07	0.00	0.03	0.07	0.00
MgO	0.10	0.15	0.16	0.15	0.05	0.16	0.20
CaO	10.92	11.93	11.60	12.26	6.49	12.19	10.73
FeO	0.72	0.50	0.81	0.70	0.69	0.55	1.92
MnO	0.00	0.00	0.00	0.03	0.00	0.03	0.00
Na_2O	5.68	5.20	5.28	4.74	8.05	4.96	4.41
K_2O	0.33	0.22	0.24	0.20	0.70	0.23	0.42
Total	**99.79**	**100.17**	**100.26**	**99.67**	**100.93**	**99.57**	**100.40**
Structural Formulae							
Cations per 8 Oxygen							
Si	2.49	2.42	2.44	2.41	2.69	2.42	2.47
Ti	0.00	0.00	0.00	0.00	0.00	0.00	0.00
Al (IV)	1.46	1.54	1.52	1.56	1.28	1.53	1.50
Al (VI)							
Cr	0.00	0.00	0.00	0.00	0.00	0.00	0.00
Mg	0.01	0.01	0.01	0.01	0.00	0.01	0.01
Ca	0.53	0.58	0.56	0.60	0.31	0.60	0.52
Fe	0.03	0.02	0.03	0.03	0.03	0.02	0.07
Mn	0.00	0.00	0.00	0.00	0.00	0.00	0.00
Na	0.50	0.46	0.46	0.42	0.69	0.44	0.39
K	0.02	0.01	0.01	0.01	0.04	0.01	0.02
Cation sum	**5.04**	**5.04**	**5.04**	**5.03**	**5.04**	**5.04**	**4.99**
An	0.67	0.71	0.70	0.74	0.46	0.72	0.72
Ab	0.32	0.28	0.29	0.26	0.51	0.27	0.27
Or	0.01	0.01	0.01	0.01	0.03	0.01	0.02

90

Table 1U- Microprobe Analyses of Plagioclase Phenocrysts

	GRB-SBM2269-1pl	GRB-SBM2269-2pl	GRB-SBM2269-2pl	GRB-SBM2269-4pl	GRB-SBM2269-4pl	GRB-SBM2269-6pl	GRB-SBM2269-6pl
SiO2	54.86	54.23	55.16	53.64	54.50	54.32	54.02
TiO2	0.12	0.22	0.23	0.17	0.19	0.20	0.19
Al2O3	28.93	27.92	27.31	27.33	27.46	27.79	28.03
Cr2O3	0.00	0.17	0.14	0.16	0.11	0.15	0.16
MgO	0.11	0.31	0.29	0.32	0.34	0.29	0.31
CaO	11.26	12.17	11.29	12.15	12.00	11.95	12.36
FeO	0.65	0.70	0.76	0.86	0.88	0.66	0.82
MnO	0.01	0.12	0.11	0.06	0.08	0.09	0.12
Na2O	4.76	4.52	4.89	4.41	4.43	4.53	4.41
K2O	0.28	0.30	0.42	0.32	0.37	0.33	0.30
Total	**100.97**	**100.64**	**100.60**	**99.42**	**100.36**	**100.29**	**100.73**
Structural Formulae							
Cations per 8 Oxygen							
Si	2.46	2.46	2.50	2.46	2.47	2.47	2.45
Ti	0.00	0.00	0.00	0.00	0.00	0.00	0.00
Al (IV)	1.53	1.49	1.46	1.48	1.47	1.49	1.50
Al (VI)							
Cr	0.00	0.00	0.00	0.00	0.00	0.00	0.00
Mg	0.01	0.02	0.02	0.02	0.02	0.02	0.02
Ca	0.54	0.59	0.55	0.60	0.58	0.58	0.60
Fe	0.02	0.03	0.03	0.03	0.03	0.02	0.03
Mn	0.00	0.00	0.00	0.00	0.00	0.00	0.00
Na	0.41	0.40	0.43	0.39	0.39	0.40	0.39
K	0.02	0.02	0.02	0.02	0.02	0.02	0.02
Cation Sum	**4.99**	**5.00**	**5.00**	**5.00**	**5.00**	**5.00**	**5.00**
An	0.72	0.74	0.71	0.74	0.74	0.74	0.75
Ab	0.27	0.25	0.28	0.24	0.25	0.25	0.24
Or	0.01	0.01	0.02	0.01	0.01	0.01	0.01

91

Table 1V- Microprobe Analyses of Plagioclase Phenocrysts

	GRB-SBM2269-6pl	GRB-SBM2269-6pl	GRB-SBM2269-7pl	GRB-SBM2269-8pl	GRB-SBM2269-8pl	GRB-SM2570-1pl	GRB-SBM2570-1pl
SiO2	54.21	54.08	49.24	58.10	55.03	53.79	53.80
TiO2	0.24	0.21	0.01	0.07	0.00	0.03	0.09
Al2O3	26.87	27.91	31.73	25.24	27.62	28.75	28.76
Cr2O3	0.12	0.18	0.01	0.00	0.00	0.00	0.03
MgO	0.34	0.34	0.18	0.03	0.03	0.15	0.16
CaO	11.29	12.37	16.44	8.73	11.30	12.55	12.48
FeO	1.07	0.73	0.40	0.62	0.69	0.62	0.53
MnO	0.08	0.14	0.01	0.03	0.02	0.04	0.01
Na2O	4.57	4.39	2.09	6.17	4.64	3.94	4.09
K2O	0.40	0.33	0.06	0.50	0.29	0.21	0.20
Total	**99.17**	**100.69**	**100.16**	**99.49**	**99.61**	**100.08**	**100.14**
Structural Formulae							
Cations per 8 Oxygen							
Si	2.49	2.45	2.25	2.63	2.50	2.44	2.44
Ti	0.00	0.00	0.00	0.00	0.00	0.00	0.00
Al (IV)	1.46	1.49	1.71	1.34	1.48	1.54	1.54
Al (VI)							
Cr	0.00	0.00	0.00	0.00	0.00	0.00	0.00
Mg	0.02	0.02	0.01	0.00	0.00	0.01	0.01
Ca	0.56	0.60	0.81	0.42	0.55	0.61	0.61
Fe	0.04	0.03	0.02	0.02	0.03	0.02	0.02
Mn	0.00	0.00	0.00	0.00	0.00	0.00	0.00
Na	0.41	0.39	0.19	0.54	0.41	0.35	0.36
K	0.02	0.02	0.00	0.03	0.02	0.01	0.01
Cation sum	**5.00**	**5.00**	**4.99**	**4.99**	**4.98**	**4.97**	**4.98**
An	0.72	0.75	0.90	0.60	0.72	0.77	0.77
Ab	0.26	0.24	0.10	0.38	0.27	0.22	0.23
Or	0.02	0.01	0.00	0.02	0.01	0.01	0.01

Table 1W- Microprobe Analyses of Plagioclase Phenocrysts

	GRB-SBM2570-1pl	GRB-SBM2570-4pl	GRB-SBM2570-6pl	GRB-SBM2570-6pl	GRB-SBM2570-6pl	GRB-SBM2570-7pl	GRB-SBM2570-7pl
SiO_2	53.25	55.73	55.00	53.18	55.48	52.86	54.48
TiO_2	0.09	0.03	0.11	0.07	0.10	0.03	0.01
Al_2O_3	28.87	27.31	27.65	28.59	27.28	28.91	27.98
Cr_2O_3	0.00	0.00	0.00	0.00	0.00	0.01	0.00
MgO	0.13	0.10	0.14	0.15	0.10	0.16	0.16
CaO	12.86	11.11	11.50	12.47	11.11	12.13	11.61
FeO	0.69	0.71	0.58	0.76	0.74	0.64	0.68
MnO	0.00	0.00	0.02	0.00	0.01	0.00	0.00
Na_2O	4.06	4.78	4.94	4.40	5.19	4.31	4.64
K_2O	0.20	0.28	0.30	0.22	0.40	0.22	0.30
Total	**100.14**	**100.04**	**100.25**	**99.84**	**100.41**	**99.27**	**99.87**
Structural Formulae							
Cations per 8 Oxygen							
Si	2.42	2.52	2.49	2.42	2.51	2.42	2.47
Ti	0.00	0.00	0.00	0.00	0.00	0.00	0.00
Al (IV)	1.55	1.45	1.47	1.54	1.45	1.56	1.50
Al (VI)							
Cr	0.00	0.00	0.00	0.00	0.00	0.00	0.00
Mg	0.01	0.01	0.01	0.01	0.01	0.01	0.01
Ca	0.63	0.54	0.56	0.61	0.54	0.59	0.56
Fe	0.03	0.03	0.02	0.03	0.03	0.02	0.03
Mn	0.00	0.00	0.00	0.00	0.00	0.00	0.00
Na	0.36	0.42	0.43	0.39	0.45	0.38	0.41
K	0.01	0.02	0.02	0.01	0.02	0.01	0.02
Cation Sum	**4.99**	**4.97**	**5.00**	**5.01**	**5.01**	**5.00**	**4.99**
An	0.77	0.71	0.71	0.75	0.69	0.75	0.73
Ab	0.22	0.28	0.28	0.24	0.29	0.24	0.26
Or	0.01	0.01	0.01	0.01	0.01	0.01	0.01

Table 1X- Microprobe Analyses of Plagioclase Phenocrysts

	GRB-SBM2570-7pl	GRB-U3406-1pl	GRB-U3406-1pl	GRB-U3406-1pl	GRB-U3406-4pl	GRB-U3406-5pl
SiO2	55.66	56.85	56.29	56.51	55.02	55.02
TiO2	0.09	0.06	0.11	0.04	0.07	0.12
Al2O3	27.04	25.97	27.13	26.54	27.55	26.83
Cr2O3	0.00	0.00	0.03	0.00	0.00	0.00
MgO	0.07	0.27	0.13	0.14	0.14	0.29
CaO	10.68	9.74	10.28	10.28	11.44	10.68
FeO	0.64	1.22	0.87	0.92	0.62	1.14
MnO	0.00	0.00	0.04	0.02	0.03	0.06
Na2O	5.18	5.33	5.36	5.35	4.61	4.74
K2O	0.39	0.41	0.29	0.36	0.23	0.29
Total	**99.75**	**99.86**	**100.52**	**100.15**	**99.72**	**99.15**
Structural Formulae						
Cations per 8 Oxygen						
Si	2.52	2.57	2.53	2.55	2.50	2.51
Ti	0.00	0.00	0.00	0.00	0.00	0.00
Al (IV)	1.44	1.38	1.44	1.41	1.47	1.45
Al (VI)						
Cr	0.00	0.00	0.00	0.00	0.00	0.00
Mg	0.00	0.02	0.01	0.01	0.01	0.02
Ca	0.52	0.47	0.50	0.50	0.56	0.52
Fe	0.02	0.05	0.03	0.03	0.02	0.04
Mn	0.00	0.00	0.00	0.00	0.00	0.00
Na	0.46	0.47	0.47	0.47	0.41	0.42
K	0.02	0.02	0.02	0.02	0.01	0.02
Cation sum	**4.99**	**4.98**	**4.99**	**4.99**	**4.98**	**4.98**
An	0.68	0.66	0.67	0.67	0.73	0.71
Ab	0.30	0.33	0.32	0.32	0.26	0.28
Or	0.01	0.02	0.01	0.01	0.01	0.01

Table 2A- Microprobe Analyses of Pyroxene Phenocrysts

	GRB-2-1ac	GRB2-1br1	GRB2-1b2	GRB2-1b3	GRB2-1c1	GRB2-1c2	GRB2-1c3
SiO_2	51.60	52.67	51.31	50.77	51.85	50.74	49.79
TiO_2	0.80	0.92	1.02	1.01	0.72	1.01	0.70
Al_2O_3	3.21	1.87	3.62	3.70	0.47	3.27	4.08
Cr_2O_3	0.05	0.01	0.05	0.05	0.03	0.03	0.05
MgO	16.07	14.67	14.66	14.70	11.61	15.10	13.26
CaO	15.67	17.39	17.85	17.03	15.80	16.63	13.95
FeO	12.70	13.10	11.55	11.67	19.57	12.39	15.26
MnO	0.32	0.26	0.31	0.27	0.48	0.30	0.28
Na_2O	0.37	0.32	0.46	0.40	0.25	0.34	0.32
K_2O	0.00	0.00	0.00	0.01	0.02	0.00	0.11
Total	**100.79**	**101.21**	**100.83**	**99.61**	**100.80**	**99.81**	**97.80**
Structural Formulae							
Cations per 6 Oxygen							
Si	1.91	1.95	1.90	1.90	1.90	1.90	1.92
Ti	0.02	0.03	0.03	0.03	0.03	0.03	0.02
Al (IV)	0.09	0.05	0.10	0.10	0.10	0.10	0.08
Al (VI)	0.05	0.03	0.06	0.06	0.00	0.05	0.10
Cr	0.00	0.00	0.00	0.00	0.06	0.00	0.00
Mg	0.89	0.81	0.81	0.82	0.00	0.84	0.76
Ca	0.62	0.69	0.71	0.68	0.82	0.67	0.57
Fe	0.39	0.41	0.36	0.37	0.68	0.39	0.49
Mn	0.01	0.01	0.01	0.01	0.37	0.01	0.01
Na	0.03	0.02	0.03	0.03	0.01	0.02	0.02
K	0.00	0.00	0.00	0.00	0.03	0.00	0.01
$Fe3+$	0.06	0.06	0.05	0.05	0.10	0.06	0.07
$Fe2+$	0.33	0.34	0.30	0.30	0.57	0.32	0.41
M1	1.02	0.93	0.95	0.97	0.20	0.98	0.96
M2	0.98	1.05	1.04	1.02	1.40	1.02	1.01
Cation Sum	**4.00**	**3.99**	**4.00**	**4.00**	**3.99**	**4.00**	**3.98**
Mg #	0.69	0.67	0.70	0.69	0.52	0.69	0.61

95

Table 2B- Microprobe Analyses of Pyroxene Phenocrysts

	GRB2-14	GRB2-2ac	GRB2-2b1r	GRB2-2b2	GRB2-2b3	GRB2-2b4	GRB-3-3pyc
SiO2	51.33	51.39	52.17	51.05	49.79	51.17	52.72
TiO2	0.87	1.02	0.83	0.89	1.22	1.04	0.15
Al2O3	3.37	3.68	1.89	3.50	4.30	3.87	0.44
Cr2O3	0.04	0.04	0.02	0.01	0.03	0.04	0.00
MgO	15.70	15.54	14.71	15.04	14.05	15.21	20.41
CaO	15.12	16.58	17.68	17.29	16.77	16.29	4.20
FeO	12.54	12.65	12.80	11.55	13.35	12.19	21.45
MnO	0.29	0.31	0.36	0.30	0.31	0.35	0.50
Na2O	0.38	0.39	0.30	0.42	0.45	0.40	0.05
K2O	0.00	0.01	0.01	0.00	0.00	0.00	0.00
Total	**99.63**	**101.61**	**100.77**	**100.06**	**100.26**	**100.56**	**99.91**
Structural Formulae							
Cations per 6 Oxygen							
Si	1.92	1.89	1.94	1.90	1.87	1.90	1.98
Ti	0.02	0.03	0.02	0.02	0.03	0.03	0.00
Al (IV)	0.08	0.11	0.06	0.10	0.13	0.10	0.02
Al (VI)	0.07	0.05	0.03	0.06	0.06	0.07	0.00
Cr	0.00	0.00	0.00	0.00	0.00	0.00	0.00
Mg	0.87	0.85	0.82	0.84	0.79	0.84	1.14
Ca	0.61	0.65	0.71	0.69	0.67	0.65	0.17
Fe	0.39	0.39	0.40	0.36	0.42	0.38	0.67
Mn	0.01	0.01	0.01	0.01	0.01	0.01	0.02
Na	0.03	0.03	0.02	0.03	0.03	0.03	0.00
K	0.00	0.00	0.00	0.00	0.00	0.00	0.00
Fe3+	0.06	0.06	0.06	0.05	0.06	0.06	0.10
Fe2+	0.33	0.32	0.33	0.30	0.35	0.32	0.56
M1	1.02	0.99	0.93	0.97	0.94	0.99	1.25
M2	0.96	1.01	1.06	1.02	1.06	0.99	0.73
Cation Sum	**3.99**	**4.01**	**4.00**	**4.00**	**4.01**	**4.00**	**4.00**
Mg #	0.69	0.69	0.67	0.70	0.65	0.69	0.63

96

Table 2C- Microprobe Analyses of Pyroxene Phenocrysts

	GRB-3-3ln4c1	GRB-3-3ln42	GRB-3-3ln43	GRB-3-3ln44	GRB-3-3pyr	GRB-3-3pyr2	GRB-3-3pyr3
SiO_2	53.55	53.76	52.57	52.18	53.54	51.32	51.98
TiO_2	0.23	0.15	0.31	0.46	0.19	0.33	0.41
Al_2O_3	0.77	1.76	0.82	1.86	1.75	1.33	1.72
Cr_2O_3	0.00	0.00	0.00	0.00	0.00	0.00	0.00
MgO	20.62	22.63	18.63	16.16	22.38	13.45	15.64
CaO	4.42	5.26	5.64	15.20	5.97	13.68	14.50
FeO	19.92	15.11	20.82	12.83	16.52	19.98	15.94
MnO	0.46	0.38	0.44	0.31	0.37	0.50	0.33
Na_2O	0.05	0.08	0.08	0.18	0.12	0.23	0.22
K_2O	0.00	0.00	0.00	0.00	0.01	0.00	0.00
Total	**100.02**	**99.12**	**99.31**	**99.18**	**100.84**	**100.82**	**100.74**

Structural Formulae

Cations per 6 Oxygen

Si	1.99	1.98	1.99	1.96	1.95	1.95	1.95
Ti	0.01	0.00	0.01	0.01	0.01	0.01	0.01
Al (IV)	0.01	0.02	0.01	0.04	0.05	0.05	0.05
Al (VI)	0.02	0.05	0.02	0.04	0.03	0.01	0.02
Cr	0.00	0.00	0.00	0.00	0.00	0.00	0.00
Mg	1.14	1.24	1.05	0.90	1.22	0.76	0.87
Ca	0.18	0.21	0.23	0.61	0.23	0.56	0.58
Fe	0.62	0.46	0.66	0.40	0.50	0.64	0.50
Mn	0.01	0.01	0.01	0.01	0.01	0.02	0.01
Na	0.00	0.01	0.01	0.01	0.01	0.02	0.02
K	0.00	0.00	0.00	0.00	0.00	0.00	0.00
Fe^{3+}	0.09	0.07	0.10	0.06	0.08	0.10	0.07
Fe^{2+}	0.52	0.39	0.55	0.34	0.42	0.53	0.42
M1	1.27	1.37	1.18	1.02	1.33	0.88	0.98
M2	0.70	0.60	0.78	0.96	0.66	1.11	1.01
Cation Sum	**3.98**	**3.98**	**3.98**	**3.99**	**4.00**	**4.00**	**4.00**
Mg #	0.65	0.73	0.62	0.69	0.71	0.55	0.64

97

Table 2D- Microprobe Analyses of Pyroxene Phenocrysts

	GRB-3-3lnc1	GRB-3-3ln2	GRB-3-3ln3	GRB-3-3pc	GRB-3-3p1r	GRB-3-6p2	GRB-3-6p2
SiO_2	51.90	52.39	52.00	51.89	51.26	51.82	52.07
TiO_2	0.35	0.40	0.18	0.39	0.29	0.14	0.19
Al_2O_3	1.54	1.47	0.56	1.54	1.08	0.55	0.64
Cr_2O_3	0.00	0.00	0.00	0.00	0.00	0.00	0.00
MgO	15.00	15.00	17.66	14.85	13.07	15.95	19.83
CaO	17.03	17.30	4.53	16.99	12.43	3.84	4.38
FeO	12.64	13.14	25.00	12.97	21.03	26.57	21.76
MnO	0.36	0.26	0.57	0.30	0.40	0.53	0.42
Na_2O	0.20	0.24	0.07	0.24	0.21	0.05	0.08
K_2O	0.00	0.00	0.00	0.01	0.00	0.01	0.00
Total	**99.02**	**100.19**	**100.57**	**99.18**	**99.77**	**99.46**	**99.37**
Structural Formulae							
Cations per 6 Oxygen							
Si	1.96	1.96	1.98	1.96	1.97	2.00	1.97
Ti	0.01	0.01	0.01	0.01	0.01	0.00	0.01
Al (IV)	0.04	0.04	0.02	0.04	0.03	0.00	0.03
Al (VI)	0.03	0.03	0.00	0.03	0.02	0.03	0.00
Cr	0.00	0.00	0.00	0.00	0.00	0.00	0.00
Mg	0.85	0.84	1.00	0.84	0.75	0.92	1.12
Ca	0.69	0.69	0.18	0.69	0.51	0.16	0.18
Fe	0.40	0.41	0.79	0.41	0.68	0.86	0.69
Mn	0.01	0.01	0.02	0.01	0.01	0.02	0.01
Na	0.01	0.02	0.01	0.02	0.02	0.00	0.01
K	0.00	0.00	0.00	0.00	0.00	0.00	0.00
Fe3+	0.06	0.06	0.12	0.06	0.10	0.13	0.10
Fe2+	0.33	0.34	0.66	0.34	0.56	0.71	0.57
M1	0.95	0.94	1.13	0.94	0.88	1.08	1.23
M2	1.04	1.05	0.85	1.05	1.09	0.88	0.76
Cation Sum	**3.99**	**4.00**	**4.00**	**4.00**	**3.99**	**3.97**	**4.00**
Mg #	0.68	0.67	0.56	0.67	0.53	0.52	0.62

98

Table 2E- Microprobe Analyses of Pyroxene Phenocrysts

	GRB-3-6cpc	GRB-8-2pyxr	GRB-8-2pyx2c	GRB-10-1py	GRB-10-2py	GRB-13-3PY	GRB-16-3py
SiO_2	51.91	51.78	51.35	53.01	51.14	51.14	51.75
TiO_2	0.14	0.87	1.15	0.46	0.93	0.90	0.84
Al_2O_3	0.51	3.55	2.58	2.33	2.80	2.61	2.51
Cr_2O_3	0.00	0.25	0.16	0.21	0.06	0.06	0.19
MgO	16.55	16.39	16.58	16.38	14.98	15.16	16.73
CaO	3.76	16.80	12.89	19.04	17.73	16.68	15.30
FeO	29.02	9.87	14.62	7.99	10.53	12.74	10.67
MnO	0.57	0.25	0.37	0.20	0.28	0.30	0.31
Na_2O	0.05	0.32	0.24	0.29	0.31	0.32	0.26
K_2O	0.00	0.02	0.01	0.00	0.00	0.00	0.00
Total	**102.51**	**100.10**	**99.96**	**99.90**	**98.75**	**99.91**	**98.55**
Structural Formulae							
Cations per 6 Oxygen							
Si	1.97	1.91	1.92	1.95	1.93	1.92	1.94
Ti	0.00	0.02	0.03	0.01	0.03	0.03	0.02
Al (IV)	0.03	0.09	0.08	0.05	0.07	0.08	0.06
Al (VI)	-0.01	0.06	0.03	0.05	0.05	0.03	0.05
Cr	0.00	0.01	0.00	0.01	0.00	0.00	0.01
Mg	0.93	0.90	0.92	0.90	0.84	0.85	0.93
Ca	0.15	0.66	0.52	0.75	0.72	0.67	0.61
Fe	0.92	0.30	0.46	0.25	0.33	0.40	0.33
Mn	0.02	0.01	0.01	0.01	0.01	0.01	0.01
Na	0.00	0.02	0.02	0.02	0.02	0.02	0.02
K	0.00	0.00	0.00	0.00	0.00	0.00	0.00
Fe3+	0.14	0.05	0.07	0.04	0.05	0.06	0.05
Fe2+	0.77	0.25	0.38	0.20	0.28	0.33	0.28
M1	1.06	1.04	1.06	1.01	0.97	0.97	1.06
M2	0.92	0.94	0.91	0.98	1.01	1.03	0.91
Cation Sum	**4.01**	**3.99**	**3.99**	**3.99**	**3.99**	**4.00**	**3.98**
Mg #	0.51	0.75	0.67	0.79	0.72	0.68	0.74

99

Table 2F- Microprobe Analyses of Pyroxene Phenocrysts

	GRB-16-5pyc	GRB-16-5pyr	GRB-16-6py	GRB-16-7pyc	GRB-16-7pyr	GRB-17-1pyc	GRB-18-1
SiO2	51.89	51.69	51.59	53.24	51.46	50.01	51.85
TiO2	0.84	0.92	0.91	0.40	0.79	0.48	0.34
Al2O3	1.80	3.05	2.65	0.90	2.61	3.31	4.05
Cr2O3	0.07	0.16	0.08	0.05	0.23	0.52	0.03
MgO	14.61	15.98	17.33	20.40	16.04	14.95	15.11
CaO	17.49	16.23	14.11	4.70	16.32	18.00	16.00
FeO	12.61	11.12	12.29	20.15	10.94	9.76	13.82
MnO	0.26	0.28	0.32	0.46	0.27	0.26	0.34
Na2O	0.28	0.28	0.20	0.07	0.30	0.28	0.33
K2O	0.00	0.00	0.00	0.00	0.01	0.02	0.01
Total	**99.84**	**99.70**	**99.48**	**100.37**	**98.97**	**97.58**	**101.88**
Structural Formulae							
Cations per 6 Oxygen							
Si	1.95	1.92	1.92	1.98	1.93	1.91	1.91
Ti	0.02	0.03	0.03	0.01	0.02	0.01	0.01
Al (IV)	0.05	0.08	0.08	0.02	0.07	0.09	0.09
Al (VI)	0.03	0.06	0.04	0.02	0.04	0.05	0.08
Cr	0.00	0.00	0.00	0.00	0.01	0.02	0.00
Mg	0.82	0.89	0.96	1.13	0.90	0.85	0.83
Ca	0.70	0.65	0.56	0.19	0.66	0.74	0.63
Fe	0.40	0.35	0.38	0.63	0.34	0.31	0.42
Mn	0.01	0.01	0.01	0.01	0.01	0.01	0.01
Na	0.02	0.02	0.01	0.01	0.02	0.02	0.02
K	0.00	0.00	0.00	0.00	0.00	0.00	0.00
Fe3+	0.06	0.05	0.06	0.09	0.05	0.05	0.06
Fe2+	0.33	0.29	0.32	0.52	0.29	0.26	0.35
M1	0.93	1.02	1.09	1.25	1.02	0.98	0.98
M2	1.05	0.95	0.90	0.71	0.96	1.01	1.01
Cation Sum	**3.99**	**3.99**	**3.99**	**3.98**	**3.99**	**4.00**	**4.00**
Mg #	0.68	0.72	0.72	0.65	0.72	0.73	0.66

100

Table 2G- Microprobe Analyses of Pyroxene Phenocrysts

	CHI-16-1py	CHI-1-16-py1	CHI-16-2pyln1	CHI-16-2pyln2	CHI-17-1py	CHI-17-2cplnc1	CHI-17-2cpln2
SiO2	51.50	52.87	50.44	50.04	50.74	49.99	50.85
TiO2	0.89	0.86	0.87	1.22	0.98	0.99	0.73
Al2O3	3.64	2.56	3.10	3.63	2.66	4.30	3.40
Cr2O3	0.05	0.05	0.08	0.01	0.04	0.04	0.04
MgO	14.96	15.03	14.96	14.35	15.15	14.67	15.06
CaO	16.69	18.08	17.60	17.72	14.34	16.42	16.27
FeO	12.20	11.56	11.20	12.72	14.72	12.22	12.49
MnO	0.29	0.26	0.32	0.32	0.42	0.32	0.31
Na2O	0.37	0.34	0.39	0.36	0.27	0.39	0.38
K2O	0.00	0.00	0.00	0.01	0.00	0.00	0.01
Total	**100.59**	**101.60**	**98.95**	**100.37**	**99.33**	**99.34**	**99.55**
Structural Formulae							
Cations per 6 Oxygen							
Si	1.91	1.94	1.90	1.88	1.92	1.88	1.91
Ti	0.02	0.02	0.02	0.03	0.03	0.03	0.02
Al (IV)	0.09	0.06	0.10	0.12	0.08	0.12	0.09
Al (VI)	0.07	0.05	0.04	0.04	0.04	0.07	0.06
Cr	0.00	0.00	0.00	0.00	0.00	0.00	0.00
Mg	0.83	0.82	0.84	0.80	0.85	0.82	0.84
Ca	0.66	0.71	0.71	0.71	0.58	0.66	0.65
Fe	0.38	0.35	0.35	0.40	0.47	0.38	0.39
Mn	0.01	0.01	0.01	0.01	0.01	0.01	0.01
Na	0.03	0.02	0.03	0.03	0.02	0.03	0.03
K	0.00	0.00	0.00	0.00	0.00	0.00	0.00
Fe3+	0.06	0.05	0.05	0.06	0.07	0.06	0.06
Fe2+	0.32	0.30	0.29	0.33	0.39	0.32	0.33
M1	0.98	0.95	0.96	0.93	0.99	0.98	0.98
M2	1.01	1.03	1.04	1.07	0.99	1.01	1.01
Cation Sum	**3.99**	**3.99**	**4.01**	**4.01**	**3.99**	**4.00**	**4.00**
Mg #	0.69	0.70	0.71	0.67	0.65	0.68	0.68

101

Table 2H - Microprobe Analyses of Pyroxene Phenocrysts

	CHI-17-2cpln3	CHI-17-2cpln4	CHI-17-3py	CHI-19-1pyo	CHI-19-2pyc	CHI-19-2py2r	CHI-19-3pyln1
SiO_2	51.35	51.28	50.27	51.75	51.40	51.56	50.85
TiO_2	0.70	0.81	0.90	0.92	0.93	0.83	0.78
Al_2O_3	3.06	1.67	3.95	1.54	3.06	1.49	2.22
Cr_2O_3	0.07	0.00	0.04	0.06	0.19	0.07	0.14
MgO	15.40	14.52	14.11	14.55	16.85	14.76	15.81
CaO	16.76	16.29	17.14	17.32	15.21	15.82	16.54
FeO	11.93	14.16	12.20	12.16	11.67	14.04	11.48
MnO	0.32	0.32	0.28	0.32	0.26	0.29	0.31
Na_2O	0.34	0.28	0.34	0.23	0.30	0.17	0.22
K_2O	0.01	0.00	0.00	0.02	0.00	0.00	0.00
Total	**99.94**	**99.33**	**99.23**	**98.87**	**99.86**	**99.02**	**98.34**
Structural Formulae							
Cations per 6 Oxygen							
Si	1.92	1.94	1.90	1.96	1.91	1.96	1.93
Ti	0.02	0.02	0.03	0.03	0.03	0.02	0.02
Al (IV)	0.08	0.06	0.10	0.04	0.09	0.04	0.07
Al (VI)	0.05	0.02	0.07	0.03	0.04	0.02	0.03
Cr	0.00	0.00	0.00	0.00	0.01	0.00	0.00
Mg	0.86	0.82	0.79	0.82	0.93	0.83	0.89
Ca	0.67	0.66	0.69	0.70	0.61	0.64	0.67
Fe	0.37	0.45	0.38	0.38	0.36	0.45	0.36
Mn	0.01	0.01	0.01	0.01	0.01	0.01	0.01
Na	0.02	0.02	0.03	0.02	0.02	0.01	0.02
K	0.00	0.00	0.00	0.00	0.00	0.00	0.00
Fe3+	0.06	0.07	0.06	0.06	0.05	0.07	0.05
Fe2+	0.31	0.37	0.32	0.32	0.30	0.37	0.30
M1	0.99	0.93	0.95	0.93	1.06	0.95	1.00
M2	1.01	1.06	1.04	1.04	0.93	1.03	0.99
Cation Sum	**4.00**	**4.00**	**4.00**	**3.98**	**4.00**	**3.98**	**4.00**
Mg #	0.70	0.65	0.68	0.68	0.72	0.65	0.71

102

Table 2I- Microprobe Analyses of Pyroxene Phenocrysts

	CHI-19-3pyln2	CHI-19-3pyln3	CHI-19-3pyln4	CHI-20-2	CHI-21-1cpx	CHI-21-2	CHI-22-1cp
SiO2	51.96	52.03	51.02	53.67	52.66	53.67	52.09
TiO2	0.80	0.78	0.85	0.21	0.76	0.67	0.75
Al2O3	1.57	1.36	1.54	0.94	2.17	1.54	1.48
Cr2O3	0.09	0.08	0.02	0.00	0.00	0.00	0.01
MgO	15.85	15.34	13.98	20.40	14.74	15.78	14.78
CaO	15.66	16.65	15.23	5.22	15.88	13.44	16.34
FeO	12.99	11.85	16.37	19.99	13.42	14.93	13.83
MnO	0.37	0.26	0.38	0.50	0.54	0.58	0.31
Na2O	0.20	0.21	0.21	0.06	0.41	0.32	0.24
K2O	0.01	0.01	0.00	0.00	0.07	0.07	0.01
Total	**99.50**	**98.57**	**99.59**	**100.99**	**100.64**	**101.00**	**99.83**
Structural Formulae							
Cations per 6 Oxygen							
Si	1.95	1.97	1.94	1.98	1.96	1.98	1.96
Ti	0.02	0.02	0.02	0.01	0.02	0.02	0.02
Al (IV)	0.05	0.03	0.06	0.02	0.04	0.02	0.04
Al (VI)	0.02	0.03	0.01	0.02	0.05	0.05	0.02
Cr	0.00	0.00	0.00	0.00	0.00	0.00	0.00
Mg	0.89	0.86	0.79	1.12	0.82	0.87	0.83
Ca	0.63	0.67	0.62	0.21	0.63	0.53	0.66
Fe	0.41	0.37	0.52	0.62	0.42	0.46	0.44
Mn	0.01	0.01	0.01	0.02	0.02	0.02	0.01
Na	0.01	0.02	0.02	0.00	0.03	0.02	0.02
K	0.00	0.00	0.00	0.00	0.00	0.00	0.00
Fe3+	0.06	0.06	0.08	0.09	0.06	0.07	0.07
Fe2+	0.34	0.31	0.43	0.51	0.35	0.38	0.36
M1	0.99	0.97	0.91	1.24	0.95	1.01	0.94
M2	0.98	1.00	1.07	0.73	1.01	0.94	1.04
Cation Sum	**3.99**	**3.98**	**4.00**	**3.98**	**3.98**	**3.97**	**3.99**
Mg #	0.69	0.70	0.60	0.65	0.66	0.65	0.66

103

Table 2J- Microprobe Analyses of Pyroxene Phenocrysts

	CHI-24-6py	CHI-28-1pyc	CHI-28-1py2r	CHI-28-3pyc1	CHI-28-3py2	CHI-28-3py3	CHI-28-3pyr
SiO2	52.38	51.15	52.69	52.85	52.01	52.52	52.68
TiO2	0.88	1.07	0.72	0.70	0.72	0.69	0.88
Al2O3	3.19	2.58	1.73	2.72	3.24	2.46	1.78
Cr2O3	0.06	0.20	0.13	0.32	0.36	0.34	0.10
MgO	15.13	16.20	15.75	17.05	15.85	15.81	15.28
CaO	17.09	16.50	18.45	15.97	18.52	18.83	17.40
FeO	11.20	12.15	10.73	9.64	8.58	8.33	11.38
MnO	0.23	0.26	0.25	0.27	0.17	0.20	0.28
Na2O	0.32	0.23	0.23	0.24	0.27	0.28	0.21
K2O	0.02	0.00	0.01	0.00	0.01	0.00	0.00
Total	**100.49**	**100.34**	**100.69**	**99.75**	**99.74**	**99.46**	**99.99**
Structural Formulae							
Cations per 6 Oxygen							
Si	1.93	1.90	1.95	1.95	1.92	1.95	1.96
Ti	0.02	0.03	0.02	0.02	0.02	0.02	0.02
Al (IV)	0.07	0.10	0.05	0.05	0.08	0.05	0.04
Al (VI)	0.07	0.02	0.02	0.06	0.06	0.05	0.04
Cr	0.00	0.01	0.00	0.01	0.01	0.01	0.00
Mg	0.83	0.90	0.87	0.94	0.87	0.87	0.85
Ca	0.68	0.66	0.73	0.63	0.73	0.75	0.69
Fe	0.35	0.38	0.33	0.30	0.27	0.26	0.35
Mn	0.01	0.01	0.01	0.01	0.01	0.01	0.01
Na	0.02	0.02	0.02	0.02	0.02	0.02	0.02
K	0.00	0.00	0.00	0.00	0.00	0.00	0.00
Fe3+	0.05	0.06	0.05	0.04	0.04	0.04	0.05
Fe2+	0.29	0.32	0.28	0.25	0.22	0.22	0.29
M1	0.98	1.01	0.96	1.07	1.01	0.99	0.96
M2	0.99	0.99	1.02	0.89	0.97	0.98	1.00
Cation Sum	**3.98**	**4.01**	**4.00**	**3.98**	**3.99**	**3.98**	**3.98**
Mg #	0.71	0.70	0.73	0.76	0.77	0.77	0.71

104

Table 2K- Microprobe Analyses of Pyroxene Phenocrysts

	CHI-36-3pylnc1	CHI-36-3pyln2	CHI-36-3pyln3	CHI-36-3pyc	CHI-36-3pyc2	CHI-36-3pyr	CHI-36-3pyr2
SiO_2	53.50	52.32	50.59	52.18	53.11	51.12	51.76
TiO_2	0.65	0.83	1.00	0.78	0.61	0.71	0.71
Al_2O_3	1.00	1.42	1.11	0.88	0.95	0.81	0.76
Cr_2O_3	0.19	0.17	0.17	0.21	0.18	0.19	0.16
MgO	20.47	17.08	10.25	16.89	20.25	14.56	15.11
CaO	5.23	13.02	16.00	5.83	5.59	4.69	4.97
FeO	19.58	16.24	20.32	22.83	18.46	27.91	26.20
MnO	0.00	0.00	0.00	0.00	0.00	0.00	0.00
Na_2O	0.19	0.28	0.38	0.20	0.22	0.20	0.21
K_2O	0.09	0.10	0.10	0.09	0.07	0.08	0.09
Total	**100.90**	**101.46**	**99.92**	**99.87**	**99.44**	**100.27**	**99.98**
Structural Formulae							
Cations per 6 Oxygen							
Si	1.97	1.94	1.96	1.98	1.98	1.98	1.99
Ti	0.02	0.02	0.03	0.02	0.02	0.02	0.02
Al (IV)	0.03	0.06	0.04	0.02	0.02	0.02	0.01
Al (VI)	0.02	0.00	0.01	0.02	0.02	0.01	0.02
Cr	0.01	0.01	0.01	0.01	0.01	0.01	0.00
Mg	1.13	0.94	0.59	0.96	1.13	0.84	0.87
Ca	0.21	0.52	0.66	0.24	0.22	0.19	0.20
Fe	0.60	0.50	0.66	0.72	0.58	0.90	0.84
Mn	0.00	0.00	0.00	0.00	0.00	0.00	0.00
Na	0.01	0.02	0.03	0.01	0.02	0.01	0.02
K	0.00	0.00	0.01	0.00	0.00	0.00	0.00
Fe3+	0.09	0.08	0.10	0.11	0.09	0.14	0.13
Fe2+	0.50	0.42	0.55	0.60	0.48	0.75	0.70
M1	1.26	1.05	0.74	1.11	1.26	1.01	1.04
M2	0.72	0.96	1.24	0.86	0.72	0.96	0.92
Cation Sum	**3.98**	**4.01**	**3.99**	**3.97**	**3.98**	**3.98**	**3.97**
Mg #	0.65	0.65	0.48	0.57	0.66	0.48	0.51

105

Table 2L- Microprobe Analyses of Pyroxene Phenocrysts

	CHI-36-3pyr3	CHI-45-1py2r	CHI-45-1py2bc	CHI-45-1pyc	CHI-45-1pybr	CHI-45-3pyc	CHI-45-3pyr
SiO2	52.02	51.36	54.32	53.58	51.68	49.78	51.57
TiO2	0.93	1.17	0.50	0.63	1.06	1.38	1.04
Al2O3	1.54	2.58	0.90	1.15	1.29	3.74	1.85
Cr2O3	0.18	0.17	0.15	0.20	0.18	0.20	0.18
MgO	14.37	15.78	23.19	22.35	12.60	15.23	14.73
CaO	16.69	15.65	4.79	4.90	14.64	14.72	16.88
FeO	14.81	12.89	16.10	16.59	19.74	14.23	13.85
MnO	0.00	0.16	0.16	0.17	0.17	0.17	0.18
Na2O	0.33	0.37	0.23	0.22	0.38	0.52	0.39
K2O	0.08	0.09	0.08	0.08	0.14	0.07	0.09
Total	**100.95**	**100.23**	**100.41**	**99.86**	**101.88**	**100.05**	**100.76**
Structural Formulae							
Cations per 6 Oxygen							
Si	1.95	1.92	1.98	1.97	1.95	1.87	1.93
Ti	0.03	0.03	0.01	0.02	0.03	0.04	0.03
Al (IV)	0.05	0.08	0.02	0.03	0.05	0.13	0.07
Al (VI)	0.01	0.03	0.02	0.02	0.01	0.04	0.01
Cr	0.01	0.01	0.00	0.01	0.01	0.01	0.01
Mg	0.80	0.88	1.26	1.22	0.71	0.85	0.82
Ca	0.67	0.63	0.19	0.19	0.59	0.59	0.68
Fe	0.46	0.40	0.49	0.51	0.62	0.45	0.43
Mn	0.00	0.01	0.00	0.01	0.01	0.01	0.01
Na	0.02	0.03	0.02	0.02	0.03	0.04	0.03
K	0.00	0.00	0.00	0.00	0.01	0.00	0.00
Fe3+	0.07	0.06	0.07	0.08	0.09	0.07	0.06
Fe2+	0.39	0.34	0.41	0.43	0.52	0.37	0.36
M1	0.92	1.00	1.37	1.34	0.84	1.00	0.93
M2	1.08	0.99	0.61	0.63	1.14	1.00	1.07
Cation Sum	**4.00**	**4.00**	**3.99**	**3.99**	**4.00**	**4.02**	**4.01**
Mg #	0.64	0.69	0.72	0.71	0.53	0.66	0.66

Table 2M- Microprobe Analyses of Pyroxene Phenocrysts

	GRB-O4014-1py	GRB-O4014-2py	GRB-O4014-2py	GRB-O4014-5py	GRB-O4014-6py	GRB-O4014-6py	GRB-O4014-6py
SiO_2	52.54	50.31	51.09	50.41	52.29	53.57	51.95
TiO_2	0.47	1.13	0.75	0.99	0.40	0.25	0.71
Al_2O_3	1.37	2.25	0.92	2.23	0.77	0.80	1.43
Cr_2O_3	0.01	0.00	0.01	0.00	0.00	0.08	0.00
MgO	20.81	13.11	12.04	15.02	20.01	24.10	15.18
CaO	5.37	17.98	10.76	16.48	5.05	2.00	16.43
FeO	19.42	14.17	24.53	13.39	21.31	18.89	12.52
MnO	0.32	0.25	0.47	0.19	0.32	0.34	0.22
Na_2O	0.15	0.36	0.15	0.30	0.08	0.02	0.26
K_2O	0.02	0.00	0.00	0.00	0.00	0.01	0.00
Total	**100.45**	**99.57**	**100.71**	**99.01**	**100.23**	**100.04**	**98.70**
Structural Formulae							
Cations per 6 Oxygen							
Si	1.95	1.92	1.97	1.91	1.96	1.87	1.96
Ti	0.01	0.03	0.02	0.03	0.01	0.01	0.02
Al (IV)	0.05	0.08	0.03	0.09	0.04	0.13	0.04
Al (VI)	0.01	0.02	0.01	0.01	0.00	-0.10	0.03
Cr	0.00	0.00	0.00	0.00	0.00	0.00	0.00
Mg	1.15	0.74	0.69	0.85	1.12	1.57	0.86
Ca	0.21	0.73	0.44	0.67	0.20	0.07	0.67
Fe	0.60	0.45	0.79	0.43	0.67	0.55	0.40
Mn	0.01	0.01	0.02	0.01	0.01	0.00	0.01
Na	0.01	0.03	0.01	0.02	0.01	0.00	0.02
K	0.00	0.00	0.00	0.00	0.00	0.00	0.00
Fe3+	0.09	0.07	0.12	0.06	0.10	0.13	0.06
Fe2+	0.50	0.38	0.66	0.35	0.56	0.31	0.33
M1	1.27	0.86	0.85	0.96	1.23	1.99	0.96
M2	0.73	1.14	1.12	1.05	0.77	-	1.01
Cation Sum	**4.00**	**4.01**	**3.98**	**4.01**	**4.00**	**3.99**	**3.99**
Mg #	0.66	0.62	0.47	0.67	0.63	0.70	0.69

107

Table 2N- Microprobe Analyses of Pyroxene Phenocrysts

	GRB-O4014-6py	GRB-O4014-6py	GRB-O4014-7py	GRB-O4014-7py	GRB-O4014-7py	GRB-O4014-7py	GRB-O4014-7py
SiO_2	51.07	50.55	49.45	50.58	50.45	50.40	50.27
TiO_2	0.61	1.03	1.19	0.69	0.82	0.50	0.96
Al_2O_3	0.73	1.58	2.88	1.28	2.50	0.91	1.45
Cr_2O_3	0.00	0.10	0.02	0.09	0.10	0.00	0.01
MgO	13.97	13.70	14.22	16.31	14.64	15.14	14.50
CaO	4.94	15.48	16.75	10.43	17.58	4.39	13.09
FeO	28.94	16.87	13.92	18.25	12.51	28.57	19.02
MnO	0.38	0.31	0.14	0.35	0.25	0.49	0.22
Na_2O	0.13	0.29	0.30	0.15	0.37	0.08	0.21
K_2O	0.03	0.00	0.01	0.01	0.00	0.03	0.02
Total	**100.80**	**99.90**	**98.88**	**98.13**	**99.21**	**100.50**	**99.73**
Structural Formulae							
Cations per 6 Oxygen							
Si	1.98	1.93	1.89	1.95	1.91	1.95	1.93
Ti	0.02	0.03	0.03	0.02	0.02	0.01	0.03
Al (IV)	0.02	0.07	0.11	0.05	0.09	0.05	0.07
Al (VI)	0.01	0.00	0.02	0.01	0.02	-0.01	-0.01
Cr	0.00	0.00	0.00	0.00	0.00	0.00	0.00
Mg	0.81	0.78	0.81	0.94	0.83	0.87	0.83
Ca	0.20	0.63	0.69	0.43	0.71	0.18	0.54
Fe	0.94	0.54	0.45	0.59	0.40	0.93	0.61
Mn	0.01	0.01	0.00	0.01	0.01	0.02	0.01
Na	0.01	0.02	0.02	0.01	0.03	0.01	0.02
K	0.00	0.00	0.00	0.00	0.00	0.00	0.00
$Fe3+$	0.14	0.08	0.07	0.09	0.06	0.14	0.09
$Fe2+$	0.78	0.45	0.37	0.49	0.33	0.77	0.51
M1	0.97	0.89	0.93	1.05	0.94	1.02	0.94
M2	0.99	1.10	1.08	0.93	1.07	0.96	1.06
Cation Sum	**3.98**	**4.01**	**4.01**	**4.00**	**4.01**	**4.00**	**4.01**
Mg #	0.46	0.59	0.65	0.62	0.68	0.49	0.58

108

Table 2O- Microprobe Analyses of Pyroxene Phenocrysts

	GRB-O4014-9py	GRB-O4014-13py	GRB-O4014-13pyc	GRB-O4014-13pyr	GRB-O4014-13py	GRB-O4014-13py	GRB-O4014-13py
SiO_2	51.52	51.30	51.86	50.17	50.47	51.20	49.59
TiO_2	0.70	0.67	0.50	1.16	0.96	0.66	1.31
Al_2O_3	1.46	1.93	2.20	1.33	1.42	1.04	1.33
Cr_2O_3	0.00	0.17	0.02	0.00	0.02	0.02	0.05
MgO	14.76	15.87	17.46	12.47	14.05	14.87	11.11
CaO	16.59	15.99	4.82	12.73	15.08	12.06	15.67
FeO	13.04	12.98	21.07	21.04	15.87	19.35	19.21
MnO	0.23	0.26	0.28	0.29	0.30	0.28	0.37
Na_2O	0.29	0.22	0.37	0.22	0.25	0.24	0.26
K_2O	0.00	0.00	0.25	0.02	0.01	0.00	0.00
Total	**98.58**	**99.38**	**98.83**	**99.43**	**98.43**	**99.73**	**98.89**
Structural Formulae							
Cations per 6 Oxygen							
Si	1.96	1.93	1.97	1.95	1.94	1.96	1.94
Ti	0.02	0.02	0.01	0.03	0.03	0.02	0.04
Al (IV)	0.04	0.07	0.03	0.05	0.06	0.04	0.06
Al (VI)	0.02	0.02	0.07	0.01	0.01	0.00	0.00
Cr	0.00	0.01	0.00	0.00	0.00	0.00	0.00
Mg	0.84	0.89	0.99	0.72	0.81	0.85	0.65
Ca	0.68	0.65	0.20	0.53	0.62	0.49	0.66
Fe	0.41	0.41	0.67	0.68	0.51	0.62	0.63
Mn	0.01	0.01	0.01	0.01	0.01	0.01	0.01
Na	0.02	0.02	0.03	0.02	0.02	0.02	0.02
K	0.00	0.00	0.01	0.00	0.00	0.00	0.00
Fe^{3+}	0.06	0.06	0.10	0.10	0.08	0.09	0.09
Fe^{2+}	0.35	0.34	0.56	0.57	0.43	0.52	0.52
M1	0.94	0.99	1.17	0.86	0.92	0.96	0.78
M2	1.04	1.00	0.78	1.11	1.07	1.03	1.20
Cation Sum	**3.99**	**4.00**	**3.97**	**3.99**	**4.00**	**4.00**	**3.99**
Mg #	0.67	0.69	0.60	0.52	0.61	0.58	0.51

109

Table 2P- Microprobe Analyses of Pyroxene Phenocrysts

	GRB-O4352-2py	GRB-O4352-2py	GRB-O4352-2py	GRB-O4352-2pyc	GRB-O4352-2pyr	GRB-O4352-3py	GRB-O4352-3py
SiO2	51.16	50.85	48.83	50.36	50.69	51.11	50.69
TiO2	0.73	0.87	1.57	1.14	1.06	0.73	1.00
Al2O3	1.85	2.30	3.34	2.85	1.49	2.14	1.29
Cr2O3	0.03	0.07	0.00	0.06	0.04	0.00	0.00
MgO	19.04	16.05	12.80	15.60	12.91	15.92	12.80
CaO	6.95	13.86	18.04	13.19	14.77	11.70	14.61
FeO	19.24	15.30	13.82	16.74	17.79	18.06	18.26
MnO	0.31	0.27	0.15	0.33	0.30	0.28	0.39
Na2O	0.15	0.29	0.30	0.34	0.29	0.17	0.24
K2O	0.02	0.00	0.02	0.00	0.00	0.00	0.03
Total	**99.48**	**99.86**	**98.87**	**100.60**	**99.33**	**100.11**	**99.30**
Structural Formulae							
Cations per 6 Oxygen							
Si	1.93	1.92	1.87	1.89	1.95	1.93	1.95
Ti	0.02	0.02	0.05	0.03	0.03	0.02	0.03
Al (IV)	0.07	0.08	0.13	0.11	0.05	0.07	0.05
Al (VI)	0.01	0.02	0.03	0.02	0.02	0.03	0.01
Cr	0.00	0.00	0.00	0.00	0.00	0.00	0.00
Mg	1.07	0.90	0.73	0.87	0.74	0.90	0.73
Ca	0.28	0.56	0.74	0.53	0.61	0.47	0.60
Fe	0.61	0.48	0.44	0.53	0.57	0.57	0.59
Mn	0.01	0.01	0.00	0.01	0.01	0.01	0.01
Na	0.01	0.02	0.02	0.02	0.02	0.01	0.02
K	0.00	0.00	0.00	0.00	0.00	0.00	0.00
Fe3+	0.09	0.07	0.07	0.08	0.09	0.09	0.09
Fe2+	0.51	0.40	0.37	0.44	0.48	0.48	0.49
M1	1.20	1.02	0.87	1.01	0.87	1.03	0.86
M2	0.80	0.98	1.13	1.00	1.11	0.96	1.11
Cation Sum	**4.00**	**4.01**	**4.01**	**4.01**	**3.99**	**4.00**	**3.99**
Mg #	0.64	0.65	0.62	0.63	0.57	0.61	0.56

110

Table 2Q- Microprobe Analyses of Pyroxene Phenocrysts

	GRB-O4352-3py	GRB-O4352-3py	GRB-O4352-4py	GRB-O4352-4py	GRB-O4352-4py	GRB-O4352-4py	GRB-O4352-5py
SiO_2	50.86	50.39	50.16	50.94	50.90	50.96	53.58
TiO_2	0.95	1.05	0.96	0.89	0.83	1.05	0.21
Al_2O_3	1.40	3.00	3.26	2.42	2.15	1.50	1.02
Cr_2O_3	0.04	0.08	0.04	0.04	0.07	0.08	0.05
MgO	14.14	14.53	15.01	15.16	15.85	13.16	24.28
CaO	13.83	17.09	17.24	16.38	14.49	16.26	2.14
FeO	17.69	12.98	11.67	13.20	14.43	16.25	18.91
MnO	0.24	0.20	0.17	0.16	0.23	0.25	0.31
Na_2O	0.25	0.39	0.35	0.36	0.33	0.33	0.02
K_2O	0.01	0.01	0.00	0.00	0.00	0.02	0.00
Total	99.39	99.72	98.85	99.54	99.28	99.85	100.53
Structural Formulae							
Cations per 6 Oxygen							
Si	1.95	1.90	1.90	1.92	1.92	1.94	1.86
Ti	0.03	0.03	0.03	0.03	0.02	0.03	0.01
Al (IV)	0.05	0.10	0.10	0.08	0.08	0.06	0.14
Al (VI)	0.01	0.03	0.04	0.03	0.02	0.01	-0.09
Cr	0.00	0.00	0.00	0.00	0.00	0.00	0.00
Mg	0.81	0.82	0.85	0.85	0.89	0.75	1.57
Ca	0.57	0.69	0.70	0.66	0.59	0.66	0.08
Fe	0.57	0.41	0.37	0.42	0.46	0.52	0.55
Mn	0.01	0.01	0.01	0.01	0.01	0.01	0.00
Na	0.02	0.03	0.03	0.03	0.02	0.02	0.00
K	0.00	0.00	0.00	0.00	0.00	0.00	0.00
Fe^{3+}	0.08	0.06	0.06	0.06	0.07	0.08	0.13
Fe^{2+}	0.47	0.34	0.31	0.35	0.38	0.43	0.31
M1	0.93	0.94	0.97	0.97	1.01	0.87	1.99
M2	1.06	1.06	1.03	1.03	0.99	1.12	-
Cation Sum	**3.99**	**4.01**	**4.01**	**4.01**	**4.01**	**4.00**	**4.00**
Mg #	0.59	0.67	0.70	0.67	0.66	0.59	0.70

111

Table 2R- Microprobe Analyses of Pyroxene Phenocrysts

	GRB-O4352-5pyc	GRB-O4352-5pyr	GRB-O4352-6pyc	GRB-O4352-6pyr	GRB-O4352-7pyc	GRB-O4352-7pyr	GRB-O4352-7pyc
SiO_2	51.42	51.24	50.26	51.36	51.41	50.33	51.13
TiO_2	0.39	0.88	1.18	0.84	0.78	0.75	0.87
Al_2O_3	0.87	2.04	2.73	2.22	2.22	0.78	2.62
Cr_2O_3	0.00	0.00	0.06	0.03	0.12	0.02	0.06
MgO	17.12	14.52	14.32	16.06	15.33	11.78	15.16
CaO	4.93	18.06	15.50	13.49	17.50	9.59	16.63
FeO	24.18	11.83	15.03	14.40	11.36	26.25	12.59
MnO	0.30	0.25	0.32	0.26	0.23	0.39	0.33
Na_2O	0.11	0.35	0.33	0.25	0.34	0.17	0.33
K_2O	0.01	0.01	0.00	0.02	0.03	0.00	0.02
Total	**99.31**	**99.18**	**99.73**	**98.92**	**99.32**	**100.06**	**99.74**
Structural Formulae							
Cations per 6 Oxygen							
Si	1.97	1.94	1.90	1.94	1.93	1.97	1.92
Ti	0.01	0.03	0.03	0.02	0.02	0.02	0.02
Al (IV)	0.03	0.06	0.10	0.06	0.07	0.03	0.08
Al (VI)	0.01	0.03	0.03	0.04	0.03	0.00	0.04
Cr	0.00	0.00	0.00	0.00	0.00	0.00	0.00
Mg	0.98	0.82	0.81	0.90	0.86	0.69	0.85
Ca	0.20	0.73	0.63	0.55	0.70	0.40	0.67
Fe	0.78	0.37	0.48	0.45	0.36	0.86	0.40
Mn	0.01	0.01	0.01	0.01	0.01	0.01	0.01
Na	0.01	0.03	0.02	0.02	0.02	0.01	0.02
K	0.00	0.00	0.00	0.00	0.00	0.00	0.00
$Fe3+$	0.12	0.06	0.07	0.07	0.05	0.13	0.06
$Fe2+$	0.65	0.31	0.40	0.38	0.30	0.72	0.33
M1	1.12	0.92	0.94	1.04	0.97	0.84	0.97
M2	0.86	1.07	1.05	0.94	1.03	1.13	1.02
Cation Sum	**3.99**	**4.00**	**4.00**	**3.99**	**4.00**	**3.98**	**4.00**
Mg #	0.56	0.69	0.63	0.67	0.71	0.45	0.68

Table 2S- Microprobe Analyses of Pyroxene Phenocrysts

	GRB-O4352-7pyr	GRB-O4352-7pyr	GRB-O4352-11py	GRB-O4352-11py	GRB-O4352-11py	GRB-SB-2978-3py	GRB-SB2978-4py
SiO2	50.77	49.39	52.00	49.60	52.25	52.09	51.93
TiO2	1.08	0.71	0.64	1.01	0.44	0.63	0.68
Al2O3	1.47	0.56	1.27	2.86	0.64	2.16	2.57
Cr2O3	0.00	0.00	0.00	0.01	0.00	0.06	0.11
MgO	13.15	10.21	17.88	14.78	19.09	16.44	16.87
CaO	15.00	5.35	9.02	16.28	4.63	17.09	16.36
FeO	16.74	33.19	19.15	12.65	22.08	9.90	10.37
MnO	0.25	0.53	0.40	0.20	0.34	0.19	0.15
Na2O	0.24	0.09	0.15	0.34	0.12	0.30	0.39
K2O	0.03	0.01	0.02	0.00	0.01	0.01	0.01
Total	**98.72**	**100.03**	**100.52**	**97.72**	**99.60**	**98.88**	**99.43**
Structural Formulae							
Cations per 6 Oxygen							
Si	1.95	1.97	1.95	1.90	1.98	1.95	1.93
Ti	0.03	0.02	0.02	0.03	0.01	0.02	0.02
Al (IV)	0.05	0.03	0.05	0.10	0.02	0.05	0.07
Al (VI)	0.02	0.00	0.01	0.03	0.01	0.04	0.04
Cr	0.00	0.00	0.00	0.00	0.00	0.00	0.00
Mg	0.75	0.61	1.00	0.85	1.08	0.92	0.93
Ca	0.62	0.23	0.36	0.67	0.19	0.68	0.65
Fe	0.54	1.11	0.60	0.41	0.70	0.31	0.32
Mn	0.01	0.02	0.01	0.01	0.01	0.01	0.00
Na	0.02	0.01	0.01	0.03	0.01	0.02	0.03
K	0.00	0.00	0.00	0.00	0.00	0.00	0.00
Fe3+	0.08	0.17	0.09	0.06	0.10	0.05	0.05
Fe2+	0.45	0.92	0.50	0.34	0.58	0.26	0.27
M1	0.89	0.80	1.11	0.97	1.20	1.02	1.05
M2	1.09	1.16	0.87	1.03	0.78	0.96	0.95
Cation Sum	**3.98**	**3.98**	**4.00**	**4.01**	**3.99**	**3.99**	**4.00**
Mg #	0.59	0.36	0.63	0.68	0.61	0.75	0.75

113

Table 2T - Microprobe Analyses of Pyroxene Phenocrysts

	GRB-SB2978-4py	GRB-SB2978-4py	GRB-SB2978-7pyc	GRB-SB2978-7pyr	GRB-SBM2269-3py	GRB-SBM2269-3py	GRB-SBM2269-5py
SiO_2	50.33	50.33	51.37	50.37	52.20	50.14	51.77
TiO_2	0.86	0.86	0.84	0.94	0.56	1.10	0.76
Al_2O_3	1.08	1.08	3.22	1.26	2.57	1.61	2.65
Cr_2O_3	0.03	0.03	0.02	0.03	0.20	0.06	0.18
MgO	11.46	11.46	15.43	11.58	16.89	11.72	16.45
CaO	13.63	13.63	18.41	16.89	17.50	13.57	17.81
FeO	21.88	21.88	8.92	17.97	9.66	21.72	9.71
MnO	0.37	0.37	0.12	0.26	0.16	0.26	0.15
Na_2O	0.24	0.24	0.38	0.30	0.22	0.23	0.18
K_2O	0.01	0.01	0.00	0.02	0.00	0.03	0.00
Total	**99.88**	**99.88**	**98.71**	**99.61**	**99.95**	**100.43**	**99.65**
Structural Formulae							
Cations per 6 Oxygen							
Si	1.96	1.96	1.92	1.95	1.93	1.93	1.92
Ti	0.03	0.03	0.02	0.03	0.02	0.03	0.02
Al (IV)	0.04	0.04	0.08	0.05	0.07	0.07	0.08
Al (VI)	0.00	0.00	0.06	0.00	0.04	0.01	0.04
Cr	0.00	0.00	0.00	0.00	0.01	0.00	0.01
Mg	0.66	0.66	0.86	0.67	0.93	0.67	0.91
Ca	0.57	0.57	0.74	0.70	0.69	0.56	0.71
Fe	0.71	0.71	0.28	0.58	0.30	0.70	0.30
Mn	0.01	0.01	0.00	0.01	0.00	0.01	0.00
Na	0.02	0.02	0.03	0.02	0.02	0.02	0.01
K	0.00	0.00	0.00	0.00	0.00	0.00	0.00
Fe^{3+}	0.11	0.11	0.04	0.09	0.04	0.11	0.05
Fe^{2+}	0.59	0.59	0.23	0.48	0.25	0.58	0.25
M1	0.80	0.80	0.99	0.78	1.04	0.82	1.02
M2	1.18	1.18	1.00	1.21	0.96	1.16	0.97
Cation Sum	**3.99**	**3.99**	**3.99**	**4.00**	**4.00**	**3.99**	**4.00**
Mg #	0.48	0.48	0.76	0.54	0.76	0.49	0.75

114

Table 2U- Microprobe Analyses of Pyroxene Phenocrysts

	GRB-SBM2269-6py	GRB-SBM2269-6py	GRB-SBM2570-2py	GRB-SBM2570-2py	GRB-SBM2570-2py	GRB-SBM2570-2py	GRB-SBM2570-5py
SiO_2	52.33	52.43	52.08	51.85	53.16	50.47	52.64
TiO_2	0.60	0.54	0.73	0.63	0.45	0.77	0.53
Al_2O_3	1.39	1.73	2.61	2.30	1.20	1.47	2.56
Cr_2O_3	0.06	0.14	0.17	0.05	0.06	0.09	0.19
MgO	16.68	17.15	15.89	16.61	19.24	12.18	20.17
CaO	14.95	15.94	19.06	17.00	8.76	13.90	10.86
FeO	13.55	11.19	9.80	10.72	18.11	21.03	13.45
MnO	0.14	0.21	0.14	0.16	0.30	0.35	0.19
Na_2O	0.15	0.22	0.29	0.25	0.10	0.19	0.19
K_2O	0.03	0.00	0.00	0.00	0.00	0.03	0.00
Total	**99.88**	**99.56**	**100.76**	**99.58**	**101.37**	**100.46**	**100.77**
Structural Formulae							
Cations per 6 Oxygen							
Si	1.96	1.95	1.92	1.93	1.96	1.94	1.92
Ti	0.02	0.02	0.02	0.02	0.01	0.02	0.01
Al (IV)	0.04	0.05	0.08	0.07	0.04	0.06	0.08
Al (VI)	0.02	0.03	0.03	0.03	0.01	0.01	0.03
Cr	0.00	0.00	0.00	0.00	0.00	0.00	0.01
Mg	0.93	0.95	0.87	0.92	1.06	0.70	1.10
Ca	0.60	0.64	0.75	0.68	0.35	0.57	0.43
Fe	0.42	0.35	0.30	0.33	0.56	0.68	0.41
Mn	0.00	0.01	0.00	0.01	0.01	0.01	0.01
Na	0.01	0.02	0.02	0.02	0.01	0.01	0.01
K	0.00	0.00	0.00	0.00	0.00	0.00	0.00
$Fe3+$	0.06	0.05	0.05	0.05	0.08	0.10	0.06
$Fe2+$	0.35	0.29	0.25	0.28	0.47	0.56	0.34
M1	1.03	1.05	0.98	1.02	1.17	0.83	1.22
M2	0.96	0.94	1.03	0.97	0.82	1.15	0.78
Cation Sum	**4.00**	**4.00**	**4.01**	**4.00**	**4.00**	**4.00**	**4.00**
Mg #	0.69	0.73	0.74	0.74	0.66	0.51	0.73

Table 2V - Microprobe Analyses of Pyroxene Phenocrysts

	GRB-SBM2570-6py	GRB-SBM2570-8pyc	GRB-SBM2570-8pyr	GRB-U3406-1py	GRB-U3406-1py	GRB-U3406-1py	GRB-U3406-2py
SiO_2	51.99	52.40	50.88	50.16	51.93	50.63	50.92
TiO_2	0.75	0.80	1.08	1.24	0.68	0.51	0.87
Al_2O_3	2.22	2.85	1.65	3.22	2.70	3.15	3.46
Cr_2O_3	0.06	0.06	0.00	0.08	0.16	0.11	0.08
MgO	17.75	17.43	11.78	14.05	17.43	15.24	15.84
CaO	10.76	15.64	15.79	17.83	14.45	17.30	17.56
FeO	16.86	11.74	18.87	12.90	12.07	10.74	9.76
MnO	0.24	0.24	0.25	0.16	0.20	0.11	0.13
Na_2O	0.14	0.27	0.31	0.36	0.26	0.30	0.35
K_2O	0.02	0.02	0.04	0.00	0.00	0.01	0.00
Total	**100.78**	**101.46**	**100.66**	**99.99**	**99.89**	**98.08**	**98.97**
Structural Formulae							
Cations per 6 Oxygen							
Si	1.93	1.92	1.94	1.89	1.93	1.92	1.90
Ti	0.02	0.02	0.03	0.04	0.02	0.01	0.02
Al (IV)	0.07	0.08	0.06	0.11	0.07	0.08	0.10
Al (VI)	0.03	0.04	0.02	0.03	0.04	0.06	0.06
Cr	0.00	0.00	0.00	0.00	0.00	0.00	0.00
Mg	0.98	0.95	0.67	0.79	0.96	0.86	0.88
Ca	0.43	0.61	0.65	0.72	0.57	0.70	0.70
Fe	0.52	0.36	0.60	0.41	0.37	0.34	0.31
Mn	0.01	0.01	0.01	0.01	0.01	0.00	0.00
Na	0.01	0.02	0.02	0.03	0.02	0.02	0.03
K	0.00	0.00	0.00	0.00	0.00	0.00	0.00
Fe^{3+}	0.08	0.05	0.09	0.06	0.06	0.05	0.05
Fe^{2+}	0.44	0.30	0.50	0.34	0.31	0.28	0.25
M1	1.11	1.07	0.81	0.92	1.09	0.99	1.01
M2	0.87	0.93	1.17	1.08	0.90	1.01	0.98
Cation Sum	**3.99**	**4.00**	**3.99**	**4.01**	**4.00**	**4.00**	**4.00**
Mg #	0.65	0.73	0.53	0.66	0.72	0.72	0.74

Table 2W- Microprobe Analyses of Pyroxene Phenocrysts

	GRB-U3406-2py	GRB-U3406-3py	GRB-U3406-3py	GRB-U3406-3py	GRB-U3406-3py
SiO_2	51.93	51.73	51.88	52.14	50.58
TiO_2	0.69	0.71	0.61	0.56	0.91
Al_2O_3	1.72	1.95	1.38	1.32	3.52
Cr_2O_3	0.12	0.21	0.12	0.12	0.12
MgO	15.72	15.88	15.86	15.92	15.65
CaO	17.20	16.60	16.66	16.68	17.41
FeO	11.89	12.29	12.51	11.96	10.34
MnO	0.19	0.19	0.20	0.19	0.18
Na_2O	0.25	0.28	0.24	0.24	0.32
K_2O	0.02	0.00	0.01	0.02	0.00
Total	**99.72**	**99.85**	**99.48**	**99.14**	**99.02**
Structural Formulae			Cations per 6 Oxygen		
Si	1.94	1.94	1.95	1.96	1.90
Ti	0.02	0.02	0.02	0.02	0.03
Al (IV)	0.06	0.06	0.05	0.04	0.10
Al (VI)	0.02	0.02	0.01	0.02	0.05
Cr	0.00	0.01	0.00	0.00	0.00
Mg	0.88	0.89	0.89	0.89	0.87
Ca	0.69	0.67	0.67	0.67	0.70
Fe	0.37	0.38	0.39	0.38	0.32
Mn	0.01	0.01	0.01	0.01	0.01
Na	0.02	0.02	0.02	0.02	0.02
K	0.00	0.00	0.00	0.00	0.00
Fe3+	0.06	0.06	0.06	0.06	0.05
Fe2+	0.31	0.32	0.33	0.31	0.27
M1	0.98	0.99	0.98	0.99	1.01
M2	1.02	1.01	1.02	1.00	0.99
Cation Sum	**4.00**	**4.00**	**4.00**	**4.00**	**4.00**
Mg #	0.70	0.70	0.69	0.71	0.73

117

Table 3A- Microprobe Analyses of Groundmass Plagioclase

	GR-2-1f	GR-3-09	GR-3-10	GR-13-7pl	GR-13-7pl2	GR-18-1plgm	GR-18-5plgm
SiO_2	55.82	58.49	55.37	58.43	57.04	59.44	58.60
TiO_2	0.07	0.07	0.17	0.13	0.09	0.06	0.02
Al_2O_3	26.90	26.71	26.76	25.58	27.47	26.00	25.85
Cr_2O_3	0.02	0.00	0.00	0.01	0.00	0.00	0.02
MgO	0.09	0.04	0.25	0.27	0.08	0.07	0.09
CaO	10.26	8.89	9.62	8.49	10.55	9.06	9.37
FeO	0.94	0.90	2.02	1.79	0.96	1.06	1.20
MnO	0.01	0.00	0.01	0.01	0.01	0.02	0.03
Na_2O	5.51	6.01	4.70	5.46	5.14	6.05	5.82
K_2O	0.34	0.46	0.48	0.49	0.43	0.40	0.36
Totals	**99.95**	**101.56**	**99.39**	**100.66**	**101.76**	**102.15**	**101.36**
Structural Formulae							
Cations per 8 Oxygen							
Si	2.53	2.59	2.53	2.62	2.53	2.62	2.60
Ti	0.00	0.00	0.00	0.00	0.00	0.00	0.00
Al (IV)	1.44	1.39	1.44	1.35	1.44	1.35	1.35
Al (VI)							
Cr	0.00	0.00	0.00	0.00	0.00	0.00	0.00
Mg	0.01	0.00	0.02	0.02	0.00	0.00	0.01
Ca	0.50	0.42	0.47	0.41	0.50	0.43	0.45
Fe	0.04	0.03	0.08	0.07	0.04	0.04	0.04
Mn	0.00	0.00	0.00	0.00	0.00	0.00	0.00
Na	0.48	0.52	0.42	0.47	0.44	0.52	0.50
K	0.02	0.03	0.03	0.03	0.02	0.02	0.02
Cation Sum	**5.01**	**4.98**	**4.98**	**4.96**	**4.98**	**4.98**	**4.98**
An	0.66	0.61	0.68	0.62	0.68	0.61	0.63
Ab	0.32	0.37	0.30	0.36	0.30	0.37	0.35
Or	0.01	0.02	0.02	0.02	0.02	0.02	0.01

118

Table 3B- Microprobe Analyses of Groundmass Plagioclase

	CHI-16-1-plgm	CHI-16-1-plgm2	CHI-16-2-plgm	CHI-24-6plgm	CHI-24-6plgm2	CHI-28-1plgm	CHI-28-5plgm
SiO2	57.62	55.78	57.25	59.34	57.47	55.16	56.13
TiO2	0.12	0.15	0.12	0.08	0.11	0.09	0.11
Al2O3	25.99	26.15	26.16	24.67	26.50	27.79	27.52
Cr2O3	0.00	0.00	0.02	0.00	0.02	0.01	0.02
MgO	0.09	0.11	0.13	0.05	0.05	0.13	0.15
CaO	9.52	9.77	10.15	7.81	9.76	11.78	11.32
FeO	1.25	1.11	1.05	1.03	0.87	0.85	0.80
MnO	0.03	0.00	0.00	0.00	0.01	0.05	0.01
Na2O	5.56	5.48	5.49	6.29	5.72	4.37	4.45
K2O	0.35	0.36	0.34	0.66	0.43	0.28	0.31
Totals	**100.53**	**98.91**	**100.71**	**99.92**	**100.94**	**100.50**	**100.81**
Structural Formulae							
Cations per 8 Oxygen							
Si	2.59	2.55	2.57	2.67	2.57	2.49	2.52
Ti	0.00	0.00	0.00	0.00	0.00	0.00	0.00
Al (IV)	1.38	1.41	1.38	1.31	1.40	1.48	1.45
Al (VI)							
Cr	0.00	0.00	0.00	0.00	0.00	0.00	0.00
Mg	0.01	0.01	0.01	0.00	0.00	0.01	0.01
Ca	0.46	0.48	0.49	0.38	0.47	0.57	0.54
Fe	0.05	0.04	0.04	0.04	0.03	0.03	0.03
Mn	0.00	0.00	0.00	0.00	0.00	0.00	0.00
Na	0.48	0.49	0.48	0.55	0.50	0.38	0.39
K	0.02	0.02	0.02	0.04	0.02	0.02	0.02
Cation Sum	**4.98**	**5.00**	**4.99**	**4.97**	**4.99**	**4.97**	**4.96**
An	0.65	0.65	0.66	0.56	0.64	0.74	0.73
Ab	0.34	0.33	0.32	0.41	0.34	0.25	0.26
Or	0.01	0.01	0.01	0.03	0.02	0.01	0.01

119

Table 3C- Microprobe Analyses of Groundmass Plagioclase

	CHI-36-1plgm	CHI-36-1pl	CHI-36-2gmpl	GR-O4014-1plgm	GR-O4014-1plgm	GR-O4014-1plgm	GR-O4014-2plgm
SiO_2	56.25	55.32	55.02	57.94	55.01	55.44	54.68
TiO_2	0.27	0.28	0.28	0.11	0.08	0.07	0.39
Al_2O_3	26.16	26.20	25.69	25.82	27.31	26.83	26.94
Cr_2O_3	0.15	0.15	0.16	0.06	0.00	0.00	0.16
MgO	0.20	0.22	0.20	0.05	0.07	0.05	0.25
CaO	9.47	10.99	10.38	8.15	10.24	10.00	10.73
FeO	1.03	0.97	1.07	0.77	1.07	0.98	1.11
MnO	0.16	0.00	0.18	0.00	0.04	0.00	0.08
Na_2O	5.47	4.93	5.18	7.19	5.58	6.14	5.81
K_2O	0.39	0.39	0.37	0.58	0.63	0.54	0.46
Totals	**99.54**	**99.43**	**98.53**	**100.67**	**100.04**	**100.04**	**100.60**
Structural Formulae							
Cations per 8 Oxygen							
Si	2.56	2.53	2.54	2.60	2.50	2.52	2.49
Ti	0.00	0.00	0.00	0.00	0.00	0.00	0.00
Al (IV)	1.40	1.41	1.40	1.37	1.46	1.44	1.45
Al (VI)							
Cr	0.00	0.00	0.00	0.00	0.00	0.00	0.00
Mg	0.01	0.02	0.01	0.00	0.00	0.00	0.02
Ca	0.46	0.54	0.51	0.39	0.50	0.49	0.52
Fe	0.04	0.04	0.04	0.03	0.04	0.04	0.04
Mn	0.00	0.00	0.00	0.00	0.00	0.00	0.00
Na	0.48	0.44	0.46	0.63	0.49	0.54	0.51
K	0.02	0.02	0.02	0.03	0.04	0.03	0.03
Cation Sum	**4.99**	**4.99**	**5.00**	**5.05**	**5.03**	**5.05**	**5.06**
An	0.65	0.70	0.68	0.54	0.65	0.63	0.66
Ab	0.34	0.28	0.31	0.43	0.32	0.35	0.32
Or	0.02	0.01	0.01	0.02	0.02	0.02	0.02

Table 3D - Microprobe Analyses of Groundmass Plagioclase

	GR-O4014-2plgm	GR-O4014-3pl	GR-O4014-4plmp	GR-O4014-8plgm	GR-O4014-8plgm	GR-O4014-10pl	GR-O4014-10pl
SiO_2	56.00	54.53	53.80	53.77	54.73	54.14	54.97
TiO_2	0.39	0.39	0.08	0.08	0.07	0.06	0.08
Al_2O_3	26.26	27.03	27.69	27.39	26.89	28.00	27.11
Cr_2O_3	0.14	0.14	0.04	0.00	0.00	0.01	0.00
MgO	0.22	0.21	0.13	0.12	0.07	0.08	0.09
CaO	9.73	11.02	11.53	11.19	10.67	11.05	10.01
FeO	1.09	1.07	1.03	0.86	0.96	0.87	0.81
MnO	0.11	0.14	0.02	0.00	0.00	0.00	0.06
Na_2O	6.27	5.52	5.35	5.55	5.96	5.54	5.94
K_2O	0.62	0.52	0.27	0.35	0.38	0.34	0.48
Totals	**100.82**	**100.57**	**99.94**	**99.30**	**99.73**	**100.07**	**99.55**
Structural Formulae							
Cations per 8 Oxygen							
Si	2.54	2.48	2.45	2.47	2.50	2.46	2.51
Ti	0.00	0.00	0.00	0.00	0.00	0.00	0.00
Al (IV)	1.40	1.45	1.49	1.48	1.45	1.50	1.46
Al (VI)							
Cr	0.00	0.00	0.00	0.00	0.00	0.00	0.00
Mg	0.01	0.01	0.01	0.01	0.01	0.01	0.01
Ca	0.47	0.54	0.56	0.55	0.52	0.54	0.49
Fe	0.04	0.04	0.04	0.03	0.04	0.03	0.03
Mn	0.00	0.00	0.00	0.00	0.00	0.00	0.00
Na	0.55	0.49	0.47	0.49	0.53	0.49	0.53
K	0.04	0.03	0.02	0.02	0.02	0.02	0.03
Cation Sum	**5.05**	**5.05**	**5.04**	**5.05**	**5.06**	**5.04**	**5.04**
An	0.62	0.68	0.70	0.68	0.66	0.68	0.64
Ab	0.36	0.31	0.29	0.31	0.33	0.31	0.34
Or	0.02	0.02	0.01	0.01	0.01	0.01	0.02

121

Table 3E- Microprobe Analyses of Groundmass Plagioclase

	GR-O4014-10pl	GR-O4014-11pl	GR-O4014-11pl	GR-O4014-12plg	GR-O4014-12plg	GR-O4014-12plg	GR-O4014-13plg
SiO_2	54.72	54.51	54.46	56.77	54.92	56.99	55.12
TiO_2	0.08	0.06	0.11	0.12	0.07	0.13	0.09
Al_2O_3	27.67	27.43	27.88	26.29	27.54	26.58	26.99
Cr_2O_3	0.00	0.00	0.02	0.03	0.06	0.00	0.00
MgO	0.08	0.11	0.09	0.03	0.11	0.04	0.14
CaO	10.34	10.67	10.61	8.94	10.25	9.00	10.28
FeO	0.89	0.83	0.93	0.83	0.77	0.80	0.73
MnO	0.00	0.00	0.00	0.02	0.01	0.00	0.08
Na_2O	5.93	5.72	5.82	6.66	5.91	6.73	6.05
K_2O	0.44	0.37	0.36	0.63	0.37	0.54	0.38
Totals	**100.13**	**99.70**	**100.29**	**100.32**	**100.02**	**100.81**	**99.84**
Structural Formulae							
Cations per 8 Oxygen							
Si	2.48	2.48	2.47	2.56	2.49	2.56	2.51
Ti	0.00	0.00	0.00	0.00	0.00	0.00	0.00
Al (IV)	1.48	1.47	1.49	1.40	1.47	1.41	1.45
Al (VI)							
Cr	0.00	0.00	0.00	0.00	0.00	0.00	0.00
Mg	0.01	0.01	0.01	0.00	0.01	0.00	0.01
Ca	0.50	0.52	0.52	0.43	0.50	0.43	0.50
Fe	0.03	0.03	0.04	0.03	0.03	0.03	0.03
Mn	0.00	0.00	0.00	0.00	0.00	0.00	0.00
Na	0.52	0.51	0.51	0.58	0.52	0.59	0.53
K	0.03	0.02	0.02	0.04	0.02	0.03	0.02
Cation Sum	**5.05**	**5.04**	**5.05**	**5.05**	**5.04**	**5.05**	**5.05**
An	0.65	0.66	0.66	0.58	0.65	0.58	0.64
Ab	0.34	0.32	0.33	0.39	0.34	0.40	0.34
Or	0.02	0.01	0.01	0.02	0.01	0.02	0.01

122

Table 3F- Microprobe Analyses of Groundmass Plagioclase

	GR-O4014-13plg	GR-O4014-13plg	GR-O4352-1plgm	GR-O4352-1plgm	GR-O4352-1plgm	GR-O4352-1plgm	GR-O4352-1plgm
SiO_2	54.33	55.08	54.91	55.68	67.28	55.20	55.26
TiO_2	0.09	0.10	0.09	0.08	0.18	0.10	0.07
Al_2O_3	27.81	27.38	27.29	26.87	18.88	27.28	27.22
Cr_2O_3	0.01	0.00	0.01	0.00	0.01	0.01	0.00
MgO	0.08	0.10	0.08	0.11	0.01	0.07	0.05
CaO	11.10	10.50	10.58	9.83	1.95	10.35	10.52
FeO	0.87	0.75	0.99	0.81	0.60	0.93	0.88
MnO	0.10	0.00	0.05	0.03	0.00	0.00	0.00
Na_2O	5.74	6.09	6.23	6.25	7.54	6.27	5.93
K_2O	0.38	0.37	0.37	0.45	4.22	0.41	0.41
Totals	**100.49**	**100.37**	**100.58**	**100.11**	**100.66**	**100.61**	**100.34**
Structural Formulae							
Cations per 8 Oxygen							
Si	2.46	2.49	2.49	2.52	2.98	2.50	2.50
Ti	0.00	0.00	0.00	0.00	0.00	0.00	0.00
Al (IV)	1.49	1.46	1.46	1.44	0.99	1.45	1.45
Al (VI)							
Cr	0.00	0.00	0.00	0.00	0.00	0.00	0.00
Mg	0.01	0.01	0.01	0.01	0.00	0.00	0.00
Ca	0.54	0.51	0.51	0.48	0.09	0.50	0.51
Fe	0.03	0.03	0.04	0.03	0.02	0.04	0.03
Mn	0.00	0.00	0.00	0.00	0.00	0.00	0.00
Na	0.51	0.53	0.55	0.55	0.65	0.55	0.52
K	0.02	0.02	0.02	0.03	0.24	0.02	0.02
Cation Sum	**5.06**	**5.05**	**5.07**	**5.05**	**4.97**	**5.06**	**5.04**
An	0.67	0.65	0.64	0.62	0.17	0.64	0.65
Ab	0.31	0.34	0.34	0.36	0.60	0.35	0.33
Or	0.01	0.01	0.01	0.02	0.22	0.02	0.02

123

Table 3G- Microprobe Analyses of Groundmass Plagioclase

	GR-O4352-2plgm	GR-O4352-2plgm	GR-O4352-2plgm	GR-O4352-2plgm	GR-O4352-3pl	GR-O4352-4plgm	GR-O4352-4plgm
SiO_2	55.30	55.27	55.61	55.18	55.33	54.02	54.40
TiO_2	0.38	0.38	0.38	0.39	0.40	0.37	0.38
Al_2O_3	26.92	26.52	26.31	26.24	26.59	27.55	27.24
Cr_2O_3	0.26	0.29	0.29	0.32	0.13	0.14	0.17
MgO	0.30	0.28	0.30	0.25	0.26	0.27	0.29
CaO	10.33	10.43	10.01	10.13	10.09	11.41	11.23
FeO	1.07	1.01	1.13	1.08	1.10	0.90	1.07
MnO	0.14	0.14	0.11	0.12	0.13	0.08	0.13
Na_2O	6.00	6.09	6.18	6.28	6.40	5.64	5.59
K_2O	0.42	0.47	0.62	0.53	0.54	0.37	0.38
Totals	**101.13**	**100.87**	**100.93**	**100.52**	**100.97**	**100.75**	**100.88**
Structural Formulae							
Cations per 8 Oxygen							
Si	2.50	2.51	2.52	2.52	2.52	2.46	2.47
Ti	0.00	0.00	0.00	0.00	0.00	0.00	0.00
Al (IV)	1.44	1.42	1.41	1.41	1.41	1.48	1.46
Al (VI)							
Cr	0.00	0.00	0.00	0.00	0.00	0.00	0.00
Mg	0.02	0.02	0.02	0.02	0.00	0.02	0.02
Ca	0.50	0.51	0.49	0.50	0.02	0.56	0.55
Fe	0.04	0.04	0.04	0.04	0.50	0.03	0.04
Mn	0.00	0.00	0.00	0.00	0.00	0.00	0.00
Na	0.53	0.54	0.54	0.56	0.00	0.50	0.49
K	0.02	0.03	0.04	0.03	0.56	0.02	0.02
Cation Sum	**5.05**	**5.06**	**5.06**	**5.07**	**5.00**	**5.06**	**5.05**
An	0.65	0.64	0.63	0.63	0.62	0.68	0.68
Ab	0.34	0.34	0.35	0.35	0.36	0.30	0.31
Or	0.02	0.02	0.02	0.02	0.02	0.01	0.01

Table 3H- Microprobe Analyses of Groundmass Plagioclase

	GR-O4352-4plgm	GR-O4352-6pl	GR-O4352-6pl	GR-O4352-8pl	GR-O4352-8pl	GR-O4352-8pl	GR-O4352-9plgm
SiO_2	54.40	54.15	54.79	54.68	55.41	55.82	54.04
TiO_2	0.38	0.37	0.36	0.37	0.38	0.39	0.38
Al_2O_3	27.24	27.61	27.15	25.26	26.44	26.41	27.63
Cr_2O_3	0.17	0.21	0.13	0.12	0.13	0.16	0.12
MgO	0.29	0.29	0.29	0.31	0.26	0.24	0.26
CaO	11.23	11.32	10.55	9.59	10.19	9.77	11.11
FeO	1.07	1.11	1.08	2.44	1.01	1.09	0.93
MnO	0.13	0.12	0.15	0.12	0.12	0.10	0.12
Na_2O	5.59	5.69	5.98	5.66	6.05	6.67	5.72
K_2O	0.38	0.40	0.50	0.50	0.79	0.60	0.39
Total	**100.88**	**101.26**	**100.97**	**99.06**	**100.79**	**101.24**	**100.71**
Structural Formulae							
Cations per 8 Oxygen							
Si	2.47	2.46	2.49	2.53	2.52	2.52	2.46
Ti	0.00	0.00	0.00	0.00	0.00	0.00	0.00
Al (IV)	1.46	1.48	1.45	1.38	1.42	1.41	1.48
Al (VI)							
Cr	0.00	0.00	0.00	0.00	0.00	0.00	0.00
Mg	0.02	0.02	0.02	0.02	0.02	0.02	0.02
Ca	0.55	0.55	0.51	0.48	0.50	0.47	0.54
Fe	0.04	0.04	0.04	0.09	0.04	0.04	0.04
Mn	0.00	0.00	0.00	0.00	0.00	0.00	0.00
Na	0.49	0.50	0.53	0.51	0.53	0.58	0.50
K	0.02	0.02	0.03	0.03	0.05	0.03	0.02
Cation Sum	**5.05**	**5.07**	**5.07**	**5.05**	**5.06**	**5.08**	**5.06**
An	0.68	0.68	0.65	0.64	0.63	0.60	0.67
Ab	0.31	0.31	0.33	0.34	0.34	0.37	0.31
Or	0.01	0.01	0.02	0.02	0.03	0.02	0.01

125

Table 3I- Microprobe Analyses of Groundmass Plagioclase

	GR-O4352-9plgm	GR-O4352-10pl	GR-O4352-11pl	GR-O4352-11pl	GR-O4352-11pl	GR-O4352-11pl	GR-O4352-12plg
SiO_2	54.52	54.82	56.20	54.78	56.78	55.33	56.81
TiO_2	0.38	0.39	0.07	0.10	0.12	0.07	0.38
Al_2O_3	27.19	27.14	26.55	26.68	25.70	26.92	25.74
Cr_2O_3	0.15	0.19	0.10	0.00	0.03	0.00	0.19
MgO	0.24	0.23	0.12	0.13	0.05	0.11	0.27
CaO	10.85	10.34	9.81	10.28	8.63	9.99	9.44
FeO	1.21	1.09	0.82	0.88	0.86	0.89	0.89
MnO	0.09	0.08	0.03	0.03	0.08	0.00	0.11
Na_2O	5.97	6.24	6.24	6.12	6.93	6.05	6.40
K_2O	0.38	0.46	0.37	0.42	0.57	0.43	0.56
Total	**100.97**	**100.98**	**100.31**	**99.41**	**99.75**	**99.80**	**100.78**
Structural Formulae							
Cations per 8 Oxygen							
Si	2.48	2.49	2.54	2.51	2.58	2.51	2.57
Ti	0.00	0.00	0.00	0.00	0.00	0.00	0.00
Al (IV)	1.46	1.45	1.41	1.44	1.38	1.44	1.37
Al (VI)							
Cr	0.00	0.00	0.00	0.00	0.00	0.00	0.00
Mg	0.02	0.02	0.01	0.01	0.00	0.01	0.02
Ca	0.53	0.50	0.48	0.50	0.42	0.49	0.46
Fe	0.05	0.04	0.03	0.03	0.03	0.03	0.03
Mn	0.00	0.00	0.00	0.00	0.00	0.00	0.00
Na	0.53	0.55	0.55	0.54	0.61	0.53	0.56
K	0.02	0.03	0.02	0.02	0.03	0.02	0.03
Cation Sum	**5.07**	**5.07**	**5.04**	**5.06**	**5.05**	**5.04**	**5.04**
An	0.66	0.64	0.63	0.64	0.57	0.64	0.61
Ab	0.33	0.35	0.36	0.34	0.41	0.35	0.37
Or	0.01	0.02	0.01	0.02	0.02	0.02	0.02

Table 3J - Microprobe Analyses of Groundmass Plagioclase

	GR-O4352-12plg	GR-O4352-12plg	GR-O4352-12plg	GR-O4352-13pl	GR-O4352-13pl	GR-O4352-13pl	GR-O4352-13pl
SiO_2	56.13	66.11	55.15	54.76	55.34	55.97	55.04
TiO_2	0.39	0.50	0.37	0.07	0.09	0.09	0.09
Al_2O_3	25.96	19.19	26.73	27.21	27.01	26.33	26.98
Cr_2O_3	0.13	0.17	0.11	0.00	0.01	0.06	0.02
MgO	0.28	0.16	0.24	0.10	0.11	0.03	0.08
CaO	10.04	2.82	10.54	10.92	10.03	9.44	10.48
FeO	0.96	0.92	1.00	0.72	0.79	0.95	0.94
MnO	0.08	0.11	0.10	0.00	0.00	0.00	0.01
Na_2O	6.42	7.40	5.97	5.68	6.22	6.42	5.97
K_2O	0.50	3.49	0.47	0.33	0.41	0.46	0.35
Total	**100.88**	**100.85**	**100.68**	**99.79**	**100.00**	**99.74**	**99.94**
Structural Formulae							
Cations per 8 Oxygen							
Si	2.54	2.95	2.50	2.49	2.51	2.54	2.50
Ti	0.00	0.00	0.00	0.00	0.00	0.00	0.00
Al (IV)	1.39	1.01	1.43	1.46	1.45	1.41	1.45
Al (VI)							
Cr	0.00	0.00	0.00	0.00	0.00	0.00	0.00
Mg	0.02	0.01	0.02	0.01	0.01	0.00	0.01
Ca	0.49	0.13	0.51	0.53	0.49	0.46	0.51
Fe	0.04	0.03	0.04	0.03	0.03	0.04	0.04
Mn	0.00	0.00	0.00	0.00	0.00	0.00	0.00
Na	0.56	0.64	0.53	0.50	0.55	0.57	0.53
K	0.03	0.20	0.03	0.02	0.02	0.03	0.02
Cation Sum	**5.06**	**4.97**	**5.06**	**5.04**	**5.05**	**5.05**	**5.05**
An	0.62	0.24	0.65	0.67	0.63	0.61	0.65
Ab	0.36	0.58	0.33	0.32	0.35	0.37	0.34
Or	0.02	0.18	0.02	0.01	0.02	0.02	0.01

Table 3K- Microprobe Analyses of Groundmass Plagioclase

	GR-SB2978-1pl	GR-SB2978-1pl	GR-SB2978-2pl	GR-SB2978-2pl	GR-SB2978-2pl	GR-SB2978-2pl	GR-SB2978-3plg
SiO_2	53.32	53.28	53.69	56.65	53.50	54.90	54.41
TiO_2	0.07	0.04	0.07	0.09	0.05	0.06	0.06
Al_2O_3	27.59	29.28	28.60	26.92	28.40	27.92	28.12
Cr_2O_3	0.07	0.02	0.01	0.00	0.00	0.01	0.04
MgO	0.26	0.07	0.09	0.06	0.14	0.06	0.09
CaO	11.31	12.06	11.76	9.30	11.68	10.63	10.88
FeO	2.00	0.89	0.71	0.77	1.15	0.93	0.82
MnO	0.00	0.01	0.00	0.00	0.00	0.00	0.00
Na_2O	5.18	4.89	5.22	6.26	5.17	5.83	5.73
K_2O	0.28	0.26	0.24	0.45	0.26	0.28	0.30
Total	**100.07**	**100.80**	**100.39**	**100.50**	**100.34**	**100.61**	**100.44**
Structural Formulae							
Cations per 8 Oxygen							
Si	2.50	2.41	2.43	2.55	2.43	2.48	2.46
Ti	0.00	0.00	0.00	0.00	0.00	0.00	0.00
Al (IV)	1.45	1.56	1.53	1.43	1.52	1.49	1.50
Al (VI)							
Cr	0.00	0.00	0.00	0.00	0.00	0.00	0.00
Mg	0.01	0.00	0.01	0.00	0.01	0.00	0.01
Ca	0.51	0.58	0.57	0.45	0.57	0.51	0.53
Fe	0.04	0.03	0.03	0.03	0.04	0.03	0.03
Mn	0.00	0.00	0.00	0.00	0.00	0.00	0.00
Na	0.53	0.43	0.46	0.55	0.46	0.51	0.50
K	0.02	0.01	0.01	0.03	0.02	0.02	0.02
Cation Sum	**5.05**	**5.03**	**5.04**	**5.03**	**5.04**	**5.04**	**5.05**
An	0.70	0.72	0.71	0.61	0.71	0.66	0.67
Ab	0.29	0.27	0.28	0.37	0.28	0.33	0.32
Or	0.01	0.01	0.01	0.02	0.01	0.01	0.01

128

Table 3L- Microprobe Analyses of Groundmass Plagioclase

	GR-SB2978-3plg	GR-SB2978-3plg	GR-SB2978-3plg	GR-SB2978-4plg	GR-SB2978-4plg	GR-SB2978-4plg	GR-SB2978-4plg
SiO2	54.09	53.15	53.50	54.37	53.99	54.96	54.00
TiO2	0.05	0.09	0.06	0.07	0.06	0.09	0.11
Al2O3	28.07	26.79	28.59	26.96	27.94	26.92	27.76
Cr2O3	0.00	0.03	0.06	0.00	0.01	0.04	0.00
MgO	0.09	0.56	0.14	0.22	0.08	0.09	0.08
CaO	11.25	10.41	11.77	10.23	10.77	10.46	10.86
FeO	0.62	2.77	0.66	1.75	0.91	0.80	0.66
MnO	0.02	0.00	0.00	0.00	0.00	0.05	0.05
Na2O	5.57	5.32	5.15	5.73	5.71	5.96	5.74
K2O	0.28	0.33	0.33	0.34	0.31	0.32	0.29
Total	**100.05**	**99.45**	**100.26**	**99.69**	**99.78**	**99.70**	**99.54**
Structural Formulae							
Cations per 8 Oxygen							
Si	2.46	2.45	2.43	2.49	2.46	2.50	2.47
Ti	0.00	0.00	0.00	0.00	0.00	0.00	0.00
Al (IV)	1.50	1.46	1.53	1.45	1.50	1.45	1.49
Al (VI)							
Cr	0.00	0.00	0.00	0.00	0.00	0.00	0.00
Mg	0.01	0.04	0.01	0.01	0.01	0.01	0.01
Ca	0.55	0.51	0.57	0.50	0.53	0.51	0.53
Fe	0.02	0.11	0.03	0.07	0.03	0.03	0.03
Mn	0.00	0.00	0.00	0.00	0.00	0.00	0.00
Na	0.49	0.48	0.45	0.51	0.50	0.53	0.51
K	0.02	0.02	0.02	0.02	0.02	0.02	0.02
Cation Sum	**5.04**	**5.07**	**5.04**	**5.05**	**5.05**	**5.04**	**5.05**
An	0.68	0.68	0.71	0.66	0.67	0.65	0.67
Ab	0.31	0.31	0.28	0.33	0.32	0.34	0.32
Or	0.01	0.01	0.01	0.01	0.01	0.01	0.01

Table 3M- Microprobe Analyses of Groundmass Plagioclase

	GR-SB2978-4plg	GR-SB2978-5pl	GR-SB2978-5pl	GR-SB2978-5pl	GR-SB2978-6pl	GR-SB2978-6pl	GR-SB2978-6pl
SiO_2	53.45	52.55	53.54	53.23	53.49	53.06	53.46
TiO_2	0.08	0.08	0.07	0.07	0.06	0.06	0.04
Al_2O_3	28.51	28.94	28.25	28.29	28.94	28.23	28.40
Cr_2O_3	0.00	0.00	0.00	0.04	0.02	0.00	0.03
MgO	0.09	0.13	0.14	0.06	0.08	0.14	0.07
CaO	11.73	12.03	11.48	11.72	11.99	12.01	11.41
FeO	0.77	0.76	0.82	0.71	0.73	0.63	0.81
MnO	0.00	0.00	0.01	0.00	0.03	0.00	0.02
Na_2O	5.28	5.03	5.07	5.12	5.06	5.08	5.19
K_2O	0.21	0.22	0.22	0.29	0.27	0.25	0.25
Total	**100.12**	**99.74**	**99.59**	**99.52**	**100.66**	**99.44**	**99.67**
Structural Formulae							
Cations per 8 Oxygen							
Si	2.43	2.40	2.44	2.44	2.42	2.43	2.44
Ti	0.00	0.00	0.00	0.00	0.00	0.00	0.00
Al (IV)	1.53	1.56	1.52	1.53	1.54	1.52	1.53
Al (VI)							
Cr	0.00	0.00	0.00	0.00	0.00	0.00	0.00
Mg	0.01	0.01	0.01	0.00	0.01	0.01	0.00
Ca	0.57	0.59	0.56	0.57	0.58	0.59	0.56
Fe	0.03	0.03	0.03	0.03	0.03	0.02	0.03
Mn	0.00	0.00	0.00	0.00	0.00	0.00	0.00
Na	0.47	0.45	0.45	0.45	0.44	0.45	0.46
K	0.01	0.01	0.01	0.02	0.02	0.01	0.01
Cation Sum	**5.04**	**5.05**	**5.03**	**5.04**	**5.04**	**5.04**	**5.03**
An	0.71	0.72	0.71	0.71	0.72	0.72	0.70
Ab	0.29	0.27	0.28	0.28	0.27	0.27	0.29
Or	0.01	0.01	0.01	0.01	0.01	0.01	0.01

130

Table 3N- Microprobe Analyses of Groundmass Plagioclase

	GR-SB2978-6pl	GR-SB2978-7plg	GR-SB2978-7plg	GR-SB2978-7plg	GR-SB2978-7plg	GR-SBM2269-1pl	GR-SBM2269-1pl
SiO2	54.38	52.99	53.29	54.34	53.00	55.34	54.42
TiO2	0.10	0.11	0.08	0.09	0.09	0.03	0.06
Al2O3	28.02	28.68	27.97	27.77	28.92	27.52	29.56
Cr2O3	0.00	0.00	0.00	0.02	0.00	0.00	0.00
MgO	0.11	0.10	0.09	0.11	0.05	0.16	0.08
CaO	10.95	12.05	11.44	11.11	11.91	10.34	11.61
FeO	0.68	0.89	0.65	0.81	0.89	1.50	0.69
MnO	0.05	0.05	0.04	0.00	0.02	0.01	0.00
Na2O	5.70	5.03	5.27	5.64	5.14	4.66	4.44
K2O	0.30	0.27	0.27	0.28	0.25	0.36	0.39
Total	**100.30**	**100.17**	**99.10**	**100.17**	**100.28**	**99.92**	**101.25**
Structural Formulae							
Cations per 8 Oxygen							
Si	2.46	2.41	2.45	2.47	2.41	2.51	2.43
Ti	0.00	0.00	0.00	0.00	0.00	0.00	0.00
Al (IV)	1.50	1.54	1.51	1.49	1.55	1.47	1.56
Al (VI)							
Cr	0.00	0.00	0.00	0.00	0.00	0.00	0.00
Mg	0.01	0.01	0.01	0.01	0.00	0.01	0.01
Ca	0.53	0.59	0.56	0.54	0.58	0.50	0.56
Fe	0.03	0.03	0.02	0.03	0.03	0.06	0.03
Mn	0.00	0.00	0.00	0.00	0.00	0.00	0.00
Na	0.50	0.44	0.47	0.50	0.45	**0.41**	0.39
K	0.02	0.02	0.02	0.02	0.01	0.02	0.02
Cation Sum	**5.05**	**5.04**	**5.04**	**5.05**	**5.05**	**4.97**	**4.99**
An	0.67	0.72	0.70	0.68	0.71	0.70	0.73
Ab	0.32	0.27	0.29	0.31	0.28	0.29	0.25
Or	0.01	0.01	0.01	0.01	0.01	0.01	0.01

Table 3O- Microprobe Analyses of Groundmass Plagioclase

	GR-SBM2269-3pl	GR-SBM2269-3pl	GR-SBM2269-3pl	GR-SBM2269-5pl	GR-SBM2269-5pl	GR-SBM2269-5pl	GR-SBM2269-7pl
SiO_2	53.89	55.72	55.46	54.27	55.14	53.99	55.24
TiO_2	0.22	0.25	0.22	0.24	0.20	0.20	0.05
Al_2O_3	27.71	26.66	26.97	26.86	27.01	27.69	27.28
Cr_2O_3	0.15	0.21	0.17	0.16	0.16	0.12	0.01
MgO	0.29	0.31	0.27	0.31	0.27	0.28	0.10
CaO	11.92	10.63	11.20	11.16	11.50	12.14	11.07
FeO	0.91	0.89	0.69	2.50	0.91	0.93	0.74
MnO	0.11	0.14	0.08	0.10	0.09	0.08	0.02
Na_2O	4.57	5.18	5.02	4.53	4.83	4.41	4.85
K_2O	0.37	0.40	0.39	0.44	0.38	0.33	0.36
Total	**100.13**	**100.39**	**100.46**	**100.57**	**100.48**	**100.18**	**99.72**
Structural Formulae							
Cations per 8 Oxygen							
Si	2.46	2.53	2.51	2.48	2.50	2.46	2.51
Ti	0.00	0.00	0.00	0.00	0.00	0.00	0.00
Al (IV)	1.49	1.42	1.44	1.45	1.44	1.49	1.46
Al (VI)							
Cr	0.00	0.00	0.00	0.00	0.00	0.00	0.00
Mg	0.02	0.02	0.02	0.02	0.02	0.02	0.01
Ca	0.58	0.52	0.54	0.55	0.56	0.59	0.54
Fe	0.03	0.03	0.03	0.10	0.03	0.04	0.03
Mn	0.00	0.00	0.00	0.00	0.00	0.00	0.00
Na	0.40	0.46	0.44	0.40	0.42	0.39	0.43
K	0.02	0.02	0.02	0.03	0.02	0.02	0.02
Cation Sum	**5.01**	**5.00**	**5.00**	**5.01**	**5.00**	**5.00**	**4.99**
An	0.73	0.68	0.70	0.72	0.71	0.74	0.71
Ab	0.25	0.30	0.28	0.26	0.27	0.24	0.28
Or	0.01	0.02	0.01	0.02	0.01	0.01	0.01

132

Table 3P- Microprobe Analyses of Groundmass Plagioclase

	GR-SBM2269-7pl	GR-SBM2269-7pl	GR-SBM2570-1pl	GR-SBM2570-1pl	GR-SBM2570-2pl	GR-SBM2570-2pl	GR-SBM2570-2pl
SiO2	54.58	55.05	55.57	55.27	55.58	54.91	54.65
TiO2	0.08	0.10	0.09	0.10	0.04	0.13	0.06
Al2O3	27.91	27.50	27.61	27.37	27.32	28.06	27.88
Cr2O3	0.03	0.04	0.00	0.03	0.00	0.00	0.00
MgO	0.07	0.15	0.09	0.10	0.18	0.16	0.14
CaO	11.42	11.32	11.01	10.79	11.37	11.80	11.41
FeO	0.71	0.55	0.76	0.97	0.82	0.73	0.68
MnO	0.04	0.00	0.00	0.00	0.03	0.00	0.00
Na2O	4.62	4.67	5.14	5.05	4.63	4.52	4.63
K2O	0.25	0.27	0.37	0.36	0.30	0.24	0.26
Total	99.71	99.65	100.62	100.03	100.26	100.56	99.72
Structural Formulae							
Cations per 8 Oxygen							
Si	2.48	2.50	2.50	2.50	2.51	2.48	2.48
Ti	0.00	0.00	0.00	0.00	0.00	0.00	0.00
Al (IV)	1.49	1.47	1.47	1.46	1.45	1.49	1.49
Al (VI)							
Cr	0.00	0.00	0.00	0.00	0.00	0.00	0.00
Mg	0.00	0.01	0.01	0.01	0.01	0.01	0.01
Ca	0.56	0.55	0.53	0.52	0.55	0.57	0.55
Fe	0.03	0.02	0.03	0.04	0.03	0.03	0.03
Mn	0.00	0.00	0.00	0.00	0.00	0.00	0.00
Na	0.41	0.41	0.45	0.44	0.41	0.40	0.41
K	0.01	0.02	0.02	0.02	0.02	0.01	0.01
Cation Sum	**4.98**	**4.98**	**5.00**	**5.00**	**4.98**	**4.98**	**4.98**
An	0.72	0.72	0.69	0.69	0.72	0.74	0.72
Ab	0.27	0.27	0.29	0.29	0.27	0.26	0.27
Or	0.01	0.01	0.01	0.01	0.01	0.01	0.01

133

Table 3Q- Microprobe Analyses of Groundmass Plagioclase

	GR-SBM2570-2pl	GR-SBM2570-2pl	GR-SBM2570-4pl	GR-SBM2570-4pl	GR-SBM2570-4pl	GR-SBM2570-4pl	GR-SBM2570-5pl
SiO_2	59.50	55.07	54.68	55.07	54.72	54.38	56.06
TiO_2	0.10	0.07	0.08	0.13	0.01	0.07	0.09
Al_2O_3	24.80	27.52	27.85	28.14	27.56	27.73	27.05
Cr_2O_3	0.02	0.00	0.00	0.00	0.00	0.00	0.00
MgO	0.03	0.15	0.11	0.09	0.08	0.10	0.06
CaO	8.31	11.55	11.36	11.46	11.49	11.57	10.64
FeO	0.65	0.84	0.73	0.63	0.80	0.64	1.01
MnO	0.04	0.03	0.01	0.04	0.02	0.03	0.02
Na_2O	6.18	4.73	4.56	4.67	4.88	4.69	5.12
K_2O	0.64	0.25	0.25	0.31	0.33	0.26	0.35
Total	**100.27**	**100.20**	**99.63**	**100.53**	**99.88**	**99.47**	**100.40**
Structural Formulae							
Cations per 8 Oxygen							
Si	2.66	2.49	2.48	2.48	2.48	2.48	2.53
Ti	0.00	0.00	0.00	0.00	0.00	0.00	0.00
Al (IV)	1.31	1.47	1.49	1.49	1.47	1.49	1.44
Al (VI)							
Cr	0.00	0.00	0.00	0.00	0.00	0.00	0.00
Mg	0.00	0.01	0.01	0.01	0.01	0.01	0.00
Ca	0.40	0.56	0.55	0.55	0.56	0.56	0.51
Fe	0.02	0.03	0.03	0.02	0.03	0.02	0.04
Mn	0.00	0.00	0.00	0.00	0.00	0.00	0.00
Na	0.54	0.41	0.40	0.41	0.43	0.41	0.45
K	0.04	0.01	0.01	0.02	0.02	0.02	0.02
Cation Sum	**4.97**	**4.99**	**4.98**	**4.98**	**5.00**	**4.99**	**4.99**
An	0.58	0.72	0.73	0.72	0.71	0.72	0.69
Ab	0.39	0.27	0.26	0.27	0.27	0.27	0.30
Or	0.03	0.01	0.01	0.01	0.01	0.01	0.01

134

Table 3R- Microprobe Analyses of Groundmass Plagioclase

	GR-SBM2570-5pl	GR-SBM2570-8pl	GR-SBM2570-8pl	GR-SBM2570-8pl	GR-SBM2570-8pl	GR-U3406-2pl	GR-U3406-2pl
SiO2	55.21	55.01	55.31	55.23	54.59	55.91	55.25
TiO2	0.16	0.09	0.12	0.09	0.03	0.07	0.06
Al2O3	27.35	27.95	27.37	27.37	28.28	26.76	27.33
Cr2O3	0.00	0.03	0.03	0.02	0.00	0.06	0.03
MgO	0.05	0.17	0.08	0.11	0.09	0.09	0.14
CaO	11.06	11.54	11.00	10.80	11.55	10.51	11.01
FeO	0.88	0.81	0.90	0.79	0.69	0.87	0.80
MnO	0.00	0.02	0.00	0.04	0.00	0.00	0.01
Na2O	5.00	4.79	5.07	5.12	4.75	5.35	4.76
K2O	0.35	0.34	0.32	0.35	0.30	0.27	0.25
Total	**100.06**	**100.76**	**100.20**	**99.92**	**100.27**	**99.90**	**99.63**
Structural Formulae							
Cations per 8 Oxygen							
Si	2.50	2.48	2.50	2.50	2.47	2.53	2.51
Ti	0.00	0.00	0.00	0.00	0.00	0.00	0.00
Al (IV)	1.46	1.48	1.46	1.46	1.51	1.43	1.46
Al (VI)							
Cr	0.00	0.00	0.00	0.00	0.00	0.00	0.00
Mg	0.00	0.01	0.01	0.01	0.01	0.01	0.01
Ca	0.54	0.56	0.53	0.52	0.56	0.51	0.54
Fe	0.03	0.03	0.03	0.03	0.03	0.03	0.03
Mn	0.00	0.00	0.00	0.00	0.00	0.00	0.00
Na	0.44	0.42	0.44	0.45	0.42	0.47	0.42
K	0.02	0.02	0.02	0.02	0.02	0.02	0.01
Cation Sum	**5.00**	**5.00**	**5.00**	**5.00**	**5.00**	**5.00**	**4.98**
An	0.70	0.72	0.70	0.69	0.72	0.68	0.71
Ab	0.29	0.27	0.29	0.30	0.27	0.31	0.28
Or	0.01	0.01	0.01	0.01	0.01	0.01	0.01

Table 3S- Microprobe Analyses of Groundmass Plagioclase

	GR-U3406-2pl	GR-U3406-3pl	GR-U3406-3pl	GR-U3406-3pl	GR-U3406-7pl	GR-U3406-7pl	GR-U3406-7pl	GR-U3406-7pl
SiO_2	54.79	54.43	54.92	56.00	55.49	55.40	55.21	55.59
TiO_2	0.10	0.06	0.07	0.06	0.11	0.08	0.13	0.17
Al_2O_3	27.46	27.72	27.40	26.78	26.41	26.34	27.22	26.83
Cr_2O_3	0.01	0.02	0.02	0.00	0.05	0.00	0.00	0.00
MgO	0.17	0.14	0.15	0.17	0.23	0.22	0.12	0.14
CaO	11.49	11.62	10.84	10.63	10.51	10.76	11.03	10.33
FeO	0.84	0.77	0.88	0.88	0.82	0.92	0.96	0.92
MnO	0.00	0.02	0.00	0.00	0.00	0.00	0.04	0.00
Na_2O	4.62	4.41	4.69	4.91	5.04	4.86	4.72	5.16
K_2O	0.27	0.29	0.28	0.33	0.33	0.31	0.26	0.30
Total	**99.74**	**99.47**	**99.26**	**99.76**	**98.98**	**98.88**	**99.69**	**99.43**
Structural Formulae								
Cations per 8 Oxygen								
Si	2.49	2.48	2.50	2.54	2.54	2.53	2.51	2.53
Ti	0.00	0.00	0.00	0.00	0.00	0.00	0.00	0.00
Al (IV)	1.47	1.49	1.47	1.43	1.42	1.42	1.46	1.44
Al (VI)								
Cr	0.00	0.00	0.00	0.00	0.00	0.00	0.00	0.00
Mg	0.01	0.01	0.01	0.01	0.02	0.01	0.01	0.01
Ca	0.56	0.57	0.53	0.52	0.51	0.53	0.54	0.50
Fe	0.03	0.03	0.03	0.03	0.03	0.04	0.04	0.03
Mn	0.00	0.00	0.00	0.00	0.00	0.00	0.00	0.00
Na	0.41	0.39	0.41	0.43	0.45	0.43	0.42	0.46
K	0.02	0.02	0.02	0.02	0.02	0.02	0.02	0.02
Cation Sum	**4.99**	**4.98**	**4.98**	**4.98**	**4.99**	**4.98**	**4.98**	**4.99**
An	0.73	0.74	0.71	0.70	0.69	0.70	0.71	0.68
Ab	0.26	0.25	0.28	0.29	0.30	0.29	0.28	0.31
Or	0.01	0.01	0.01	0.01	0.01	0.01	0.01	0.01

Table 4A - Microprobe Analyses of Groundmass Pyroxene

	GR-3-08-1cp	GR-13-1pig	GR-13-2py	GR-13-4py1	GR-13-4py2	GR-13-5py1	GR-13-6py1
SiO2	52.72	49.62	48.57	50.97	51.73	52.31	52.15
TiO2	0.80	0.36	0.77	1.01	0.91	0.88	0.95
Al2O3	2.72	0.51	1.25	1.63	1.47	1.50	1.79
Cr2O3	0.15	0.00	0.01	0.04	0.02	0.05	0.05
MgO	15.93	12.39	11.54	14.47	13.27	14.65	14.65
CaO	16.91	5.59	14.65	15.23	15.72	17.09	17.11
FeO	10.69	31.68	21.39	15.34	15.64	13.40	12.37
MnO	0.24	0.65	0.52	0.34	0.40	0.34	0.31
Na2O	0.29	0.07	0.29	0.20	0.27	0.23	0.21
K2O	0.34	0.00	0.00	0.00	0.00	0.01	0.00
Totals	**100.79**	**100.86**	**98.99**	**99.23**	**99.43**	**100.46**	**99.59**
Structural Formulae			Cations per 6 oxygen				
Si	1.94	1.96	1.92	1.94	1.97	1.96	1.96
Ti	0.02	0.01	0.02	0.03	0.03	0.02	0.03
Al (IV)	0.06	0.04	0.08	0.06	0.03	0.04	0.04
Al (VI)	0.06	-0.02	-0.02	0.01	0.03	0.02	0.04
Cr	0.00	0.00	0.00	0.00	0.00	0.00	0.00
Mg	0.87	0.73	0.68	0.82	0.75	0.82	0.82
Ca	0.67	0.24	0.62	0.62	0.64	0.68	0.69
Fe	0.33	1.04	0.71	0.49	0.50	0.42	0.39
Mn	0.01	0.02	0.02	0.01	0.01	0.01	0.01
Na	0.02	0.01	0.02	0.01	0.02	0.02	0.02
K	0.02	0.00	0.00	0.00	0.00	0.00	0.00
Fe3+	0.05	0.16	0.11	0.07	0.07	0.06	0.06
Fe2+	0.27	0.87	0.59	0.41	0.41	0.35	0.32
M1	1.01	0.87	0.78	0.94	0.89	0.93	0.94
M2	0.96	1.11	1.23	1.04	1.08	1.05	1.03
Cation Sum	**3.99**	**4.01**	**4.03**	**3.99**	**3.98**	**3.99**	**3.98**
Mg#	72.80	41.26	49.21	62.89	60.38	66.26	68.02

137

Table 4B- Microprobe Analyses of Groundmass Pyroxene

	GR-13-7pig	GR-18-4pygm	GR-18-5pygm	GR-18-pygm2	GR-18-2pygm	CHI-16-2-ygm	CHI-18-1pya
SiO_2	53.20	50.95	53.37	51.67	50.71	51.50	50.47
TiO_2	0.38	0.29	0.23	0.31	0.27	0.81	1.49
Al_2O_3	0.61	1.98	1.23	2.52	3.33	2.16	5.94
Cr_2O_3	0.00	0.00	0.00	0.00	0.05	0.03	0.00
MgO	18.82	13.89	20.27	15.91	15.54	15.58	9.51
CaO	3.84	14.90	5.06	13.33	14.73	15.01	12.39
FeO	23.09	16.80	20.66	16.18	13.60	12.72	19.16
MnO	0.55	0.34	0.39	0.34	0.27	0.38	0.46
Na_2O	0.03	0.24	0.11	0.25	0.32	0.35	1.31
K_2O	0.01	0.05	0.00	0.02	0.01	0.00	0.07
Totals	**100.52**	**99.45**	**101.31**	**100.53**	**98.82**	**98.54**	**100.80**
Structural Formulae		Cations per 6 oxygen					
Si	1.99	1.95	1.97	1.93	1.92	1.95	1.91
Ti	0.01	0.01	0.01	0.01	0.01	0.02	0.04
Al (IV)	0.01	0.05	0.03	0.07	0.08	0.05	0.09
Al (VI)	0.02	0.03	0.02	0.04	0.07	0.04	0.17
Cr	0.00	0.00	0.00	0.00	0.00	0.00	0.00
Mg	1.05	0.79	1.11	0.89	0.88	0.88	0.54
Ca	0.15	0.61	0.20	0.53	0.60	0.61	0.50
Fe	0.72	0.54	0.64	0.51	0.43	0.40	0.61
Mn	0.02	0.01	0.01	0.01	0.01	0.01	0.01
Na	0.00	0.02	0.01	0.02	0.02	0.03	0.10
K	0.00	0.00	0.00	0.00	0.00	0.00	0.00
Fe3+	0.11	0.08	0.10	0.08	0.06	0.06	0.09
Fe2+	0.60	0.45	0.53	0.42	0.36	0.34	0.50
M1	1.19	0.91	1.24	1.02	1.02	1.01	0.84
M2	0.76	1.07	0.74	0.97	0.98	0.97	1.10
Cation Sum	**3.97**	**4.00**	**3.99**	**4.00**	**4.00**	**3.99**	**3.96**
Mg #	59.42	59.76	63.80	63.85	67.25	68.75	47.13

138

Table 4C- Microprobe Analyses of Groundmass Pyroxene

	CHI-18-1pyb	CHI-20-1cpx	CHI-22-3pygm	CHI-24-6GM	CHI-24-6CPGM	CHI-24-6CPGM2	CHI-28-5pygm
SiO2	49.36	52.57	51.80	51.53	52.03	51.79	52.30
TiO2	1.65	0.43	0.90	0.64	0.93	0.99	0.82
Al2O3	1.90	1.52	1.60	1.01	1.56	1.73	1.71
Cr2O3	0.01	0.00	0.05	0.02	0.02	0.01	0.13
MgO	12.48	14.54	14.75	12.75	14.74	14.37	15.79
CaO	11.52	16.88	15.55	14.05	15.33	16.61	16.76
FeO	21.54	12.77	14.58	19.53	15.68	14.26	11.30
MnO	0.59	0.27	0.29	0.44	0.41	0.35	0.34
Na2O	0.27	0.20	0.22	0.20	0.22	0.27	0.23
K2O	0.00	0.02	0.01	0.00	0.00	0.00	0.00
Totals	**99.32**	**99.19**	**99.74**	**100.17**	**100.92**	**100.38**	**99.39**
Structural Formulae			Cations per 6 oxygen				
Si	1.92	1.98	1.95	1.97	1.95	1.94	1.96
Ti	0.05	0.01	0.03	0.02	0.03	0.03	0.02
Al (IV)	0.08	0.02	0.05	0.03	0.05	0.06	0.04
Al (VI)	0.01	0.05	0.02	0.02	0.02	0.02	0.03
Cr	0.00	0.00	0.00	0.00	0.00	0.00	0.00
Mg	0.72	0.82	0.83	0.73	0.82	0.80	0.88
Ca	0.48	0.68	0.63	0.58	0.61	0.67	0.67
Fe	0.70	0.40	0.46	0.63	0.49	0.45	0.35
Mn	0.02	0.01	0.01	0.01	0.01	0.01	0.01
Na	0.02	0.01	0.02	0.01	0.02	0.02	0.02
K	0.00	0.00	0.00	0.00	0.00	0.00	0.00
Fe3+	0.11	0.06	0.07	0.09	0.07	0.07	0.05
Fe2+	0.58	0.34	0.38	0.52	0.41	0.37	0.29
M1	0.88	0.94	0.95	0.86	0.94	0.92	0.99
M2	1.08	1.03	1.03	1.11	1.04	1.06	0.98
Cation Sum	**3.99**	**3.98**	**3.99**	**3.98**	**3.99**	**3.99**	**3.98**
Mg #	51.00	67.16	64.50	53.97	62.81	64.41	71.51

Table 4D- Microprobe Analyses of Groundmass Pyroxene

	CHI-36-1py3c	CHI-36-1py3br	CHI-36-1py3r2	CHI-36-1gmpy	CHI-36-1gmpig	CHI-36-1gmpy2	CHI-36-2gmpy
SiO2	51.69	51.42	52.13	51.71	50.72	51.36	51.27
TiO2	1.14	0.73	1.20	0.68	0.68	0.94	1.17
Al2O3	1.47	0.68	1.42	0.70	0.56	1.56	1.31
Cr2O3	0.18	0.18	0.19	0.16	0.18	0.14	0.16
MgO	12.97	14.77	12.63	15.40	14.53	14.32	12.33
CaO	16.84	5.43	16.64	5.34	5.88	15.33	16.65
FeO	16.09	26.14	15.86	25.52	26.57	16.56	17.88
MnO	0.18	0.00	0.00	0.21	0.19	0.19	0.00
Na2O	0.36	0.20	0.39	0.20	0.22	0.34	0.36
K2O	0.08	0.08	0.08	0.09	0.09	0.08	0.07
Totals	**101.00**	**99.62**	**100.55**	**100.00**	**99.62**	**100.82**	**101.21**
Structural Formulae		Cations per 6 oxygen					
Si	1.95	1.99	1.97	1.98	1.97	1.94	1.94
Ti	0.03	0.02	0.03	0.02	0.02	0.03	0.03
Al (IV)	0.05	0.01	0.03	0.02	0.03	0.06	0.06
Al (VI)	0.01	0.02	0.03	0.02	0.00	0.00	0.00
Cr	0.01	0.01	0.01	0.00	0.01	0.00	0.00
Mg	0.73	0.85	0.71	0.88	0.84	0.80	0.70
Ca	0.68	0.22	0.67	0.22	0.25	0.62	0.68
Fe	0.51	0.84	0.50	0.82	0.86	0.52	0.57
Mn	0.01	0.00	0.00	0.01	0.01	0.01	0.00
Na	0.03	0.01	0.03	0.02	0.02	0.03	0.03
K	0.00	0.00	0.00	0.00	0.00	0.00	0.00
Fe3+	0.08	0.13	0.08	0.12	0.13	0.08	0.08
Fe2+	0.42	0.70	0.42	0.68	0.72	0.43	0.47
M1	0.85	1.02	0.85	1.04	1.00	0.92	0.82
M2	1.13	0.94	1.12	0.92	0.98	1.08	1.17
Cation Sum	**3.99**	**3.97**	**3.97**	**3.97**	**3.99**	**4.01**	**4.00**
Mg #	59.15	50.37	58.86	52.01	49.55	60.83	55.33

Table 4E- Microprobe Analyses of Groundmass Pyroxene

	CHI-45-5ingmQ	GR-O4014-1py	GR-O4014-1py	GR-O4014-2py	GR-O4014-2py	GR-O4014-py	GR-O4014-pygm
SiO2	51.59	51.48	52.50	50.38	50.69	50.03	51.59
TiO2	1.18	0.86	0.53	0.82	1.05	1.06	0.80
Al2O3	1.69	1.29	0.89	1.28	1.28	1.45	1.24
Cr2O3	0.21	0.00	0.00	0.02	0.06	0.00	0.01
MgO	14.51	15.13	19.79	13.74	13.41	13.00	15.19
CaO	13.94	12.71	4.79	10.49	13.05	14.59	14.11
FeO	16.18	18.66	21.38	22.61	19.78	18.57	16.64
MnO	0.17	0.29	0.34	0.29	0.27	0.31	0.29
Na2O	0.37	0.19	0.05	0.15	0.23	0.26	0.24
K2O	0.09	0.03	0.03	0.00	0.02	0.02	0.00
Totals	**99.93**	**100.62**	**100.30**	**99.79**	**99.85**	**99.28**	**100.09**
Structural Formulae			Cations per 6 oxygen				
Si	1.95	1.95	1.97	1.95	1.95	1.93	1.95
Ti	0.03	0.02	0.01	0.02	0.03	0.03	0.02
Al (IV)	0.05	0.05	0.03	0.05	0.05	0.07	0.05
Al (VI)	0.02	0.00	0.01	0.00	0.00	0.00	0.01
Cr	0.01	0.00	0.00	0.00	0.00	0.00	0.00
Mg	0.82	0.85	1.10	0.79	0.77	0.75	0.86
Ca	0.56	0.51	0.19	0.43	0.54	0.60	0.57
Fe	0.51	0.59	0.67	0.73	0.64	0.60	0.53
Mn	0.01	0.01	0.01	0.01	0.01	0.01	0.01
Na	**0.03**	0.01	0.00	0.01	0.02	0.02	0.02
K	0.00	0.00	0.00	0.00	0.00	0.00	0.00
Fe3+	0.08	0.09	0.10	0.11	0.10	0.09	0.08
Fe2+	0.43	0.49	0.56	0.61	0.53	0.50	0.44
M1	0.96	0.97	0.97	0.93	0.90	0.87	0.96
M2	1.02	1.02	0.75	1.05	1.08	1.12	1.03
Cation Sum	**3.98**	**4.00**	**3.99**	**3.99**	**3.99**	**4.00**	**4.00**
Mg #	61.70	59.29	62.44	52.19	54.91	55.71	62.12

Table 4F- Microprobe Analyses of Groundmass Pyroxene

	GR-O4014-pygm	GR-O4014-3pygm	GR-O4014-4py	GR-O4014-4py	GR-O4014-4py	GR-O4014-4py	GR-O4014-5py
SiO2	51.22	50.32	52.78	53.17	53.75	52.44	52.47
TiO2	0.90	0.63	0.39	0.36	0.28	0.63	0.44
Al2O3	1.54	1.09	1.03	0.67	0.78	1.08	0.72
Cr2O3	0.00	0.00	0.00	0.01	0.01	0.04	0.00
MgO	15.37	9.21	23.27	21.74	23.63	18.81	20.42
CaO	13.35	6.02	2.25	2.97	2.09	6.74	4.26
FeO	16.74	32.26	20.06	21.03	19.33	18.75	20.73
MnO	0.22	0.44	0.31	0.34	0.32	0.29	0.22
Na2O	0.20	0.13	0.03	0.08	0.06	0.14	0.06
K2O	0.00	0.48	0.01	0.00	0.00	0.01	0.00
Totals	**99.54**	**100.58**	**100.13**	**100.37**	**100.24**	**98.93**	**99.32**
Structural Formulae		Cations per 6 oxygen					
Si	1.94	1.99	1.84	1.83	1.87	1.98	1.97
Ti	0.03	0.02	0.01	0.01	0.01	0.02	0.01
Al (IV)	0.06	0.01	0.16	0.17	0.13	0.02	0.03
Al (VI)	0.01	0.04	-0.12	-0.14	-0.10	0.03	0.01
Cr	0.00	0.00	0.00	0.00	0.00	0.00	0.00
Mg	0.87	0.54	1.57	1.55	1.56	1.06	1.15
Ca	0.54	0.26	0.08	0.11	0.08	0.27	0.17
Fe	0.53	1.07	0.58	0.61	0.56	0.59	0.65
Mn	0.01	0.01	0.00	0.00	0.00	0.01	0.01
Na	0.01	0.01	0.00	0.01	0.00	0.01	0.00
K	0.00	0.02	0.00	0.00	0.00	0.00	0.00
Fe3+	0.08	0.16	0.13	0.14	0.13	0.09	0.10
Fe2+	0.44	0.89	0.33	0.34	0.31	0.49	0.54
M1	0.99	0.77	2.01	2.01	1.99	1.19	1.26
M2	1.00	1.16	-	-	-	0.78	0.72
Cation Sum	**3.99**	**3.96**	**4.01**	**4.02**	**4.00**	**3.98**	**3.99**
Mg #	62.26	33.90	67.57	64.99	68.71	64.30	63.89

142

Table 4G- Microprobe Analyses of Groundmass Pyroxene

	GR-O4014-5py	GR-O4014-6pyc	GR-O4014-6pyr	GR-O4014-6pyc2	GR-O4014-6pyr2	GR-O4014-6py	GR-O4014-8pygm
SiO_2	49.36	52.29	53.57	51.95	51.07	50.55	52.11
TiO_2	1.29	0.40	0.25	0.71	0.61	1.03	0.58
Al_2O_3	1.69	0.77	0.80	1.43	0.73	1.58	1.39
Cr_2O_3	0.05	0.00	0.08	0.00	0.00	0.10	0.08
MgO	11.55	20.01	24.10	15.18	13.97	13.70	20.26
CaO	12.24	5.05	2.00	16.43	4.94	15.48	4.62
FeO	21.68	21.31	18.89	12.52	28.94	16.87	20.49
MnO	0.28	0.32	0.34	0.22	0.38	0.31	0.30
Na_2O	0.26	0.08	0.02	0.26	0.13	0.29	0.13
K_2O	0.00	0.00	0.01	0.00	0.03	0.00	0.00
Total	**98.41**	**100.23**	**100.04**	**98.70**	**100.80**	**99.90**	**99.97**
Structural Formulae	Cations per 6 oxygen						
Si	1.94	1.96	1.87	1.96	1.98	1.93	1.95
Ti	0.04	0.01	0.01	0.02	0.02	0.03	0.02
Al (IV)	0.06	0.04	0.13	0.04	0.02	0.07	0.05
Al (VI)	0.02	0.00	-0.10	0.03	0.01	0.00	0.01
Cr	0.00	0.00	0.00	0.00	0.00	0.00	0.00
Mg	0.68	1.12	1.57	0.86	0.81	0.78	1.13
Ca	0.52	0.20	0.07	0.67	0.20	0.63	0.19
Fe	0.71	0.67	0.55	0.40	0.94	0.54	0.64
Mn	0.01	0.01	0.00	0.01	0.01	0.01	0.01
Na	0.02	0.01	0.00	0.02	0.01	0.02	0.01
K	0.00	0.00	0.00	0.00	0.00	0.00	0.00
Fe^{3+}	0.11	0.10	0.13	0.06	0.14	0.08	0.10
Fe^{2+}	0.59	0.56	0.31	0.33	0.78	0.45	0.53
M1	0.84	1.23	1.99	0.96	0.97	0.89	1.26
M2	1.13	0.77	-	1.01	0.99	1.10	0.73
Cation Sum	**3.98**	**4.00**	**3.99**	**3.99**	**3.98**	**4.01**	**4.00**
Mg #	48.91	62.78	69.62	68.52	46.44	59.33	63.99

143

Table 4H- Microprobe Analyses of Groundmass Pyroxene

	GR-O4014-8pygm	GR-O4014-8pygm	GR-O4014-8pygm	GR-O4014-9py	GR-O4014-9py	GR-O4014-9py	GR-O4014-9py
SiO_2	52.12	51.41	51.34	51.52	50.88	51.16	51.85
TiO_2	0.56	0.79	0.90	0.70	0.75	0.64	0.52
Al_2O_3	1.04	1.45	1.48	1.46	1.45	1.00	0.69
Cr_2O_3	0.03	0.03	0.12	0.00	0.07	0.03	0.01
MgO	18.28	16.46	14.95	14.76	14.67	17.26	17.10
CaO	9.28	12.64	14.68	16.59	17.86	6.59	5.82
FeO	18.11	16.40	15.23	13.04	12.91	22.92	24.08
MnO	0.29	0.26	0.19	0.23	0.23	0.27	0.36
Na_2O	0.18	0.17	0.24	0.29	0.25	0.09	0.11
K_2O	0.00	0.01	0.00	0.00	0.00	0.02	0.00
Total	**99.87**	**99.61**	**99.11**	**98.58**	**99.06**	**99.97**	**100.55**
Structural Formulae	Cations per 6 oxygen						
Si	1.96	1.94	1.95	1.96	1.94	1.95	1.97
Ti	0.02	0.02	0.03	0.02	0.02	0.02	0.01
Al (IV)	0.04	0.06	0.05	0.04	0.06	0.05	0.03
Al (VI)	0.00	0.01	0.02	0.02	0.00	0.00	0.00
Cr	0.00	0.00	0.00	0.00	0.00	0.00	0.00
Mg	1.02	0.93	0.85	0.84	0.83	0.98	0.97
Ca	0.37	0.51	0.60	0.68	0.73	0.27	0.24
Fe	0.57	0.52	0.48	0.41	0.41	0.73	0.76
Mn	0.01	0.01	0.01	0.01	0.01	0.01	0.01
Na	0.01	0.01	0.02	0.02	0.02	0.01	0.01
K	0.00	0.00	0.00	0.00	0.00	0.00	0.00
Fe^{3+}	0.09	0.08	0.07	0.06	0.06	0.11	0.11
Fe^{2+}	0.47	0.43	0.40	0.35	0.34	0.61	0.64
M1	1.13	1.04	0.97	0.94	0.92	1.11	1.10
M2	0.86	0.96	1.02	1.04	1.09	0.88	0.88
Cation Sum	**4.00**	**4.00**	**3.99**	**3.99**	**4.01**	**4.00**	**3.99**
Mg #	64.46	64.33	63.81	67.03	67.12	57.49	56.06

144

Table 4I- Microprobe Analyses of Groundmass Pyroxene

	GR-O4014-10pyg	GR-O4014-10pyg	GR-O4014-10pyg	GR-O4014-10pyg	GR-O4352-1pygm	GR-O4352-1pygmc2	GR-O4352-1pygmr2
SiO2	51.41	49.88	51.94	50.23	49.57	51.36	49.71
TiO2	0.78	0.52	0.45	0.77	1.19	0.48	0.87
Al2O3	1.45	0.62	1.06	0.87	3.29	0.59	0.72
Cr2O3	0.08	0.00	0.03	0.00	0.03	0.03	0.01
MgO	15.13	11.13	19.20	14.09	13.53	15.69	9.96
CaO	16.60	7.52	4.22	11.18	18.22	5.26	7.56
FeO	13.94	30.05	22.06	21.72	12.20	26.77	31.37
MnO	0.21	0.51	0.20	0.31	0.17	0.47	0.46
Na2O	0.29	0.12	0.13	0.19	0.37	0.10	0.12
K2O	0.02	0.01	0.02	0.02	0.01	0.01	0.01
Total	**99.90**	**100.37**	**99.30**	**99.39**	**98.57**	**100.75**	**100.78**
Structural Formulae	Cations per 6 oxygen						
Si	1.94	1.97	1.97	1.95	1.89	1.97	1.97
Ti	0.02	0.02	0.01	0.02	0.03	0.01	0.03
Al (IV)	0.06	0.03	0.03	0.05	0.11	0.03	0.03
Al (VI)	0.00	0.00	0.02	-0.01	0.04	0.00	0.00
Cr	0.00	0.00	0.00	0.00	0.00	0.00	0.00
Mg	0.85	0.66	1.08	0.81	0.77	0.90	0.59
Ca	0.67	0.32	0.17	0.46	0.75	0.22	0.32
Fe	0.44	0.99	0.70	0.70	0.39	0.86	1.04
Mn	0.01	0.02	0.01	0.01	0.01	0.02	0.02
Na	0.02	0.01	0.01	0.01	0.03	0.01	0.01
K	0.00	0.00	0.00	0.00	0.00	0.00	0.00
Fe3+	0.07	0.15	0.10	0.11	0.06	0.13	0.16
Fe2+	0.37	0.83	0.58	0.59	0.32	0.72	0.86
M1	0.94	0.82	1.22	0.93	0.90	1.04	0.77
M2	1.06	1.15	0.76	1.07	1.10	0.94	1.19
Cation Sum	**4.01**	**3.99**	**3.99**	**4.01**	**4.01**	**3.99**	**3.98**
Mg #	66.09	39.96	60.99	53.83	66.58	51.29	36.32

145

Table 4J- Microprobe Analyses of Groundmass Pyroxene

	GR-O4352-1pygmc3	GR-O4352-1pygm	GR-O4352-5py	GR-O4352-6py	GR-O4352-6py	GR-O4352-7py	GR-O4352-8pygm
SiO2	51.05	50.99	52.22	50.38	52.32	49.62	49.74
TiO2	0.95	0.85	0.64	1.01	0.67	1.52	1.25
Al2O3	1.60	1.30	1.85	3.19	2.02	2.68	2.86
Cr2O3	0.03	0.00	0.07	0.04	0.08	0.01	0.00
MgO	14.49	14.76	16.55	14.09	20.16	12.40	15.01
CaO	15.63	15.27	16.39	18.75	7.73	16.34	14.44
FeO	15.47	15.39	10.98	11.25	16.53	15.92	15.55
MnO	0.32	0.22	0.26	0.09	0.19	0.20	0.25
Na2O	0.24	0.25	0.33	0.38	0.17	0.32	0.24
K2O	0.00	0.01	0.01	0.02	0.00	0.01	0.01
Total	**99.77**	**99.04**	**99.29**	**99.20**	**99.87**	**99.00**	**99.33**
Structural Formulae	Cations per 6 oxygen						
Si	1.94	1.95	1.95	1.90	1.94	1.94	1.89
Ti	0.03	0.02	0.02	0.03	0.02	0.02	0.04
Al (IV)	0.06	0.05	0.05	0.10	0.06	0.06	0.11
Al (VI)	0.01	0.00	0.03	0.04	0.03	0.00	0.02
Cr	0.00	0.00	0.00	0.00	0.00	0.03	0.00
Mg	0.82	0.84	0.92	0.79	1.11	0.00	0.85
Ca	0.64	0.62	0.66	0.76	0.31	1.11	0.59
Fe	0.49	0.49	0.34	0.36	0.51	0.31	0.49
Mn	0.01	0.01	0.01	0.00	0.01	0.51	0.01
Na	0.02	0.02	0.02	0.03	0.01	0.01	0.02
K	0.00	0.00	0.00	0.00	0.00	0.01	0.00
Fe3+	0.07	0.07	0.05	0.05	0.08	0.05	0.07
Fe2+	0.41	0.41	0.29	0.30	0.43	0.26	0.41
M1	0.93	0.94	1.02	0.92	1.24	0.10	0.98
M2	1.06	1.05	0.97	1.08	0.75	1.38	1.02
Cation Sum	**4.00**	**4.00**	**4.00**	**4.01**	**3.99**	**4.00**	**4.01**
Mg #	62.72	63.27	73.02	69.23	68.66	58.31	63.43

146

Table 4K- Microprobe Analyses of Groundmass Pyroxene

	GR-O4352-8pygm	GR-O4352-8pygm	GR-O4352-8pygm	GR-O4352-9pygm	GR-O4352-9pygm	GR-O4352-9pygm	GR-O4352-12pygc1
SiO_2	51.19	51.18	49.88	50.96	50.07	52.24	53.80
TiO_2	0.84	0.90	1.14	0.81	1.11	0.52	0.24
Al_2O_3	1.99	1.30	1.61	1.69	2.75	1.54	0.70
Cr_2O_3	0.00	0.06	0.06	0.00	0.08	0.03	0.03
MgO	14.98	14.46	12.39	15.36	15.46	20.64	23.05
CaO	16.14	15.50	15.16	14.45	14.40	4.38	3.84
FeO	13.39	15.24	17.37	14.66	14.75	20.48	17.97
MnO	0.23	0.25	0.23	0.29	0.14	0.40	0.29
Na_2O	0.30	0.30	0.22	0.29	0.26	0.07	0.09
K_2O	0.02	0.00	0.00	0.00	0.00	0.00	0.00
Total	**99.10**	**99.17**	**98.07**	**98.51**	**99.01**	**100.29**	**99.99**
Structural Formulae							
Cations per 6 oxygen							
Si	1.94	1.95	1.94	1.94	1.90	1.95	1.98
Ti	0.02	0.03	0.03	0.02	0.03	0.01	0.01
Al (IV)	0.06	0.05	0.06	0.06	0.10	0.05	0.02
Al (VI)	0.03	0.01	0.02	0.02	0.03	0.01	0.01
Cr	0.00	0.00	0.00	0.00	0.00	0.00	0.00
Mg	0.85	0.82	0.72	0.87	0.88	1.15	1.26
Ca	0.65	0.63	0.63	0.59	0.59	0.17	0.15
Fe	0.42	0.49	0.57	0.47	0.47	0.64	0.55
Mn	0.01	0.01	0.01	0.01	0.00	0.01	0.01
Na	0.02	0.02	0.02	0.02	0.02	0.00	0.01
K	0.00	0.00	0.00	0.00	0.00	0.00	0.00
Fe3+	0.06	0.07	0.08	0.07	0.07	0.10	0.08
Fe2+	0.35	0.40	0.47	0.39	0.39	0.53	0.46
M1	0.96	0.93	0.86	0.99	1.00	1.27	1.36
M2	1.03	1.06	1.12	1.00	1.00	0.71	0.62
Cation Sum	**4.00**	**4.00**	**3.98**	**4.00**	**4.00**	**4.00**	**3.99**
Mg #	66.77	63.01	56.17	65.31	65.30	64.42	69.73

Table 4L- Microprobe Analyses of Groundmass Pyroxene

	GR-O4352-12pyGR1	GR-O4352-12pyg	GR-O4352-12pyg	GR-SB2978-1pyg	GR-SB2978-1pyg	GR-SB2978-1pyg	GR-SB2978-1pyg
SiO_2	50.32	50.18	51.84	50.01	51.22	50.66	52.07
TiO_2	0.95	0.95	0.46	0.63	1.00	0.70	0.58
Al_2O_3	3.12	2.73	1.64	0.76	1.49	0.74	0.94
Cr_2O_3	0.05	0.00	0.00	0.00	0.04	0.01	0.04
MgO	14.63	15.14	20.53	10.90	14.03	14.09	18.91
CaO	15.76	16.10	4.62	12.08	16.34	6.90	6.16
FeO	13.41	12.53	19.88	24.16	15.26	25.70	20.96
MnO	0.28	0.22	0.35	0.38	0.29	0.42	0.36
Na_2O	0.41	0.39	0.10	0.19	0.26	0.14	0.07
K_2O	0.00	0.03	0.01	0.02	0.01	0.01	0.00
Total	**98.92**	**98.28**	**99.42**	**99.13**	**99.93**	**99.39**	**100.09**
Structural Formulae							
Cations per 6 oxygen							
Si	1.91	1.91	1.95	1.97	1.94	1.97	1.96
Ti	0.03	0.03	0.01	0.02	0.03	0.02	0.02
Al (IV)	0.09	0.09	0.05	0.03	0.06	0.03	0.04
Al (VI)	0.05	0.03	0.02	0.01	0.01	0.01	0.00
Cr	0.00	0.00	0.00	0.00	0.00	0.00	0.00
Mg	0.83	0.86	1.15	0.64	0.79	0.82	1.06
Ca	0.64	0.66	0.19	0.51	0.66	0.29	0.25
Fe	0.43	0.40	0.62	0.80	0.48	0.84	0.66
Mn	0.01	0.01	0.01	0.01	0.01	0.01	0.01
Na	0.03	0.03	0.01	0.01	0.02	0.01	0.01
K	0.00	0.00	0.00	0.00	0.00	0.00	0.00
Fe^{3+}	0.06	0.06	0.09	0.12	0.07	0.13	0.10
Fe^{2+}	0.35	0.33	0.52	0.66	0.40	0.70	0.55
M1	0.97	0.98	1.27	0.78	0.90	0.97	1.18
M2	1.03	1.02	0.71	1.19	1.09	1.00	0.80
Cation Sum	**4.00**	**4.01**	**4.00**	**3.99**	**4.00**	**3.98**	**3.99**
Mg #	66.20	68.45	64.97	44.75	62.29	49.62	61.84

Table 4M - Microprobe Analyses of Groundmass Pyroxene

	GR-SB-2978-3py	GR-SB2978-7py	GR-SB2978-7py	GR-SB2978-7py	GR-SB2978-7py	GR-SB2978-7py	GR-SBM2269-1py
SiO2	50.31	52.41	52.27	50.65	50.94	52.57	51.52
TiO2	0.64	0.70	0.75	0.70	1.23	0.53	0.65
Al2O3	0.96	1.32	1.49	0.75	2.41	1.16	0.97
Cr2O3	0.00	0.03	0.04	0.00	0.01	0.06	0.00
MgO	12.05	16.19	16.13	13.07	14.82	16.64	14.90
CaO	12.53	16.96	16.44	9.52	16.41	16.82	7.84
FeO	21.57	11.10	12.51	25.89	12.94	11.31	23.61
MnO	0.34	0.23	0.22	0.48	0.21	0.23	0.37
Na2O	0.22	0.24	0.24	0.14	0.30	0.25	0.11
K2O	0.01	0.01	0.01	0.00	0.01	0.01	0.00
Total	98.61	99.18	100.09	101.19	99.28	99.57	99.97
Structural Formulae	Cations per 6 oxygen						
Si	1.97	1.96	1.95	1.95	1.92	1.96	1.98
Ti	0.02	0.02	0.02	0.02	0.04	0.01	0.02
Al (IV)	0.03	0.04	0.05	0.05	0.08	0.04	0.02
Al (VI)	0.01	0.02	0.01	-0.01	0.03	0.01	0.02
Cr	0.00	0.00	0.00	0.00	0.00	0.00	0.00
Mg	0.70	0.90	0.90	0.75	0.83	0.93	0.85
Ca	0.53	0.68	0.66	0.39	0.66	0.67	0.32
Fe	0.71	0.35	0.39	0.84	0.41	0.35	0.76
Mn	0.01	0.01	0.01	0.02	0.01	0.01	0.01
Na	0.02	0.02	0.02	0.01	0.02	0.02	0.01
K	0.00	0.00	0.00	0.00	0.00	0.00	0.00
Fe3+	0.11	0.05	0.06	0.13	0.06	0.05	0.11
Fe2+	0.59	0.29	0.33	0.70	0.34	0.29	0.63
M1	0.84	1.00	0.99	0.88	0.96	1.01	1.00
M2	1.13	0.99	1.00	1.10	1.03	0.98	0.96
Cation Sum	**3.99**	**3.99**	**4.00**	**4.00**	**3.99**	**4.00**	**3.98**
Mg #	50.08	72.38	69.85	47.56	67.28	72.55	53.14

149

Table 4N- Microprobe Analyses of Groundmass Pyroxene

	GR-SBM2269-1py	GR-SBM2269-1py	GR-SBM2269-1py	GR-SBM2269-2py	GR-BM2269-2py	GR-BM2269-2py	GR-SBM2269-2py
SiO2	53.46	53.21	52.55	53.17	51.59	52.20	51.18
TiO2	0.42	0.46	0.52	0.60	0.80	0.69	0.92
Al2O3	1.01	1.19	1.38	1.50	0.84	1.73	1.15
Cr2O3	0.04	0.04	0.00	0.04	0.05	0.06	0.00
MgO	19.56	21.59	16.56	17.04	13.61	15.53	11.49
CaO	8.83	6.17	15.45	15.05	11.30	16.93	15.59
FeO	16.09	15.83	12.09	11.92	23.01	12.48	19.73
MnO	0.22	0.32	0.16	0.26	0.23	0.22	0.28
Na2O	0.12	0.07	0.20	0.19	0.17	0.23	0.23
K2O	0.00	0.00	0.00	0.01	0.02	0.01	0.01
Total	**99.76**	**98.86**	**98.91**	**99.77**	**101.61**	**100.07**	**100.58**
Structural Formulae							
Cations per 6 oxygen							
Si	1.98	1.98	1.97	1.97	1.96	1.95	1.96
Ti	0.01	0.01	0.01	0.02	0.02	0.02	0.03
Al (IV)	0.02	0.02	0.03	0.03	0.04	0.05	0.04
Al (VI)	0.03	0.03	0.03	0.04	0.00	0.03	0.01
Cr	0.00	0.00	0.00	0.00	0.00	0.00	0.00
Mg	1.08	1.19	0.93	0.94	0.77	0.86	0.66
Ca	0.35	0.25	0.62	0.60	0.46	0.68	0.64
Fe	0.50	0.49	0.38	0.37	0.73	0.39	0.63
Mn	0.01	0.01	0.01	0.01	0.01	0.01	0.01
Na	0.01	0.01	0.01	0.01	0.01	0.02	0.02
K	0.00	0.00	0.00	0.00	0.00	0.00	0.00
Fe3+	0.07	0.07	0.06	0.06	0.11	0.06	0.09
Fe2+	0.42	0.41	0.32	0.31	0.61	0.32	0.53
M1	1.20	1.31	1.03	1.05	0.90	0.97	0.79
M2	0.78	0.66	0.95	0.92	1.08	1.02	1.18
Cation Sum	**3.98**	**3.98**	**3.99**	**3.98**	**3.99**	**3.99**	**3.98**
Mg #	68.59	71.01	71.11	71.97	51.52	69.09	51.12

Table 4O- Microprobe Analyses of Groundmass Pyroxene

	GR-SBM2269-2py	GR-SBM2269-3py	GR-SBM2269-4py	GR-SBM2269-4py	GR-SBM2269-4py	GR-SBM2269-4py	GR-SBM2269-5py
SiO_2	50.55	52.17	52.01	51.13	51.83	51.75	50.44
TiO_2	1.00	0.49	0.48	0.94	0.37	0.63	1.00
Al_2O_3	1.20	1.29	0.61	0.83	0.61	1.01	1.22
Cr_2O_3	0.00	0.03	0.06	0.00	0.00	0.00	0.02
MgO	12.34	16.86	17.64	13.20	20.34	16.03	11.94
CaO	12.64	16.10	4.63	14.43	4.82	14.19	13.49
FeO	22.50	11.60	23.72	19.11	21.56	15.12	22.10
MnO	0.30	0.24	0.34	0.25	0.31	0.26	0.27
Na_2O	0.18	0.22	0.09	0.26	0.13	0.16	0.21
K_2O	0.01	0.01	0.02	0.04	0.03	0.01	0.00
Total	**100.72**	**99.01**	**99.60**	**100.19**	**100.00**	**99.17**	**100.70**
Structural Formulae							
Cations per 6 oxygen							
Si	1.95	1.96	1.98	1.96	1.95	1.96	1.94
Ti	0.03	0.01	0.01	0.03	0.01	0.02	0.03
Al (IV)	0.05	0.04	0.02	0.04	0.05	0.04	0.06
Al (VI)	0.00	0.01	0.01	-0.01	-0.02	0.01	0.00
Cr	0.00	0.00	0.00	0.00	0.00	0.00	0.00
Mg	0.71	0.94	1.00	0.75	1.14	0.90	0.69
Ca	0.52	0.65	0.19	0.59	0.19	0.58	0.56
Fe	0.72	0.36	0.76	0.61	0.68	0.48	0.71
Mn	0.01	0.01	0.01	0.01	0.01	0.01	0.01
Na	0.01	0.02	0.01	0.02	0.01	0.01	0.02
K	0.00	0.00	0.00	0.00	0.00	0.00	0.00
Fe3+	0.11	0.05	0.11	0.09	0.10	0.07	0.11
Fe2+	0.60	0.30	0.63	0.51	0.57	0.40	0.59
M1	0.85	1.03	1.14	0.87	1.24	1.00	0.82
M2	1.14	0.97	0.83	1.12	0.77	0.99	1.17
Cation Sum	**3.99**	**4.00**	**3.98**	**4.00**	**4.02**	**4.00**	**4.00**
Mg #	49.63	72.30	57.19	55.37	62.89	65.56	49.24

151

Table 4P- Microprobe Analyses of Groundmass Pyroxene

	GR-SBM2269-6py	GR-BM2269-7py	GR-SBM2269-7py	GR-SBM2269-7py	GR-SBM2269-8py	GR-SBM2269-8pyc	GR-SBM2269-8pyr
SiO2	51.02	52.33	52.00	53.69	52.10	53.16	50.42
TiO2	0.54	0.45	0.54	0.35	0.78	0.38	0.96
Al2O3	1.27	1.21	1.95	0.71	1.57	0.71	1.50
Cr2O3	0.08	0.10	0.04	0.00	0.00	0.09	0.01
MgO	15.83	19.06	16.56	22.50	15.17	20.40	12.44
CaO	13.88	12.12	17.62	4.64	18.64	8.29	14.04
FeO	15.22	13.49	9.64	18.43	10.51	17.00	19.96
MnO	0.18	0.27	0.25	0.28	0.21	0.26	0.28
Na2O	0.19	0.16	0.26	0.06	0.20	0.11	0.31
K2O	0.01	0.01	0.01	0.00	0.02	0.01	0.05
Total	**98.22**	**99.19**	**98.86**	**100.65**	**99.18**	**100.42**	**99.97**
Structural Formulae							
Cations per 6 oxygen							
Si	1.95	1.95	1.95	1.97	1.96	1.97	1.94
Ti	0.02	0.01	0.02	0.01	0.02	0.01	0.03
Al (IV)	0.05	0.05	0.05	0.03	0.04	0.03	0.06
Al (VI)	0.01	0.01	0.03	0.00	0.02	0.00	0.01
Cr	0.00	0.00	0.00	0.00	0.00	0.00	0.00
Mg	0.90	1.06	0.92	1.23	0.85	1.13	0.71
Ca	0.57	0.48	0.71	0.18	0.75	0.33	0.58
Fe	0.49	0.42	0.30	0.57	0.33	0.53	0.64
Mn	0.01	0.01	0.01	0.01	0.01	0.01	0.01
Na	0.01	0.01	0.02	0.00	0.01	0.01	0.02
K	0.00	0.00	0.00	0.00	0.00	0.00	0.00
Fe3+	0.07	0.06	0.05	0.08	0.05	0.08	0.10
Fe2+	0.41	0.35	0.25	0.47	0.27	0.44	0.54
M1	1.00	1.15	1.02	1.33	0.94	1.22	0.85
M2	0.99	0.85	0.98	0.66	1.04	0.78	1.14
Cation Sum	**4.00**	**4.00**	**4.00**	**4.00**	**3.99**	**4.00**	**4.00**
Mg #	65.14	71.74	75.54	68.69	72.17	68.30	52.81

152

Table 4Q- Microprobe Analyses of Groundmass Pyroxene

	GR-BM2570-1py	GR-SBM2570-1pyc2	GR-SBM2570-1pyr2	GR-SBM2570-1py	GR-SBM2570-1py	GR-SBM2570-2py	GR-SBM2570-2py
SiO2	51.87	52.58	50.43	52.62	50.96	52.72	51.31
TiO2	0.74	0.74	0.99	0.65	0.94	0.62	0.82
Al2O3	1.65	1.58	1.72	1.39	1.53	1.42	2.74
Cr2O3	0.06	0.03	0.00	0.08	0.04	0.01	0.11
MgO	15.37	16.18	12.57	16.73	13.92	15.92	15.47
CaO	18.09	15.34	17.16	15.03	16.24	15.13	18.00
FeO	11.82	14.38	17.61	13.66	16.53	14.65	10.37
MnO	0.16	0.22	0.25	0.24	0.21	0.25	0.16
Na2O	0.22	0.19	0.30	0.21	0.24	0.22	0.27
K2O	0.00	0.02	0.02	0.00	0.00	0.00	0.02
Total	**99.98**	**101.26**	**101.05**	**100.63**	**100.63**	**100.93**	**99.25**
Structural Formulae							
Cations per 6 oxygen							
Si	1.94	1.95	1.92	1.95	1.93	1.96	1.92
Ti	0.02	0.02	0.03	0.02	0.03	0.02	0.02
Al (IV)	0.06	0.05	0.08	0.05	0.07	0.04	0.08
Al (VI)	0.01	0.02	0.00	0.01	0.00	0.02	0.04
Cr	0.00	0.00	0.00	0.00	0.00	0.00	0.00
Mg	0.86	0.89	0.71	0.93	0.79	0.88	0.86
Ca	0.73	0.61	0.70	0.60	0.66	0.60	0.72
Fe	0.37	0.45	0.56	0.42	0.52	0.46	0.32
Mn	0.01	0.01	0.01	0.01	0.01	0.01	0.00
Na	0.02	0.01	0.02	0.02	0.02	0.02	0.02
K	0.00	0.00	0.00	0.00	0.00	0.00	0.00
Fe3+	0.06	0.07	0.08	0.06	0.08	0.07	0.05
Fe2+	0.31	0.37	0.47	0.35	0.44	0.38	0.27
M1	0.95	1.00	0.82	1.02	0.89	0.99	0.98
M2	1.05	0.99	1.19	0.97	1.11	1.00	1.01
Cation Sum	**4.00**	**4.00**	**4.02**	**4.00**	**4.01**	**3.99**	**4.00**
Mg #	70.03	66.90	56.19	68.75	60.20	66.14	72.82

153

Table 4R- Microprobe Analyses of Groundmass Pyroxene

	GR-BM2570-2py	GR-SBM2570-4pyc1	GR-SBM2570-4pyr1	GR-SBM2570-4pyc2	GR-SBM2570-4pyr2	GR-SBM2570-4py	GR-SBM2570-4pyc
SiO2	54.24	50.99	50.57	53.90	50.85	52.98	54.02
TiO2	0.25	0.95	0.96	0.41	0.95	0.49	0.25
Al2O3	0.58	3.16	1.26	1.53	1.29	1.94	0.63
Cr2O3	0.08	0.08	0.06	0.08	0.00	0.01	0.00
MgO	23.54	16.81	12.82	23.77	11.39	21.15	23.96
CaO	3.71	13.80	13.67	4.81	16.33	9.21	3.79
FeO	18.56	14.59	21.57	16.62	19.24	13.79	17.17
MnO	0.30	0.31	0.34	0.25	0.27	0.23	0.32
Na2O	0.06	0.25	0.23	0.07	0.23	0.13	0.06
K2O	0.02	0.00	0.00	0.00	0.01	0.00	0.00
Total	**101.35**	**100.93**	**101.49**	**101.42**	**100.54**	**99.93**	**100.18**
Structural Formulae							
Cations per 6 oxygen							
Si	1.97	1.89	1.93	1.95	1.95	1.95	1.98
Ti	0.01	0.03	0.03	0.01	0.03	0.01	0.01
Al (IV)	0.03	0.11	0.07	0.05	0.05	0.05	0.02
Al (VI)	0.00	0.03	-0.01	0.01	0.01	0.03	0.00
Cr	0.00	0.00	0.00	0.00	0.00	0.00	0.00
Mg	1.28	0.93	0.73	1.28	0.65	1.16	1.31
Ca	0.14	0.55	0.56	0.19	0.67	0.36	0.15
Fe	0.56	0.45	0.69	0.50	0.62	0.42	0.53
Mn	0.01	0.01	0.01	0.01	0.01	0.01	0.01
Na	0.00	0.02	0.02	0.00	0.02	0.01	0.00
K	0.00	0.00	0.00	0.00	0.00	0.00	0.00
Fe3+	0.08	0.07	0.10	0.08	0.09	0.06	0.08
Fe2+	0.47	0.38	0.57	0.42	0.51	0.35	0.44
M1	1.37	1.06	0.85	1.38	0.78	1.26	1.40
M2	0.62	0.94	1.15	0.61	1.20	0.72	0.59
Cation Sum	**4.00**	**4.01**	**4.01**	**4.00**	**3.99**	**4.00**	**4.00**
Mg #	69.50	67.41	51.64	71.98	51.53	73.37	71.48

154

Table 4S- Microprobe Analyses of Groundmass Pyroxene

	GR-SBM2570-4pyr	GR-SBM2570-4py	GR-BM2570-5py	GR-SBM2570-6py	GR-SBM2570-6py	GR-BM2570-7py	GR-BM2570-7py
SiO_2	51.33	52.51	52.04	51.08	52.28	52.91	52.72
TiO_2	0.61	0.75	0.66	0.96	0.58	0.62	0.69
Al_2O_3	0.79	1.56	2.36	1.43	1.42	1.42	1.53
Cr_2O_3	0.00	0.03	0.14	0.00	0.06	0.01	0.03
MgO	15.51	15.56	17.40	12.26	16.00	16.14	16.46
CaO	5.03	18.06	14.75	15.98	16.40	15.99	16.25
FeO	26.72	11.32	13.22	18.19	12.85	12.67	12.85
MnO	0.41	0.20	0.27	0.20	0.16	0.22	0.25
Na_2O	0.10	0.23	0.16	0.27	0.20	0.23	0.19
K_2O	0.01	0.00	0.00	0.03	0.00	0.01	0.03
Total	**100.52**	**100.24**	**101.00**	**100.40**	**99.96**	**100.21**	**100.99**
Structural Formulae							
Cations per 6 oxygen							
Si	1.97	1.95	1.92	1.95	1.95	1.97	1.95
Ti	0.02	0.02	0.02	0.03	0.02	0.02	0.02
Al (IV)	0.03	0.05	0.08	0.05	0.05	0.03	0.05
Al (VI)	0.01	0.02	0.02	0.01	0.02	0.03	0.02
Cr	0.00	0.00	0.00	0.00	0.00	0.00	0.00
Mg	0.89	0.86	0.96	0.70	0.89	0.89	0.91
Ca	0.21	0.72	0.58	0.65	0.66	0.64	0.64
Fe	0.86	0.35	0.41	0.58	0.40	0.39	0.40
Mn	0.01	0.01	0.01	0.01	0.01	0.01	0.01
Na	0.01	0.02	0.01	0.02	0.01	0.02	0.01
K	0.00	0.00	0.00	0.00	0.00	0.00	0.00
Fe^{3+}	0.13	0.05	0.06	0.09	0.06	0.06	0.06
Fe^{2+}	0.71	0.29	0.34	0.48	0.33	0.33	0.33
M1	1.04	0.96	1.06	0.83	0.99	1.00	1.00
M2	0.93	1.03	0.93	1.16	1.01	0.98	0.99
Cation Sum	**3.98**	**3.99**	**4.01**	**3.99**	**4.00**	**3.99**	**4.00**
Mg #	51.06	71.17	70.27	54.78	69.09	69.58	69.71

155

Table 4T- Microprobe Analyses of Groundmass Pyroxene

	GR-SBM2570-7py	GR-SBM2570-7py	GR-U3406-2py	GR-U3406-2py	GR-U3406-3py	GR-U3406-7py	GR-U3406-7py	GR-U3406-7py
SiO_2	52.07	52.67	49.12	49.50	51.26	47.46	47.14	46.73
TiO_2	0.77	0.69	1.82	1.32	0.91	2.15	1.99	2.38
Al_2O_3	1.60	1.65	3.59	3.12	2.16	4.80	3.95	4.70
Cr_2O_3	0.05	0.03	0.01	0.01	0.01	0.00	0.00	0.03
MgO	15.64	16.40	12.96	12.90	14.71	11.31	11.41	11.06
CaO	16.78	14.74	16.17	16.62	16.98	16.03	14.00	15.71
FeO	13.15	14.51	16.07	15.49	12.84	16.61	20.02	17.85
MnO	0.20	0.15	0.16	0.20	0.19	0.22	0.35	0.17
Na_2O	0.24	0.15	0.30	0.31	0.27	0.40	0.37	0.38
K_2O	0.00	0.00	0.02	0.06	0.01	0.11	0.01	0.03
Total	**100.50**	**101.00**	**100.20**	**99.52**	**99.32**	**99.09**	**99.25**	**99.04**
Structural Formulae		Cations per 6 oxygen						
Si	1.94	1.95	1.87	1.89	1.93	1.83	1.84	1.82
Ti	0.02	0.02	0.05	0.04	0.03	0.06	0.06	0.07
Al (IV)	0.06	0.05	0.13	0.11	0.07	0.17	0.16	0.18
Al (VI)	0.01	0.02	0.03	0.03	0.03	0.05	0.02	0.03
Cr	0.00	0.00	0.00	0.00	0.00	0.00	0.00	0.00
Mg	0.87	0.91	0.73	0.73	0.83	0.65	0.66	0.64
Ca	0.67	0.59	0.66	0.68	0.69	0.66	0.59	0.66
Fe	0.41	0.45	0.51	0.50	0.41	0.54	0.65	0.58
Mn	0.01	0.00	0.01	0.01	0.01	0.01	0.01	0.01
Na	0.02	0.01	0.02	0.02	0.02	0.03	0.03	0.03
K	0.00	0.00	0.00	0.00	0.00	0.01	0.00	0.00
Fe^{3+}	0.06	0.07	0.08	0.07	0.06	0.08	0.10	0.09
Fe^{2+}	0.34	0.37	0.43	0.41	0.34	0.45	0.54	0.48
M1	0.97	1.02	0.89	0.88	0.94	0.85	0.84	0.83
M2	1.03	0.97	1.11	1.12	1.04	1.14	1.16	1.17
Cation Sum	**4.00**	**3.99**	**4.00**	**4.00**	**3.99**	**4.00**	**4.01**	**4.01**
Mg #	68.12	66.99	59.16	59.94	67.29	55.01	50.59	52.67

156

Table 5A - Microprobe Analyses of Olivine in Groundmass

	GR-13-4OL	GR-13-7OL	CHI-16-1ol	CHI-16-1ol3	CHI-16-2-olin	CHI-16-2-ol	CHI-16-2-ol2
SiO2	33.14	33.48	36.44	36.95	36.41	36.21	36.13
TiO2	0.01	0.06	0.07	0.09	0.07	0.03	0.06
Al2O3	0.00	0.00	0.03	0.01	0.04	0.00	0.08
Cr2O3	0.02	0.00	0.00	0.01	0.00	0.00	0.01
MgO	13.01	13.37	27.48	27.50	27.95	28.52	28.00
CaO	0.29	0.11	0.33	0.32	0.62	0.32	0.34
FeO	55.16	54.19	36.52	35.82	32.88	38.23	36.54
MnO	0.82	0.77	0.48	0.56	0.54	0.52	0.62
Na2O	0.00	0.00	0.02	0.00	0.03	0.00	0.04
K2O	0.00	0.00	0.01	0.00	0.01	0.00	0.00
Total	102.46	101.97	101.39	101.26	98.55	103.83	101.82
Structural Formulae							
Cations per 4 Oxygen							
Si	1.00	1.01	1.00	1.01	1.02	0.98	0.99
Ti	0.00	0.00	0.00	0.00	0.00	0.00	0.00
Al (IV)	0.00	0.00	0.00	0.00	0.00	0.00	0.00
Al (VI)	0.00	0.00	0.00	0.00	0.00	0.00	0.00
Cr	0.00	0.00	0.00	0.00	0.00	0.00	0.00
Mg	0.58	0.60	1.13	1.12	1.16	1.15	1.15
Ca	0.01	0.00	0.01	0.01	0.02	0.01	0.01
Fe	1.39	1.36	0.84	0.82	0.77	0.87	0.84
Mn	0.02	0.02	0.01	0.01	0.01	0.01	0.01
Na	0.00	0.00	0.00	0.00	0.00	0.00	0.00
K	0.00	0.00	0.00	0.00	0.00	0.00	0.00
Cation Sum	**3.00**	**2.99**	**3.00**	**2.98**	**2.98**	**3.02**	**3.01**
Mg#	29.76	30.71	57.48	57.97	60.43	57.27	57.92

157

Table 5B- Microprobe Analyses of Olivine in Groundmass

	CHI-16-2-ol3	CHI-16-2-ol4	CHI-16-2-ol5	CHI-19-1ol	CHI-21-2oll	CHI-21-2ol	CHI-22-3OL
SiO2	36.11	36.14	36.34	33.44	35.82	35.89	33.38
TiO2	0.04	0.06	0.06	0.05	0.30	0.31	0.10
Al2O3	0.01	0.01	0.01	0.02	0.20	0.17	0.01
Cr2O3	0.00	0.00	0.01	0.00	0.00	0.00	0.04
MgO	28.31	28.17	27.90	16.20	24.99	24.94	14.12
CaO	0.37	0.37	0.34	0.33	0.50	0.50	0.30
FeO	37.38	34.53	36.70	51.10	38.69	38.90	52.07
MnO	0.63	0.61	0.59	0.70	0.82	0.82	0.83
Na2O	0.01	0.00	0.00	0.00	0.16	0.20	0.00
K2O	0.00	0.00	0.00	0.00	0.10	0.09	0.00
Total	**102.87**	**99.89**	**101.95**	**101.84**	**101.57**	**101.81**	**100.86**
Structural Formulae							
Cations per 4 Oxygen							
Si	0.98	1.00	1.00	1.00	1.00	1.00	1.01
Ti	0.00	0.00	0.00	0.00	0.01	0.01	0.00
Al (IV)	0.00	0.00	0.00	0.00	0.00	0.00	0.00
Al (VI)	0.00	0.00	0.00	0.00	0.00	0.00	0.00
Cr	0.00	0.00	0.00	0.00	0.00	0.00	0.00
Mg	1.15	1.17	1.14	1.14	1.04	1.04	0.64
Ca	0.01	0.01	0.01	0.01	0.01	0.02	0.01
Fe	0.85	0.80	0.84	0.84	0.90	0.91	1.31
Mn	0.01	0.01	0.01	0.01	0.02	0.02	0.02
Na	0.00	0.00	0.00	0.00	0.01	0.01	0.00
K	0.00	0.00	0.00	0.00	0.00	0.00	0.00
Cation Sum	**3.01**	**3.00**	**3.00**	**3.00**	**3.00**	**3.00**	**2.99**
Mg#	57.63	59.44	57.73	36.28	53.71	53.52	32.75

Table 5C- Microprobe Analyses of Olivine in Groundmass

	CHI-22-3OL1	CHI-22-3OL2	CHI-24-7OL	GR-U3406-7ol	GR-U3406-7ol	GR-U3406-2py	GR-U3406-2py
SiO2	33.25	33.14	33.85	36.63	34.62	35.96	36.19
TiO2	0.05	0.06	0.02	40.50	48.98	36.13	35.58
Al2O3	0.02	0.00	0.00	0.85	0.47	0.34	0.31
Cr2O3	0.00	0.00	0.01	0.24	0.25	0.00	0.00
MgO	13.53	13.27	15.59	0.19	0.30	0.06	0.06
CaO	0.37	0.34	0.33	1.65	0.67	0.02	0.03
FeO	55.33	55.25	52.48	0.32	0.46	0.38	0.27
MnO	0.88	0.87	0.82	0.09	0.27	0.00	0.01
Na2O	0.00	0.02	0.00	18.89	13.14	27.66	26.77
K2O	0.01	0.00	0.02	0.00	0.01	0.01	0.00
Total	**103.43**	**102.96**	**103.12**	**99.36**	**99.15**	**100.56**	**99.22**
Structural Formulae							
Cations per 4 Oxygen							
Si	0.99	0.99	1.00	0.95	0.88	0.94	0.94
Ti	0.00	0.00	0.00	0.79	0.94	0.71	0.71
Al (IV)	0.00	0.00	0.00	0.00	0.00	0.00	0.00
Al (VI)	0.00	0.00	0.00	0.00	0.00	0.00	0.00
Cr	0.00	0.00	0.00	0.00	0.00	0.00	0.00
Mg	0.60	0.59	0.68	0.01	0.01	0.00	0.00
Ca	0.01	0.01	0.01	0.05	0.02	0.00	0.00
Fe	1.38	1.38	1.29	0.01	0.01	0.01	0.01
Mn	0.02	0.02	0.02	0.00	0.01	0.00	0.00
Na	0.00	0.00	0.00	0.95	0.65	1.40	1.40
K	0.00	0.00	0.00	0.00	0.00	0.00	0.00
Cation Sum	**3.01**	**3.01**	**3.00**	**2.74**	**2.51**	**3.05**	**3.05**
Mg#	30.52	30.14	34.79	51.92	54.39	21.27	28.45

159

CHAPTER 4.

MODELING OF MELTING CONDITIONS

Introduction

Most geologists consider all large igneous provinces (LIPs) to have a similar mode of origin no matter what the ages, volumes or petrologic characteristics. As pointed out earlier (Chapter 1), the most popular hypothesis has been LIP magma generation by melting of large plume "heads" that rise from the deep mantle, perhaps the D" layer. In such models, the "tail" of a plume persists for millions of years and generates volcanic chains on a moving plate (Richards et al. 1989). However, LIPs differ substantially in age, location, and geochemistry.

The CRBG (particularly, GRB) is different from other LIPs, such as the Deccan Traps (e.g., Hooper, 1997) and from active hot spot basalts e.g. Iceland and Hawaii in terms of all major oxides except SiO_2 (Figure 32). From this, one could argue that GRB lavas were derived in some manner that differed from these other provinces. Is this difference attributable to varying source compositions, melting conditions (temperature, pressure, volatile abundance), or ascent paths (i.e., crystallization, crustal contamination, and magma mixing, isobaric vs. polybaric evolution etc.)? These questions can only be answered by modeling of the formation and ascent histories of individual provinces. In this chapter I use geochemical modeling techniques to illustrate the origin of GRB magmas; a comparative analysis with other LIPs will be a future endeavor.
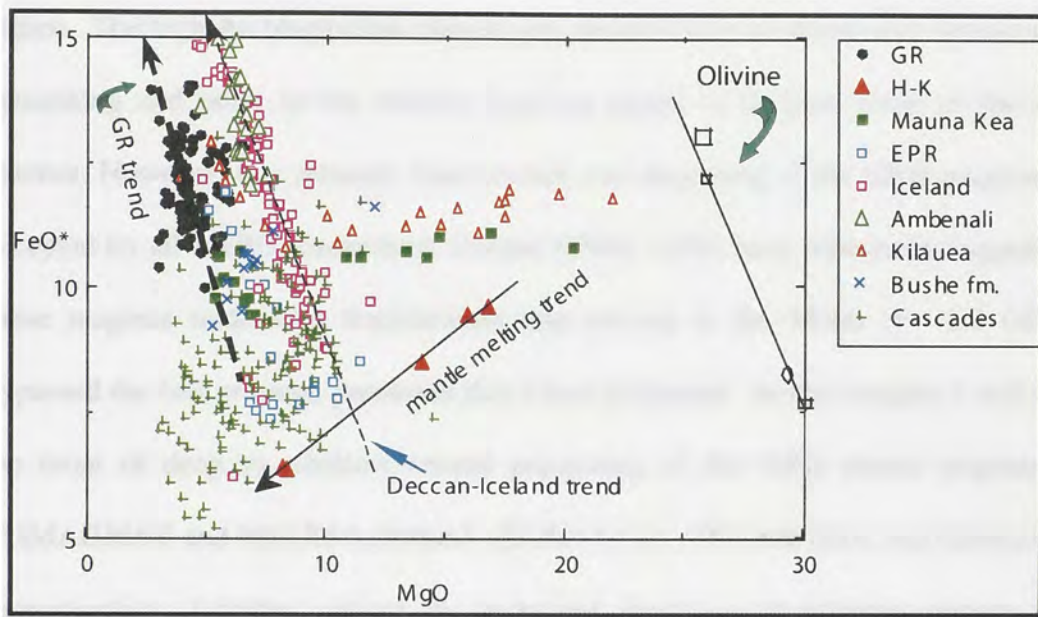
Figure 32- Plot showing how different GRB lavas are from other LIPs and presently active hot spots or plume basalts such as Iceland, Deccan (Ambenali Fm.), and Hawaii in terms of the major oxides, FeO and MgO. Data obtained from the GEOROC database (http://georoc.mpch-mainz.gwdg.de/georoc/).

In Chapters 2 and 3, based on phenocryst assemblages, textural features, and projected phase compositions on pseudoternary phase diagrams, I concluded that GRB lava was processed in shallow crustal magma chambers. Low-pressure fractionation, magma mixing and mingling, and degassing processes have obliterated the geochemical and physical characteristics that the magma batches inherited from their mantle source region. The high-An plagioclase phenocrysts seem to have survived such intense shallow processing and point to the initially hydrous nature of at least some of the magma batches. However, low pressure fractionation and degassing of the GRB magmas is not accepted by all CRBG researchers, Hooper (1984, 1988) have repeatedly suggested that these magmas underwent fractionation and mixing at the Moho (P ~1.2 GPa) and bypassed the low pressure processes that I have proposed. In this chapter, I will explore the issue of deep vs. shallow crustal processing of the GRB parent magmas using COMAGMAT and MELTS softwares (Ariskin et al., 1993 and Sack and Ghiorso, 1994, respectively). I further extend the numerical modeling to estimate primary magma compositions and their formation conditions (i.e., P, T, and $XH2O$), and to evaluate the nature of the source rocks (peridotite and/or eclogite).

In this study, I use the terms "primary" magma, "primitive" magma and "parental" magma in the same sense as detailed in Basaltic Volcanism on Terrestrial Planets (BVTP, 1981). A primary magma is one that has equilibrated with the source rock, whether it is a peridotite or an eclogite. It is often thought that tiny fractions of partial melt are generated within the source materials (peridotite, eclogite) over a wide volume (i.e., P-T space), and that these melts accumulate into larger bodies that equilibrate with the upper mantle before ascending toward the crust. I consider the

accumulated melt volume that equilibrated last with the source mantle volume to be primary magma, although every tiny fraction of melt that contributed to it can also be primary magma. In a suite of genetically related lavas, the one with the highest Mg/[Mg+Fe*] ratio is considered to be the parental or primitive magma because the idea is that such a magma could differentiate in conduits and generate the other less magnesian lavas. A primitive magma, on the other hand, is any lava with a fairly high Mg/[Mg+Fe*]. Thus, a primary magma is both primitive and parental to a suite of lavas, but the inverse is not necessarily true.

Geochemical Modeling

Forward and Inverse Modeling of Major Elements

I carried out both forward and inverse modeling to answer some of the questions outlined above. In inverse modeling, the usual approach is to start with the most magnesian lava (preferably aphyric, because only aphyric or glassy lavas are closest approximations of liquids) in a cogenetic suite of lavas and take it as the parent magma composition. Using partition coefficients or multi-saturation concepts (e.g., BVTP 1981, Herzberg and O'Hara 2002; Asimow and Longhi 2004) one can deduce whether such a composition could have equilibrated with a plausible upper mantle source rock. If a convincing case can be made, such a composition may be considered a primary magma. The P,T, and X_{H2O} conditions at which this primary magma is found to be in equilibrium with the source rock(s) are then considered to be the last mantle equilibration conditions of such a magma (Figure 33).
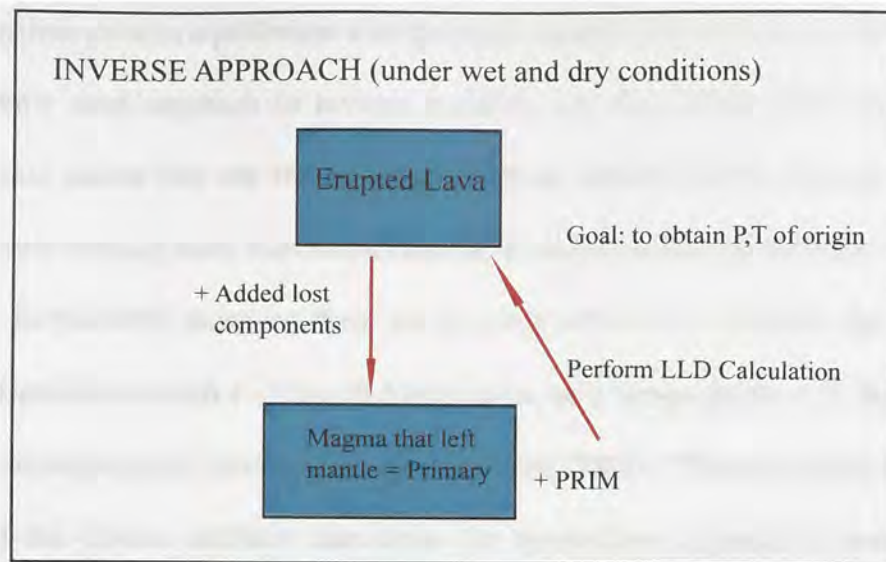
Figure 33- Schematic depicting the Inverse method used to model GRB magma under hydrous and anhydrous conditions at different pressures with a peridotitic starting material.

In reality, however, it is nearly impossible to find a glassy lava with appropriate MgO required to be in equilibrium with mantle; one rare exception to this is the recent finding by Clague and Moore, (1991) of glass fragments with 15% MgO from submarine landslides off Hawaiian shield volcanoes. Such high-MgO glasses could arguably be the best candidates for primary magmas in modern times. More typically, one has to use the most MgO-rich lava and, if possible demonstrate that such lava has not gained its high MgO by accumulation of olivine phenocrysts, but represents a liquid or near-liquid composition. If this lava has only olivine phenocrysts, then clearly, it has not reached multiphase saturation; and one could argue that such a lava composition can be extrapolated to a mantle-equilibrated primary magma composition by incrementally adding olivine while maintaining appropriate olivine-liquid equilibrium partition coefficient (K_d=0.3 for FeO, MgO exchange equilibrium between olivine and basaltic melt (Herzberg and O'Hara, 2002). The calculated primary magma must have the right

composition to be in equilibrium with the upper mantle olivine (Fo_{89-92}). This is the most commonly used approach in inverse modeling (cf. Sen 1994) and it works well for peridotitic source but not for an eclogitic upper mantle simply because eclogites are chemically nothing more than basalts and these compositions can therefore vary greatly.

In the GRB, however, there are no lavas with 15 wt. % MgO, nor are there any lava magnesian enough (~ 8 wt. % MgO) to be only olivine-phyric. In fact, these lavas are all ol+aug+pig+pl saturated (Durand and Sen, 2004). Thus, one must employ a step beyond the olivine addition calculation for the inverse approach to work. Tholeiitic basalts become olivine-saturated at ~ 8 wt. % MgO (Herzberg and O'Hara, 2002), therefore, I extrapolated a linear regression through the GRB data to 8 wt. % MgO, and selected that to be the parental magma to GRB basalts. Although I concluded earlier that the GRB trend is caused by mixing, the mafic mixing end member (B) lies along the 1 atm cotectic (Figure 28). Thus, for most major elements, the extrapolated 8 wt. % MgO parental magma is close to a composition that could form through LLD from a primary magma. To this parental composition, I then added olivine incrementally (in 2 wt% steps) until a reasonable primary magma composition was obtained (PRIM). This approach is also justified because the evolved mixing end member (A, in figure 28) also lies along the 1 atm cotectic. To check whether the 8 wt. % MgO parental melt so calculated can generate a liquid line of descent (LLD) through the GRB data, I ran that primary composition using COMAGMAT to simulate the LLD at P<0.6 GPa (required by our mineral data, see chapter 2). In this exercise I assume that the erupted GRB basalts were derived from more primitive magma, and are not primary magmas from eclogitic sources (Chapter 3).

At this stage I (1) compared my primary magma with experimental melts, and (2) crystallized them at various pressure using pMELTS (Paul Asimow, CalTech, ran these) to look for multiphase saturation points. Multiphase saturation points are "points" defined by intersection of several phase-saturation curves in P-T space (Asimow and Longhi, 2004). For natural magma compositions these are often not points but a fairly tight P,T area where several mineral phases are stable along with the calculated melt phase. The significance of such points is a matter of some debate but in general, these are thought to represent the P, T at which the primary magma would have equilibrated with the source rock (e.g., BVTP 1981, but see Asimow and Longhi, 2004).

In the forward modeling approach, I chose starting magma compositions from published data on experimentally generated partial melts of peridotite and eclogite sources at a variety of pressure, temperature, and volatile-bearing (mainly H_2O) conditions. Using COMAGMAT and pMELTS, I modeled the compositions of these magmas from their P, T of last mantle equilibration to the surface, while crystallizing in magma conduits at a single pressure or multiple pressures. The goal of such exercise was to see if I could derive the tightly grouped GRB liquid compositions from any experimentally produced melt by modeling the crystallization of the parent melt under any set of conditions.

As with all modeling efforts, there exist certain caveats: [1] COMAGMAT and pMELTS (and pHMELTS) have upper pressure limits of 1.5 and 3 GPa, respectively (Ariskin et al. 1993; Sack and Ghiorso, 1994). [2] The few melting studies of hydrous peridotite and eclogite mean that the quantitative effect of H_2O on phase equilibrium is not well constrained. [3] The few high-pressure crystallization studies of basaltic or

andesitic magmas mean that polybaric crystallization is also not well modeled by these simulations. Temperature, melt fraction, and phase compositions sometimes do not exactly duplicate experimental conditions; however, the overall trends match in most cases [e.g. Asimow and Longhi 2004; Asimow and Longhi 2004; Hirschmann et al., 1998, 1999].

The goal of both inverse and forward modeling was to determine at what P, T such magmas could form from an appropriate (eclogite or peridotite) source. Finally, I took the best model primary compositions and then performed a sort of "synthetic reversal experiment"; I took that primary magma composition and ran LLD calculations at various pressures using COMAGMAT in order to simulate the magma's chemical journey from its point of origin to eruption. This exercise revealed surprisingly tight constraints on P, T, X_{H2O} conditions for the primary GRB magma as described below.

RESULTS AND DISCUSSION

Inverse Modeling of Dry Primary Magma

A parental magma composition was obtained for the GR basalts by extrapolating a linear regression through the GRB data to 8 wt. % MgO. Olivine was added to this composition until a liquid composition could be found that would be in equilibrium with upper mantle olivine (Fo_{89}). The parent and primary magma compositions thus calculated are listed in as PAM and PRIM, respectively in Table 6. Using COMAGMAT, PRIM was then modeled to fractionally crystallize at 2.0 kb, 10 kb and 15 kb. These LLD's are shown in Figure 34 (a-d) and the temperature and phase appearance for 2 and 10 kb are shown for comparison in Table 7.

MgO vs. FeO and SiO₂ plots (Figure 34 a,c) show that all four LLD's could explain the GR data within the margin of error determined from comparisons with experimental data of Grove and Bryan (1983), and Tormey et al. (1987). However, MgO vs. Al₂O₃ and CaO plots (Figure 34 b,d) clearly show that the GRB data cannot be explained by high pressure (i.e., 10 or 15 kb) fractionation. At such higher pressures, augite appears before plagioclase and, thus, olivine + augite fractionation leaves the residual liquid with high Al₂O₃ and low CaO, which is seen in Table 7. The trend of MgO vs. CaO/ Al₂O₃ ratio in GRB can only be explained by low pressure (shallow crust) fractionation; higher pressure fractionation results in lower CaO/Al₂O₃ at an early stage of fractionation (Figure 35). This finding is consistent with the phenocryst assemblage and phase equilibria of GRB (Durand and Sen, 2004).

The LLD at 2 kb displays the best fit with regard to all the major oxides shown here. However, the 2 kb LLD seems to miss the bulk of the GRB MgO-SiO₂ and –FeO data (although within uncertainty). Because the presence of high-An phenocrysts signifies that GRB magmas may have been hydrous; therefore, a new set of calculations was performed with variable amounts of dissolved H₂O in the PRIM.

Table 6- Starting Compositions for Inverse Modeling

	8 wt. % MgO Composition (PAM)	Olivine addition Composition (PRIM)
SiO2	52.0	51.16
TiO2	0.82	0.76
Al2O3	17.5	16.16
FeO*	7.5	7.86
MgO	8.0	11.07
CaO	11.5	10.62
Na2O	2.57	2.37
Total	100.0	100.0

Table 7. Comparison of PRIM Phase Assemblages for best fit 2 and 10 kb dry runs.

Temperature	Phases	Temperature	Phases
T °C	2.0 kb	T °C	10 kb
1280	Ol+L	1311	Ol+L
1233	Ol+Plag.+L	1280	Ol+Aug.
1189	Ol+ Plag.+ Aug. +L	1278	Aug.
1144	Plag.+Aug.+Pig.	1265	Aug.+Plag.
1101	Plag.+Aug.+L	1259	Plag.+Aug.+Ol
1068	Plag.+Aug.+Mt+L	1219	Plag.+Aug.
1025	Plag.+Aug.+il+L		
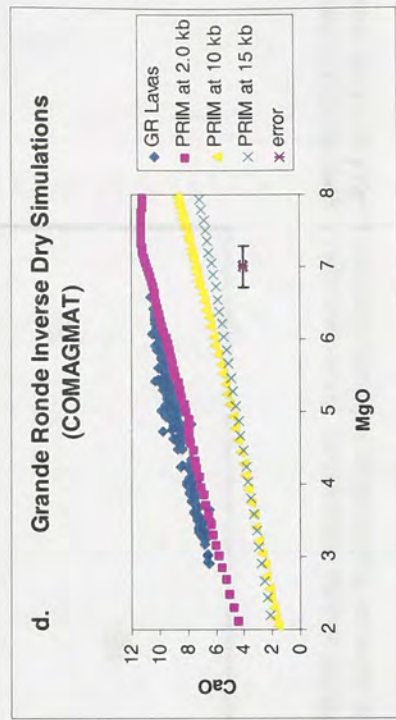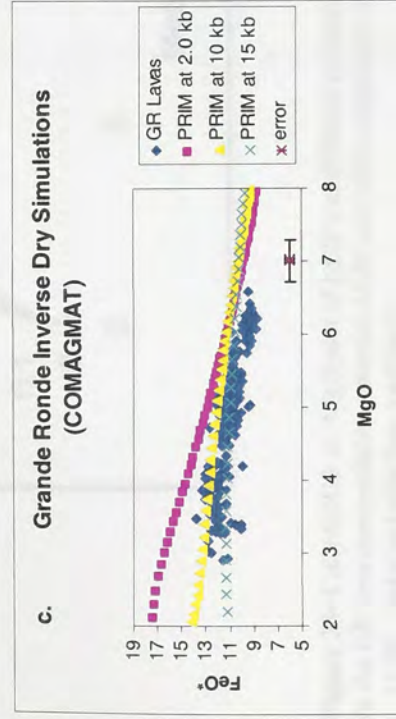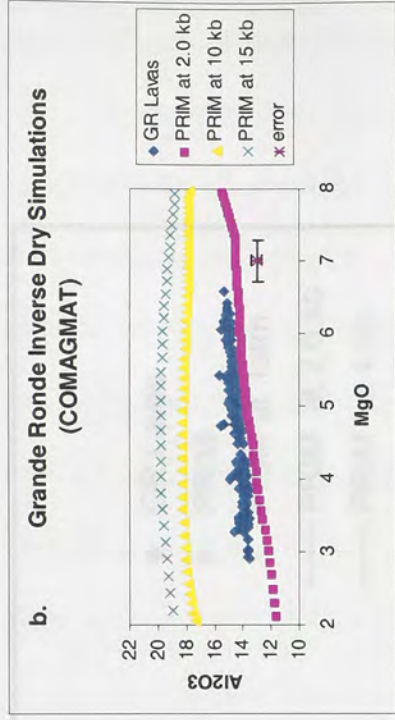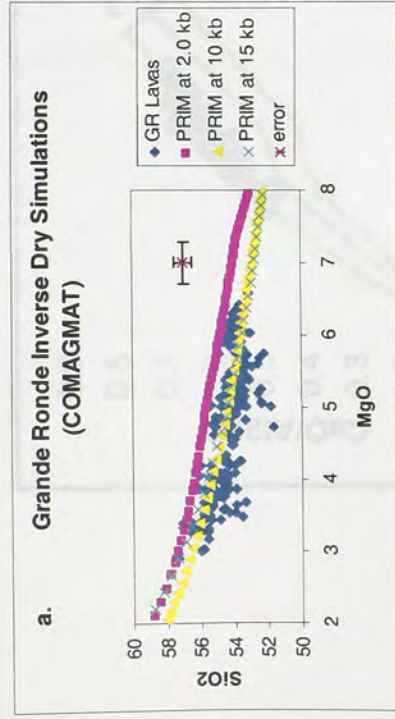
Figure 34-a-d shows inverse models for the best fit liquid lines of descent for a calculated PRIM composition (see text for explanation), a typical upper mantle peridotite melt, fractionated at different pressures (2.0, 10 and 15 kb). (a). SiO2 vs. MgO plot. (b). Al_2O_3 vs. MgO plot. (c). FeO* vs. MgO. (d). CaO vs. MgO. Error bars show mean error determined by comparisons of modeled LLD with experimental results of Grove and Bryan, 1983; and Tormey et al., 1987). Figures b and d clearly show that 10 and 15 kb LLDs cannot reproduce the GRB trend. The 2 kb LLD works well for MgO-CaO and MgO-Al_2O_3 but not for FeO, SiO₂ (a, c). Addition of small % of H_2O significantly improves the fit with the 2 kb LLD (Figure 36)

170
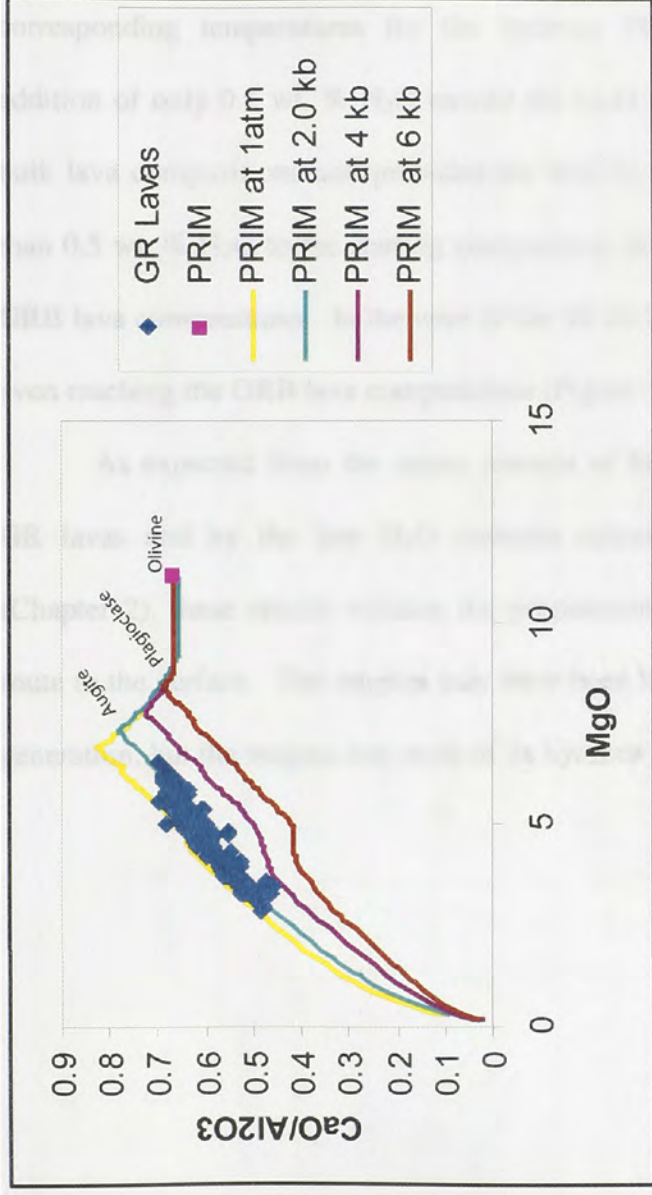
Figure 35- CaO/Al2O3 *vs.* MgO plot of LLD's at different pressures from a parental (PRIM) magma composition. Lower pressure (1 atm-2kb) LLD's best fit the GR lava compositions, whereas LLD's of >2kb completely miss the GR data. This rules out fractionation in magma chambers at the base of the crust (~13 kb), under volatile-free conditions.

Inverse Hydrous Models:
Role of Water in Shallow Fractionation

From 0.5 to 5 wt. % water was added to PRIM and then LLD's were generated at 2, 10, and 15 kb pressures. Table 8 displays the order of phase appearance and the corresponding temperatures for the hydrous PRIM composition simulations. The addition of only 0.5 wt. % H_2O moved the LLD's for SiO_2 and FeO towards the GRB bulk lava compositions and provided the best fit to the GRB lavas. Addition of more than 0.5 wt. % H_2O to the starting composition shifted the LLD's too far away from the GRB lava compositions. In the case of the 10 kb LLD, the hydrous melt runs out before even reaching the GRB lava compositions (Figure 36; a-d).

As expected from the minor amount of high-An plagioclase phenocrysts in the GR lavas and by the low H_2O contents calculated with Putirka's (2005) equation (Chapter 2), these results validate the proposition that the magma largely degassed en route to the surface. The magma may have been highly hydrous at the source of magma generation, but the magma lost most of its hydrous signature as it rose to the surface.

Table 8- Comparison of PRIM phase assemblages for best fit hydrous runs.

Temperature T °C	Phases 2.0 kb (0.5 wt. % H_2O)	Temperature T °C	Phases 2.0 kb (1.0 wt. % H_2O)
1272	Ol+L	1263	Ol+Plag.
1209	Ol+Plag.+L	1184	Ol+Plag.+Aug.
1157	Ol+ Plag.+L	1127	Ol+Plag.+Aug.+Pig.
1107	Ol+ Plag.+ Aug. +L	1086	Plag.+Aug.+Pig.
1037	Plag.+Aug.+Pig.	1083	Plag.+Aug.+Mt.
1030	Plag.+Aug.	1000	Ol.+Plag.
1272	Plag.+Aug.+Mt.		

173
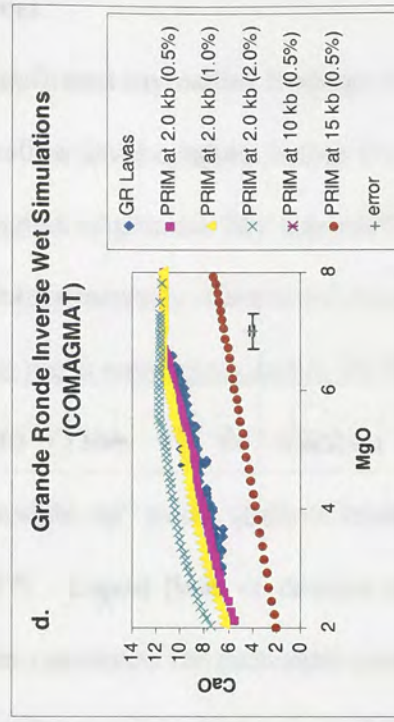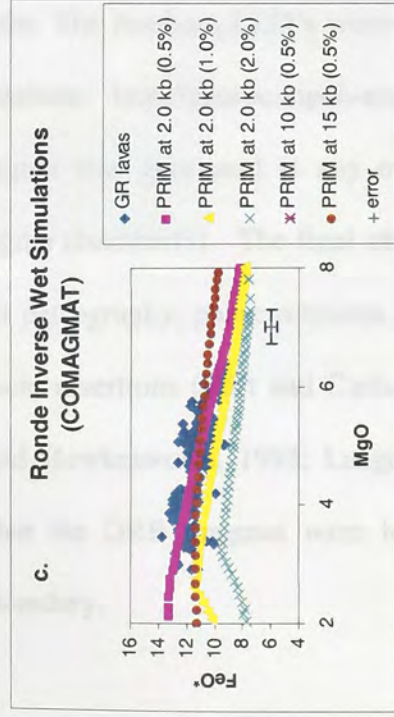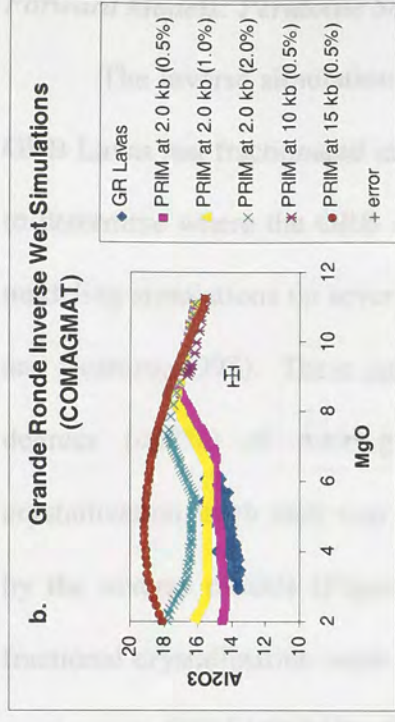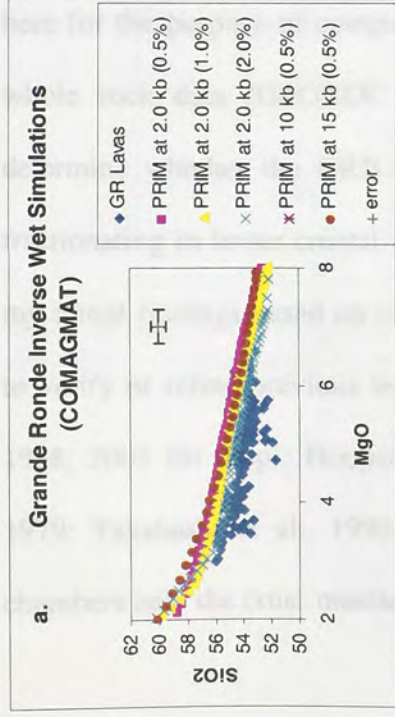
Figure 36-a-d show best fit liquid lines of descent of inverse models for a parental PRIM composition (see text for explanation), fractionated at different pressures (2.0, 10 and 15 kb) and under different water conditions (0.5%, 1.0% and 2.0 wt. %). (a). SiO_2 vs. MgO plot. (b). CaO vs. MgO plot. (c). FeO^* vs. MgO. (d). Al_2O_3 vs. MgO. Error bars show mean error determined by comparisons of modeled LLD with experimental results of Grove and Bryan, 1983; and Tormey et al., 1987).

Forward Models: Peridotite Sources

The inverse simulations confirmed my earlier findings (Chapter 2 and 3) that the GRB Lavas last fractionated in shallow-level conduits before erupting. My next goal was to determine where the GRB magmas originated. My approach was to conduct forward modeling simulations on several experimentally-determined mantle compositions (Hirose and Kushiro, 1993). These partial melts were generated at 10-30 kb by low to moderate degrees (<17%) of melting (F) (Table 9). To simulate low-pressure fractional crystallization, each melt was "brought up" to the shallow-levels previously constrained by the inverse models (Figure 37). Liquid lines of descent for both equilibrium and fractional crystallization were then calculated for each melt composition over a pressure range using COMAGMAT. In addition to simulating crystallization under volatile-free conditions, 0.5-2 wt. % H2O was added to each of the starting melts and LLD's were calculated at various pressures. Only the best-fit or most relevant models are discussed here for the purpose of comparison. The resultant LLD's were then compared with GR whole rock data (GEOROC database: http://georoc.mpch-mainz.gwdg.de/georoc/) to determine whether the GRB magma was generated at any of these pressures before fractionating in lower crustal magma chamber(s). The final objective was to (1) verify my initial findings based on GRB petrography, phase relations and H_2O content and (2) to verify or refute previous workers assertions (Hart and Carlson, 1987; Hooper, 1984, 1988, 2005 (in prep); Hooper and Hawkesworth, 1993; Lange, 2001; Swanson et al., 1979: Takahashi et al., 1998) that the GRB magmas were last processed in magma chambers near the crust-mantle boundary.

Table 9- Starting experimental compositions (Hirose and Kushiro, 1993)

	P (Kbar)	T	F	SiO2	TiO2	Al2O3	FeO*	MnO	MgO	CaO	Na2O	K2O
KLB-1	10.00	1250	0.07	51.32	1.09	19.09	6.38	0.23	8.14	8.85	4.60	0.27
	15.00	1300	0.06	50.71	1.04	19.31	6.37	0.14	8.31	7.75	5.47	0.73
	20.00	1375	0.14	47.47	0.75	15.53	8.51	0.18	13.94	11.11	2.22	0.08
	30.00	1500	0.17	45.67	0.99	14.33	9.59	0.17	16.73	10.64	1.80	0.07
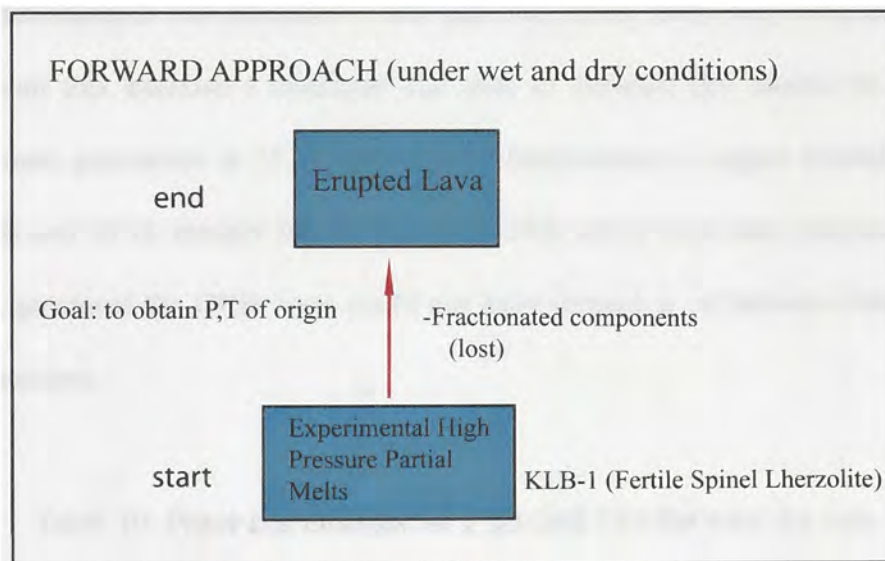
Figure 37-Schematic depicting the Forward method used to model GRB magma under hydrous and anhydrous conditions at different pressures with a peridotitic starting material.

Figure 38 shows oxide-oxide plots (Al_2O_3-MgO, FeO-MgO, CaO-MgO, and SiO_2-MgO) comparing GRB whole rock data with liquid lines of descent (LLD) for the different experimental partial melts. Liquid lines of descent for fractional crystallization of dry melt were calculated for each melt composition over this pressure range using COMAGMAT. All melts were fractionally crystallized at 1 atm and 2 kb and the results are shown in Table10.

Table 10 shows the phase appearance and corresponding temperatures of these best fit dry models. Figure 38 shows that 2 kb LLD's generated from 10, 20, and 30 kb melts do not at all resemble the GRB data. On the other hand, the melt generated at 15 kb and fractionated at low pressures (1 atm and 2 kb) fit the GRB data remarkably well.

From this exercise I conclude that best fit forward dry model for all oxides involves melt generation at 15 kb followed by fractionation in upper crustal chambers. The 20 kb and 30 kb models fall far from the GRB whole rock data indicating that the melt that generated the GRB lavas could not have formed at or between either of these higher pressures.

Table 10- Phase assemblages for 1 atm and 2 kb Forward dry runs

Temperature	Phases (15 kb)	Temperature	Phases (15 kb)
T °C	1 atm	T °C	2.0 kb
1364	Ol+L	1361	Ol+L
1216	Ol+Plag.	1223	Ol+Plag.
1186	Ol+Plag.+Aug.	1206	Ol+Plag.+Aug.
1146	Ol+Plag.+Aug.+Pig.	1157	Plag.+Aug.+Pig.
1144	Plag.+Aug.+Pig.	1116	Plag.+Aug.
1115	Plag.+Aug.	1361	Ol+L
1364	Ol+L		
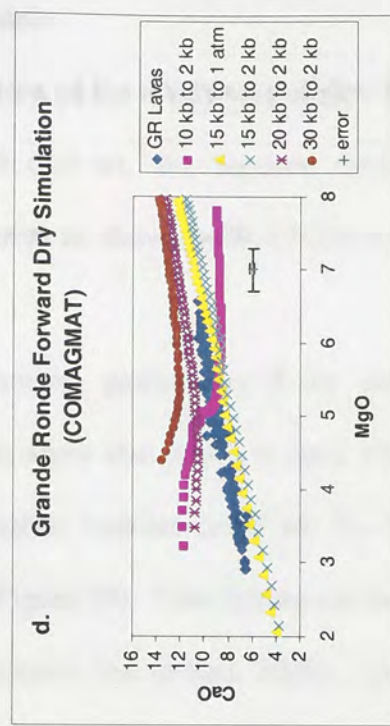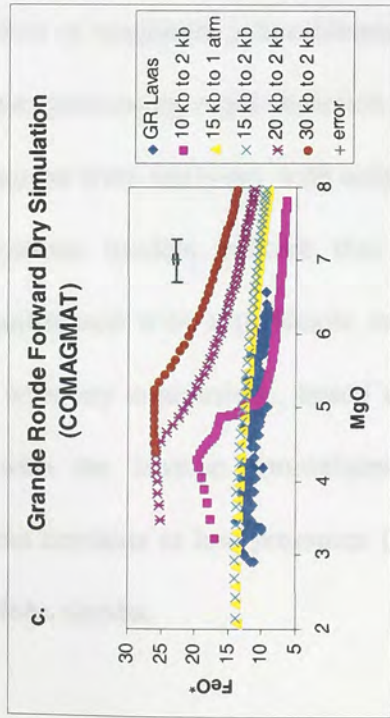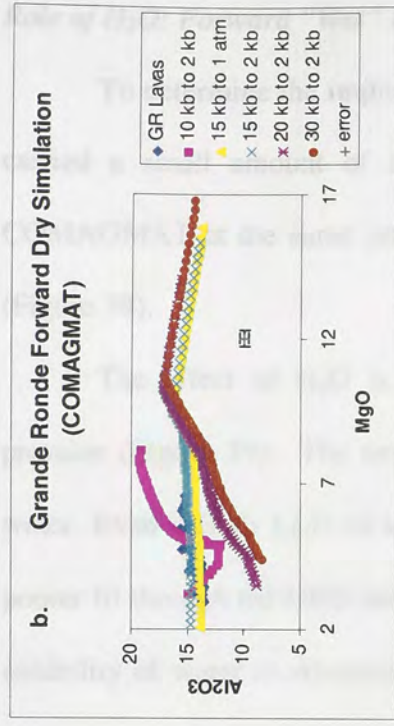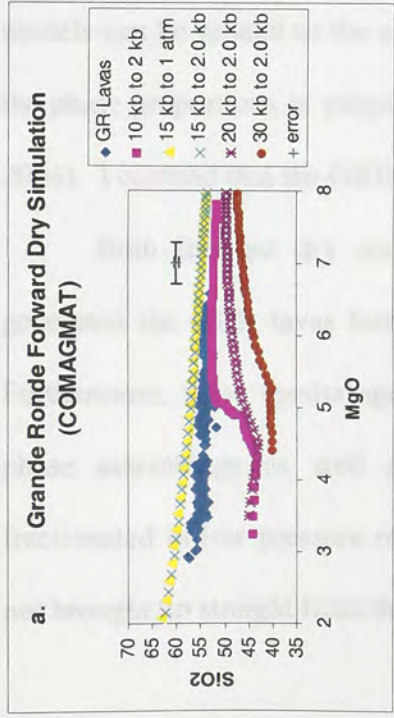
Figure 38- a-d shows the best fit liquid lines of descent for an experimentally determined composition, KLB-1 (Hirose and Kushiro, 1993). Forward dry models were run at different starting pressures (10, 15, 20, 30 kb) and fractionated at 2.0 kb. (a). SiO2 *vs.* MgO plot. (b). Al₂O₃ *vs.* MgO plot. (c). FeO* *vs.* MgO. (d). CaO vs. MgO. Error bars show mean error determined by comparisons of modeled LLD with experimental results of Grove and Bryan, 1983; and Tormey et al., 1987).

Role of H₂O: Forward "Wet" Models:

To determine the implications of the inverse simulation finding that GRB magma carried a small amount of H_2O (0.5 wt. %), forward simulations were run using COMAGMAT at the same pressures as above, with 0.5-2.0 wt. % H_2O added to them (Figure 39).

The effect of H_2O is dramatic, particularly if the melt crystallizes at higher pressure (Figure 39). The models show that Al_2O_3 is most affected by the addition of water. Even a 2 kb LLD of a slightly hydrous (>0.5 wt. %) 15 kb magma generate a poorer fit through the GRB data (Figure 39). This finding can be explained by the higher solubility of water in Alumina (Litasov and Ohtani, 2002). Litasov and Ohtani (2002) experimentally determined that water content in periclase and ferropericlase increases with increasing temperature and Al_2O_3 content and that this could be the result of the incorporation of trivalent cations to the structure. Furthermore, the kinks seen in the models can be related to the addition of magnetite ± hornblende which seems to change the phase proportions of plagioclase, preventing rapid depletion of Al_2O_3 (Almeev et al., 2004). I contend that the GRB magmas were fairly dry with only 0.5 wt. % H_2O.

Both forward dry and hydrous models indicate that the primary melts that generated the GRB lavas last equilibrated with a peridotite source at 15 kb pressure. Furthermore, these results agree with my conclusions, based on lava petrography and phase assemblage as well as with the inverse simulations, that GRB lavas last fractionated in low-pressure magma conduits at low pressures (2 kb to 1 atm) and were not brought up straight from the Moho depths.

Table 11- Phase assemblages for 2 kb Forward wet runs

Temperature	Phases	Temperature	Phases
T °C	2 kb (0.5 wt. % H_2O)	T °C	2 kb (1.0 wt. % H_2O)
1353	Ol+L	1344	Ol+L
1197	Ol+Plag.	1171	Ol+Plag.
1178	Ol.+Plag.+Aug.	1151	Ol.+Plag.+Aug.
1128	Ol.+Plag.+Aug.+Pig.	1105	Plag.+Aug.+Pig.
1125	Plag.+Aug.+Pig.	993	Plag.+Aug.+Mt.
1053	Plag.+Aug.	938	Aug.+Mt.
1005	Plag.+Aug.+Mt.		
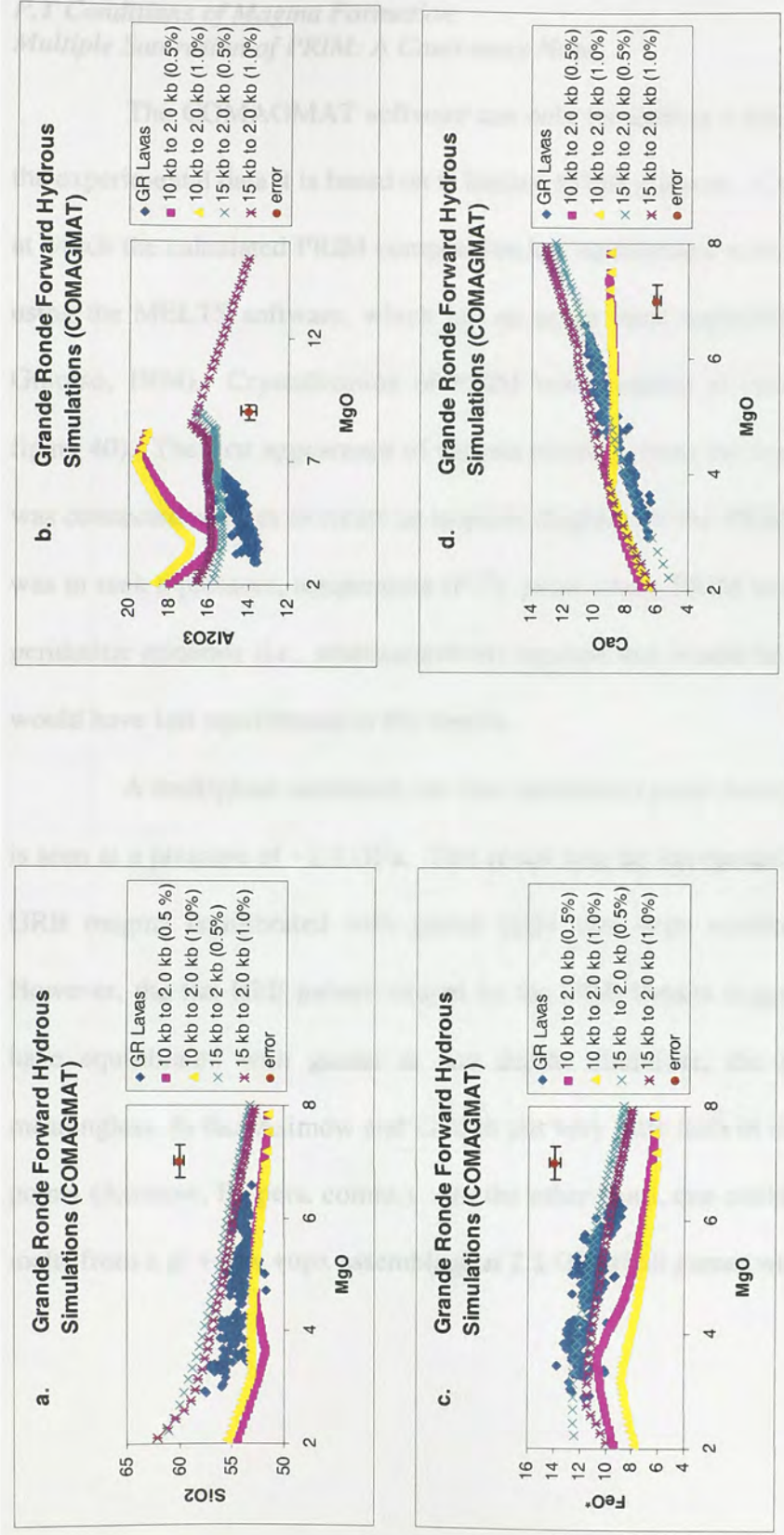
Figure 39-a-d shows the best fit liquid lines of descent for an experimentally determined composition, KLB-1 (Hirose and Kushiro, 1993). Forward wet models were run at different starting pressures (10 and 15 kb) and fractionated at 2.0 kb with different water contents (0.5% and 1.0%). (a). SiO2 vs. MgO plot. (b). Al₂O₃ vs. MgO plot. (c). FeO*(total FeO) vs. MgO. (d). CaO vs. MgO. Error bars show mean error determined by comparisons of modeled LLD with experimental results of Grove and Bryan, 1983; and Tormey et al., 1987).

181

The COMAGMAT software can only be used to a maximum of 15 kb because the experimental data it is based on is limited to this pressure. Consequently, the pressure at which the calculated PRIM composition last equilibrated with the mantle was modeled using the MELTS software, which has an upper limit applicability of 30 kb (Sack and Ghiorso, 1994). Crystallization of PRIM was modeled at various pressures (0-30 kb; figure 40). The first appearance of various minerals from the liquid at different pressures was connected as lines to create an isopleth diagram for the PRIM composition. The goal was to seek a pressure, temperature (P,T) point where PRIM would be saturated with all peridotitic minerals (i.e., multisaturation) because that would be the P,T at which PRIM would have last equilibrated in the mantle.

A multiphase saturation (or near saturation) point involving garnet, opx and cpx is seen at a pressure of ~2.3 GPa. This result may be interpreted to indicate that primary GRB magma equilibrated with garnet (gt)+ opx +cpx residue at 2.3 GPa (60 km). However, the flat REE pattern shown by the GRB basalts suggests that these could not have equilibrated with garnet at any depth. Therefore, the multisaturation point is meaningless. In fact Asimow and Longhi put very little faith in the use of multisaturation points (Asimow, P., pers. comm.). On the other hand, one could generate GRB primary melts from a gt + cpx +opx assemblage at 2.3 GPa if all garnet were melted (i.e., high F).
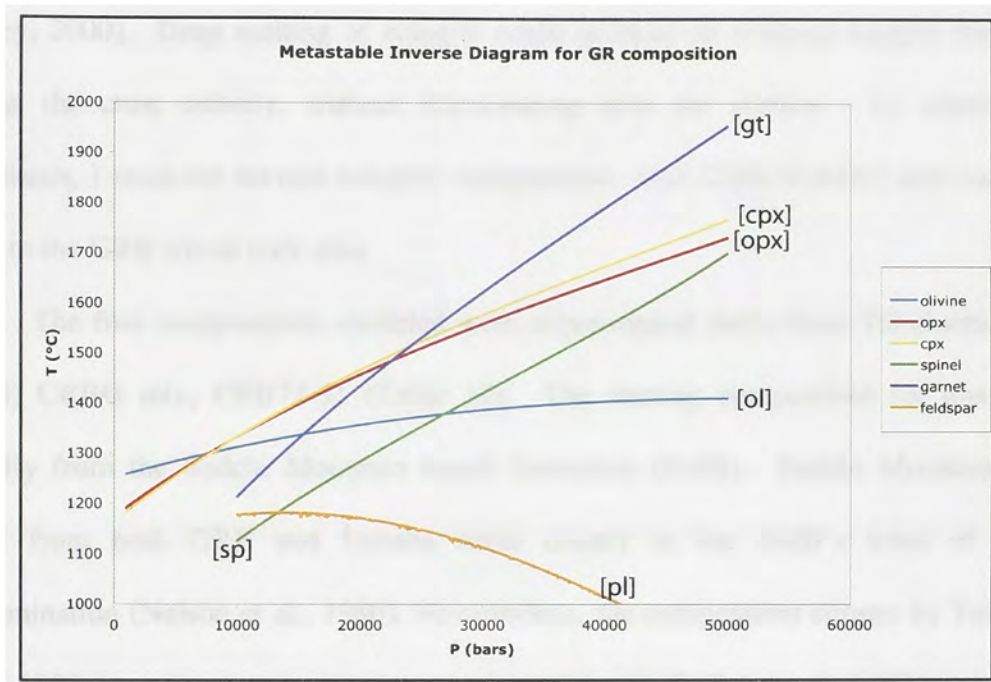
Figure 40- Phase diagram for PRIM depicting the multiphase saturation of garnet, orthoclinopyroxene (opx), clinopyroxene (cpx), point for this GRB composition. The curves show the temperature at which each phase is saturated in the bulk liquid composition. The curves meet at ~2 GPa and ~1450 °C. This plot also shows the stability or saturation curves for olivine, plagioclase feldspar and spinel.

Eclogite source: forward models

I wanted to test the hypothesis that an eclogitic source is required to account for the unique characteristics (aphyric, evolved nature) exhibited by the GRB lavas. Because eclogite (as a subducted component), is chemically akin to basalt, the melt product has higher SiO_2 and FeO than a peridotite at any pressure (Takahashi, 1998; Wright, 1989; Yaxley, 2000). Deep melting of eclogite could produce an evolved magma that could bypass the crust entirely, without fractionating near the surface. To address this hypothesis, I modeled several eclogitic compositions with COMAGMAT and compared them to the GRB whole rock data.

The first compositions modeled were experimental melts from Takahashi et al's (1998) CRBG mix, CRB72-31 (Table 12). The starting composition for this run is actually from the Saddle Mountain basalt formation (SMB). Saddle Mountain lavas differ from both GRB and Imnaha lavas mainly in the SMB's level of crustal contamination (Nelson et al., 1980). Nevertheless, the composition chosen by Takahashi et al., 1998, was the most magnesian member of the SMB (8.2 wt. % MgO) and closely resembles a typical MORB composition in major elements. Table 13 shows the resultant phases for the two compositions used in Table 12.

Liquid lines of descent at 2 kb for compositions of partial melts generated at 15 kb, 20 kb, and 30 kb were derived using COMAGMAT. LLD's for all major oxides (SiO_2, FeO, CaO and Al_2O_3) under dry conditions indicate that none of the models fit the GRB data because in all cases the starting melts have lower initial MgO concentrations than the GRB data (Figure 41). The initial increase in MgO in all of our models is a very interesting feature of all the LLD's, which are not duplicated by the GRB data.

Table 12- Starting Melt Compositions for Eclogite CRB72-31

CRB72-31 (F=0.4-0.5)		
	2.0 GPa	**3.0 GPa**
SiO2	54.5	59.0
TiO2	1.7	2.1
Al2O3	17.9	16.0
FeO*	8.2	6.7
MnO	0.1	0.1
MgO	4.6	3.3
CaO	9.1	8.4
Na2O	3.0	3.2
K2O	0.8	1.2
Total	100.0	100.0

Table 13- Comparison of Eclogite (CRB72-31) phase assemblages for 2 and 3 GPa
Forward runs

Temperature	Phases	Temperature	Phases
T °C	**2.0 GPa**	T °C	**3.0 GPa**
1225	Plag.+L	1176	Plag.+L
1157	Plag.+Ol+L	1139	Plag.+Aug.+L
1147	Plag.+Ol+Aug.+L	1088	Plag.+Aug.+IL+L
1146	Plag.+Aug.+L (Ol-out)		
1087	Plag.+Aug.+IL+L		
1086	Plag.+Aug.+IL+Mt.+L		
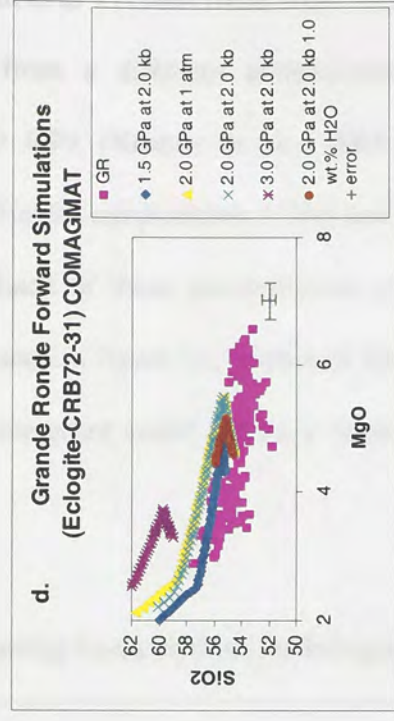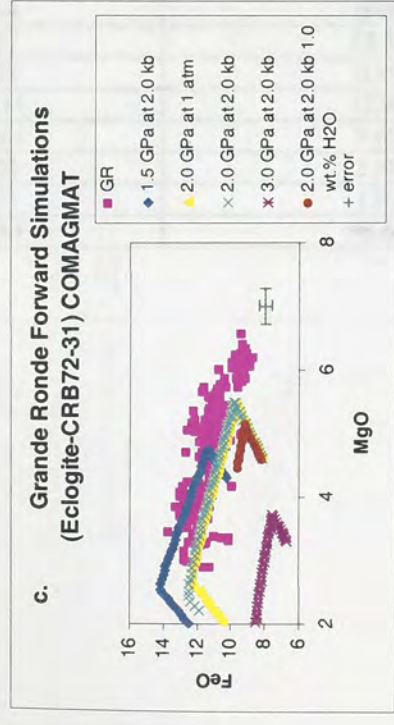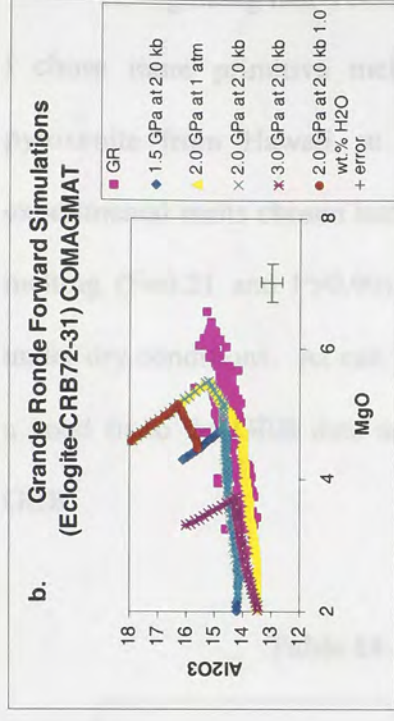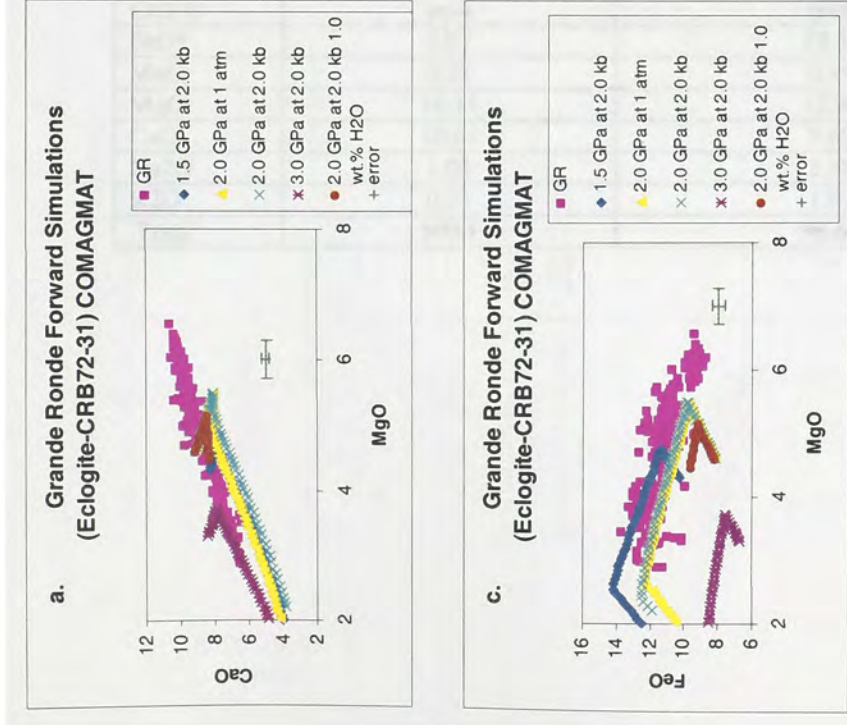
Figure 41-Models derived from the COMAGMAT Software showing the Fractional crystallization of an experimentally derived eclogitic composition, CRB72-31 (Takahashi et al., 1998) at different starting pressures, 15 kb, 20 kb and 30 kb fractionated at 1 atm and 2.0 kb. Compositions were modeled under both wet and dry conditions and wet conditions. The results suggest that that eclogite compositions were not responsible for the generation of the GR lavas under either condition. (a). SiO2 vs. MgO plot. (b). CaO vs. MgO plot. (c). FeO* vs. MgO. (d). Al_2O_3 vs. MgO.

186

Recognizing that Takahashi et al's (1998) melts were inappropriate starting melts, I chose more primitive melts from a different composition (77SL-582), a garnet pyroxenite from Hawaii, at 2.0 GPa (Keshav et al., 2004; Table 14). The two experimental melts chosen had different temperatures (1340 and 1440 °C) and degrees of melting (F=0.21 and F>0.90). Each of these compositions were fractionated at 2 kb under dry conditions. As can be seen in figure 42, neither of these compositions provide a good fit to the GRB data and therefore could not have been parental magmas to the GRB.

Table 14- Starting Compositions for Eclogite 77SL-582

77SL-582 (P=2.0 GPa)		
	T=1340, F=0.21	T=1440, F=>0.9
SiO2	45.99	44.12
TiO2	0.69	1.51
Al2O3	16.17	13.18
Cr2O3	0.14	0.08
FeO*	8.97	13.37
MnO	0.21	0.19
MgO	16.11	12.94
CaO	10.61	9.69
Na2O	1.01	2.58
K2O	0.21	1.02
Total	100.1	98.68
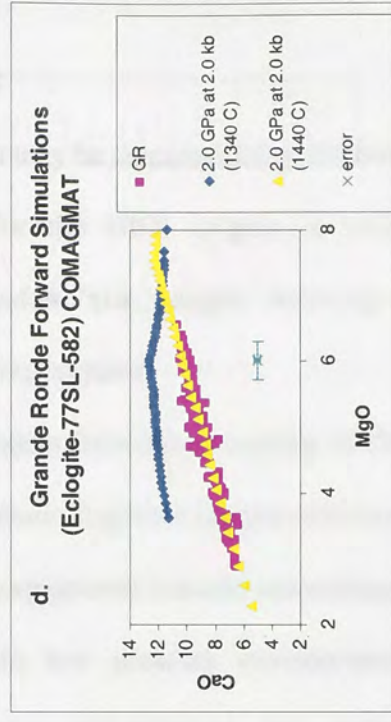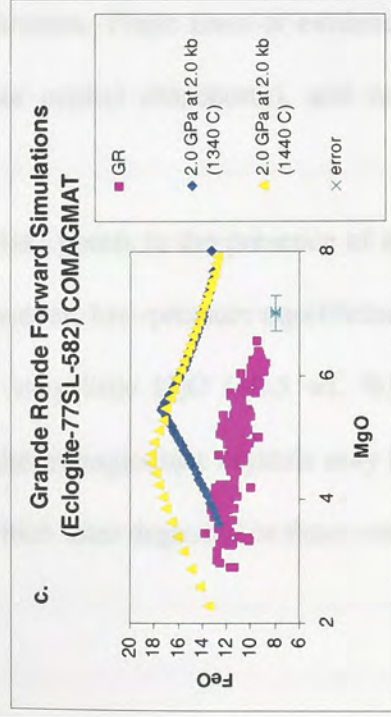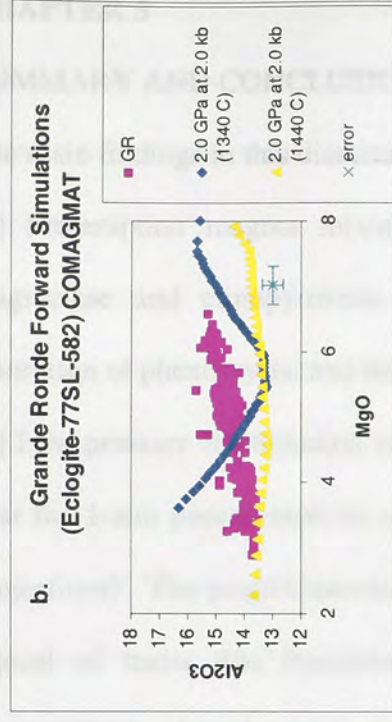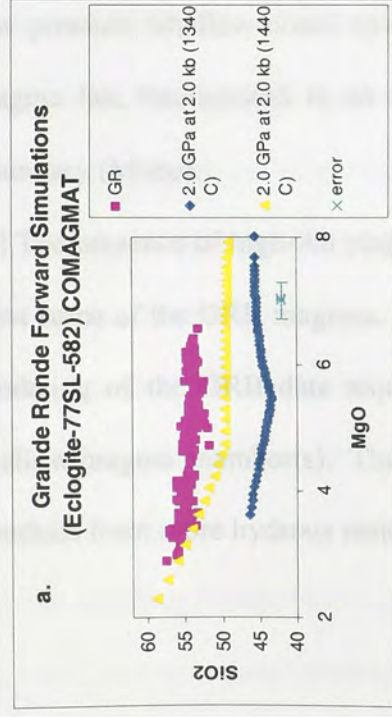
Figure 42-Models derived from the COMAGMAT Software showing the Fractional crystallization of an experimentally derived eclogitic composition, 77SL-582 (Keshav et al., 2004) at 2.0 GPa (1340 °C and 1440 °C) and fractionated at 2.0 kb. Compositions were modeled under dry conditions. Again the results suggest that that eclogite compositions were not responsible for the generation of the GR lavas (a). SiO2 vs. MgO plot. (b). CaO vs. MgO plot. (c). FeO* vs. MgO. (d). Al₂O₃ vs. MgO.

CHAPTER 5

SUMMARY AND CONCLUSIONS

The main findings in this dissertation may be summarized as follows:

[1] Pre-eruption magma mixing for the GRB magma is evident from zoning of plagioclase and clinopyroxene crystals, (i.e., augite rimming opx and pigeonite), resorption of phenocrysts, and mingling textures.

[2] Low pressure fractionation is evident from the clustering of GRB lava compositions near the 1-atm pseudo-cotectic on phase diagrams (augite-olivine-quartz pseudo ternary projections). The plagioclase+augite+pigeonite basaltic assemblage of the GRB lavas, is typical of melts that fractionate in low pressure environments. Additionally, cpx compositions plotted on a pyroxene quadrilateral also point to a low-pressure fractionation environment for the GRB magmas. Thermometry and barometry calculations (Putirka, 2005) provide further evidence that these lavas last equilibrated in low-pressure (shallow crust) environments. These lines of evidence show that the GRB magma last fractionated in an upper crustal chamber(s), and not at the crust-mantle boundary (Moho).

[3] The presence of high-An plagioclase points to the presence of a hydrous source for at least some of the GRB magmas. However, low-pressure equilibrium and inverse/forward modeling of the GRB data require very little H_2O (~0.5 wt. %) to be present in the shallow magma chamber(s). Thus, these plagioclase crystals may have formed in deeper conduits from more hydrous melts which later degassed or these can be xenocrysts.

[4] Most of the CRBG magmas were formed, or last equilibrated, with a fertile spinel lherzolite at approximately 15 kb (45 km), these conclusions/observations allow me to develop a reasonable petrotectonic model for the generation of the GRB.

Alternative Models to the Plume Hypothesis

As stated in the Introduction, there are essentially two types of tectonic models that try to explain the generation of the CRBG magmas – one of these calls for plume melting and the other – backarc spreading. I evaluate these hypotheses in a general way on the basis of my new findings.

It is clear from the present study that the primary magmas were generated at 15 kb, very close to the Moho. For this to occur, the lithosphere had to be greatly thinned underneath the plateau allowing hot asthenosphere, possibly hydrated by the fluids released from the subducting Farallon plate, to rise to shallow depths (~45-50 km). A recent seismic tomography model noted the occurrence of a thick, high-density horizon beneath the Wallowa Mountains (Columbia plateau), and interpreted it to be residues of the CRBG melting event (Hales et al., 2005). Hales et al. (2005) further inferred that thinning of the lithosphere was caused by the continued back-arc extension created by subduction to the west. This resulted in the dislodging of a large piece of the lower lithosphere. This is entirely consistent with the depth constraints of magma generation mechanism that I discussed above.

Current conditions below the Cascade Arc could have been similar in the mid-Miocene, when the bulk of the CRBG lavas were erupted. Compositions of parental liquids and temperatures were calculated from the most primitive Cascade arc samples available, this was done by using Fe-Mg equilibrium with a mantle peridotite (Leeman et

al., 2004). They assumed that magmas ascended from accumulation zones and estimated pressure and temperature of segregation of these magmas. Leeman et al. (2004) determined that the temperature beneath the Cascade Arc today is warmer than in normal arc settings. If conditions were similar 17 to 16 million years ago, it could explain the melting of larger volumes of lava beneath the plateau. The elevated temperatures due to the subduction of a younger slab (Farallon plate), could have raised the temperature above the slab. The combination of detachment of the lower lithosphere, and addition of fluids to the asthenosphere maybe have created an unusual hot and wet situation to exist in the asthenosphere reaching close to the Moho, resulting in sudden production of melts that became the GRB primary magmas. This model is presented schematically in figure 43. The magmas are generated or last equilibrated with largely peridotitic material at a shallow depth (45 km). Such magmas escaped through the feeder dikes that formed during the back-arc extension event. In this view, the presence of a hot plume is not necessary. However, a plume is not entirely ruled out by this model.

Back to the Plume Model Hypothesis

Although the back arc spreading model offers some convincing alternatives to the plume model, the large magma volumes present in the CRBG plateau continue to be a troubling aspect and cannot be fully explained by the back arc spreading model. Furthermore, considering that there are other areas with similar tectonic settings, where LIPs are not present, it seems unlikely that this model alone can explain the voluminous GRB lavas. There are aspects of this model however that can be used in conjunction with a plume model to explain the unique characteristics seen in the CRBG. For example, crustal thinning and the formation of fissures due to back arc spreading may have

191

facilitated the upward mobility of magma. This tectonic scenario could have allowed large volumes of magma from the plume to follow a "path of least resistance" and briefly fractionate underneath the plateau before erupting. Because seismic tomography detects an area where a large amount of melt was extracted beneath the CRBG plateau, it is clear that magma chamber(s) or conduits are present beneath the plateau. Therefore, as my work shows, the lavas last fractionated in crustal chamber beneath the plateau and large collapse structures are not required (see discussion in INTRODUCTION; Hooper et al., 1982).

The problem with the absence of the plume source beneath the plateau can be explained in a manner similar to what Geist and Richards (1993; figure 3) and/or Camp et al. (2004) have proposed. The first scenario calls for the shearing and deflection of the Yellowstone plume head by the subducting Farallon plate resulting in the plume head moving northward underneath the Columbia Plateau. The alternative model of Camp et al. (2004) calls for the presence of giant radiating dike swarms that traveled approximately 500 km north to the Columbia plateau. Either way, once the magma reached the area, it had to fractionate for a short period of time in crustal chambers before erupting and forming the CRBG as is indicated by the seismic tomography (Hales, 2005).

Future Work

Because my geochemical models indicate that the GRB magma last equilibrated with a spinel lherzolite source at approximately 15 kb, experiments at this pressure are necessary to constrain and verify the geochemical modeling results I obtained. Furthermore, the addition of various amount of H_2O to these experiments would also serve to constrain what if any amount of H_2O was present in the magma at this depth. An

additional method that I would like to utilize to determine the amount of H_2O in the CRBG magma would be to analyze melt inclusions in the Imnaha Formation. The Imnaha Formation would be ideal because of the higher abundance of phenocrysts in the lavas. Finally, it is apparent that the controversy of plume vs. non-plume sources for the CRBG has not yet been resolved. Therefore, I will continue to investigate the tectonic setting in the plateau so that I can better constrain the source for the generation of the CRBG continental flood basalt.
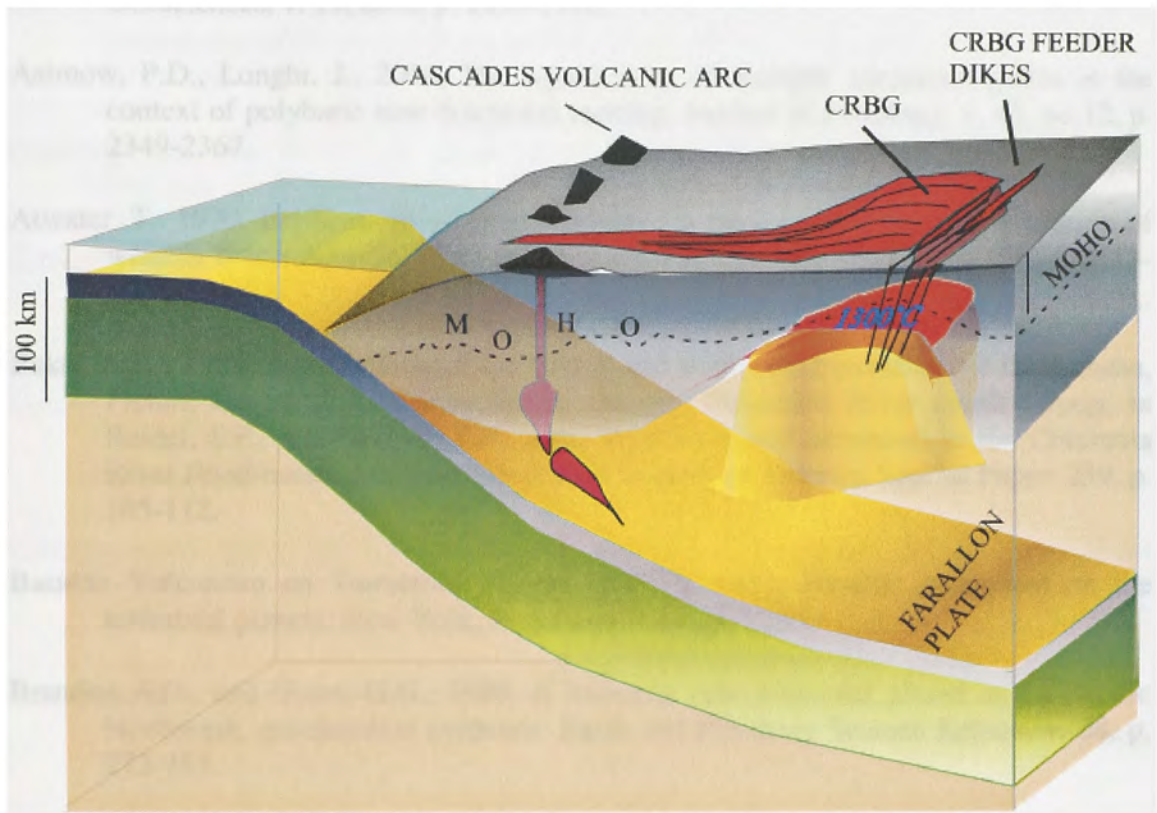
Figure 43-Diagram depicting the conditions that led to magma segregation below the CRBG plateau. As the Farallon Plate was being subducted under the North America Plate, the release of volatile caused melting to occur above the Farallon Plate. In addition, the extensional environment in this area caused thinning of the lithosphere. As a consequence, decompressional melting occurred. It is possible that a combination of two or more processes combined to form the large volumes of lava erupted to produce the flood basalt province.

REFERENCES CITED

Almeev, R., Ozerov, A., Ariskin, A.A., Kimura, J., *in* http://www.ozerov.ru/papers/k080-p004_e.pdf.

Ariskin, A.A., Frenkel, M.Y., Barmina, G.S., Nielsen, R.L., 1993, COMAGMAT: a FORTRAN program to model magma differentiation processes: Computers and Geosciences, v. 19, no.8, p. 1155-1170.

Asimow, P.D., Longhi, J., 2004, The significance of multiple saturation points in the context of polybaric near-fractional melting: Journal of Petrology, v. 45, no.12, p. 2349-2367.

Atwater, T., 1970, Implications of plate tectonics for the Cenozoic tectonic evolution of western North America: Geological Society of America Bulletin, v. 81, p. 3513-3536.

Baksi, A.K., 1989, Reevaluation of the timing and duration of extrusion of the Imnaha, Picture Gorge, and Grande Ronde Basalts, Columbia River basalt Group, in Reidel, S.P., and Hooper, P.R., eds., Volcanism and tectonism in the Columbia River flood-basalt province: Geological Society of America Special Paper 239, p. 105-112.

Basaltic Volcanism on Terrestrial Planets (BVTP), 1981, Basaltic volcanism on the terrestrial planets: New York, Pergamon Press, p. 1286.

Brandon A.D., and Goles, G.G., 1988, A Miocene subcontinental plume in the Pacific Northwest, geochemical evidence: Earth and Planetary Science Letters, v. 88, p. 273-283.

Campbell, S.M. and Griffiths, R.W., 1990, Implications of mantle plumes for the evolution of basalts: Earth and Planetary Science Letters, v. 99, p. 79-93.

Camp, V.C., 1976, Petrochemical stratigraphy and structure of the Columbia River basalt, Lewiston basin area, Idaho-Washington: Washington State University, PhD. Dissertation.

Camp, V.E., Hooper, P.R., 1981, Geologic studies of the Columbia Plateau: Part I. Late Cenozoic evolution of the southeast part of the Columbia River Basalt Province: Geological Society of America Bulletin, v. 92, no.9, p. 659-668.

Camp, V.E., 1995, Mid-Miocene propagation of the Yellowstone mantle plume head beneath the Columbia River basalt source region: Geology, v. 23, no. 5, p. 435–438.

Camp, V.E., Ross, M.E., and Hanson, W.E., 2003, Genesis of flood basalts and Basin and Range volcanic rocks from Steens Mountain to the Malheur River Gorge, Oregon: Geological Society of America Bulletin, v. 115, p. 105–128.

Camp, V.E., Ross, M.E., 2004, Mantle dynamics and genesis of mafic magmatism in the intermontane Pacific Northwest: Journal of Geophysical Research B: Solid Earth, v. 109, no.8 p. B08204 1-14.

Caprarelli, G., and Reidel, S.P., 2005, A clinopyroxene-basalt geothermobarometry perspective of Columbia Plateau (NW-USA) Miocene magmatism: Terra Nova, v. 17, p. 265-277.

Caprarelli, G., and Reidel, S. P., 2004, Physical evolution of Grande Ronde Basalt magmas, Columbia River Basalt Group, north-western USA: Mineralogy and Petrology, v. 80, p. 1-25.

Carlson, R.W., Lugmair, G.W., Macdougall, J.D., 1981, Columbia River Volcanism: the question of mantle heterogeneity or crustal contamination: Geochimica, Cosmochimica Acta, v. 45, p. 2483-2499.

Carlson, R.W., 1984, Isotopic Constraints on Columbia River flood basalt fenesis and the nature of the subcontinental mantle: Geochimica, Cosmochimica Acta, v. 48, p. 2357-2372.

Carlson, R.W., Hart, W.K., 1988, Flood basalt volcanism in the northwestern United States: in Macdougall, J.D. eds., Continental Flood Basalts, Dordrecht, Kluwer Academic, p. 35-61.

Cashman, K.V., Mangan, M.T., Newman, S., 1994, Surface degassing and modifications to vesicle size distributions in active basalt flows: Journal of Volcanology and Geothermal Research, v. 61, no.1-2, p. 45-68.

Catchings, R.D.; Mooney, W.D., 1988, Crustal structure of east central Oregon: relation between Newberry Volcano and regional crustal structure: Journal of Geophysical Research, v. 93, no.B9, p. 10 081-10 094.

Christiansen, R.L., Lipman, P.W., 1972, Cenozoic volcanism and plate-tectonic evolution of the western United States. II Late Cenozoic: Philosophical Transactions of the Royal Society of London, v. 271, v. 271 p. 249-284.

Clague, D.A., Moore, J.G., 1991, Geology and petrology of Mahukona volcano, Hawaii: Bulletin of Volcanology, v. 53, no.3, p. 159-172.

Coe, R.S., Stock, G.M., Lyons, J.J., Beitler, B., Bowen, G.J., 2005, Yellowstone hotspot volcanism in California? A paleomagnetic test of the Lovejoy flood basalt hypothesis: Geology: v. 33, no. 9, p. 697–700.

Cordrey, M.J., Davies, G.F., Campbell, I.H., 1997, Genesis of flood basalts from eclogite-bearing mantle plumes: Journal of Geophysical Research, v. 102, no. 20, p. 179-197.

Decker, R.W., Wright, T.L., Stauffer, P.H., 1987, Volcanism in Hawaii: U.S. Geological Survey Professional Papers 1350, p. 1667.

De Paolo, D. J., Wasserburg, G. J., 1977, Nd in island arc and continental volcanic rocks: Eos, Transactions, American Geophysical Union, v. 58, no.6, p.533.

Dickinson, W.R., 1997, OVERVIEW: Tectonic implications of Cenozoic volcanism in coastal California: Geological Society of America Bulletin, v. 109, no. 8, p. 936–954.

Dodson, A., Kennedy, B.M., DePaolo, D.J., 1997, Helium and neon isotopes in the Imnaha Basalt, Columbia River Basalt Group: Evidence for a Yellowstone plume source: Earth and Planetary Science Letters, v. 150, p. 443-451.

Duncan, R.A., Richards, M.A., 1991, Hotspots, mantle plumes, flood basalts, and true polar wander: Reviews of Geophysics, v. 29, no.1 p. 31-50.

Engebretson, D.C., Cox, A., Thompson, G.A., 1984, Correlation of plate motions with continental tectonics: Laramide to Basin-Range (North America): Tectonics, v. 3, no.2, p. 115-119.

Erlank, A.J., Allsopp, H.L., Rickard, R.S., Menzies, M.A., Waters, F.G., Hawkesworth C.J., Haggerty, S.E., 1987, Evidence for mantle metasomatism in peridotite nodules from the Kimberley pipes, South Africa: In: Mantle Metasomatism Editor: Menzies M.A.; Hawkesworth C.J., Academic Press Year, p. 221-311.

Ernst, R.E., Wilson, L., Head, J.W., Parfitt, E., Grosfils, E., 1995, Giant radiating dyke swarms on Earth and Venus: Earth-Science Reviews, v. 39, no.1-2, p. 1-58.

Ernst, R.E., Buchanan, K.L., 2003, Recognizing mantle plumes in the geological record: Annual Review of Earth and Planetary Sciences, v. 31 p. 469-523.

Geist, D., and Richards, M., 1993, Origin of the Columbia Plateau and Snake River plain: Deflection of the Yellowstone plume: Geology v. 21, p. 789-792.

Goldstein, J.I., Newbury, D.E., Echlin, P., Joy, D.C., Romig, A.D., Lyman, C.E., Fiori, C., Lifshin, E., 1992, Scanning Electron Microscopy and X-Ray Microanalysis: New York, Plenum Press.

Ghiorso, M.S., 1994, Algorithms for the estimation of phase stability in heterogeneous thermodynamic systems: Geochimica et Cosmochimica Acta, v. 58, no.24, p. 5489-5501.

Grove, T. L.; Bence, A. E., 1977, Experimental study of pyroxene-liquid interaction in quartz-normative basalt 15597: in Proceedings of the Eighth lunar science conference; petrogenetic studies of mare and highland rocks, eds. Merrill, R. B. Blanchard, D. D., Lofgren, G. E., Mendell, W. W., Gibson, M. S., Robertson, P. C., Gunter, K., Ancelin, M. A., Ridings, R., Eighth lunar science conference, Houston, Tex., United States, Pergamon Press, New York, N.Y., United States (USA).

Grove, T.L., Garlach, D.C., and Sando, I.W., 1982, Origin of calc-alkaline series lavas at Medicine Lake volcano by fractionation, assimilation, and mixing: Contributions to Mineralogy and Petrology, v. 80, p. 160–182.

Grove, T.L., and Bryan, W.B., 1983, Fractionation of pyroxene-phyric MORB at low pressure: an experimental study: Contributions to Mineralogy and Petrology, v. 84, p. 293-309.

Grove, T.L., Juster, T.C., and Perfit, M.R., 1989, Experimental investigations of low-Ca pyroxene stability and olivine-pyroxene-liquid equilibria at 1-atm in natural basaltic and andesitic liquids: Contributions to Mineralogy and Petrology, v. 103, p. 287-305.

Hales, T.C., Abt, D.L., Humphreys, E.D., Roering, J.J., 2005, A lithospheric instability origin for Columbia River flood basalts and Wallowa Mountains uplift in northeast Oregon: Nature, v. 438, no.7069, p. 842-845.

Hart W.K., Carlson, R.W., 1987, Tectonic controls on magma genesis and evolution in the northwestern United States: Journal of Volcanology and Geothermal Research, v. 32, p. 119-135.

Hawkesworth, C.J., Hergt, J.M., McDermott, F., Ellam, R.M.,1991, Destructive margin magmatism and the contributions from the mantle wedge and subducted crust: Australian Journal of Earth Sciences, v. 38, no.5, p. 577-594.

Helz, R.T., Wright, T.L., 1992, Differentiation and magma mixing on Kilauea's east rift zone: a further look at the eruptions of 1955 and 1960. Part I, the late 1955 lavas: Bulletin of Volcanology, v. 54, no.5, p. 361-384.

Herzberg, C., O'Hara, M.J., 2002, Plume-associated ultramafic magmas of phanerozoic age: Journal of Petrology, v. 43, no.10, p. 1857-1883.

Hirschmann, M. M., Ghiorso, M. S., Wasylenki, L. E., Asimow, P. D., Stolper, E. M., 1998, Calculation of peridotite partial melting from thermodynamic models of minerals and melts; I, Review of methods and comparison with experiments: Journal of Petrology, v.39, no.6, p.1091-1115.

Hirschmann, M. M., Asimow, P. D., Ghiorso, M. S., Stolper, E. M., 1999, Calculation of peridotite partial melting from thermodynamic models of minerals and metals; III, Controls on isobaric melt production and the effect of water on melt production: Journal of Petrology, v.40, no.5, p.831-851.

Hirose, K., Kushiro, I., 1992, Partial melting of dry peridotites at high pressures: determination of compositions of melts segregated from peridotite using aggregates of diamond: Earth and Planetary Science Letters, v. 114, no.1, p. 477-489.

Hon, K., Kauahikaua, J., Denlinger, R., 1994, Emplacement and inflation of pahoehoe sheet flows: Observations and measurements of active lava flows on Kilauea Volcano, Hawaii: Geological Society of America Bulletin, v. 106, no. 3, p. 351–370.

Ho, A.M., Cashman, K.V., 1997, Temperature constraints on the Ginkgo Flow of the Columbia River Basalt Group: Geology, v. 25, no.5, pp.403-406.

Hooper, P.R., 1982, The Columbia River Basalts: Science, v. 215, p. 1463–8.

Hooper, P.R., 1984, Physical and chemical constraints on the evolution of the Columbia River basalt: Geology, v. 12, p. 495-499.

Hooper P.R., Thiessen R.L., Kleck W.D., Knowles, C.R., Reidel, S.P., 1984, Imnaha basalt, Columbia River basalt group; Journal of Petrology v. 25, n. 2, p. 473-500.

Hooper, P.R., 1985, A case of simple magma mixing in the Columbia River Basalt Group: The Wilbur Creek, Lapwai, and Asotin Flows, Saddle Mountain Formation: Contributions to Mineralogy and Petrology, v. 91, p. 66-73.

Hooper, P.R., 1988, The Columbia River Basalt: in Macdougall, J.D. eds., Continental Flood Basalts, Dordrecht, Kluwer Academic, p. 1-33.

Hooper, P.R., and Reidel, S.P., 1989, Dikes and Vents Feeding the Columbia River Basalts: in Joseph, N.L., and others, eds., Geologic guidebook for Washington and adjacent areas: Washington Division of Geology and Earth Resources Information Circular 86, p. 255-273.

Hooper, P.R., 1990, The timing of crustal extension and the eruption of continental flood basalts: Nature, v. 345, p. 246-249.

Hooper, P.R., and Hawkesworth, C.J., 1993, Isotopic and geochemical constraints on the origin and evolution of the Columbia River Basalt: Journal of Petrology, v. 34, p. 1203–1246.

Hooper, P.R., 1997, The Columbia River Flood Basalt Province: Current status, in J. H. Mahoney and M.F. Coffin eds., Large Igneous Provinces: Continental, Oceanic, and Planetary Flood Volcanism: Geophysical Monogram Services, Washington, D.C., v. 100, p. 1-27.

Hooper, P. R., 2000, Chemical Discrimination of Columbia River basalt flows: Geochemical Geophysical Geosystems, v. 1, Paper number 2000GC000040.

Hooper, P.R., Binger, G.B., and Lees, K.R., 2002, Ages of the Steens and Columbia River flood basalts and their relationship to extension-related calc-alkalic volcanism in eastern Oregon: Geological Society of America Bulletin, v. 114, p. 43–50.

Hooper, P.R., 2003, The Columbia River Basalts & Yellowstone Hot Spot: A Mantle Plume? http:/www.mantleplumes.org/CRB.html.

Jackson, E. D., Silver, E. A., Dalrymple, G. B., 1972, Hawaiian-Emperor Chain and its Relation to Cenozoic Circumpacific Tectonics: Geological Society of America Bulletin, v. 83, no. 3, p. 601-617.

Keshav, S., Fei, Y., Gudfinnsson, G.H., Sen, G., 2004, High-pressure melting experiments on garnet clinopyroxenite and the alkalic to tholeiitic transition in ocean-island basalts: Earth and Planetary Science Letters, v 223, no.3-4, p. 365-379.

Keshav, S., Sen, G., 2001, Majoritic garnets in Hawaiian xenoliths: Preliminary results: Geophysical Research Letters, v. 28, no.18, p. 3509-3512.

Keszthelyi, L. ; Self, S., 1998, Some physical requirements for the emplacement of long basaltic lava flows: Journal of Geophysical Research B: Solid Earth, v.103, no.11, p. 27,447-27,464.

Kuo, L.C., and Kirkpatrick, R.J., 1982, Preeruption history of phyric basalts from DSDP Legs 45 and 46: Evidence from morphology and zoning patterns in plagioclase: Contributions to Mineralogy and Petrology, v. 79, p. 13–27.

Kushiro, I., 1972, Determination of liquidus relations in synthetic silicate systems with electron probe analysis: the system forsterite-diopside-silica at 1 atmosphere: American Mineralogist, v. 57, p. 1260-1271.

Latypov, R., Dubrovskii, M.M., Alapieti, T. T., 2001, Graphical analysis of the orthopyroxene-pigeonite-augite-plagioclase equilibrium at liquidus temperatures and low pressures: American Mineralogist, v. 86, p. 547-554.

Lange, R., 2002, Constraints on the preeruptive volatile concentrations in the Columbia River flood basalts: Geology, v. 30, p. 179–182.

Leeman, W.P., Conrey, R.M., Streck, M.J., Lewis, J.F., Evarts, R.C., 2005, Petrologic constraints on the thermal structure of the Cascades arc: Journal of Volcanology and Geothermal Research, v. 140, no.1-3, p. 67-105.

Lindsley, D.H., 1983, Pyroxene thermometry: American Mineralogist, v. 68, p. 477–493.

Litasov, K.D., Ohtani, E., 2003, Effect of Alumina on Water Solubility in Lower Mantle Ferropericlase: Preliminary Results, Geophysical Research Abstracts, European Geophysical Society, v. 5, 05875.

Long P.E., and Wood, B.J., 1987, Structures, textures, and cooling histories of Columbia River basalt flows (USA): Geological Society of America Bulletin, v. 97, no.9 p. 1144-1155.

McDougall, I., 1976, Geochemistry and origin of basalt of the Columbia River Group, Oregon and Washington: Geological Society of America Bulletin, v.87, no.5, p.777-792.Mangan, M.T., Wright, T.L., Swanson, D.A., and Byerly, G.R., 1986, Regional correlation of Grande Ronde Basalt flows, Columbia River Basalt Group, Washington, Oregon, and Idaho: Geological Society of America Bulletin, v. 97, p. 1300–1318.

Mankinen, E.A., Larson, E.E., Gromme, C.S., Prevot, M., Coe, R.S., 1987, The Steens Mountain (Oregon) geomagnetic polarity transition: 3. Its regional significance: Journal of Geophysical Research, v. 92, p. 8057–8076.

Marsh, B.D., 1989, Magma chambers: Annual Review of Earth and Planetary Sciences, v. 17, p. 439–474.

Marsh, B.D., 1996, Solidification fronts and magmatic evolution: Mineralogical Magazine, v. 60, p. 5–40.

McKee, E.H., Swanson, D.A., Wright, T.L., 1977, Duration and volume of Columbia River basalt volcanics, Washington, Oregon, and Idaho: Geological Society of America Abstract, Program 9, p. 463.

McKee, E.H., Hooper, P.R., Kleck, W.D., 1981, Age of Imnaha Basalt-oldest basalt flow of the Colombia River Basalt Group, northwestern U.S.: Isochron/West, v. 31, p. 31-33.

Meibom, A., and Anderson, D.L., 2003, The statistical upper mantle assemblage: Earth and Planetary Science Letters, v. 217, p. 123-139.

Nelson, D.O., 1980, Strontium isotopic and trace element geochemistry of the Saddle Mountains and Grande Ronde Basalts of the Columbia River Basalt Group: Ph.D. Thesis Oregon State University, Corvallis.

Nelson, D.O., 1989, Geochemistry of the Grande Ronde Basalt of the Columbia River Basalt Group; A reevaluation of source control and assimilation effects: in Reidel, S.P., and Hooper, P.R., eds., Volcanism and Tectonism in the Columbia River flood-basalt province: Geological Society of America Special Paper 239, p. 333–342.

Pearce, T.H., 1984, The analysis of zoning in magmatic crystals with emphasis on olivine: Contributions to Mineralogy and Petrology, v. 86, no.2, p. 149-154.

Philpotts, A.R., and Carroll, M., 1996, Physical properties of partly melted tholeiitic basalt: Geology, v. 24, no. 11, p. 1029-1032.

Pierce, K.L., Morgan, L.A., 1992, The track of the Yellowstone hot spot: Volcanism, faulting, and uplift: in Link, P.K. Kuntz, M.A., Platt, L.B., eds., Regional Geology of Eastern Idaho and Western Wyoming: Geological Society of America Memoir 179, p. 1-53.

Putirka, K.D., 2005, Igneous thermometers and barometers based on plagioclase + liquid equilibria: Tests of some existing models and new calibrations: American Mineralogist, v. 90, no. 2-3, p. 336-346.

Ragland, P.C., 1989, Basic Analytical Petrology: New York, Oxford University Press, p. 122-123.

Ramos, F.C., Wolff, J.A., Tollstrup, D.L., 2005, Sr isotope disequilibrium in Columbia River flood basalts: Evidence for rapid shallow-level open-systems processes: Geology, v. 33, no.6, p. 457-460.

Rampino, M., and Self, S., 2000, Volcanism and biotic extinctions, in Sigurdsson, H., et al., eds., The encyclopedia of volcanology: San Diego, Academic Press, p. 1083–1091.

Reichow, M.K., Al'Mukhamedov A.I., Medvedev, A.I., Kirda N.P., Saunders A.D., White, R.V. , Pringle M.S., 2002, $^{40}Ar/^{39}Ar$ dates from the West Siberian Basin: Siberian flood basalt province doubled: Science, v. 296, no. 5574, p. 1846-1849.

Reidel, S. P., 1978, The Stratigraphy and Petrogenesis of the Grande Ronde Basalt in the Lower Salmon and Adjacent Snake River Canyons: Ph.D Dissertation, Washington State University.

Reidel, S. P., 1983, Stratigraphy and Petrogenesis of the Grande Ronde Basalt from the Deep Canyon Country of Washington, Oregon, and Idaho: Geological Society of America Bulletin, v. 44, p. 519-542.

Reidel, S.P., Dick, B., Scott, G.R., Bazard, D.R., Cross, R.W., 1984, Post-12 million year clockwise rotation in the central Columbia Plateau, Washington: Tectonics, v. 3, no.2, p. 251-273.

Reidel, S.P., Tolan, T.L., Hooper, P.R., Beeson, M.H., Fecht, K.R., Bentley, R.D., and Anderson, J.L., 1989, The Grande Ronde Basalt, Columbia River Basalt Group: Stratigraphic descriptions and correlations in Washington, Oregon, and Idaho, in Reidel, S.P., and Hooper, P.R., eds., Volcanism and tectonism in the Columbia River flood-basalt province: Geological Society of America Special Paper 239, p. 21–53.

Reidel, S.P., and Tolan, T.L., 1992, Eruption and emplacement of flood basalt: An example from the large-volume Teepee Butte Member, Columbia River Basalt Group: Geological Society of America Bulletin, v. 104, p. 1650–1671.

Reidel, S.P., 1998, Emplacement of Columbia River flood basalt: Journal of Geophysical Research, v. 103, p. 27393-27410.

Reidel, S. P., 2005, A lava Flow without a Source: The Cohassett Flow and Its Compositional Components, Sentinel Bluffs Member, Columbia River Basalt Group: Journal of Geology, v. 113, p. 1-21.

Renne, P.R., 2002, Geology: Flood Basalts- Bigger and badder: Science, v. 296, no. 5574, p. 1812-1813.

Richards, M.A., Duncan, R.A., Courtillot, V., 1989, Flood basalts and hot spot tracks: plume heads and tails: Science, v. 246, p. 103-107.

Russell, J.K., Nicholls, J., 1990, Magma mixing processes: insights and constraints from Thermodynamic calculations: in Modern methods of igneous petrology, understanding magmatic processes, Reviews in Mineralogy, v. 24, p. 153-190.

Sack, R.O. ; Ghiorso, M.S., 1994, Thermodynamics of multicomponent pyroxenes: I. Formulation of a general model: Contributions to Mineralogy and Petrology, v. 116, no.3, p. 277-286.

Saltus, R.W., 1993, Upper-crustal structure beneath the Columbia River Basalt Group, Washington: gravity interpretation controlled by borehole and seismic studies: Geological Society of America Bulletin, v. 105, no.9, p. 1247-1259.

Schiffman, P., Lofgren, G.E., 1982, Dynamic Crystallization Studies On the Grande Ronde Pillow Basalts, Central Washington: Journal of Geology, v. 90, p. 49-78.

Self, S., Thordarson, T., and Keszthelyi, L., 1997, Emplacement of continental flood basalt lava flows, in Mahoney, J., and Coffin, M.F., eds., Large igneous provinces: Continental, oceanic, and planetary flood volcanism: American Geophysical Union Geophysical Monograph 100, p. 381–410.

Sen, G., 1983, Deccan Trap intrusion: Magma mixing in the Chalka-Delakhari sill, Chindwara district, Madhya Pradesh: Geological Society of India Journal, v. 24, no. 8, p. 381–393.

Sen, G., 2001, Earth's materials: Minerals and rocks: New Jersey, Prentice-Hall, 542 p.

Shaw, H. R.; Swanson, D. A., 1969, Eruption and flow rates of flood basalts: in 2nd Columbia River basalt symposium; proceedings, eds. Gilmour, Ernest H; Stradling, Dale, 2nd Columbia River basalt symposium, Cheney, WA, United States, Eastern Washington State College Press, Cheney, WA, United States (USA).

Shaw, H.R., Swanson, D.A, 1970, Eruption and flow rates of flood basalts: 2nd Columbia River basalt symposium; proceedings, Eastern Washington State College Press, Cheney, WA.

Sisson, T.W., and Grove, T.L., 1993, Experimental investigations of the role of H_2O in calc-alkaline differentiation and subduction zone magmatism, Contributions to Mineralogy and Petrology, v. 113, p. 143-166.

Smith, A.D., 1992, Back-arc convection model for Columbia River basalt genesis: Tectonophysics, v. 207, p. 269-285.

Sugawara T., 2001, Ferric iron partitioning between plagioclase and silicate liquid: Thermodynamics and petrological applications: Contributions to Mineralogy and Petrology, v. 141, no.6, p. 659-686.

Swanson, D. A.,1972, Magma Supply Rate at Kilauea Volcano, 1952-1971: Science, v.175, no.4018, p.169-170.

Swanson, D.A., Wright, T.L., Helz, R.T., 1975, Linear Vent Systems and Estimated Rates of Magma Production and Eruption for Yakima Basalt on Columbia Plateau: American Journal of Science, v. 275, p. 877-905.

Swanson, D.A., Wright, T.L., Hooper, P.R., and Bentley, R.D., 1979, Revisions in stratigraphic nomenclature of the Columbia River Basalt Group: U.S. Geological Survey Bulletin 1457G, p. 1–59.

Swanson, D.A., Cameron, Evarts, Pringle, and Vance, 1989, IGC Field Trip T106: Cenozoic Volcanism in the Cascade Range and Columbia Plateau, Southern Washington and Northernmost Oregon: American Geophysical Union Field Trip Guidebook T106, p.21-24.

Takahashi, E., Nakajima, K., and Wright, T.L., 1998, Origin of the Columbia River basalts: Melting model of a heterogeneous plume head: Earth and Planetary Science Letters, v. 162, p. 63–80.

Thordarson, T., Self, S., 1996, Sulfur, chlorine and fluorine degassing and atmospheric loading by the Roza eruption, Columbia River Basalt Group, Washington, USA: Journal of Volcanology and Geothermal Research, v. 74, p. 49-73.

Thy, P., Lesher, E.E., and Mayfield, J.D., 1999, Low-pressure melting studies of basalt and basaltic andesite from the South-East Greenland continental margin and the origin of dacites at Site 917, in Larsen, H.C., Duncan, R.A., et al., Proceedings of the Ocean Drilling Program: Scientific results, Volume 163: College Station, Texas, Ocean Drilling Program, p. 95–112.

Tolan, T.L., Reidel, S.P., Beeson, M.H., Anderson, J.L., Fecht, K.R., and Swanson, D.A., 1989, Revisions to the estimates of the areal extent and volume of the Columbia River Basalt Group, in Reidel, S.P., and Hooper, P.R., eds., Volcanism and tectonism in the Columbia River flood-basalt province: Geological Society of America Special Paper 239, p. 1–20.

Tormey, D.R., Grove, T.L., Bryan, W.B., 1987, Experimental petrology of normal MORB near the Kane Fracture Zone: 22°-25° N, mid-Atlantic ridge near: Contribution to Mineralogy and Petrology, v. 96, p. 121-139.

Walker, D., Shibata, T., and DeLong, S.E., 1979, Abyssal tholeiites from the Oceanographer Fracture Zone: II. Phase equilibria and mixing: Contributions to Mineralogy and Petrology, v. 70, p. 111–125.

Waters, A.C., 1961, Stratigraphy and lithologic variations in the Columbia River basalt: American Journal of Science, v. 259, p. 583-611.

Watkins A.C., Baksi A.K., 1974, Magnetostratigraphy and oroclinal folding of the Columbia River, Steens, and Owyhee basalts in Oregon, Washington, and Idaho: American Journal of Science, v. 274, p. 148-189.

White, R., Mckenzie, D., 1989, Magmatism at Rift Zones- The Generation of Volcanic Continental Margins and Flood Basalts: Journal of Geophysical Research- Solid Earth and Planets, v. 94, p. 7685-7729.

Yang, H., Kinzler, R.J., Grove, T.L., 1996, Experiments and models of anhydrous, basaltic olivine-plagioclase-augite saturated melts from 0.001 to 10 kbar: Contributions to Mineralogy and Petrology, v.124, p. 1-18.

Yaxley G.M.,2000, Experimental study of the phase and melting relations of homogeneous basalt + peridotite mixtures and implications for the petrogenesis of flood basalts: Contributions to Mineralogy and Petrology, v. 139, no.3, p. 326-338.

Table 6A- Microprobe Analyses of Immaha Dike Plagioclase Phenocrysts

	Im-15c-1pl	Im-B15c-2pl	Im-B15c-2pl	Im-B15c-2pl	Im-B15c-2pl	Im-B15c-2pl	Im-B15c-3pl
SiO2	52.38	52.71	53.55	51.87	50.10	51.80	55.45
TiO2	0.06	0.12	0.18	0.20	0.07	0.16	0.11
Al2O3	31.33	29.24	29.09	28.95	29.78	29.76	26.27
MgO	0.07	0.04	0.07	0.08	0.07	0.06	0.10
CaO	13.13	13.15	12.96	12.97	13.90	13.45	9.78
FeO	0.52	0.58	0.59	0.60	0.58	0.59	0.63
Na2O	4.07	4.13	4.45	4.22	3.58	4.02	6.04
K2O	0.21	0.24	0.23	0.23	0.18	0.22	0.41
SrO	0.00	0.00	0.00	0.00	0.00	0.02	0.02
Total	**101.77**	**100.22**	**101.13**	**99.11**	**98.26**	**100.06**	**98.81**
Structural Formulae							
Cations per 8 Oxygen							
Si	2.35	2.40	2.42	2.39	2.34	2.37	2.55
Ti	0.00	0.01	0.01	0.01	0.01	0.01	0.01
Al	1.66	1.57	1.55	1.57	1.64	1.60	1.42
Mg	0.00	0.00	0.00	0.01	0.00	0.00	0.01
Ca	0.63	0.64	0.63	0.64	0.69	0.66	0.48
Fe	0.02	0.02	0.02	0.02	0.02	0.02	0.02
Na	0.31	0.32	0.34	0.33	0.28	0.31	0.46
K	0.01	0.01	0.01	0.01	0.01	0.01	0.02
Sr	0.00	0.00	0.00	0.00	0.00	0.00	0.00
Cation Sum	**4.98**	**4.98**	**4.98**	**4.99**	**4.99**	**4.99**	**4.98**
An	77.5	77.2	75.7	76.7	80.6	78.1	63.1
Ab	21.7	21.9	23.5	22.5	18.8	21.1	35.3
Or	0.7	0.9	0.8	0.8	0.6	0.8	1.6

Table 6B- Microprobe Analyses of Imnaha Dike Plagioclase Phenocrysts

	Im-B15c-3pl	Im-B15c-3pl	Im-B15c-3pl	Im-B15c-4pl	Im-B15c-4pl	Im-B15c-4pl	Im-B15c-4pl
	2.00	3.00	4.00	1.00	2.00	3.00	4.00
SiO2	56.69	55.85	53.87	52.76	51.51	53.16	53.35
TiO2	0.18	0.06	0.09	0.05	0.11	0.10	0.09
Al2O3	26.07	26.47	26.40	28.31	28.92	28.18	27.99
MgO	0.05	0.06	1.12	0.10	0.06	0.07	0.09
CaO	9.32	10.17	10.70	12.42	13.32	12.52	12.42
FeO	0.57	0.69	1.05	0.85	0.72	0.76	0.59
Na2O	6.64	6.00	4.85	4.37	3.87	4.33	4.51
K2O	0.54	0.46	0.33	0.29	0.26	0.25	0.27
SrO	0.00	0.04	0.00	0.00	0.00	0.00	0.00
Total	**100.07**	**99.80**	**98.41**	**99.15**	**98.76**	**99.38**	**99.30**
Structural Formulae							
Cations per 8 Oxygen							
Si	2.57	2.55	2.49	2.43	2.39	2.44	2.45
Ti	0.01	0.00	0.01	0.00	0.01	0.01	0.01
Al	1.40	1.42	1.44	1.54	1.58	1.53	1.52
Mg	0.00	0.00	0.08	0.01	0.00	0.00	0.01
Ca	0.45	0.50	0.53	0.61	0.66	0.62	0.61
Fe	0.02	0.03	0.04	0.03	0.03	0.03	0.02
Na	0.50	0.46	0.38	0.34	0.30	0.33	0.35
K	0.03	0.03	0.02	0.02	0.02	0.01	0.02
Sr	0.00	0.00	0.00	0.00	0.00	0.00	0.00
Cation Sum	**5.00**	**4.98**	**4.98**	**4.98**	**4.98**	**4.97**	**4.97**
An	59.54	64.06	70.02	75.06	78.47	75.47	74.54
Ab	38.39	34.22	28.68	23.88	20.64	23.63	24.49
Or	2.07	1.72	1.30	1.05	0.89	0.91	0.98

208

Table 6C- Microprobe Analyses of Imnaha Dike Plagioclase Phenocrysts

	Im-B15c-5pl	Im-B15c-5pl	Im-B15c-5pl	Im-B15c-5pl	Im-B15c-7pl	Im-B15c-8pl	Im-B15c-8pl
SiO_2	53.43	52.03	51.44	55.26	55.84	52.41	52.66
TiO_2	0.07	0.16	0.06	0.18	0.18	0.02	0.06
Al_2O_3	28.02	28.81	29.35	26.27	26.20	29.02	28.92
MgO	0.11	0.07	0.06	0.04	0.09	0.06	0.07
CaO	11.96	13.31	13.94	10.36	13.02	12.61	12.69
FeO	0.41	0.57	0.56	0.60	0.59	0.60	0.59
Na_2O	4.85	3.81	3.73	5.52	3.17	3.97	4.05
K_2O	0.27	0.25	0.17	0.48	0.56	0.23	0.21
SrO	0.00	0.00	0.00	0.00	0.00	0.00	0.00
Total	**99.12**	**99.00**	**99.31**	**98.72**	**99.65**	**98.92**	**99.24**
Structural Formulae							
Cations per 8 Oxygen							
Si	2.46	2.40	2.37	2.54	2.54	2.41	2.42
Ti	0.01	0.01	0.00	0.01	0.01	0.00	0.00
Al	1.52	1.57	1.59	1.43	1.40	1.58	1.57
Mg	0.01	0.00	0.00	0.00	0.01	0.00	0.00
Ca	0.59	0.66	0.69	0.51	0.63	0.62	0.62
Fe	0.02	0.02	0.02	0.02	0.02	0.02	0.02
Na	0.37	0.29	0.29	0.43	0.24	0.31	0.31
K	0.02	0.01	0.01	0.03	0.03	0.01	0.01
Sr	0.00	0.00	0.00	0.00	0.00	0.00	0.00
Cation Sum	**4.98**	**4.97**	**4.98**	**4.97**	**4.89**	**4.96**	**4.96**
An	72.44	78.74	80.07	66.23	80.27	77.19	77.00
Ab	26.60	20.39	19.36	31.94	17.68	21.96	22.25
Or	0.96	0.87	0.57	1.83	2.04	0.85	0.74

Table 6D- Microprobe Analyses of Imnaha Dike Plagioclase Phenocrysts

	Im-B15c-8pl	Im-B15c-8pl	Im-B15c-10pl	Im-B15c-10pl	Im-B15c-10pl	Im-B15c-10pl	Im-B15c-10pl
SiO2	53.69	51.02	54.12	54.77	51.89	52.05	57.09
TiO2	0.15	0.01	0.15	0.18	0.06	0.14	0.17
Al2O3	28.36	29.47	27.80	27.96	29.03	29.42	26.28
MgO	0.05	0.05	0.09	0.09	0.09	0.05	0.09
CaO	11.61	12.56	11.50	11.49	12.70	13.58	9.48
FeO	0.69	0.69	0.53	0.60	0.52	0.53	0.66
Na2O	4.59	3.94	4.60	4.59	3.98	3.49	5.80
K2O	0.30	0.26	0.27	0.28	0.22	0.20	0.51
SrO	0.00	0.00	0.00	0.00	0.00	0.00	0.00
Total	**99.43**	**97.99**	**99.05**	**99.96**	**98.49**	**99.45**	**100.06**
Structural Formulae							
Cations per 8 Oxygen							
Si	2.46	2.38	2.48	2.49	2.40	2.39	2.58
Ti	0.01	0.00	0.01	0.01	0.00	0.01	0.01
Al	1.53	1.62	1.50	1.50	1.58	1.59	1.40
Mg	0.00	0.00	0.01	0.01	0.01	0.00	0.01
Ca	0.57	0.63	0.56	0.56	0.63	0.67	0.46
Fe	0.03	0.03	0.02	0.02	0.02	0.02	0.02
Na	0.35	0.31	0.35	0.35	0.31	0.27	0.44
K	0.02	0.02	0.02	0.02	0.01	0.01	0.03
Sr	0.00	0.00	0.00	0.00	0.00	0.00	0.00
Cation Sum	**4.96**	**4.98**	**4.95**	**4.95**	**4.97**	**4.96**	**4.95**
An	72.81	77.17	72.67	72.71	77.31	80.55	63.09
Ab	26.06	21.89	26.31	26.24	21.91	18.74	34.89
Or	1.12	0.95	1.02	1.05	0.78	0.70	2.02

Table 6E- Microprobe Analyses of Immaha Dike Plagioclase Phenocrysts

	Im-b15c-11pl	Im-b15c-11pl	Im-b15c-11pl	Im-b15c-12pl	Im-B15c-13pl	Im-B15c-13pl	Im-B15c-13pl
SiO2	52.92	52.02	52.89	48.64	52.40	50.80	49.52
TiO2	0.07	0.08	0.14	0.06	0.01	0.07	0.02
Al2O3	29.30	29.23	28.68	31.70	28.92	27.55	29.41
MgO	0.04	0.04	0.05	0.10	0.06	1.27	0.05
CaO	13.14	12.99	12.36	15.58	12.44	11.90	13.49
FeO	0.59	0.49	0.58	0.51	0.49	1.46	0.62
Na2O	3.80	3.80	4.18	2.15	4.09	3.73	3.62
K2O	0.21	0.17	0.28	0.08	0.21	0.24	0.21
SrO	0.00	0.00	0.00	0.00	0.00	0.00	0.00
Total	**100.07**	**98.81**	**99.15**	**98.81**	**98.62**	**97.02**	**96.94**
Structural Formulae							
Cations per 8 Oxygen							
Si	2.41	2.40	2.43	2.26	2.42	2.40	2.34
Ti	0.00	0.01	0.01	0.00	0.00	0.00	0.00
Al	1.57	1.59	1.55	1.73	1.57	1.53	1.64
Mg	0.00	0.00	0.00	0.01	0.00	0.09	0.00
Ca	0.64	0.64	0.61	0.77	0.62	0.60	0.68
Fe	0.02	0.02	0.02	0.02	0.02	0.06	0.02
Na	0.29	0.29	0.32	0.17	0.32	0.29	0.29
K	0.01	0.01	0.02	0.00	0.01	0.01	0.01
Sr	0.00	0.00	0.00	0.00	0.00	0.00	0.00
Cation Sum	**4.95**	**4.96**	**4.96**	**4.96**	**4.96**	**4.99**	**4.99**
An	78.65	78.58	75.78	88.66	76.48	77.16	79.88
Ab	20.59	20.79	23.19	11.07	22.74	21.91	19.37
Or	0.76	0.63	1.03	0.27	0.78	0.92	0.75

211

Table 6F- Microprobe Analyses of Immaha Dike Plagioclase Phenocrysts

	Im-18c-1pl5	Im-18c-1plc2	Im-18c-1plc3	Im-18c-1plc	Im-18c-1plr2	Im-18c-1plr3	Im-18c-1plr
SiO2	50.61	52.47	52.77	51.32	65.18	62.03	55.93
TiO2	0.10	0.15	0.16	0.21	0.18	0.08	0.14
Al2O3	30.73	29.57	30.01	29.67	20.42	23.53	26.98
MgO	0.10	0.10	0.10	0.09	0.00	0.05	0.05
CaO	13.83	13.04	12.64	12.75	2.45	5.65	9.86
FeO	0.37	0.38	0.47	0.59	0.45	0.31	0.58
Na2O	3.76	4.38	4.63	4.59	9.63	8.88	6.30
K2O	0.16	0.19	0.22	0.23	2.52	0.90	0.43
SrO	0.00	0.06	0.00	0.00	0.00	0.02	0.02
Total	**99.67**	**100.34**	**101.00**	**99.45**	**100.83**	**101.45**	**100.29**
Structural Formulae							
Cations per 8 Oxygen							
Si	2.32	2.39	2.39	2.36	2.91	2.75	2.54
Ti	0.01	0.01	0.01	0.01	0.01	0.01	0.01
Al	1.66	1.59	1.60	1.61	1.07	1.23	1.44
Mg	0.01	0.01	0.01	0.01	0.00	0.00	0.00
Ca	0.68	0.64	0.61	0.63	0.12	0.27	0.48
Fe	0.01	0.01	0.02	0.02	0.02	0.01	0.02
Na	0.29	0.33	0.35	0.35	0.72	0.66	0.48
K	0.01	0.01	0.01	0.01	0.14	0.05	0.03
Sr	0.00	0.00	0.00	0.00	0.00	0.00	0.00
Cation Sum	**4.99**	**4.99**	**5.00**	**5.01**	**4.99**	**4.99**	**4.99**
An	79.82	76.21	74.54	74.83	19.31	39.72	62.32
Ab	19.62	23.14	24.68	24.37	68.83	56.51	36.05
Or	0.56	0.65	0.78	0.80	11.86	3.77	1.63

212

Table 6G- Microprobe Analyses of Imnaha Dike Plagioclase
Phenocrysts

	Im-18c-3pllc	Im-18c-3pllr	Im-18c-3plc2	Im-18c-3plc3	Im-18c-3plc4	Im-18c-3plc5	Im-18c-3plc6
SiO2	51.23	60.46	51.62	50.87	51.54	54.53	52.27
TiO2	0.09	0.18	0.08	0.11	0.16	0.13	0.13
Al2O3	29.35	23.36	30.09	30.46	30.32	27.99	29.63
MgO	0.09	0.02	0.06	0.06	0.07	0.05	0.09
CaO	13.09	5.76	13.55	13.79	13.69	11.12	13.77
FeO	0.47	0.58	0.72	0.69	0.58	0.73	0.68
Na2O	4.40	8.73	4.06	3.98	4.02	5.76	4.11
K2O	0.21	0.98	0.14	0.18	0.15	0.31	0.20
SrO	0.00	0.00	0.00	0.00	0.00	0.00	0.00
Total	**98.92**	**100.06**	**100.32**	**100.14**	**100.53**	**100.61**	**100.87**
Structural Formulae							
Cations per 8 Oxygen							
Si	2.37	2.73	2.36	2.33	2.35	2.47	2.37
Ti	0.01	0.01	0.01	0.01	0.01	0.01	0.01
Al	1.60	1.24	1.62	1.64	1.63	1.50	1.59
Mg	0.01	0.00	0.00	0.00	0.00	0.00	0.01
Ca	0.65	0.28	0.66	0.68	0.67	0.54	0.67
Fe	0.02	0.02	0.03	0.03	0.02	0.03	0.03
Na	0.34	0.66	0.31	0.30	0.31	0.44	0.31
K	0.01	0.06	0.01	0.01	0.01	0.02	0.01
Sr	0.00	0.00	0.00	0.00	0.00	0.00	0.00
Cation Sum	**5.00**	**5.01**	**4.99**	**5.01**	**5.00**	**5.01**	**4.99**
An	76.15	40.43	78.30	78.84	78.60	67.34	78.19
Ab	23.14	55.47	21.21	20.56	20.90	31.54	21.13
Or	0.71	4.10	0.49	0.60	0.50	1.12	0.68

Table 6H- Microprobe Analyses of Imnaha Dike Plagioclase Phenocrysts

	Im-18c-3plr2	Im-18c-4plph1	Im-18c-6pl1	Im-18c-6pl	Im-18c-7pl1	Im-18c-8plph	Im-18c-8plphr
SiO_2	66.78	53.85	51.55	52.42	52.86	53.99	60.45
TiO_2	0.03	0.18	0.13	0.19	0.05	0.04	0.00
Al_2O_3	18.79	28.07	30.69	29.44	29.42	28.95	24.50
MgO	0.00	0.06	0.07	0.08	0.09	0.07	0.05
CaO	0.45	12.36	14.04	13.40	12.47	12.69	6.81
FeO	0.26	0.72	0.55	0.52	0.61	0.51	0.57
Na_2O	6.91	5.01	3.18	3.35	4.15	3.93	6.63
K_2O	7.40	0.28	0.16	0.21	0.22	0.26	0.66
SrO	0.00	0.00	0.00	0.00	0.00	0.00	0.03
Total	**100.61**	**100.54**	**100.35**	**99.61**	**99.86**	**100.43**	**99.70**
Structural Formulae							
Cations per 8 Oxygen							
Si	3.00	2.45	2.34	2.40	2.41	2.44	2.72
Ti	0.00	0.01	0.01	0.01	0.00	0.00	0.00
Al	1.00	1.51	1.65	1.59	1.58	1.54	1.30
Mg	0.00	0.00	0.00	0.01	0.01	0.00	0.00
Ca	0.02	0.60	0.68	0.66	0.61	0.62	0.33
Fe	0.01	0.03	0.02	0.02	0.02	0.02	0.02
Na	0.52	0.38	0.24	0.26	0.32	0.30	0.50
K	0.42	0.02	0.01	0.01	0.01	0.01	0.04
Sr	0.00	0.00	0.00	0.00	0.00	0.00	0.00
Cation Sum	**4.97**	**5.00**	**4.96**	**4.95**	**4.96**	**4.94**	**4.90**
An	4.04	72.45	82.53	80.92	76.24	77.38	51.61
Ab	56.28	26.57	16.92	18.31	22.97	21.69	45.44
Or	39.67	0.98	0.54	0.77	0.79	0.93	2.95

214

Table 6I- Microprobe Analyses of Imnaha Dike Plagioclase Phenocrysts

	Im-18c-8plph2	Im-18c-9pl3	Im-18c-9plc1	Im-18c-9plc2	Im-18c-9plr1	Im-18c-9plr2	Im-18c-10plc
SiO_2	51.97	53.09	54.08	52.67	64.60	59.92	51.77
TiO_2	0.21	0.11	0.20	0.06	0.05	0.08	0.23
Al_2O_3	28.94	28.18	28.18	29.69	20.53	23.55	30.05
MgO	0.09	0.08	0.09	0.09	0.00	0.03	0.08
CaO	12.85	11.78	12.20	14.00	2.97	7.42	14.40
FeO	0.49	0.73	0.53	0.42	0.31	0.46	0.30
Na_2O	3.74	4.31	4.12	3.28	7.73	6.33	3.09
K_2O	0.24	0.24	0.25	0.20	2.05	0.73	0.16
SrO	0.00	0.00	0.00	0.00	0.00	0.00	0.00
Total	**98.53**	**98.53**	**99.66**	**100.41**	**98.23**	**98.51**	**100.07**
Structural Formulae							
Cations per 8 Oxygen							
Si	2.40	2.45	2.46	2.39	2.92	2.73	2.36
Ti	0.01	0.01	0.01	0.00	0.00	0.01	0.02
Al	1.58	1.53	1.51	1.59	1.10	1.26	1.62
Mg	0.01	0.01	0.01	0.01	0.00	0.00	0.01
Ca	0.64	0.58	0.60	0.68	0.14	0.36	0.70
Fe	0.02	0.03	0.02	0.02	0.01	0.02	0.01
Na	0.29	0.33	0.31	0.25	0.58	0.48	0.24
K	0.01	0.01	0.01	0.01	0.12	0.04	0.01
Sr	0.00	0.00	0.00	0.00	0.00	0.00	0.00
Cation Sum	**4.96**	**4.96**	**4.94**	**4.95**	**4.88**	**4.90**	**4.96**
An	78.46	74.43	75.91	81.93	26.54	54.61	83.28
Ab	20.67	24.66	23.18	17.39	62.55	42.19	16.15
Or	0.86	0.92	0.91	0.68	10.91	3.19	0.56

Table 6J- Microprobe Analyses of Imnaha Dike Plagioclase Phenocrysts

	Im-18c-10pllnr	Im-18c-10plln	Im-18c-10pllnc	Im-18c-10pllnc	Im-18c-10plln	Im-18c-10pllnr	Im-18c-10plr
SiO2	51.96	48.78	50.42	51.40	51.95	55.37	55.28
TiO2	0.05	0.00	0.13	0.03	0.14	0.19	0.11
Al2O3	30.22	31.65	30.13	29.84	29.09	27.53	27.03
MgO	0.08	0.13	0.14	0.09	0.11	0.10	0.09
CaO	13.15	15.59	14.31	14.03	13.51	10.26	11.11
FeO	0.37	0.53	0.47	0.41	0.57	0.58	0.61
Na2O	3.63	2.21	2.92	3.14	3.54	4.91	4.61
K2O	0.18	0.08	0.12	0.15	0.19	0.38	0.35
SrO	0.00	0.00	0.00	0.00	0.00	0.00	0.00
Total	**99.63**	**98.96**	**98.63**	**99.09**	**99.09**	**99.31**	**99.18**
Structural Formulae							
Cations per 8 Oxygen							
Si	2.37	2.26	2.33	2.37	2.39	2.52	2.53
Ti	0.00	0.00	0.01	0.00	0.01	0.01	0.01
Al	1.63	1.73	1.65	1.62	1.58	1.48	1.46
Mg	0.01	0.01	0.01	0.01	0.01	0.01	0.01
Ca	0.64	0.77	0.71	0.69	0.67	0.50	0.54
Fe	0.01	0.02	0.02	0.02	0.02	0.02	0.02
Na	0.28	0.17	0.23	0.24	0.27	0.37	0.35
K	0.01	0.00	0.01	0.01	0.01	0.02	0.02
Sr	0.00	0.00	0.00	0.00	0.00	0.00	0.00
Cation Sum	**4.96**	**4.97**	**4.96**	**4.95**	**4.96**	**4.94**	**4.93**
An	79.51	88.40	84.07	82.71	80.31	68.75	71.74
Ab	19.84	11.32	15.50	16.77	19.03	29.74	26.92
Or	0.65	0.28	0.43	0.52	0.66	1.51	1.33

Table 6K- Microprobe Analyses of Imnaha Dike Plagioclase Phenocrysts

	Im-18c-11plc	Im-18c-13plc1	Im-18c-13plr3	Im-18c-13plc4	Im-18c-13plr2	Im-18c-13plr3	Im-18c-13plr
SiO2	52.81	53.27	53.14	52.81	55.13	65.24	56.80
TiO2	0.06	0.18	0.08	0.03	0.10	0.14	0.08
Al2O3	28.31	29.21	29.81	29.05	26.98	20.65	26.51
MgO	0.13	0.07	0.05	0.05	0.07	0.00	0.04
CaO	13.30	13.37	13.66	12.72	10.76	2.35	9.22
FeO	0.36	0.42	0.49	0.72	0.78	0.32	0.74
Na2O	3.57	3.53	3.36	3.55	4.82	7.38	5.68
K2O	0.17	0.23	0.18	0.22	0.35	3.15	0.43
SrO	0.02	0.00	0.00	0.00	0.00	0.00	0.00
Total	**98.73**	**100.27**	**100.76**	**99.14**	**98.98**	**99.23**	**99.49**
Structural Formulae							
Cations per 8 Oxygen							
Si	2.43	2.42	2.40	2.42	2.53	2.93	2.58
Ti	0.00	0.01	0.01	0.00	0.01	0.01	0.01
Al	1.54	1.56	1.59	1.57	1.46	1.09	1.42
Mg	0.01	0.00	0.00	0.00	0.00	0.00	0.00
Ca	0.66	0.65	0.66	0.63	0.53	0.11	0.45
Fe	0.01	0.02	0.02	0.03	0.03	0.01	0.03
Na	0.28	0.27	0.25	0.27	0.37	0.55	0.43
K	0.01	0.01	0.01	0.01	0.02	0.18	0.02
Sr	0.01	0.00	0.00	0.00	0.00	0.00	0.00
Cation Sum	**4.94**	**4.94**	**4.94**	**4.94**	**4.94**	**4.89**	**4.94**
An	79.95	80.06	81.29	79.22	70.18	21.52	63.11
Ab	19.44	19.14	18.08	19.97	28.47	61.24	35.16
Or	0.62	0.80	0.63	0.81	1.36	17.23	1.74

217

Table 6L- Microprobe Analyses of Imnaha Dike Plagioclase Phenocrysts

	Im-B19c-1pl	Im-B19c-1plb	Im-B19c-1plc	Im-B19c-2pl1	Im-B19c-2pl2c	Im-B19c-2pl2r	Im-B19c-2pl3c
SiO2	57.38	51.43	54.18	51.62	51.81	59.25	57.69
TiO2	0.11	0.19	0.04	0.08	0.06	0.10	0.20
Al2O3	25.98	29.26	28.18	28.65	29.20	24.78	24.85
MgO	0.08	0.10	0.17	0.05	0.10	0.05	0.06
CaO	8.98	12.92	11.70	13.74	13.06	7.88	8.50
FeO	0.76	0.54	0.62	0.63	0.68	0.48	0.70
Na2O	5.78	3.69	4.29	3.26	3.70	6.08	5.89
K2O	0.46	0.20	0.25	0.17	0.19	0.63	0.56
SrO	0.00	0.00	0.00	0.00	0.00	0.00	0.00
Total	**99.52**	**98.32**	**99.42**	**98.20**	**98.79**	**99.25**	**98.44**
Structural Formulae							
Cations per 8 Oxygen							
Si	2.60	2.38	2.47	2.40	2.39	2.68	2.64
Ti	0.01	0.01	0.00	0.01	0.00	0.01	0.01
Al	1.39	1.60	1.52	1.57	1.59	1.32	1.34
Mg	0.01	0.01	0.01	0.00	0.01	0.00	0.00
Ca	0.44	0.64	0.57	0.68	0.65	0.38	0.42
Fe	0.03	0.02	0.02	0.02	0.03	0.02	0.03
Na	0.44	0.29	0.33	0.25	0.29	0.46	0.45
K	0.03	0.01	0.01	0.01	0.01	0.04	0.03
Sr	0.00	0.00	0.00	0.00	0.00	0.00	0.00
Cation Sum	**4.94**	**4.96**	**4.94**	**4.95**	**4.96**	**4.91**	**4.93**
An	64.29	75.04	73.66	80.14	79.87	45.53	60.05
Ab	35.71	24.96	26.34	19.86	20.13	54.47	58.29
Or	0.00	0.00	0.00	0.00	0.00	0.00	41.71

Table 6M- Microprobe Analyses of Imnaha Dike Plagioclase Phenocrysts

	Im-B19c-2pl3r	Im-B19c-2pl4	Im-B19c-3pl2	Im-B19c-3plout	Im-B19c-4pl1	Im-B19c-4pl2	Im-B19c-4pl3
SiO_2	58.07	52.33	54.50	59.77	53.89	53.92	58.07
TiO_2	0.11	0.00	0.05	0.16	0.19	0.16	0.14
Al_2O_3	26.38	28.27	27.30	24.28	27.85	27.68	24.64
MgO	0.03	0.06	0.12	0.03	0.08	0.09	0.03
CaO	8.83	13.11	11.71	6.84	12.21	11.99	7.93
FeO	0.66	0.67	0.84	0.50	0.50	0.52	0.46
Na_2O	5.70	3.71	4.43	6.43	4.04	4.01	6.14
K_2O	0.54	0.21	0.25	0.76	0.28	0.25	0.61
SrO	0.00	0.00	0.00	0.00	0.00	0.00	0.00
Total	**100.32**	**98.33**	**99.21**	**98.77**	**99.03**	**98.61**	**98.03**
Structural Formulae							
Cations per 8 Oxygen							
Si	2.61	2.43	2.50	2.71	2.47	2.48	2.66
Ti	0.01	0.00	0.00	0.01	0.01	0.01	0.01
Al	1.40	1.54	1.47	1.30	1.51	1.50	1.33
Mg	0.00	0.00	0.01	0.00	0.01	0.01	0.00
Ca	0.43	0.65	0.57	0.33	0.60	0.59	0.39
Fe	0.02	0.03	0.03	0.02	0.02	0.02	0.02
Na	0.43	0.29	0.34	0.49	0.31	0.31	0.47
K	0.03	0.01	0.01	0.04	0.02	0.01	0.04
Sr	0.00	0.00	0.00	0.00	0.00	0.00	0.00
Cation Sum	**4.92**	**4.95**	**4.94**	**4.91**	**4.94**	**4.93**	**4.92**
An	61.72	79.04	73.79	52.17	76.15	76.06	45.43
Ab	57.39	78.34	78.60	41.90	65.91	69.73	54.57
Or	42.61	21.66	21.40	58.10	34.09	30.27	0.00

Table 6N- Microprobe Analyses of Imnaha Dike Plagioclase Phenocrysts

	Im-B19c-5pl	Im-B19c-5pl2	Im-B19c-6plin1	Im-B19c-6plin2	Im-B19c-6plln	Im-B19c-6plln	Im-B19c-6plln
SiO2	54.57	55.86	54.55	54.67	55.77	55.41	61.40
TiO2	0.09	0.04	0.21	0.21	0.05	0.09	0.14
Al2O3	26.61	25.76	26.35	26.81	25.90	26.22	22.87
MgO	0.10	0.10	0.08	0.06	0.08	0.06	0.02
CaO	11.48	10.62	11.36	10.55	10.02	10.21	5.66
FeO	0.50	0.67	0.71	0.72	0.66	0.69	0.53
Na2O	4.41	4.90	4.47	4.80	5.19	5.00	7.13
K2O	0.27	0.38	0.28	0.36	0.37	0.35	0.91
SrO	0.00	0.00	0.00	0.00	0.00	0.00	0.00
Total	**98.02**	**98.32**	**98.00**	**98.19**	**98.04**	**98.03**	**98.66**
Structural Formulae							
Cations per 8 Oxygen							
Si	2.52	2.57	2.53	2.52	2.57	2.56	2.78
Ti	0.01	0.00	0.01	0.01	0.00	0.01	0.01
Al	1.45	1.40	1.44	1.46	1.41	1.43	1.22
Mg	0.01	0.01	0.01	0.00	0.01	0.00	0.00
Ca	0.57	0.52	0.56	0.52	0.50	0.51	0.27
Fe	0.02	0.03	0.03	0.03	0.03	0.03	0.02
Na	0.34	0.38	0.35	0.37	0.40	0.39	0.54
K	0.02	0.02	0.02	0.02	0.02	0.02	0.05
Sr	0.00	0.00	0.00	0.00	0.00	0.00	0.00
Cation Sum	**4.93**	**4.93**	**4.94**	**4.94**	**4.93**	**4.93**	**4.90**
An	67.14	69.53	72.98	68.79	65.94	68.79	38.97
Ab	32.86	66.33	73.76	7.59	8.17	7.89	10.83
Or	0.00	33.67	26.24	0.00	0.00	0.00	0.00

Table 6O- Microprobe Analyses of Imnaha Dike Plagioclase Phenocrysts

	Im-B19c-6plln	Im-B19c-6plln	Im-B19c-8plc	Im-B19c-8plr	Im-B19c-10plc	Im-B19c-10plr	Im-B19c-11plc
SiO2	65.58	65.58	50.90	57.65	51.48	55.59	47.96
TiO2	0.08	0.08	0.09	0.18	0.21	0.10	0.06
Al2O3	20.01	20.01	29.14	24.77	29.17	27.48	31.96
MgO	0.01	0.01	0.04	0.05	0.08	0.08	0.08
CaO	2.15	2.15	14.03	8.99	13.07	10.65	16.73
FeO	0.33	0.33	0.52	0.61	0.54	0.67	0.50
Na2O	7.69	7.69	3.49	6.04	3.88	5.12	1.81
K2O	2.98	2.98	0.17	0.47	0.24	0.37	0.04
SrO	0.00	0.00	0.00	0.00	0.00	0.00	0.00
Total	**98.81**	**98.81**	**98.37**	**98.76**	**98.67**	**100.07**	**99.13**
Structural Formulae							
Cations per 8 Oxygen							
Si	2.95	2.95	2.37	2.64	2.38	2.52	2.22
Ti	0.01	0.01	0.01	0.01	0.01	0.01	0.00
Al	1.06	1.06	1.60	1.34	1.59	1.47	1.75
Mg	0.00	0.00	0.00	0.00	0.01	0.01	0.01
Ca	0.10	0.10	0.70	0.44	0.65	0.52	0.83
Fe	0.01	0.01	0.02	0.02	0.02	0.03	0.02
Na	0.58	0.58	0.27	0.46	0.30	0.39	0.14
K	0.17	0.17	0.01	0.03	0.01	0.02	0.00
Sr	0.00	0.00	0.00	0.00	0.00	0.00	0.00
Cation Sum	**4.89**	**4.89**	**4.97**	**4.94**	**4.98**	**4.95**	**4.97**
An	10.89	10.89	77.32	60.99	78.17	68.68	90.97
Ab	11.56	11.56	5.62	37.12	20.97	29.90	8.91
Or	0.00	0.00	0.00	1.89	0.85	1.42	0.12

Table 6P- Microprobe Analyses of Imnaha Dike Plagioclase Phenocrysts

	Im-b21b-1pl	Im-b21b-1pl	Im-B21b-2pl	Im-B21b-3pl	Im-B21b-3pl	Im-B21b-3pl	Im-B21b-4pl
SiO2	53.34	56.91	50.78	54.43	52.22	56.00	51.33
TiO2	0.07	0.22	0.08	0.16	0.09	0.10	0.13
Al2O3	28.73	26.42	30.14	28.00	28.65	26.90	30.24
MgO	0.07	0.08	0.08	0.13	0.09	0.08	0.06
CaO	12.56	9.66	14.11	11.64	12.49	10.05	13.57
FeO	0.54	0.56	0.41	0.62	0.63	0.58	0.44
Na2O	3.76	5.49	3.18	4.65	4.05	5.35	3.51
K2O	0.19	0.41	0.15	0.26	0.21	0.37	0.14
SrO	0.00	0.00	0.00	0.00	0.00	0.00	0.00
Total	**99.26**	**99.73**	**98.92**	**99.89**	**98.42**	**99.44**	**99.40**
Structural Formulae							
Cations per 8 Oxygen							
Si	2.44	2.58	2.34	2.48	2.42	2.55	2.36
Ti	0.00	0.01	0.01	0.01	0.01	0.01	0.01
Al	1.55	1.41	1.64	1.50	1.56	1.44	1.64
Mg	0.00	0.01	0.01	0.01	0.01	0.01	0.00
Ca	0.62	0.47	0.70	0.57	0.62	0.49	0.67
Fe	0.02	0.02	0.02	0.02	0.02	0.02	0.02
Na	0.29	0.42	0.25	0.35	0.31	0.41	0.27
K	0.01	0.02	0.01	0.02	0.01	0.02	0.01
Sr	0.00	0.00	0.00	0.00	0.00	0.00	0.00
Cation Sum	**4.93**	**4.94**	**4.96**	**4.96**	**4.96**	**4.94**	**4.97**
An	78.12	64.97	82.63	72.71	76.75	66.52	80.64
Ab	21.18	33.41	16.85	26.31	22.49	32.03	18.85
Or	0.70	1.62	0.52	0.98	0.76	1.45	0.50

222

Table 6Q- Microprobe Analyses of Imnaha Dike Plagioclase Phenocrysts

	Im-B21b-4pl	Im-B21b-4pl	Im-B21b-4pl	Im-B21b-4pl	Im-B21b-4pl	Im-B21b-5pl	Im-B21b-5pl
SiO2	52.74	65.83	50.42	52.76	57.26	55.60	54.65
TiO2	0.07	0.06	0.12	0.08	0.18	0.12	0.07
Al2O3	29.03	20.20	28.47	29.40	26.48	27.18	27.55
MgO	0.06	0.00	0.84	0.07	0.03	0.09	0.23
CaO	12.74	1.86	12.72	13.20	9.26	10.87	11.57
FeO	0.66	0.32	3.14	0.48	0.64	0.74	0.73
Na2O	3.89	8.54	3.21	3.81	6.06	5.00	4.72
K2O	0.19	2.72	0.16	0.21	0.40	0.28	0.23
SrO	0.00	0.00	0.00	0.00	0.00	0.00	0.00
Total	**99.37**	**99.53**	**99.08**	**100.00**	**100.31**	**99.88**	**99.76**
Structural Formulae							
Cations per 8 Oxygen							
Si	2.42	2.95	2.35	2.40	2.58	2.52	2.49
Ti	0.00	0.00	0.01	0.01	0.01	0.01	0.00
Al	1.57	1.07	1.56	1.58	1.41	1.45	1.48
Mg	0.00	0.00	0.06	0.00	0.00	0.01	0.02
Ca	0.63	0.09	0.64	0.64	0.45	0.53	0.56
Fe	0.03	0.01	0.12	0.02	0.02	0.03	0.03
Na	0.30	0.64	0.25	0.29	0.46	0.38	0.36
K	0.01	0.16	0.01	0.01	0.02	0.02	0.01
Sr	0.00	0.00	0.00	0.00	0.00	0.00	0.00
Cation Sum	**4.95**	**4.92**	**5.00**	**4.96**	**4.95**	**4.95**	**4.96**
An	77.81	16.57	80.92	78.72	61.80	69.84	72.42
Ab	21.49	68.95	18.46	20.53	36.62	29.09	26.71
Or	0.71	14.47	0.61	0.75	1.58	1.07	0.87

223

Table 6R- Microprobe Analyses of Imnaha Dike Plagioclase Phenocrysts

	Im-B21b-5pl	Im-B21b-6pl	Im-B21b-6pl	Im-B21b-7pl	Im-B21b-7pl	Im-B21b-7pl	Im-B21b-7pl
SiO2	51.67	54.31	54.37	55.19	53.92	54.68	52.13
TiO2	0.10	0.14	0.01	0.07	0.14	0.15	0.08
Al2O3	29.57	27.71	28.61	26.53	27.54	27.00	29.31
MgO	0.04	0.11	0.06	0.08	0.10	0.05	0.07
CaO	13.04	11.54	12.20	10.14	11.41	10.69	13.11
FeO	0.65	0.63	0.53	0.62	0.65	0.87	0.64
Na2O	3.86	4.65	4.42	5.34	4.64	5.02	3.70
K2O	0.20	0.25	0.22	0.31	0.25	0.27	0.22
SrO	0.00	0.00	0.00	0.00	0.00	0.00	0.00
Total	**99.13**	**99.34**	**100.42**	**98.27**	**98.62**	**98.72**	**99.25**
Structural Formulae							
Cations per 8 Oxygen							
Si	2.38	2.48	2.46	2.54	2.48	2.51	2.40
Ti	0.01	0.01	0.00	0.00	0.01	0.01	0.01
Al	1.61	1.49	1.53	1.44	1.50	1.46	1.59
Mg	0.00	0.01	0.00	0.01	0.01	0.00	0.00
Ca	0.64	0.57	0.59	0.50	0.56	0.53	0.65
Fe	0.03	0.02	0.02	0.02	0.02	0.03	0.02
Na	0.30	0.36	0.33	0.41	0.36	0.39	0.28
K	0.01	0.01	0.01	0.02	0.01	0.02	0.01
Sr	0.00	0.00	0.00	0.00	0.00	0.00	0.00
Cation Sum	**4.97**	**4.95**	**4.95**	**4.95**	**4.95**	**4.95**	**4.96**
An	78.32	72.60	74.69	66.89	72.43	69.46	79.06
Ab	20.98	26.45	24.52	31.88	26.64	29.50	20.17
Or	0.70	0.94	0.79	1.23	0.93	1.05	0.77

224

Table 6S- Microprobe Analyses of Imnaha Dike Plagioclase Phenocrysts

	Im-B21b-7pl	Im-B21b-8pl	Im-B21b-8pl	Im-B21b-8pl	Im-B21b-8pl	Im-B21b-8pl	Im-B21b-8pl
SiO2	56.58	50.55	52.58	51.27	50.39	65.99	52.83
TiO2	0.10	0.00	0.13	0.02	0.00	0.05	0.16
Al2O3	25.85	29.15	28.89	30.25	29.44	20.77	28.97
MgO	0.05	0.04	0.07	0.07	0.05	0.00	0.05
CaO	9.39	13.07	12.19	14.31	14.05	2.87	12.90
FeO	0.76	0.51	0.61	0.50	0.51	0.31	0.50
Na2O	5.74	3.65	4.07	3.17	3.26	7.66	3.94
K2O	0.44	0.18	0.19	0.16	0.12	2.23	0.17
SrO	0.00	0.00	0.00	0.00	0.00	0.00	0.00
Total	**98.91**	**97.14**	**98.74**	**99.75**	**97.80**	**99.87**	**99.52**
Structural Formulae							
Cations per 8 Oxygen							
Si	2.59	2.37	2.42	2.35	2.35	2.93	2.42
Ti	0.01	0.00	0.01	0.00	0.00	0.00	0.01
Al	1.39	1.61	1.57	1.63	1.62	1.09	1.56
Mg	0.00	0.00	0.01	0.00	0.00	0.00	0.00
Ca	0.46	0.66	0.60	0.70	0.70	0.14	0.63
Fe	0.03	0.02	0.02	0.02	0.02	0.01	0.02
Na	0.44	0.29	0.31	0.24	0.25	0.57	0.30
K	0.03	0.01	0.01	0.01	0.01	0.13	0.01
Sr	0.00	0.00	0.00	0.00	0.00	0.00	0.00
Cation Sum	**4.95**	**4.97**	**4.96**	**4.96**	**4.96**	**4.87**	**4.96**
An	63.26	79.29	76.24	82.86	82.33	25.79	77.88
Ab	34.97	20.05	23.05	16.60	17.27	62.29	21.51
Or	1.77	0.66	0.72	0.54	0.40	11.92	0.60

225

Table 6T- Microprobe Analyses of Imnaha Dike Plagioclase Phenocrysts

	Im-B21b-9pl	Im-B21b-9pl	Im-B21b-9pl	Im-B21b-9pl	Im-B21b-9pl	Im-B21b-10pl	Im-B21b-10pl
SiO2	56.58	51.79	52.83	53.40	54.88	51.23	52.23
TiO2	0.11	0.13	0.07	0.18	0.19	0.11	0.08
Al2O3	27.31	28.79	29.24	28.03	26.78	29.62	29.21
MgO	0.07	0.08	0.10	0.06	0.07	0.07	0.07
CaO	10.92	12.55	12.91	11.91	10.31	13.51	12.93
FeO	0.58	0.50	0.46	0.67	0.64	0.46	0.52
Na2O	4.96	4.00	3.78	4.41	4.97	3.53	3.77
K2O	0.33	0.20	0.18	0.28	0.33	0.12	0.21
SrO	0.00	0.00	0.00	0.00	0.00	0.00	0.00
Total	**100.88**	**98.02**	**99.58**	**98.93**	**98.17**	**98.64**	**99.01**
Structural Formulae							
Cations per 8 Oxygen							
Si	2.54	2.41	2.41	2.46	2.53	2.37	2.40
Ti	0.01	0.01	0.00	0.01	0.01	0.01	0.01
Al	1.44	1.58	1.57	1.52	1.46	1.61	1.58
Mg	0.00	0.01	0.01	0.00	0.01	0.00	0.00
Ca	0.52	0.62	0.63	0.59	0.51	0.67	0.64
Fe	0.02	0.02	0.02	0.03	0.02	0.02	0.02
Na	0.37	0.31	0.29	0.34	0.38	0.27	0.29
K	0.02	0.01	0.01	0.02	0.02	0.01	0.01
Sr	0.00	0.00	0.00	0.00	0.00	0.00	0.00
Cation Sum	**4.93**	**4.97**	**4.95**	**4.96**	**4.94**	**4.96**	**4.96**
An	69.96	77.03	78.53	74.13	68.75	80.54	78.55
Ab	28.76	22.24	20.81	24.84	29.96	19.04	20.70
Or	1.27	0.73	0.66	1.03	1.29	0.42	0.75

Table 6U- Microprobe Analyses of Imnaha Dike Plagioclase Phenocrysts

	Im-B21b-10pl	Im-B21b-10pl	Im-B23b-2pl-1	Im-B23b-2pl-1	Im-B23b-2pl-1	Im-B23b-2pl-1	Im-B23b-2pl-1
SiO_2	53.88	52.21	54.07	56.99	56.38	57.77	54.50
TiO_2	0.02	0.05	0.01	0.10	0.23	0.10	0.14
Al_2O_3	28.20	29.43	26.88	26.04	27.13	26.78	27.06
MgO	0.27	0.12	0.07	0.07	0.10	0.05	0.04
CaO	12.02	13.50	11.71	10.33	11.34	9.80	11.76
FeO	0.95	0.76	0.67	0.78	0.72	0.61	0.81
Na_2O	4.02	3.67	4.79	5.67	4.87	5.91	5.00
K_2O	0.18	0.16	0.32	0.47	0.30	0.50	0.35
SrO	0.00	0.00	0.00	0.00	0.00	0.01	0.00
Total	**99.54**	**99.88**	**98.52**	**100.45**	**101.06**	**101.53**	**99.66**
Structural Formulae							
Cations per 8 Oxygen							
Si	2.46	2.39	2.50	2.58	2.53	2.58	2.49
Ti	0.00	0.00	0.00	0.01	0.02	0.01	0.01
Al	1.52	1.59	1.46	1.39	1.44	1.41	1.46
Mg	0.02	0.01	0.00	0.00	0.01	0.00	0.00
Ca	0.59	0.66	0.58	0.50	0.55	0.47	0.58
Fe	0.04	0.03	0.03	0.03	0.03	0.02	0.03
Na	0.31	0.28	0.37	0.43	0.37	0.44	0.38
K	0.01	0.01	0.02	0.03	0.02	0.03	0.02
Sr	0.00	0.00	0.00	0.00	0.00	0.00	0.00
Cation Sum	**4.94**	**4.96**	**4.96**	**4.96**	**4.94**	**4.95**	**4.98**
An	76.25	79.81	72.13	65.62	71.22	63.46	71.29
Ab	23.06	19.62	26.68	32.60	27.66	34.60	27.45
Or	0.70	0.58	1.19	1.78	1.12	1.94	1.26

Table 6V- Microprobe Analyses of Imnaha Dike Plagioclase Phenocrysts

	Im-B23b-3pl	Im-B23b-3pl	Im-B23b-3pl	Im-B23b-3pl	Im-B23b-3pl	Im-B23b-3pl	Im-B23b-4pl
SiO2	54.75	66.46	53.60	53.53	53.58	60.04	61.13
TiO2	0.11	0.15	0.03	0.09	0.08	0.09	0.00
Al2O3	29.09	19.19	28.95	28.20	27.70	24.09	23.91
MgO	0.05	0.00	0.05	0.11	0.04	0.02	0.04
CaO	12.44	2.23	13.22	13.02	13.09	7.70	7.31
FeO	0.73	0.20	0.68	0.84	0.54	0.47	0.40
Na2O	4.48	7.86	4.09	4.23	3.98	6.90	6.66
K2O	0.25	3.10	0.20	0.24	0.23	0.66	0.81
SrO	0.00	0.00	0.00	0.00	0.04	0.00	0.02
Total	**101.91**	**99.19**	**100.80**	**100.25**	**99.27**	**99.96**	**100.28**
Structural Formulae							
Cations per 8 Oxygen							
Si	2.45	2.98	2.43	2.44	2.46	2.70	2.73
Ti	0.01	0.01	0.00	0.01	0.01	0.01	0.00
Al	1.53	1.02	1.54	1.51	1.50	1.28	1.26
Mg	0.00	0.00	0.00	0.01	0.00	0.00	0.00
Ca	0.60	0.11	0.64	0.64	0.64	0.37	0.35
Fe	0.03	0.01	0.03	0.03	0.02	0.02	0.01
Na	0.34	0.59	0.31	0.32	0.31	0.52	0.50
K	0.01	0.18	0.01	0.01	0.01	0.04	0.05
Sr	0.00	0.00	0.00	0.00	0.00	0.00	0.00
Cation Sum	**4.96**	**4.89**	**4.96**	**4.97**	**4.95**	**4.94**	**4.91**
An	74.73	19.90	77.61	76.64	77.79	53.71	52.91
Ab	24.37	63.58	21.71	22.52	21.42	43.56	43.58
Or	0.91	16.52	0.68	0.85	0.80	2.73	3.51

228

Table 6W- Microprobe Analyses of Imnaha Dike Plagioclase Phenocrysts

	Im-B23b-4pl	Im-B23b-4pl	Im-B23b-4pl	Im-B23b-4pl	Im-B23b-5pl	Im-B23b-5pl	Im-B23b-6pl
SiO2	54.06	57.73	52.75	55.54	57.21	58.37	65.36
TiO2	0.06	0.13	0.11	0.21	0.09	0.18	0.05
Al2O3	27.97	25.45	29.69	27.00	27.05	25.57	21.60
MgO	0.11	0.04	0.05	0.06	0.10	0.07	0.00
CaO	12.56	9.66	13.90	10.40	10.02	9.53	3.80
FeO	0.61	0.73	0.64	0.76	0.57	0.58	0.26
Na2O	4.08	5.65	3.59	5.49	5.90	6.19	7.99
K2O	0.26	0.44	0.19	0.40	0.42	0.33	1.91
SrO	0.00	0.00	0.00	0.00	0.00	0.00	0.03
Total	**99.71**	**99.83**	**100.91**	**99.88**	**101.35**	**100.79**	**100.99**
Structural Formulae							
Cations per 8 Oxygen							
Si	2.47	2.61	2.39	2.53	2.56	2.62	2.89
Ti	0.00	0.01	0.01	0.01	0.01	0.01	0.00
Al	1.50	1.36	1.58	1.45	1.43	1.35	1.12
Mg	0.01	0.00	0.00	0.00	0.01	0.00	0.00
Ca	0.61	0.47	0.67	0.51	0.48	0.46	0.18
Fe	0.02	0.03	0.02	0.03	0.02	0.02	0.01
Na	0.31	0.43	0.27	0.42	0.44	0.46	0.59
K	0.02	0.03	0.01	0.02	0.02	0.02	0.11
Sr	0.00	0.00	0.00	0.00	0.00	0.00	0.00
Cation Sum	**4.95**	**4.93**	**4.96**	**4.97**	**4.96**	**4.95**	**4.90**
An	76.56	64.26	80.54	66.65	64.20	62.20	31.25
Ab	22.48	33.98	18.82	31.83	34.21	36.53	59.40
Or	0.95	1.76	0.64	1.53	1.60	1.27	9.36

229

Table 6X- Microprobe Analyses of Imnaha Dike Plagioclase Phenocrysts

	Im-B23b-6pl	Im-B23b-6pl	Im-B23b-6pl	Im-B23b-6pl	Im-B23b-6pl	Im-B23b-7pl	Im-B23b-7pl
SiO_2	63.51	63.61	64.97	62.44	65.29	53.12	56.09
TiO_2	0.00	0.06	0.00	0.23	0.05	0.21	0.00
Al_2O_3	22.75	23.25	15.20	23.96	20.53	28.70	26.96
MgO	0.01	0.03	1.72	0.00	0.00	0.07	0.12
CaO	5.88	5.66	0.43	5.94	2.82	13.66	11.26
FeO	0.43	0.41	2.94	0.54	0.56	0.37	0.72
Na_2O	7.59	7.87	3.39	7.67	7.96	3.75	5.25
K_2O	1.03	1.23	9.70	1.15	2.43	0.20	0.31
SrO	0.00	0.13	0.00	0.02	0.00	0.00	0.00
Total	**101.20**	**102.26**	**98.34**	**101.95**	**99.63**	**100.08**	**100.71**
Structural Formulae							
Cations per 8 Oxygen							
Si	2.81	2.79	3.03	2.75	2.92	2.42	2.53
Ti	0.00	0.00	0.00	0.01	0.00	0.01	0.00
Al	1.19	1.20	0.84	1.24	1.08	1.54	1.43
Mg	0.00	0.00	0.12	0.00	0.00	0.00	0.01
Ca	0.28	0.27	0.02	0.28	0.14	0.67	0.54
Fe	0.02	0.02	0.11	0.02	0.02	0.01	0.03
Na	0.56	0.58	0.26	0.56	0.60	0.29	0.40
K	0.06	0.07	0.58	0.06	0.14	0.01	0.02
Sr	0.00	0.00	0.00	0.00	0.00	0.00	0.00
Cation Sum	**4.91**	**4.93**	**4.97**	**4.94**	**4.90**	**4.96**	**4.96**
An	44.01	41.88	4.64	43.80	24.62	79.56	69.53
Ab	51.39	52.69	33.09	51.14	62.77	19.75	29.34
Or	4.60	5.42	62.27	5.06	12.62	0.69	1.13

Table 6Y - Microprobe Analyses of Imnaha Dike Plagioclase Phenocrysts

	Im-B23b-7pl	Im-B23b-7pl	Im-B23b-7pl	Im-B23b-7pl	Im-B23b-8pl	Im-B23b-8pl	Im-B23b-8pl
SiO_2	63.95	59.14	66.78	54.17	52.69	55.84	65.55
TiO_2	0.08	0.06	0.05	0.05	0.10	0.06	0.16
Al_2O_3	22.72	24.59	18.47	29.48	28.54	26.57	21.94
MgO	0.07	0.05	0.01	0.07	0.11	0.07	0.01
CaO	5.80	8.98	0.99	12.35	13.97	11.11	4.26
FeO	0.41	0.47	0.04	0.65	0.47	0.71	0.47
Na_2O	7.40	6.26	6.83	4.55	3.61	5.26	8.02
K_2O	1.01	0.48	6.29	0.29	0.17	0.39	1.60
SrO	0.02	0.00	0.00	0.00	0.00	0.00	0.01
Total	**101.44**	**100.04**	**99.45**	**101.61**	**99.65**	**100.01**	**102.04**
Structural Formulae							
Cations per 8 Oxygen							
Si	2.82	2.67	3.02	2.43	2.41	2.54	2.87
Ti	0.00	0.00	0.00	0.00	0.01	0.00	0.01
Al	1.18	1.31	0.98	1.56	1.54	1.42	1.13
Mg	0.00	0.00	0.00	0.00	0.01	0.00	0.00
Ca	0.27	0.43	0.05	0.59	0.69	0.54	0.20
Fe	0.02	0.02	0.00	0.02	0.02	0.03	0.02
Na	0.54	0.47	0.52	0.34	0.28	0.40	0.59
K	0.06	0.03	0.36	0.02	0.01	0.02	0.09
Sr	0.00	0.00	0.00	0.00	0.00	0.00	0.00
Cation Sum	**4.90**	**4.93**	**4.93**	**4.97**	**4.96**	**4.96**	**4.90**
An	44.30	60.15	9.03	74.19	80.56	69.00	34.16
Ab	51.12	37.92	56.66	24.76	18.85	29.55	58.20
Or	4.58	1.93	34.31	1.05	0.59	1.45	7.64

Table 6Z- Microprobe Analyses of Imnaha Dike Plagioclase Phenocrysts

	Im-B23b-9pl	Im-B23b-9pl	Im-B23b-9pl	Im-B23b-11plr	Im-B23b-11pl	Im-B23b-11pl	Im-B23b-11pl	Im-B23b-11pl
SiO2	53.18	58.04	54.37	63.77	55.24	54.84	58.25	52.66
TiO2	0.03	0.05	0.19	0.18	0.15	0.00	0.04	0.18
Al2O3	28.50	25.41	29.02	22.62	25.66	27.80	25.80	30.14
MgO	0.05	0.11	0.07	0.01	0.92	0.09	0.05	0.04
CaO	13.33	9.50	13.08	4.55	10.77	11.27	9.12	14.09
FeO	0.57	0.53	0.72	0.45	1.56	0.83	0.54	0.64
Na2O	4.13	5.86	4.12	7.50	4.85	5.06	6.26	3.48
K2O	0.21	0.49	0.26	1.16	0.28	0.35	0.53	0.17
SrO	0.00	0.00	0.00	0.02	0.00	0.00	0.00	0.00
Total	**99.99**	**99.98**	**101.83**	**100.26**	**99.42**	**100.24**	**100.58**	**101.39**
Structural Formulae								
Cations per 8 Oxygen								
Si	2.43	2.62	2.43	2.83	2.53	2.49	2.62	2.37
Ti	0.00	0.00	0.01	0.01	0.01	0.00	0.00	0.01
Al	1.53	1.35	1.53	1.18	1.39	1.49	1.37	1.60
Mg	0.00	0.01	0.00	0.00	0.06	0.01	0.00	0.00
Ca	0.65	0.46	0.63	0.22	0.53	0.55	0.44	0.68
Fe	0.02	0.02	0.03	0.02	0.06	0.03	0.02	0.02
Na	0.32	0.44	0.31	0.56	0.37	0.38	0.47	0.26
K	0.01	0.03	0.01	0.07	0.02	0.02	0.03	0.01
Sr	0.00	0.00	0.00	0.00	0.00	0.00	0.00	0.00
Cation Sum	**4.97**	**4.94**	**4.96**	**4.89**	**4.97**	**4.97**	**4.95**	**4.96**
An	77.55	62.92	77.12	37.84	70.27	70.22	60.38	81.27
Ab	21.72	35.14	21.97	56.44	28.65	28.50	37.52	18.14
Or	0.73	1.94	0.92	5.73	1.09	1.28	2.11	0.60

APPENDIX 2

Table 7A- Microprobe Analyses of Imnaha Dike Olivine Phenocrysts

	Im-B15C-1ol	Im-B15C-1ol	Im-B15C-1ol	Im-B15C-1ol	Im-B15c-2ol	Im-B15c-2ol	Im-B15c-2ol
SiO2	37.01	37.14	37.68	37.52	37.12	38.40	37.11
TiO2	0.02	0.02	0.00	0.02	0.00	0.03	0.09
Al2O3	0.00	0.01	0.00	0.02	0.00	0.02	0.01
Cr2O3	0.00	0.02	0.00	0.00	0.06	0.05	0.03
MgO	33.01	30.83	32.00	31.65	31.63	33.02	31.30
CaO	0.03	0.06	0.06	0.08	0.05	0.06	0.06
FeO	28.69	32.11	30.22	30.24	31.38	29.17	30.13
MnO	0.38	0.49	0.43	0.39	0.49	0.34	0.39
Na2O	0.00	0.00	0.00	0.00	0.00	0.00	0.01
K2O	0.02	0.00	0.00	0.00	0.00	0.00	0.00
Total	**99.16**	**100.68**	**100.38**	**99.92**	**100.74**	**101.10**	**99.14**
Structural Formulae	Cations per 4 Oxygen						
Si	1.00	1.01	1.01	1.01	1.00	1.02	1.01
Ti	0.00	0.00	0.00	0.00	0.00	0.00	0.00
Al (IV)	0.00	0.00	0.00	0.00	0.00	0.00	0.00
Al (VI)	0.00	0.00	0.00	0.00	0.00	0.00	0.00
Cr	0.00	0.00	0.00	0.00	0.00	0.00	0.00
Mg	1.33	1.25	1.28	1.28	1.27	1.31	1.27
Ca	0.00	0.00	0.00	0.00	0.00	0.00	0.00
Fe	0.65	0.73	0.68	0.68	0.71	0.65	0.69
Mn	0.01	0.01	0.01	0.01	0.01	0.01	0.01
Na	0.00	0.00	0.00	0.00	0.00	0.00	0.00
K	0.00	0.00	0.00	0.00	0.00	0.00	0.00
Cation Sum	**3.00**	**2.99**	**2.99**	**2.99**	**3.00**	**2.98**	**2.99**
Mg #	67.39	63.30	65.54	65.28	64.42	67.03	65.11

233

Table 7B- Microprobe Analyses of Imnaha Dike Olivine Phenocrysts

	Im-B15C-3ol	Im-B15C-3olr	Im-B15c-4ol	Im-B15c-4ol	Im-B15c-4ol	Im-B15C-5ol	Im-B15C-6ol
SiO2	38.16	37.76	37.76	36.11	37.93	36.72	36.98
TiO2	0.02	0.00	0.00	0.06	0.02	0.04	0.05
Al2O3	0.00	0.00	0.02	0.03	0.07	0.03	0.05
Cr2O3	0.00	0.00	0.04	0.03	0.00	0.00	0.02
MgO	34.85	33.36	31.99	29.48	32.27	31.36	33.71
CaO	0.06	0.07	0.01	0.02	0.08	0.05	0.03
FeO	25.89	27.22	29.20	30.95	28.88	30.62	27.42
MnO	0.36	0.33	0.38	0.34	0.39	0.43	0.32
Na2O	0.03	0.00	0.01	0.02	0.00	0.00	0.00
K2O	0.00	0.02	0.00	0.00	0.00	0.00	0.00
Total	**99.37**	**98.76**	**99.42**	**97.03**	**99.64**	**99.25**	**98.59**
Structural Formulae							
Cations per 4 Oxygen							
Si	1.02	1.02	1.02	1.01	1.02	1.00	1.00
Ti	0.00	0.00	0.00	0.00	0.00	0.00	0.00
Al (IV)	0.00	0.00	0.00	0.00	0.00	0.00	0.00
Al (VI)	0.00	0.00	0.00	0.00	0.00	0.00	0.00
Cr	0.00	0.00	0.00	0.00	0.00	0.00	0.00
Mg	1.38	1.34	1.29	1.23	1.29	1.28	1.36
Ca	0.00	0.00	0.00	0.00	0.00	0.00	0.00
Fe	0.58	0.61	0.66	0.73	0.65	0.70	0.62
Mn	0.01	0.01	0.01	0.01	0.01	0.01	0.01
Na	0.00	0.00	0.00	0.00	0.00	0.00	0.00
K	0.00	0.00	0.00	0.00	0.00	0.00	0.00
Cation Sum	**2.98**	**2.98**	**2.98**	**2.98**	**2.98**	**2.99**	**3.00**
Mg#	70.74	68.76	66.31	63.11	66.75	64.78	68.83

234

Table 7C- Microprobe Analyses of Imnaha Dike Olivine Phenocrysts

	Im-B15C-6ol	Im-B15C-6ol	Im-B15C-6ol	Im-B15C-7ol	Im-B15C-7ol	Im-B15C-7ol	Im-B15C-8ol
SiO2	36.80	37.93	37.77	37.12	38.14	37.13	37.72
TiO2	0.02	0.05	0.03	0.01	0.03	0.06	0.01
Al2O3	0.01	0.00	0.00	0.03	0.00	0.00	0.02
Cr2O3	0.02	0.02	0.02	0.02	0.00	0.02	0.06
MgO	31.93	32.52	34.07	30.11	31.97	30.58	33.90
CaO	0.05	0.07	0.05	0.05	0.09	0.04	0.06
FeO	30.07	29.14	26.23	31.56	29.87	31.82	27.39
MnO	0.40	0.45	0.36	0.43	0.43	0.43	0.38
Na2O	0.06	0.01	0.00	0.00	0.00	0.00	0.03
K2O	0.00	0.00	0.01	0.01	0.00	0.02	0.00
Total	**99.35**	**100.19**	**98.54**	**99.34**	**100.53**	**100.10**	**99.57**
Structural Formulae							
Cations per 4 Oxygen							
Si	1.00	1.02	1.02	1.02	1.02	1.01	1.01
Ti	0.00	0.00	0.00	0.00	0.00	0.00	0.00
Al (IV)	0.00	0.00	0.00	0.00	0.00	0.00	0.00
Al (VI)	0.00	0.00	0.00	0.00	0.00	0.00	0.00
Cr	0.00	0.00	0.00	0.00	0.00	0.00	0.00
Mg	1.30	1.30	1.37	1.23	1.28	1.24	1.35
Ca	0.00	0.00	0.00	0.00	0.00	0.00	0.00
Fe	0.69	0.65	0.59	0.72	0.67	0.72	0.61
Mn	0.01	0.01	0.01	0.01	0.01	0.01	0.01
Na	0.00	0.00	0.00	0.00	0.00	0.00	0.00
K	0.00	0.00	0.00	0.00	0.00	0.00	0.00
Cation Sum	**3.00**	**2.98**	**2.98**	**2.98**	**2.98**	**2.99**	**2.99**
Mg#	65.60	66.72	70.00	63.15	65.78	63.32	68.97

235

Table 7D- Microprobe Analyses of Imnaha Dike Olivine
Phenocrysts

	Im-B15C-8ol	Im-B15C-8ol	Im-B15C-8ol	Im-B15C-10ol	Im-B15C-11ol	Im-B15c-11ol	Im-B15C-11ol
SiO2	38.06	37.53	36.98	37.30	37.34	37.93	37.27
TiO2	0.05	0.01	0.02	0.00	0.04	0.01	0.03
Al2O3	0.00	0.03	0.00	0.00	0.00	0.00	0.00
Cr2O3	0.00	0.00	0.05	0.00	0.01	0.04	0.04
MgO	33.94	31.56	33.24	31.09	33.83	35.16	29.82
CaO	0.07	0.07	0.05	0.06	0.05	0.03	0.05
FeO	27.11	31.07	28.62	29.76	27.09	25.71	31.57
MnO	0.36	0.46	0.38	0.47	0.33	0.33	0.46
Na2O	0.00	0.02	0.03	0.00	0.05	0.00	0.01
K2O	0.00	0.00	0.01	0.01	0.00	0.00	0.03
Total	**99.59**	**100.75**	**99.38**	**98.70**	**98.74**	**99.21**	**99.27**
Structural Formulae							
Cations per 4 Oxygen							
Si	1.02	1.01	1.00	1.02	1.01	1.01	1.02
Ti	0.00	0.00	0.00	0.00	0.00	0.00	0.00
Al (IV)	0.00	0.00	0.00	0.00	0.00	0.00	0.00
Al (VI)	0.00	0.00	0.00	0.00	0.00	0.00	0.00
Cr	0.00	0.00	0.00	0.00	0.00	0.00	0.00
Mg	1.35	1.27	1.34	1.27	1.36	1.40	1.22
Ca	0.00	0.00	0.00	0.00	0.00	0.00	0.00
Fe	0.61	0.70	0.65	0.68	0.61	0.57	0.72
Mn	0.01	0.01	0.01	0.01	0.01	0.01	0.01
Na	0.00	0.00	0.00	0.00	0.00	0.00	0.00
K	0.00	0.00	0.00	0.00	0.00	0.00	0.00
Cation Sum	**2.98**	**2.99**	**3.00**	**2.98**	**2.99**	**2.99**	**2.98**
Mg#	69.22	64.60	67.60	65.24	69.17	71.07	62.92

236

Table 7E- Microprobe Analyses of Imnaha Dike Olivine Phenocrysts

	Im-B15C-12ol	Im-B15C-12ol	Im-B15C-12ol	Im-B18c-3ol	Im-B18c-3ol	Im-B18c-3ol	Im-B18c-3ol
SiO_2	36.66	35.69	36.38	36.03	38.11	37.16	37.28
TiO_2	0.04	0.04	0.01	0.06	0.03	0.04	0.00
Al_2O_3	0.00	0.05	0.00	0.04	0.00	0.00	0.02
Cr_2O_3	0.01	0.02	0.02	0.01	0.04	0.02	0.00
MgO	31.98	32.20	30.38	26.10	33.08	28.88	27.40
CaO	0.07	0.08	0.04	0.05	0.08	0.09	0.04
FeO	30.02	27.82	31.42	38.71	30.05	34.82	37.15
MnO	0.38	0.41	0.38	0.61	0.39	0.55	0.55
Na_2O	0.01	0.02	0.01	0.00	0.00	0.02	0.00
K_2O	0.00	0.00	0.01	0.00	0.01	0.00	0.00
Total	**99.18**	**96.32**	**98.65**	**101.61**	**101.79**	**101.57**	**102.43**
Structural Formulae							
Cations per 4 Oxygen							
Si	1.00	1.00	1.01	1.00	1.01	1.01	1.01
Ti	0.00	0.00	0.00	0.00	0.00	0.00	0.00
Al (IV)	0.00	0.00	0.00	0.00	0.00	0.00	0.00
Al (VI)	0.00	0.00	0.00	0.00	0.00	0.00	0.00
Cr	0.00	0.00	0.00	0.00	0.00	1.17	0.00
Mg	1.30	1.34	1.25	1.08	1.30	0.00	1.11
Ca	0.00	0.00	0.00	0.00	0.00	0.79	0.00
Fe	0.69	0.65	0.73	0.90	0.67	0.01	0.85
Mn	0.01	0.01	0.01	0.01	0.01	0.00	0.01
Na	0.00	0.00	0.00	0.00	0.00	0.00	0.00
K	0.00	0.00	0.00	0.00	0.00	0.00	0.00
Cation Sum	**3.00**	**3.00**	**2.99**	**3.00**	**2.99**	**2.99**	**2.99**
Mg#	65.68	67.52	63.46	54.77	66.41	59.84	56.99

237

Table 7F- Microprobe Analyses of Imnaha Dike Olivine Phenocrysts

	Im-B18c-3ol	Im-B18c-5olgmbd	Im-B18c-6ol	Im-B18c-6ol	Im-B18c-6ol	Im-B18c-6ol	Im-B18c-6ol
SiO2	36.61	37.38	38.11	36.22	37.31	37.92	37.21
TiO2	0.07	0.05	0.01	0.06	0.00	0.04	0.02
Al2O3	0.00	0.00	0.00	0.03	0.05	0.00	0.02
Cr2O3	0.00	0.02	0.03	0.00	0.02	0.00	0.06
MgO	29.37	28.43	33.10	24.59	28.11	32.54	28.40
CaO	0.07	0.08	0.07	0.07	0.09	0.08	0.06
FeO	34.26	34.75	29.64	40.37	36.17	30.47	35.79
MnO	0.47	0.46	0.35	0.61	0.50	0.40	0.48
Na2O	0.00	0.00	0.06	0.00	0.02	0.02	0.00
K2O	0.00	0.02	0.00	0.00	0.00	0.00	0.01
Total	**100.84**	**101.19**	**101.38**	**101.96**	**102.27**	**101.47**	**102.06**
Structural Formulae							
Cations per 4 Oxygen							
Si	1.00	1.02	1.01	1.01	1.01	1.01	1.01
Ti	0.00	0.00	0.00	0.00	0.00	0.00	0.00
Al (IV)	0.00	0.00	0.00	0.00	0.00	0.00	0.00
Al (VI)	0.00	0.00	0.00	0.00	0.00	0.00	0.00
Cr	0.00	0.00	0.00	0.00	0.00	0.00	0.00
Mg	1.20	1.15	1.31	1.02	1.14	1.29	1.15
Ca	0.00	0.00	0.00	0.00	0.00	0.00	0.00
Fe	0.78	0.79	0.66	0.94	0.82	0.68	0.81
Mn	0.01	0.01	0.01	0.01	0.01	0.01	0.01
Na	0.00	0.00	0.00	0.00	0.00	0.00	0.00
K	0.00	0.00	0.00	0.00	0.00	0.00	0.00
Cation Sum	**3.00**	**2.98**	**2.99**	**2.99**	**2.99**	**2.99**	**2.99**
Mg#	60.63	59.51	66.73	52.25	58.26	65.73	58.77

Table 7G- Microprobe Analyses of Imnaha Dike Olivine Phenocrysts

	Im-B18c-6ol	Im-B18c-7olc1	Im-B18c-7olr1	Im-B18c-7olc2	Im-B18c-7olr2	Im-B18c-8ol	Im-B18c-8olgm
SiO2	38.36	37.04	36.31	38.15	35.72	36.90	36.79
TiO2	0.02	0.00	0.04	0.00	0.00	0.02	0.16
Al2O3	0.01	0.00	0.01	0.00	0.00	0.00	0.19
Cr2O3	0.06	0.04	0.00	0.06	0.01	0.00	0.01
MgO	34.41	32.80	24.98	33.45	21.62	28.86	28.86
CaO	0.08	0.10	0.06	0.09	0.10	0.12	0.44
FeO	28.21	29.73	40.47	29.81	43.52	33.29	31.73
MnO	0.34	0.37	0.61	0.44	0.72	0.41	0.52
Na2O	0.02	0.00	0.00	0.03	0.00	0.00	0.18
K2O	0.00	0.00	0.00	0.01	0.00	0.02	0.10
Total	**101.51**	**100.07**	**102.48**	**102.03**	**101.69**	**99.62**	**98.96**
Structural Formulae							
Cations per 4 Oxygen							
Si	1.01	1.00	1.01	1.01	1.01	1.02	1.02
Ti	0.00	0.00	0.00	0.00	0.00	0.00	0.00
Al (IV)	0.00	0.00	0.00	0.00	0.00	0.00	0.00
Al (VI)	0.00	0.00	0.00	0.00	0.00	0.00	0.00
Cr	0.00	0.00	0.00	0.00	0.00	0.00	0.00
Mg	1.35	1.32	1.03	1.32	0.92	1.19	1.19
Ca	0.00	0.00	0.00	0.00	0.00	0.00	0.01
Fe	0.62	0.67	0.94	0.66	1.03	0.77	0.74
Mn	0.01	0.01	0.01	0.01	0.02	0.01	0.01
Na	0.00	0.00	0.00	0.00	0.00	0.00	0.00
K	0.00	0.00	0.00	0.00	0.00	0.00	0.00
Cation Sum	**2.99**	**3.00**	**2.99**	**2.99**	**2.99**	**2.98**	**2.98**
Mg#	68.66	66.46	52.58	66.84	47.16	60.89	62.03

239

Table 7H- Microprobe Analyses of Imnaha Dike Olivine Phenocrysts

	Im-B18c-9ol	Im-B18c-10ol	Im-B18c-11olc	Im-B18c-11ol	Im-B18c-11olr	Im-B18c-12olc1	Im-B18c-12olr1
SiO2	36.56	39.16	38.73	36.40	35.69	38.49	36.65
TiO2	0.01	0.00	0.00	0.03	0.05	0.00	0.09
Al2O3	0.06	0.00	0.04	0.03	0.00	0.01	0.00
Cr2O3	0.00	0.00	0.05	0.02	0.00	0.01	0.00
MgO	29.61	35.78	32.92	24.02	25.33	32.33	27.33
CaO	0.06	0.08	0.04	0.07	0.12	0.05	0.03
FeO	34.51	25.82	29.61	39.98	38.75	29.60	35.93
MnO	0.44	0.34	0.36	0.60	0.66	0.37	0.56
Na2O	0.00	0.00	0.00	0.02	0.00	0.00	0.00
K2O	0.00	0.00	0.00	0.00	0.01	0.00	0.02
Total	**101.26**	**101.18**	**101.75**	**101.16**	**100.60**	**100.86**	**100.61**
Structural Formulae							
Cations per 4 Oxygen							
Si	1.00	1.02	1.02	1.02	1.00	1.02	1.01
Ti	0.00	0.00	0.00	0.00	0.00	0.00	0.00
Al (IV)	0.00	0.00	0.00	0.00	0.00	0.00	0.00
Al (VI)	0.00	0.00	0.00	0.00	0.00	0.00	0.00
Cr	0.00	0.00	0.00	0.00	0.00	0.00	0.00
Mg	1.20	1.39	1.29	1.00	1.06	1.28	1.13
Ca	0.00	0.00	0.00	0.00	0.00	0.00	0.00
Fe	0.79	0.56	0.65	0.94	0.91	0.66	0.83
Mn	0.01	0.01	0.01	0.01	0.02	0.01	0.01
Na	0.00	0.00	0.00	0.00	0.00	0.00	0.00
K	0.00	0.00	0.00	0.00	0.00	0.00	0.00
Cation Sum	**3.00**	**2.98**	**2.98**	**2.98**	**3.00**	**2.98**	**2.99**
Mg#	60.65	71.34	66.63	51.90	54.01	66.24	57.74

240

Table 7I- Microprobe Analyses of Imnaha Dike Olivine Phenocrysts

	Im-B18c-12olr2	Im-B18c-12olr3	Im-B18c-12olc2	Im-b18c-13ol	Im-b18c-13olr	Im-b18c-13olc	Im-b18c-13olr
SiO_2	38.01	36.29	38.00	36.30	37.62	37.92	37.33
TiO_2	0.00	0.00	0.00	0.08	0.00	0.00	0.00
Al_2O_3	0.01	0.00	0.05	0.01	0.01	0.05	0.00
Cr_2O_3	0.03	0.00	0.00	0.02	0.00	0.00	0.00
MgO	30.17	24.49	32.08	31.47	29.03	32.36	25.48
CaO	0.10	0.04	0.05	0.13	0.08	0.06	0.05
FeO	32.81	40.00	30.18	32.25	35.99	30.96	38.67
MnO	0.46	0.62	0.36	0.48	0.55	0.37	0.53
Na_2O	0.00	0.00	0.02	0.03	0.05	0.01	0.05
K_2O	0.00	0.00	0.01	0.00	0.01	0.00	0.01
Total	**101.58**	**101.44**	**100.75**	**100.77**	**103.34**	**101.74**	**102.12**
Structural Formulae							
Cations per 4 Oxygen							
Si	1.02	1.01	1.02	0.99	1.01	1.01	1.03
Ti	0.00	0.00	0.00	0.00	0.00	0.00	0.00
Al (IV)	0.00	0.00	0.00	0.00	0.00	0.00	0.00
Al (VI)	0.00	0.00	0.00	0.00	0.00	0.00	0.00
Cr	0.00	0.00	0.00	0.00	0.00	0.00	0.00
Mg	1.21	1.02	1.28	1.27	1.16	1.28	1.04
Ca	0.00	0.00	0.00	0.00	0.00	0.00	0.00
Fe	0.74	0.94	0.68	0.73	0.81	0.69	0.89
Mn	0.01	0.01	0.01	0.01	0.01	0.01	0.01
Na	0.00	0.00	0.00	0.00	0.00	0.00	0.00
K	0.00	0.00	0.00	0.00	0.00	0.00	0.00
Cation Sum	**2.98**	**2.99**	**2.98**	**3.01**	**2.99**	**2.99**	**2.97**
Mg#	62.29	52.38	65.63	63.67	59.16	65.25	54.20

241

Table 7J - Microprobe Analyses of Immaha Dike Olivine Phenocrysts

	Im-b18c-13ol	Im-B19c-1ol	Im-B19c-1ol2	Im-B19c-2ol	Im-B19c-7olc	Im-B19c-7ol	Im-b19c-8ol
SiO2	36.66	36.13	36.81	36.51	39.20	35.77	36.49
TiO2	0.01	0.17	0.16	0.17	0.11	0.17	0.17
Al2O3	0.00	0.16	0.16	0.15	0.17	0.15	0.16
Cr2O3	0.03	0.01	0.01	0.01	0.01	0.01	0.01
MgO	23.10	25.76	31.37	27.43	35.98	22.94	26.36
CaO	0.01	0.45	0.43	0.43	0.38	0.42	0.44
FeO	40.09	36.73	29.59	33.95	24.65	41.88	35.02
MnO	0.46	0.52	0.44	0.46	0.42	0.63	0.52
Na2O	0.01	0.20	0.18	0.18	0.16	0.21	0.17
K2O	0.01	0.09	0.10	0.08	0.10	0.11	0.09
Total	**100.38**	**100.22**	**99.25**	**99.37**	**101.17**	**102.28**	**99.43**
Structural Formulae							
Cations per 4 Oxygen							
Si	1.03	1.01	1.01	1.02	1.02	1.01	1.02
Ti	0.00	0.00	0.00	0.00	0.00	0.00	0.00
Al (IV)	0.00	0.00	0.00	0.00	0.00	0.00	0.00
Al (VI)	0.00	0.00	0.00	0.00	0.00	0.00	0.00
Cr	0.00	0.00	0.00	0.00	0.00	0.00	0.00
Mg	0.97	1.08	1.28	1.14	1.40	0.96	1.10
Ca	0.00	0.01	0.01	0.01	0.01	0.01	0.01
Fe	0.95	0.86	0.68	0.79	0.54	0.99	0.82
Mn	0.01	0.01	0.01	0.01	0.01	0.02	0.01
Na	0.00	0.00	0.00	0.00	0.00	0.00	0.00
K	0.00	0.00	0.00	0.00	0.00	0.00	0.00
Cation Sum	**2.97**	**2.98**	**2.99**	**2.98**	**2.98**	**2.99**	**2.98**
Mg#	50.86	55.75	65.57	59.20	72.39	49.59	57.48

Table 7K- Microprobe Analyses of Imnaha Dike Olivine Phenocrysts

	Im-B19c-9ol	Im-B19c-9ol	Im-B19c-9ol	Im-B19c-9ol	Im-B19c-9ol	Im-B19c-9ol	Im-b19c-10ol
SiO2	37.59	35.86	36.77	37.27	36.15	35.31	36.62
TiO2	0.17	0.12	0.13	0.17	0.14	0.17	0.10
Al2O3	0.14	0.13	0.13	0.15	0.13	0.12	0.15
Cr2O3	0.01	0.01	0.01	0.01	0.01	0.01	0.01
MgO	30.59	26.76	30.41	31.88	25.52	23.88	29.12
CaO	0.42	0.41	0.44	0.41	0.40	0.46	0.43
FeO	30.31	34.05	30.65	28.58	36.39	37.68	32.05
MnO	0.41	0.51	0.47	0.44	0.50	0.52	0.47
Na2O	0.18	0.20	0.29	0.18	0.21	0.20	0.22
K2O	0.11	0.10	0.12	0.09	0.11	0.09	0.11
Total	**99.92**	**98.14**	**99.42**	**99.17**	**99.55**	**98.43**	**99.28**
Structural Formulae							
Cations per 4 Oxygen							
Si	1.02	1.02	1.01	1.01	1.01	1.01	1.01
Ti	0.00	0.00	0.00	0.00	0.00	0.00	0.00
Al (IV)	0.00	0.00	0.00	0.00	0.00	0.00	0.00
Al (VI)	0.00	0.00	0.00	0.00	0.00	0.00	0.00
Cr	0.00	0.00	0.00	0.00	0.00	0.00	0.00
Mg	1.24	1.13	1.24	1.29	1.24	0.00	1.20
Ca	0.01	0.01	0.01	0.01	0.01	1.29	0.01
Fe	0.69	0.81	0.70	0.65	0.70	0.65	0.74
Mn	0.01	0.01	0.01	0.01	0.01	0.01	0.01
Na	0.00	0.00	0.00	0.00	0.01	0.01	0.00
K	0.00	0.00	0.00	0.00	0.00	0.00	0.00
Cation Sum	**2.98**	**2.98**	**2.99**	**2.98**	**2.99**	**2.98**	**2.99**
Mg#	64.44	58.53	64.06	66.71	55.74	53.23	62.01

243

Table 7L- Microprobe Analyses of Imnaha Dike Olivine Phenocrysts

	Im-b19c-10ol	Im-B19c-11ol	Im-B19c-11olr1	Im-B19c-11olc2	Im-B19c-11olr2	Im-b19c-11olg2	Im-b19c-11olgm
SiO2	36.39	38.07	35.20	37.50	35.55	36.67	35.73
TiO2	0.15	0.15	0.20	0.17	0.15	0.20	0.14
Al2O3	0.13	0.14	0.12	0.12	0.11	0.15	0.16
Cr2O3	0.01	0.01	0.01	0.01	0.01	0.01	0.01
MgO	26.01	31.44	23.27	30.45	23.94	25.43	24.90
CaO	0.44	0.43	0.45	0.42	0.43	0.41	0.44
FeO	34.70	29.21	38.47	31.15	37.60	36.34	37.90
MnO	0.50	0.39	0.58	0.43	0.64	0.63	0.56
Na2O	0.19	0.17	0.18	0.19	0.21	0.19	0.21
K2O	0.10	0.09	0.08	0.09	0.11	0.08	0.11
Total	**98.63**	**100.09**	**98.56**	**100.53**	**98.75**	**100.11**	**100.17**
Structural Formulae							
Cations per 4 Oxygen							
Si	1.03	1.03	1.02	1.02	1.02	1.03	1.01
Ti	0.00	0.00	0.00	0.00	0.00	0.00	0.00
Al (IV)	0.00	0.00	0.00	0.00	0.00	0.00	0.00
Al (VI)	0.00	0.00	0.00	0.00	0.00	0.00	0.00
Cr	0.00	0.00	0.00	0.00	0.00	0.00	0.00
Mg	1.09	1.26	1.00	1.23	1.02	1.06	1.05
Ca	0.01	0.01	0.01	0.01	0.01	0.01	0.01
Fe	0.82	0.66	0.93	0.71	0.90	0.85	0.90
Mn	0.01	0.01	0.01	0.01	0.02	0.01	0.01
Na	0.00	0.00	0.00	0.00	0.00	0.00	0.00
K	0.00	0.00	0.00	0.00	0.00	0.00	0.00
Cation Sum	**2.97**	**2.97**	**2.98**	**2.98**	**2.98**	**2.97**	**2.99**
Mg#	57.38	65.91	52.07	63.72	53.35	55.69	54.13

244

Table 7M- Microprobe Analyses of Imnaha Dike Olivine Phenocrysts

	Im-b19c-11olgm	Im-B21b-2ol	Im-B21b-2ol	Im-B21b-2ol	Im-B21b-2ol	Im-B21b-3ol	Im-B21b-3ol
SiO2	36.46	37.08	37.83	36.62	34.54	34.75	38.10
TiO2	0.17	0.00	0.02	0.00	0.00	0.00	0.00
Al2O3	0.15	0.00	0.04	0.03	0.00	0.00	0.00
Cr2O3	0.01	0.00	0.00	0.02	0.00	0.03	0.01
MgO	25.79	32.90	32.50	29.06	23.06	20.35	31.39
CaO	0.42	0.06	0.05	0.09	0.07	0.07	0.09
FeO	35.85	28.80	30.49	35.04	41.68	43.92	31.62
MnO	0.49	0.37	0.38	0.54	0.73	0.73	0.38
Na2O	0.18	0.00	0.00	0.00	0.00	0.07	0.00
K2O	0.09	0.00	0.00	0.01	0.01	0.00	0.00
Total	**99.60**	**99.21**	**101.31**	**101.40**	**100.08**	**99.92**	**101.59**
Structural Formulae							
Cations per 4 Oxygen							
Si	1.02	1.00	1.01	1.00	0.99	1.01	1.02
Ti	0.00	0.00	0.00	0.00	0.00	0.00	0.00
Al (IV)	0.00	0.00	0.00	0.00	0.00	0.00	0.00
Al (VI)	0.00	0.00	0.00	0.00	0.00	0.00	0.00
Cr	0.00	0.00	0.00	0.00	0.00	0.00	0.00
Mg	1.08	1.33	1.29	1.18	0.99	0.88	1.25
Ca	0.01	0.00	0.00	0.00	0.00	0.00	0.00
Fe	0.84	0.65	0.68	0.80	1.00	1.07	0.71
Mn	0.01	0.01	0.01	0.01	0.02	0.02	0.01
Na	0.00	0.00	0.00	0.00	0.00	0.00	0.00
K	0.00	0.00	0.00	0.00	0.00	0.00	0.00
Cation Sum	**2.97**	**3.00**	**2.99**	**3.00**	**3.01**	**2.99**	**2.98**
Mg#	56.37	67.23	65.69	59.83	49.84	45.42	64.07

Table 7N- Microprobe Analyses of Imnaha Dike Olivine Phenocrysts

	Im-B21b-3ol	Im-B21b-3ol	Im-B21b-3ol	Im-B21b-4ol	Im-B21b-4ol	Im-B21b-4ol	Im-B21b-5ol
SiO2	36.76	37.95	36.34	36.29	37.40	37.06	36.09
TiO2	0.03	0.07	0.03	0.00	0.06	0.02	0.00
Al2O3	0.06	0.01	0.00	0.06	0.00	0.00	0.01
Cr2O3	0.01	0.02	0.03	0.02	0.01	0.02	0.00
MgO	29.58	33.24	26.32	26.75	29.35	31.66	25.48
CaO	0.05	0.05	0.04	0.04	0.05	0.06	0.08
FeO	32.23	30.11	37.42	36.71	33.32	30.60	38.70
MnO	0.30	0.38	0.56	0.60	0.43	0.40	0.55
Na2O	0.00	0.02	0.00	0.00	0.00	0.00	0.00
K2O	0.01	0.00	0.02	0.00	0.00	0.01	0.01
Total	**99.03**	**101.85**	**100.75**	**100.47**	**100.62**	**99.82**	**100.93**
Structural Formulae							
Cations per 4 Oxygen							
Si	1.01	1.00	1.01	1.01	1.02	1.01	1.01
Ti	0.00	0.00	0.00	0.00	0.00	0.00	0.00
Al (IV)	0.00	0.00	0.00	0.00	0.00	0.00	0.00
Al (VI)	0.00	0.00	0.00	0.00	0.00	0.00	0.00
Cr	0.00	0.00	0.00	0.00	0.00	0.00	0.00
Mg	1.22	1.31	1.09	1.11	1.19	1.28	1.06
Ca	0.00	0.00	0.00	0.00	0.00	0.00	0.00
Fe	0.74	0.67	0.87	0.85	0.76	0.69	0.90
Mn	0.01	0.01	0.01	0.01	0.01	0.01	0.01
Na	0.00	0.00	0.00	0.00	0.00	0.00	0.00
K	0.00	0.00	0.00	0.00	0.00	0.00	0.00
Cation Sum	**2.98**	**2.99**	**2.99**	**2.99**	**2.98**	**2.99**	**2.99**
Mg #	62.24	66.48	55.82	56.69	61.27	65.02	54.18

246

Table 7O - Microprobe Analyses of Imnaha Dike Olivine Phenocrysts

	Im-B21b-5ol	Im-B21b-5ol	Im-B21b-5ol	Im-B21b-6ol	Im-B21b-6ol	Im-B21b-6ol	Im-B21b-7ol
SiO2	38.21	38.04	35.88	36.96	37.31	38.06	36.16
TiO2	0.02	0.06	0.01	0.00	0.07	0.00	0.03
Al2O3	0.05	0.00	0.01	0.02	0.05	0.07	0.02
Cr2O3	0.01	0.00	0.01	0.06	0.02	0.04	0.00
MgO	37.12	35.62	24.96	31.41	31.46	35.09	24.23
CaO	0.07	0.06	0.08	0.03	0.05	0.05	0.07
FeO	23.13	27.01	38.71	31.49	30.98	26.43	38.05
MnO	0.29	0.31	0.64	0.43	0.43	0.31	0.60
Na2O	0.00	0.00	0.00	0.00	0.01	0.00	0.00
K2O	0.00	0.00	0.00	0.00	0.02	0.00	0.00
Total	**98.90**	**101.11**	**100.31**	**100.39**	**100.40**	**100.04**	**99.16**
Structural Formulae							
Cations per 4 Oxygen							
Si	1.01	1.00	1.01	1.00	1.01	1.01	1.03
Ti	0.00	0.00	0.00	0.00	0.00	0.00	0.00
Al (IV)	0.00	0.00	0.00	0.00	0.00	0.00	0.00
Al (VI)	0.00	0.00	0.00	0.00	0.00	0.00	0.00
Cr	0.00	0.00	0.00	0.00	0.00	0.00	0.00
Mg	1.46	1.40	1.05	1.27	1.27	1.39	1.03
Ca	0.00	0.00	0.00	0.00	0.00	0.00	0.00
Fe	0.51	0.59	0.91	0.71	0.70	0.59	0.90
Mn	0.01	0.01	0.02	0.01	0.01	0.01	0.01
Na	0.00	0.00	0.00	0.00	0.00	0.00	0.00
K	0.00	0.00	0.00	0.00	0.00	0.00	0.00
Cation Sum	**2.99**	**3.00**	**2.99**	**3.00**	**2.99**	**2.99**	**2.97**
Mg #	74.24	70.32	53.67	64.18	64.59	70.46	53.35

247

Table 7P- Microprobe Analyses of Imnaha Dike Olivine Phenocrysts

	Im-B21b-7ol	Im-B21b-7ol	Im-b21b-8ol	Im-B21b-9ol	Im-B21b-9ol	Im-B21b-9ol	Im-B21b-9ol
SiO2	37.03	37.55	37.61	38.09	37.24	37.02	35.93
TiO2	0.00	0.01	0.02	0.03	0.00	0.00	0.02
Al2O3	0.00	0.00	0.00	0.00	0.00	0.01	0.00
Cr2O3	0.00	0.05	0.00	0.01	0.00	0.00	0.00
MgO	28.42	30.97	33.86	32.14	28.99	30.71	28.15
CaO	0.04	0.07	0.05	0.06	0.06	0.05	0.04
FeO	35.34	31.07	29.53	29.75	33.13	32.59	35.91
MnO	0.55	0.43	0.33	0.39	0.48	0.54	0.56
Na2O	0.01	0.00	0.01	0.00	0.03	0.00	0.00
K2O	0.00	0.00	0.00	0.00	0.00	0.00	0.00
Total	**101.39**	**100.15**	**101.41**	**100.47**	**99.93**	**100.92**	**100.61**
Structural Formulae							
Cations per 4 Oxygen							
Si	1.01	1.02	1.00	1.02	1.02	1.00	1.00
Ti	0.00	0.00	0.00	0.00	0.00	0.00	0.00
Al (IV)	0.00	0.00	0.00	0.00	0.00	0.00	0.00
Al (VI)	0.00	0.00	0.00	0.00	0.00	0.00	0.00
Cr	0.00	0.00	0.00	0.00	0.00	0.00	0.00
Mg	1.16	1.25	1.34	1.28	1.18	1.24	1.16
Ca	0.00	0.00	0.00	0.00	0.00	0.00	0.00
Fe	0.81	0.70	0.66	0.67	0.76	0.74	0.83
Mn	0.01	0.01	0.01	0.01	0.01	0.01	0.01
Na	0.00	0.00	0.00	0.00	0.00	0.00	0.00
K	0.00	0.00	0.00	0.00	0.00	0.00	0.00
Cation Sum	**2.99**	**2.98**	**3.00**	**2.98**	**2.98**	**3.00**	**3.00**
Mg #	59.09	64.16	67.32	65.99	61.12	62.86	58.47

Table 7Q- Microprobe Analyses of Imnaha Dike Olivine Phenocrysts

	Im-B23b-9ol	Im-b23b-10ol	Im-b23b-10ol	Im-b23b-10ol
SiO2	38.32	38.22	37.73	37.49
TiO2	0.05	0.01	0.07	0.00
Al2O3	0.00	0.05	0.01	0.00
Cr2O3	0.06	0.05	0.00	0.03
MgO	34.24	33.59	30.53	32.00
CaO	0.06	0.04	0.08	0.06
FeO	27.77	27.33	32.44	30.79
MnO	0.38	0.42	0.43	0.39
Na2O	0.00	0.00	0.00	0.03
K2O	0.00	0.00	0.00	0.00
Total	**100.87**	**99.71**	**101.29**	**100.79**
Structural Formulae				
Cations per 4 Oxygen				
Si	1.01	1.02	1.02	1.01
Ti	0.00	0.00	0.00	0.00
Al (IV)	0.00	0.00	0.00	0.00
Al (VI)	0.00	0.00	0.00	0.00
Cr	0.00	0.00	0.00	0.00
Mg	1.35	1.34	1.22	1.28
Ca	0.00	0.00	0.00	0.00
Fe	0.61	0.61	0.73	0.69
Mn	0.01	0.01	0.01	0.01
Na	0.00	0.00	0.00	0.00
K	0.00	0.00	0.00	0.00
Cation Sum	**2.99**	**2.98**	**2.98**	**2.99**
Mg #	68.89	68.82	62.83	65.12

APPENDIX 3

Table 8A- Microprobe Analyses of Imnaha Dike Pyroxene Phenocrysts

Im	Im-B15c-1py	Im-B15c-3py	Im-B15c-3py	Im-B15c-6py	Im-B15c-7py	Im-B15c-7py	Im-B15c-7py
SiO_2	51.53	50.08	49.11	48.37	51.41	51.29	50.68
TiO_2	1.03	1.99	2.35	2.22	1.16	1.16	1.81
Al_2O_3	1.63	3.37	3.78	4.11	2.07	2.05	2.79
Cr_2O_3	0.01	0.01	0.01	0.01	0.01	0.01	0.01
MgO	14.56	13.80	14.01	13.92	14.13	14.07	14.10
CaO	19.24	19.37	19.37	18.78	18.58	19.00	19.29
FeO	9.68	8.80	9.25	9.25	10.17	9.74	9.18
MnO	0.25	0.24	0.22	0.29	0.29	0.30	0.20
Na_2O	0.57	0.67	0.64	0.67	0.59	0.64	0.64
K_2O	0.10	0.09	0.08	0.10	0.08	0.10	0.09
Total	**98.59**	**98.43**	**98.82**	**97.72**	**98.50**	**98.35**	**98.79**
Structural Formulae	Cations per 6 Oxygen						
Si	1.95	1.89	1.86	1.85	1.94	1.94	1.91
Ti	0.03	0.06	0.07	0.06	0.03	0.03	0.05
Al (IV)	0.05	0.11	0.14	0.15	0.06	0.06	0.09
Al (VI)	0.02	0.04	0.03	0.03	0.04	0.03	0.03
Cr	0.00	0.00	0.00	0.00	0.00	0.00	0.00
Mg	0.82	0.78	0.79	0.79	0.80	0.79	0.79
Ca	0.78	0.78	0.78	0.77	0.75	0.77	0.78
Fe	0.31	0.28	0.29	0.30	0.32	0.31	0.29
Mn	0.01	0.01	0.01	0.01	0.01	0.01	0.01
Na	0.04	0.05	0.05	0.05	0.04	0.05	0.05
K	0.00	0.00	0.00	0.01	0.00	0.00	0.00
Fe^{3+}	0.05	0.04	0.04	0.04	0.05	0.05	0.04
Fe^{2+}	0.26	0.23	0.24	0.25	0.27	0.26	0.24
M1	0.92	0.92	0.93	0.94	0.92	0.91	0.92
M2	1.08	1.07	1.08	1.07	1.06	1.08	1.07
Cation Sum	**4.00**	**4.00**	**4.01**	**4.02**	**3.99**	**4.00**	**4.00**
Mg #	72.98	73.80	73.11	73.00	71.39	72.17	73.40

Table 8B- Microprobe Analyses of Imnaha Dike Pyroxene Phenocrysts

Im	Im-B15c-7py	Im-B15c-7py	Im-B15c-8py	Im-B15c-8py	Im-B15c-8py	Im-B15c-9py	Im-B15c-11py
SiO2	50.54	51.08	51.44	50.56	51.44	51.44	49.79
TiO2	1.28	1.87	1.51	1.93	1.39	1.40	2.46
Al2O3	2.53	2.34	2.28	2.81	1.89	2.36	3.50
Cr2O3	0.01	0.01	0.02	0.01	0.01	0.01	0.01
MgO	14.41	14.65	14.86	14.42	15.32	14.23	13.97
CaO	18.53	19.79	19.19	18.92	18.25	19.01	19.15
FeO	10.23	9.12	9.02	8.98	8.69	9.49	9.14
MnO	0.28	0.29	0.26	0.23	0.26	0.25	0.26
Na2O	0.68	0.63	0.66	0.62	0.50	0.60	0.63
K2O	0.09	0.08	0.10	0.08	0.09	0.09	0.09
Total	**98.58**	**99.86**	**99.34**	**98.56**	**97.83**	**98.87**	**98.98**
Structural Formulae							
Cations per 6 Oxygen							
Si	1.92	1.91	1.92	1.91	1.94	1.93	1.88
Ti	0.04	0.05	0.04	0.05	0.04	0.04	0.07
Al (IV)	0.08	0.09	0.08	0.09	0.06	0.07	0.12
Al (VI)	0.03	0.01	0.03	0.03	0.03	0.04	0.03
Cr	0.00	0.00	0.00	0.00	0.00	0.00	0.00
Mg	0.81	0.82	0.83	0.81	0.86	0.80	0.78
Ca	0.75	0.79	0.77	0.76	0.74	0.77	0.77
Fe	0.32	0.28	0.28	0.28	0.27	0.30	0.29
Mn	0.01	0.01	0.01	0.01	0.01	0.01	0.01
Na	0.05	0.05	0.05	0.05	0.04	0.04	0.05
K	0.00	0.00	0.00	0.00	0.00	0.00	0.00
Fe3+	0.05	0.04	0.04	0.04	0.04	0.04	0.04
Fe2+	0.27	0.24	0.24	0.24	0.23	0.25	0.24
M1	0.93	0.92	0.94	0.94	0.97	0.92	0.93
M2	1.07	1.07	1.05	1.05	1.00	1.06	1.06
Cation Sum	**4.01**	**4.01**	**4.00**	**4.00**	**3.99**	**3.99**	**4.00**
Mg #	71.67	74.25	74.75	74.26	75.99	72.92	73.30

251

Table 8C- Microprobe Analyses of Imnaha Dike Pyroxene Phenocrysts

Im	Im-B15c-11py	Im-B15c-11py	Im-B15c-13py	Im-B18c-2py	Im-B18c-4py	Im-B18c-4pyln1	Im-B18c-4pyln2
SiO_2	50.65	49.21	49.68	51.48	50.59	51.29	51.21
TiO_2	1.72	2.24	2.21	1.60	2.00	1.84	1.91
Al_2O_3	2.92	3.74	3.33	2.99	3.70	3.41	3.59
Cr_2O_3	0.01	0.01	0.01	0.01	0.01	0.01	0.01
MgO	14.02	13.91	13.98	14.00	13.70	13.87	13.92
CaO	19.47	19.05	18.68	19.24	19.25	19.36	19.65
FeO	9.29	9.45	9.65	9.99	9.54	9.91	9.71
MnO	0.31	0.23	0.27	0.27	0.30	0.31	0.27
Na_2O	0.58	0.68	0.63	0.59	0.62	0.62	0.57
K_2O	0.10	0.08	0.09	0.09	0.07	0.08	0.09
Total	**99.07**	**98.60**	**98.52**	**100.26**	**99.76**	**100.69**	**100.91**
Structural Formulae							
Cations per 6 Oxygen							
Si	1.91	1.86	1.88	1.91	1.89	1.90	1.89
Ti	0.05	0.06	0.06	0.04	0.06	0.05	0.05
Al (IV)	0.09	0.14	0.12	0.09	0.11	0.10	0.11
Al (VI)	0.04	0.03	0.03	0.05	0.05	0.05	0.05
Cr	0.00	0.00	0.00	0.00	0.00	0.00	0.00
Mg	0.79	0.79	0.79	0.78	0.76	0.77	0.77
Ca	0.78	0.77	0.76	0.77	0.77	0.77	0.78
Fe	0.29	0.30	0.31	0.31	0.30	0.31	0.30
Mn	0.01	0.01	0.01	0.01	0.01	0.01	0.01
Na	0.04	0.05	0.05	0.04	0.04	0.04	0.04
K	0.00	0.00	0.00	0.00	0.00	0.00	0.00
Fe^{3+}	0.04	0.04	0.05	0.05	0.04	0.05	0.05
Fe^{2+}	0.24	0.25	0.25	0.26	0.25	0.26	0.25
M1	0.91	0.93	0.93	0.91	0.92	0.91	0.91
M2	1.07	1.07	1.06	1.07	1.06	1.07	1.07
Cation Sum	**4.00**	**4.01**	**4.00**	**3.99**	**3.99**	**3.99**	**3.99**
Mg #	73.06	72.57	72.24	71.56	72.06	71.55	72.02

Table 8D- Microprobe Analyses of Imnaha Dike Pyroxene Phenocrysts

Im	Im-B18c-4pyln3	Im-B18c-4pyln4	Im-B18c-4pyln5	Im-B18c-8py	Im-B18c-12py	Im-B18c-12py	Im-B18c-13py
SiO2	50.68	49.35	49.40	51.70	51.80	52.05	50.75
TiO2	2.01	2.49	2.68	1.53	1.66	0.93	1.72
Al2O3	3.92	4.40	4.47	2.71	2.69	1.39	3.80
Cr2O3	0.01	0.01	0.02	0.01	0.01	0.01	0.01
MgO	13.82	13.55	13.36	13.53	13.63	11.93	13.98
CaO	19.50	18.47	18.79	18.36	18.68	19.12	19.53
FeO	9.37	9.76	10.08	11.29	11.63	13.30	9.72
MnO	0.25	0.26	0.23	0.35	0.30	0.37	0.25
Na2O	0.58	0.65	0.66	0.65	0.62	0.73	0.61
K2O	0.10	0.10	0.09	0.08	0.09	0.10	0.09
Total	**100.25**	**99.04**	**99.77**	**100.22**	**101.11**	**99.93**	**100.45**
Structural Formulae							
Cations per 6 Oxygen							
Si	1.88	1.86	1.85	1.93	1.92	1.97	1.88
Ti	0.06	0.07	0.08	0.04	0.05	0.03	0.05
Al (IV)	0.12	0.14	0.15	0.07	0.08	0.03	0.12
Al (VI)	0.05	0.05	0.05	0.05	0.04	0.03	0.05
Cr	0.00	0.00	0.00	0.00	0.00	0.00	0.00
Mg	0.77	0.76	0.75	0.75	0.75	0.67	0.77
Ca	0.78	0.75	0.75	0.73	0.74	0.78	0.78
Fe	0.29	0.31	0.32	0.35	0.36	0.42	0.30
Mn	0.01	0.01	0.01	0.01	0.01	0.01	0.01
Na	0.04	0.05	0.05	0.05	0.04	0.05	0.04
K	0.00	0.00	0.00	0.00	0.00	0.00	0.00
Fe3+	0.04	0.05	0.05	0.05	0.05	0.06	0.05
Fe2+	0.24	0.26	0.26	0.29	0.30	0.35	0.25
M1	0.92	0.93	0.92	0.90	0.89	0.80	0.92
M2	1.06	1.05	1.07	1.08	1.09	1.18	1.07
Cation Sum	**3.99**	**3.99**	**4.00**	**3.99**	**3.99**	**3.99**	**4.00**
Mg #	72.60	71.38	70.42	68.29	67.81	61.70	72.10

Table 8E- Microprobe Analyses of Imnaha Dike Pyroxene Phenocrysts

Im	Im-B19c-2py	Im-B19c-3py1	Im-B19c-4py1	Im-B19c-5py1	Im-B19c-6py	Im-B19c-8py	Im-B19c-10py
SiO_2	50.65	51.70	50.78	49.45	49.89	50.27	50.99
TiO_2	1.82	1.40	1.66	1.96	1.93	2.01	1.34
Al_2O_3	2.65	1.94	2.28	3.21	3.32	3.30	2.54
Cr_2O_3	0.00	0.00	0.00	0.01	0.01	0.01	0.01
MgO	13.75	14.83	13.43	14.03	13.68	13.55	14.36
CaO	18.64	18.62	18.64	19.47	18.38	19.24	19.33
FeO	11.05	9.78	11.13	9.54	10.32	9.56	9.26
MnO	0.44	0.47	0.48	0.24	0.31	0.20	0.21
Na_2O	0.62	0.56	0.55	0.64	0.63	0.60	0.55
K_2O	0.09	0.12	0.09	0.09	0.08	0.09	0.09
Total	**99.72**	**99.42**	**99.04**	**98.63**	**98.56**	**98.83**	**98.68**
Structural Formulae							
Cations per 6 Oxygen							
Si	1.91	1.94	1.92	1.88	1.89	1.90	1.92
Ti	0.05	0.04	0.05	0.06	0.06	0.06	0.04
Al (IV)	0.09	0.06	0.08	0.12	0.11	0.10	0.08
Al (VI)	0.02	0.02	0.03	0.02	0.04	0.04	0.04
Cr	0.00	0.00	0.00	0.00	0.00	0.00	0.00
Mg	0.77	0.83	0.76	0.79	0.77	0.76	0.81
Ca	0.75	0.75	0.76	0.79	0.75	0.78	0.78
Fe	0.35	0.31	0.35	0.30	0.33	0.30	0.29
Mn	0.01	0.01	0.02	0.01	0.01	0.01	0.01
Na	0.05	0.04	0.04	0.05	0.05	0.04	0.04
K	0.00	0.01	0.00	0.00	0.00	0.00	0.00
Fe3+	0.05	0.05	0.05	0.05	0.05	0.05	0.04
Fe2+	0.29	0.26	0.29	0.25	0.27	0.25	0.24
M1	0.90	0.94	0.88	0.91	0.92	0.91	0.92
M2	1.09	1.04	1.09	1.09	1.07	1.07	1.06
Cation Sum	**4.00**	**4.00**	**3.99**	**4.02**	**4.00**	**3.99**	**4.00**
Mg #	69.09	73.15	68.42	72.54	70.44	71.79	73.60

254

Table 8F- Microprobe Analyses of Imnaha Dike Pyroxene Phenocrysts

Im	Im-B18c-11py	Im-B21b-1py	Im-B21b-3py	Im-B21b-4py	Im-B21b-6py	Im-B21b-7py	Im-B21b-9py
SiO2	50.83	50.09	50.01	51.01	52.25	50.92	49.86
TiO2	1.16	2.09	2.14	1.79	1.29	1.79	2.28
Al2O3	2.33	3.59	3.69	2.77	1.99	2.80	3.82
Cr2O3	0.01	0.01	0.01	0.01	0.01	0.01	0.01
MgO	12.93	13.95	13.76	13.88	14.87	13.73	13.96
CaO	18.20	19.01	19.77	19.09	19.77	18.79	19.37
FeO	12.07	10.23	9.64	11.04	9.81	11.27	9.43
MnO	0.30	0.30	0.32	0.34	0.26	0.30	0.31
Na2O	0.61	0.64	0.62	0.64	0.56	0.62	0.62
K2O	0.09	0.09	0.07	0.08	0.08	0.10	0.11
Total	**98.55**	**100.01**	**100.03**	**100.65**	**100.88**	**100.33**	**99.77**
Structural Formulae							
Cations per 6 Oxygen							
Si	1.94	1.87	1.87	1.90	1.93	1.90	1.87
Ti	0.03	0.06	0.06	0.05	0.04	0.05	0.06
Al (IV)	0.06	0.13	0.13	0.10	0.07	0.10	0.13
Al (VI)	0.04	0.03	0.03	0.02	0.02	0.03	0.03
Cr	0.00	0.00	0.00	0.00	0.00	0.00	0.00
Mg	0.73	0.78	0.77	0.77	0.82	0.77	0.78
Ca	0.74	0.76	0.79	0.76	0.78	0.75	0.78
Fe	0.39	0.32	0.30	0.34	0.30	0.35	0.30
Mn	0.01	0.01	0.01	0.01	0.01	0.01	0.01
Na	0.05	0.05	0.04	0.05	0.04	0.04	0.05
K	0.00	0.00	0.00	0.00	0.00	0.00	0.01
Fe3+	0.06	0.05	0.05	0.05	0.05	0.05	0.04
Fe2+	0.32	0.27	0.25	0.29	0.25	0.29	0.25
M1	0.87	0.92	0.91	0.90	0.92	0.90	0.92
M2	1.11	1.08	1.09	1.10	1.08	1.09	1.07
Cation Sum	**3.99**	**4.01**	**4.01**	**4.01**	**4.01**	**4.00**	**4.01**
Mg #	65.80	71.00	71.95	69.31	73.15	68.65	72.66

255

Table 8G- Microprobe Analyses of Imnaha Dike Pyroxene Phenocrysts

Im	Im-B23b-2py	Im-b23b-4py	Im-B23b-5py	Im-B23b-7py	Im-B23b-7py	Im-B23b-7py	Im-B23b-10py
SiO2	52.20	52.12	49.94	49.78	50.94	51.87	50.18
TiO2	0.98	1.36	2.67	2.26	1.95	1.00	2.06
Al2O3	1.67	1.90	3.96	3.91	2.99	1.42	3.17
Cr2O3	0.02	0.01	0.01	0.01	0.01	0.01	0.01
MgO	13.88	14.68	13.50	13.17	13.62	11.68	13.48
CaO	18.55	18.12	18.93	19.62	18.98	18.66	19.12
FeO	11.41	10.90	10.85	10.23	10.64	13.77	10.35
MnO	0.28	0.31	0.20	0.25	0.32	0.41	0.26
Na2O	0.57	0.49	0.63	0.63	0.58	0.59	0.57
K2O	0.09	0.08	0.09	0.09	0.09	0.10	0.08
Total	**99.63**	**99.97**	**100.80**	**99.93**	**100.12**	**99.53**	**99.29**
Structural Formulae							
Cations per 6 Oxygen							
Si	1.96	1.94	1.86	1.87	1.90	1.97	1.89
Ti	0.03	0.04	0.07	0.06	0.05	0.03	0.06
Al (IV)	0.04	0.06	0.14	0.13	0.10	0.03	0.11
Al (VI)	0.03	0.03	0.03	0.04	0.04	0.04	0.03
Cr	0.00	0.00	0.00	0.00	0.00	0.00	0.00
Mg	0.78	0.82	0.75	0.74	0.76	0.66	0.76
Ca	0.75	0.72	0.75	0.79	0.76	0.76	0.77
Fe	0.36	0.34	0.34	0.32	0.33	0.44	0.33
Mn	0.01	0.01	0.01	0.01	0.01	0.01	0.01
Na	0.04	0.04	0.05	0.05	0.04	0.04	0.04
K	0.00	0.00	0.00	0.00	0.00	0.01	0.00
Fe3+	0.05	0.05	0.05	0.05	0.05	0.07	0.05
Fe2+	0.30	0.28	0.28	0.27	0.28	0.37	0.27
M1	0.89	0.93	0.91	0.89	0.90	0.79	0.90
M2	1.09	1.04	1.08	1.10	1.08	1.17	1.09
Cation Sum	**3.99**	**3.99**	**4.00**	**4.00**	**3.99**	**3.98**	**4.00**
Mg #	68.61	70.75	69.09	69.82	69.69	60.38	70.04

Table 8H- Microprobe Analyses of Imnaha Dike Pyroxene Phenocrysts

Im	Im-B23b-12py	Im-B23b-12py	Im-B23b-12py
SiO2	49.98	50.27	49.51
TiO2	2.32	1.67	2.39
Al2O3	3.62	2.99	3.79
Cr2O3	0.01	0.01	0.01
MgO	13.25	13.38	13.28
CaO	19.49	19.33	19.35
FeO	10.05	10.78	10.01
MnO	0.31	0.27	0.29
Na2O	0.67	0.56	0.63
K2O	0.07	0.07	0.09
Total	**99.79**	**99.33**	**99.34**
Structural Formulae			
Cations per 6 Oxygen			
Si	1.88	1.90	1.87
Ti	0.07	0.05	0.07
Al (IV)	0.12	0.10	0.13
Al (VI)	0.04	0.03	0.04
Cr	0.00	0.00	0.00
Mg	0.74	0.75	0.75
Ca	0.78	0.78	0.78
Fe	0.32	0.34	0.32
Mn	0.01	0.01	0.01
Na	0.05	0.04	0.05
K	0.00	0.00	0.00
Fe3+	0.05	0.05	0.05
Fe2+	0.26	0.28	0.26
M1	0.89	0.88	0.90
M2	1.10	1.11	1.09
Cation Sum	**4.00**	**4.00**	**4.00**
Mg #	70.30	69.05	70.45

257

APPENDIX 4

Table 9A - Microprobe Analyses of Imnaha Groundmass Plagioclase

	Im-B15c-10gm	Im-b15c-11plgm	Im-b15c-11plgm	Im-b15c-11plgm	Im-b15c-11plgm	Im-B15c-13plgm	Im-B15c-13plgm
SiO2	51.91	51.97	50.96	51.74	54.45	57.48	57.03
TiO2	0.09	0.18	0.24	0.24	0.11	0.11	0.27
Al2O3	29.17	29.61	30.02	29.77	27.66	26.33	26.16
MgO	0.05	0.02	0.01	0.04	0.05	0.05	0.05
CaO	12.38	13.41	13.88	12.89	11.59	9.19	9.09
FeO	0.64	0.62	0.62	0.50	0.78	0.80	0.75
Na2O	3.97	3.60	3.39	3.56	4.76	5.85	5.90
K2O	0.22	0.20	0.20	0.21	0.29	0.54	0.44
Sr	0.00	0.00	0.00	0.00	0.00	0.00	0.00
Totals	98.43	99.61	99.32	98.96	99.69	100.35	99.70
Structural Formulae							
Cations per 8 Oxygen							
Si	2.40	2.38	2.35	2.38	2.49	2.59	2.59
Ti	0.01	0.01	0.02	0.02	0.01	0.01	0.02
Al	1.59	1.60	1.63	1.61	1.49	1.40	1.40
Mg	0.00	0.00	0.00	0.00	0.00	0.00	0.00
Ca	0.61	0.66	0.68	0.64	0.57	0.44	0.44
Fe	0.02	0.02	0.02	0.02	0.03	0.03	0.03
Na	0.31	0.28	0.26	0.27	0.36	0.44	0.45
K	0.01	0.01	0.01	0.01	0.02	0.03	0.03
Sr	0.00	0.00	0.00	0.00	0.00	0.00	0.00
Cation Sum	4.96	4.96	4.97	4.96	4.96	4.95	4.95
An (mol)	76.88	79.88	81.34	79.39	72.16	62.08	61.89
Ab (mol)	22.32	19.43	17.98	19.85	26.78	35.75	36.33
Or (mol)	0.80	0.70	0.68	0.76	1.06	2.17	1.78

258

Table 9B- Microprobe Analyses of Imnaha Groundmass Plagioclase

	Im-B15c-13plgm	Im-18c-4plgm2	Im-18c-4plgm	Im-18c-6plgm3	Im-18c-7pl2gm	Im-18c-7plgm3	Im-18c-8plgm
SiO_2	51.76	54.04	53.91	52.36	51.96	52.92	54.44
TiO_2	0.00	0.15	0.00	0.04	0.10	0.09	0.24
Al_2O_3	29.87	28.36	28.01	28.33	30.07	29.96	27.86
MgO	0.02	0.07	0.11	0.06	0.07	0.09	0.07
CaO	13.41	11.76	11.32	12.44	13.41	13.10	10.95
FeO	0.65	0.68	0.62	0.52	0.53	0.45	0.66
Na_2O	3.58	5.11	5.56	4.06	3.44	3.70	4.62
K_2O	0.21	0.28	0.30	0.22	0.20	0.18	0.32
Sr	0.00	0.00	0.00	0.00	0.00	0.00	0.04
Totals	**99.49**	**100.46**	**99.83**	**98.04**	**99.77**	**100.49**	**99.18**
Structural Formulae							
Cations per 8 Oxygen							
Si	2.37	2.45	2.46	2.43	2.37	2.40	2.49
Ti	0.00	0.01	0.00	0.00	0.01	0.01	0.02
Al	1.62	1.52	1.51	1.55	1.62	1.60	1.50
Mg	0.00	0.00	0.01	0.00	0.00	0.01	0.00
Ca	0.66	0.57	0.55	0.62	0.66	0.64	0.54
Fe	0.03	0.03	0.02	0.02	0.02	0.02	0.03
Na	0.27	0.39	0.42	0.32	0.26	0.28	0.35
K	0.01	0.02	0.02	0.01	0.01	0.01	0.02
Sr	0.00	0.00	0.00	0.00	0.00	0.00	0.00
Cation Sum	**4.96**	**4.99**	**5.00**	**4.96**	**4.95**	**4.95**	**4.95**
An (mol)	79.94	71.05	68.49	76.57	80.59	79.12	71.45
Ab (mol)	19.32	27.94	30.42	22.62	18.72	20.23	27.30
Or (mol)	0.74	1.00	1.09	0.81	0.70	0.65	1.25

259

Table 9C- Microprobe Analyses of Immaha Groundmass Plagioclase

	Im-B19c-6plgm	Im-B19c-8gm2	Im-B19c-8gm	Im-B19c-10plgm	Im-B23b-1plg35	Im-B23b-1plg35	Im-B23b-1plg35
SiO_2	53.22	54.73	53.11	52.49	53.36	53.51	56.98
TiO_2	0.09	0.09	0.03	0.13	0.11	0.10	0.09
Al_2O_3	29.17	26.02	27.70	28.40	29.41	29.19	24.51
MgO	0.04	0.04	0.08	0.06	0.08	0.07	0.33
CaO	11.78	11.58	12.24	13.05	13.44	13.28	8.57
FeO	0.65	0.77	0.53	0.47	0.43	0.50	1.03
Na_2O	3.87	4.62	4.33	3.88	3.74	3.80	6.14
K_2O	0.27	0.28	0.26	0.19	0.22	0.18	0.56
Sr	0.00	0.00	0.00	0.00	0.00	0.00	0.03
Totals	**99.08**	**98.12**	**98.28**	**98.66**	**100.79**	**100.62**	**98.24**
Structural Formulae							
Cations per 8 Oxygen							
Si	2.44	2.53	2.46	2.42	2.41	2.42	2.63
Ti	0.01	0.01	0.00	0.01	0.01	0.01	0.01
Al	1.57	1.42	1.51	1.55	1.57	1.56	1.33
Mg	0.00	0.00	0.01	0.00	0.01	0.00	0.02
Ca	0.58	0.57	0.61	0.65	0.65	0.64	0.42
Fe	0.02	0.03	0.02	0.02	0.02	0.02	0.04
Na	0.30	0.36	0.34	0.30	0.28	0.29	0.47
K	0.02	0.02	0.02	0.01	0.01	0.01	0.03
Sr	0.00	0.00	0.00	0.00	0.00	0.00	0.00
Cation Sum	**4.93**	**4.94**	**4.96**	**4.96**	**4.95**	**4.95**	**4.96**
An (mol)	76.26	72.71	75.06	78.28	79.28	78.95	59.28
Ab (mol)	22.69	26.25	24.00	21.04	19.96	20.43	38.40
Or (mol)	1.05	1.04	0.94	0.68	0.76	0.62	2.31

Table 9D- Microprobe Analyses of
Imnaha Groundmass Plagioclase

	Im-B23b-1plgm2	Im-b23b-1-plgm
SiO2	54.49	55.28
TiO2	0.08	0.16
Al2O3	26.68	27.18
MgO	0.05	0.07
CaO	11.48	10.97
FeO	0.88	0.63
Na2O	4.91	5.31
K2O	0.24	0.39
Sr	0.00	0.00
Totals	**98.82**	**100.00**
Structural Formulae		
Cations per 8 Oxygen		
Si	2.51	2.51
Ti	0.01	0.01
Al	1.45	1.46
Mg	0.00	0.00
Ca	0.57	0.53
Fe	0.03	0.02
Na	0.38	0.40
K	0.01	0.02
Sr	0.00	0.00
Cation Sum	**4.96**	**4.97**
An (mol)	71.45	68.52
Ab (mol)	27.67	30.02
Or (mol)	0.88	1.46

APPENDIX 5

Table 10A- Microprobe Analyses of Imnaha Dike Groundmass Pyroxene

	Im-B15c-4pygm	Im-B15c-6pygm	Im-B15c-13pygm	Im-B15c-13pygm	Im-B18c-1pygm	Im-B18c-3pygm	Im-B18c-7pygm
SiO2	50.46	49.50	48.53	51.76	52.05	50.40	52.84
TiO2	1.50	2.53	1.88	1.34	1.33	2.21	0.91
Al2O3	2.47	3.52	4.30	1.88	1.45	3.94	1.38
Cr2O3	0.02	0.01	0.01	0.01	0.01	0.01	0.01
MgO	14.13	14.26	14.52	15.58	13.48	13.86	12.84
CaO	19.08	18.56	17.69	17.89	18.44	19.09	19.11
FeO	9.25	9.30	9.10	9.32	12.11	9.54	12.67
MnO	0.23	0.26	0.23	0.30	0.32	0.27	0.35
Na2O	0.65	0.60	0.55	0.48	0.53	0.63	0.59
K2O	0.08	0.08	0.09	0.09	0.07	0.08	0.10
Total	**97.87**	**98.63**	**96.89**	**98.65**	**99.80**	**100.03**	**100.81**
Structural Formulae		Cations per 6 Oxygen					
Si	1.92	1.87	1.86	1.94	1.96	1.88	1.97
Ti	0.04	0.07	0.05	0.04	0.04	0.06	0.03
Al (IV)	0.08	0.13	0.14	0.06	0.04	0.12	0.03
Al (VI)	0.03	0.03	0.05	0.03	0.02	0.05	0.03
Cr	0.00	0.00	0.00	0.00	0.00	0.00	0.00
Mg	0.80	0.80	0.83	0.87	0.76	0.77	0.71
Ca	0.78	0.75	0.73	0.72	0.74	0.76	0.76
Fe	0.29	0.29	0.29	0.29	0.38	0.30	0.40
Mn	0.01	0.01	0.01	0.01	0.01	0.01	0.01
Na	0.05	0.04	0.04	0.03	0.04	0.05	0.04
K	0.00	0.00	0.00	0.00	0.00	0.00	0.00
Fe3+	0.04	0.04	0.04	0.04	0.06	0.04	0.06
Fe2+	0.25	0.24	0.24	0.24	0.32	0.25	0.33
M1	0.92	0.95	0.98	0.98	0.87	0.93	0.83
M2	1.07	1.04	1.01	1.00	1.10	1.06	1.14
Cation Sum	**4.00**	**4.00**	**4.01**	**3.99**	**3.99**	**3.99**	**3.99**
Mg #	73.29	73.36	74.14	75.01	66.67	72.29	64.55

Table 10B- Microprobe Analyses of Imnaha Dike Groundmass Pyroxene

	Im-B18c-7pygm	Im-B18c-8pygm	Im-B18c-8pygm	Im-B23b-1pygm	Im-B23b-1pygm	Im-B23b-1pygmc	Im-B23b 2pygm
SiO2	52.18	52.58	52.65	51.35	50.47	50.33	52.59
TiO2	0.94	1.12	0.95	1.40	1.98	1.59	0.90
Al2O3	1.69	1.73	1.69	2.17	3.45	2.46	1.36
Cr2O3	0.01	0.01	0.01	0.01	0.01	0.01	0.01
MgO	12.34	13.92	12.43	12.69	13.50	13.40	12.67
CaO	19.04	18.96	19.36	18.46	18.42	18.55	18.98
FeO	12.87	10.75	12.30	13.00	11.31	11.88	13.47
MnO	0.31	0.30	0.33	0.42	0.25	0.30	0.42
Na2O	0.72	0.52	0.60	0.60	0.62	0.61	0.60
K2O	0.08	0.10	0.10	0.10	0.11	0.11	0.10
Total	**100.19**	**100.00**	**100.42**	**100.19**	**100.12**	**99.23**	**101.10**
Structural Formulae							
Cations per 6 Oxygen							
Si	1.96	1.96	1.97	1.94	1.89	1.89	1.97
Ti	0.03	0.03	0.03	0.04	0.06	0.06	0.03
Al (IV)	0.04	0.04	0.03	0.06	0.11	0.11	0.03
Al (VI)	0.04	0.04	0.05	0.03	0.04	0.04	0.03
Cr	0.00	0.00	0.00	0.00	0.00	0.00	0.00
Mg	0.69	0.77	0.69	0.71	0.75	0.75	0.71
Ca	0.77	0.76	0.78	0.75	0.74	0.74	0.76
Fe	0.41	0.34	0.39	0.41	0.35	0.35	0.42
Mn	0.01	0.01	0.01	0.01	0.01	0.01	0.01
Na	0.05	0.04	0.04	0.04	0.05	0.05	0.04
K	0.00	0.00	0.00	0.01	0.01	0.01	0.00
Fe3+	0.06	0.05	0.06	0.06	0.05	0.05	0.06
Fe2+	0.34	0.28	0.32	0.34	0.30	0.30	0.35
M1	0.82	0.89	0.82	0.85	0.90	0.90	0.82
M2	1.16	1.08	1.14	1.13	1.08	1.08	1.15
Cation Sum	**3.99**	**3.98**	**3.98**	**3.99**	**4.00**	**4.00**	**3.99**
Mg #	63.26	69.93	64.47	63.67	68.19	66.96	62.83

Table 10C- Microprobe Analyses of Imnaha Dike Groundmass Pyroxene

	Im-B23b-3pygm	Im-B23b-3pygm
SiO2	50.96	51.81
TiO2	1.44	0.87
Al2O3	2.28	1.18
Cr2O3	0.01	0.01
MgO	12.60	11.41
CaO	18.28	19.19
FeO	12.18	14.78
MnO	0.31	0.39
Na2O	0.59	0.63
K2O	0.07	0.09
Total	**98.73**	**100.36**
Structural Formulae		
Cations per 6 Oxygen		
Si	1.94	1.97
Ti	0.04	0.02
Al (IV)	0.06	0.03
Al (VI)	0.04	0.02
Cr	0.00	0.00
Mg	0.72	0.65
Ca	0.75	0.78
Fe	0.39	0.47
Mn	0.01	0.01
Na	0.04	0.05
K	0.00	0.00
Fe3+	0.06	0.07
Fe2+	0.32	0.39
M1	0.86	0.76
M2	1.11	1.22
Cation Sum	**3.98**	**4.00**
Mg #	65.03	58.09

VITA

SEDELIA RODRIGUEZ DURAND

EDUCATION   Florida International University, Miami FL
Ph.D. Candidate in Geology
Expected Graduation Date: May 2006
Title of Dissertation: Investigation into the Petrogenesis of the Columbia
River Basalt Group of the Pacific Northwest, USA

California State University, Los Angeles
Bachelor in Geological Sciences - 1997

EXPERIENCE

Shipboard Scientist-Igneous Petrologist
IODP Expedition 309 Superfast Spreading 2, Guatemala Basin
R/V JOIDES Resolution, July-Aug 2005
Co-chief scientists: Dr. D. A. H. Teagle (Univ. of Southampton)
Dr. S. Umino (Univ. of Shizuoka)

Laboratory Instructor- Florida International University
2000-2004
Duties included: teaching, preparing lecture and laboratory materials and
grading and creating exams and lab exercises. In addition, preparing a
curriculum, implementing new topics into the existing exercises using a
variety of sources such as internet and outdoor activities.

Geologist- ATLAS Environmental Engineering
1998 – 2000
Conducted soil and groundwater sampling, site assessment, remediation
and groundwater monitoring. Interfaced with local and state agencies,
responsible for writing quarterly groundwater monitoring reports as well
as site investigation, underground storage tank (UST) and corrective
action reports.

PUBLISHED PAPERS AND ABSTRACTS

Leg 206, Expedition 309 and 312 Scientific Party (Durand, S.R.), 2006, *Drilling
to Gabbro in intact ocean crust at the East Pacific Rise*; Science, accepted.

Durand, S.R., Sen, G., Reidel, S.P., 2005, *Origin of the Grande Ronde Basalts,
Columbia River Basalt Group: Eos Tran.* AGU, 86(44), Fall Meeting
Supplement, Abstract V41C-1454.

Teagle, D.A.H., Expedition 309 Scientific Party (Durand, S.R.), 2005, The Hard Yards: Deep basement drilling of an in situ section of oceanic crust formed at a superfast spreading rate. Recent results from IODP Expedition 309 to Hole 1256D, Eastern Equatorial Pacific.

Durand, S.R., Sen, G., 2004, *Preeruption history of the Grande Ronde Formation lavas, Columbia River Basalt Group, American Northwest: Evidence from phenocrysts:* Geology, v. 32 no. 4, p. 293-296.

Durand, S.R., Sen, G., 2003, Invited presenter at the Geological Society of America's 2003 national meeting in Seattle Washington, *Evidence for Shallow Differentiation and Magma Mixing of the Grande Ronde Formation, Columbia River Basalt Group:* Abstracts with Programs- Geological Society of America Annual Meeting and Exposition, Seattle, WA.

Durand, S.R., Sen, G., 2003, *Floods of Fire: The Columbia River Flood Basalt Lava Flows: SACNAS* National Meeting, Albuquerque, New Mexico. *Received award for Best Oral Presentation.*

HONORS AND ACTIVITIES

- Lamont-Doherty Postdoctoral Research Fellowship-2006-2008

- Joint Oceanographic Institute Research Grant-2006

- Dissertation Year Fellowship 2004-2005, Florida International University

- Research Grant Recipient 2003, Geological Society of America

- Teaching Award 2002 (first place), Florida International University

- Conference Travel Grants, Graduate Student Association-Florida International University, 2002, 2003, 2005.

- Field Trip Leader: GSA 2003 Annual Meeting field trip, The Columbia Flood Basalts and the Yakima fold belt.